Titre: Title:	High-Performance Thermoplastic PEEK-Based Systems for Lunar Exploration
Auteur: Author:	Arthur Lassus
Date:	2025
Type:	Mémoire ou thèse / Dissertation or Thesis
Référence: Citation:	Lassus, A. (2025). High-Performance Thermoplastic PEEK-Based Systems for Lunar Exploration [Thèse de doctorat, Polytechnique Montréal]. PolyPublie. https://publications.polymtl.ca/69073/

POLYTECHNIQUE MONTRÉAL

affiliée à l'Université de Montréal

High-Performance Thermoplastic PEEK-based Systems for Lunar Exploration

ARTHUR LASSUS

Département de génie chimique

Thèse présentée en vue de l'obtention du diplôme de *Philosophiæ Doctor*

Génie chimique

Septembre 2025

POLYTECHNIQUE MONTRÉAL

affiliée à l'Université de Montréal

Cette thèse intitulée :

High-Performance Thermoplastic PEEK-based Systems for Lunar Exploration

présentée par **Arthur LASSUS**

en vue de l'obtention du diplôme de *Philosophiæ Doctor*

a été dûment acceptée par le jury d'examen constitué de :

Jason Robert TAVARES, président
Nick VIRGILIO, membre et directeur de recherche
Basil FAVIS, membre et codirecteur de recherche
Abdellah AJJI, membre
Pierre SARAZIN, membre externe

DEDICATION

To my family.

ACKNOWLEDGEMENTS

I would like to begin by expressing my heartfelt gratitude to my research supervisors, Prof. Basil D. Favis and Prof. Nick Virgilio, for giving me the opportunity to pursue my Ph.D. within their research group. Their kindness, invaluable help, and meticulous attention to detail have profoundly shaped the researcher I have become today. Thank you for your support and guidance throughout this pivotal chapter of my life.

I would like to sincerely thank the evaluation committee, Prof. Jason R. Tavares, Prof. Abdellah Ajji, and Dr. Pierre Sarazin, for agreeing to evaluate my thesis.

I thank all the members of the PEEKbot project for the engaging and constructive discussions during our many team meetings. Special thanks go to Professor Daniel Therriault for enabling the creation of such an ambitious project and for providing access to the essential equipment needed for my research. I thank Dr. Kambiz Chizari for his technical assistance and meticulous project oversight. My gratitude also goes to Dr. Marie-Josée Potvin, who inspired us to aim for the stars while keeping our feet firmly on the ground. Similarly, I would like to thank Dr. Romain Martin, Olivier Duchesne, and Behnam Khaledi for riding alongside me on this Ph.D. journey and for our always-enriching discussions.

I am deeply grateful to the technical and administrative staff of the Chemical Engineering department for their unwavering support. Special thanks to Matthieu Gauthier, Wendell Raphael, and Claire Cerclé for their constant help in solving daily challenges, without whom research progress would be even harder. Thank you to Gino Robin and Martine Lamarche for their invaluable expertise in planning high-risk experiments, and Alexandre Bréard for his indispensable assistance in navigating administrative complexities.

I would like to express my gratitude to Professor Antonio Nanci, Dr. Dainelys G. Bello, and Katia J. Ponce for their perpetual good spirits and their invaluable help in using the microscopy platform at UdeM, without which many of the results presented in this work would not have been possible.

I warmly thank Professor Miriam M. Unterlass for welcoming me for a short research stay in her research group in Konstanz, and for the valuable lessons I gained from this experience. Special thanks to Alonso for the warm welcome, the daily guidance during those four months to help me avoid mistakes, and for offering me a spot in your windowless office. Many thanks go to all the

group members: Rob, Fabián, Florian, Frank, Hipassia, Celine, Tobias, and Max, with whom I shared wonderful moments both at work and outside of it. I am also grateful to Mitacs for the financial support that made this exchange possible.

I would now like to thank my past and present colleagues, Parniyan, Caroline, Lauriane, Guillaume, Lisa, Vaiana, and Alex, for their extended discussions on all the technical details no one else would have wanted to hear about; your help over the years was invaluable.

A heartfelt thanks to my friends Olivier, Teodora, Helia, and Clémence for being my role models, showing me that achieving this extraordinary project was possible, and thank you for all the enjoyable moments spent outside of work.

Cristina, a special thank you for your love and support since the turbulent early days in the transport phenomena class, and especially during the mini project. This journey would not have been the same without you.

Finally, I deeply thank all my friends for helping me take my mind off work throughout these years! Especially those who became a second family to me in Montréal: Pierre, Gabrielle, Lancelot, Kassy, Louis, Benoit, Éléa, Loïc, Ambre, Paul, and Alizée.

To conclude, I would like to express my deepest love and gratitude to my wonderful family and Lila for their unwavering love, encouragement, and support, which allowed me to bring this thesis to completion.

Finis coronat opus.

RÉSUMÉ

L'exploration lunaire présente des défis uniques pour la conception de nouveaux matériaux, en particulier pour les composants qui seront exposés à de fortes variations thermiques, au régolithe lunaire abrasif, au vide spatial et aux radiations. Les thermoplastiques haute performance, tels que le poly(éther éther cétone) (PEEK) et le poly(éther imide) (PEI), offrent une bonne combinaison de propriétés, notamment une résistance thermique élevée, une excellente stabilité chimique et de bonnes propriétés mécaniques. Ainsi, les mélanger pour former des systèmes à base de PEEK/PEI présente un intérêt particulier, car ils combinent la nature cristalline et la résistance aux solvants du PEEK, avec le caractère amorphe et la température de transition vitreuse élevée du PEI. Le mélange de *méta*-PEI (*m*-PEI) ou de *para*-PEI (*p*-PEI) au PEEK permet de contrôler la morphologie, le comportement thermique et les propriétés mécaniques. Ces systèmes multiphasiques pourraient constituer une matrice idéale pour développer des composites thermoplastiques afin d'atteindre les performances mécaniques supérieures nécessaires aux pièces structurelles. Ces mélanges de polymères présentent également le potentiel de générer des structures de PEEK poreux après l'extraction sélective du PEI, permettant ainsi une réduction de masse et ouvrant la voie à de nouvelles applications. Comprendre l'influence de la composition, de la miscibilité, de la cristallisation et des traitements post-production sur ces systèmes est donc essentiel pour optimiser leurs propriétés et développer de nouveaux matériaux adaptés aux applications lunaires.

L'objectif principal de ce travail est de développer des matériaux polymères multiphasiques à base de poly(éther éther cétone) (PEEK), avec des morphologies hautement contrôlées, capables de résister à l'environnement lunaire en tant qu'élément de la structure d'un rover lunaire.

Dans la première partie, les systèmes binaires PEEK/*m*-PEI et PEEK/*p*-PEI sont étudiés, mettant en évidence leurs comportements distincts en termes de miscibilité et de morphologie. Le PEEK/*m*-PEI est confirmé comme étant totalement miscible à l'état amorphe, tandis que le PEEK/*p*-PEI est démontré partiellement miscible, formant des morphologies submicroniques co-continues ou dispersées à l'état fondu. La tension interfaciale du système PEEK/*p*-PEI a été mesurée à une valeur très faible (0,14 mN/m), permettant un contrôle de la morphologie par recuit au-dessus du point de fusion du PEEK. Pour le PEEK/*m*-PEI, la cristallisation du PEEK est contrôlée par traitements thermiques, provoquant la ségrégation du *m*-PEI à des échelles allant du

nanomètre au micromètre. Prenant compte des deux systèmes binaires, ce travail démontre un contrôle morphologique sur près de quatre ordres de grandeur (~5 nm à plus de 15 µm), permettant la préparation de monolithes de PEEK poreux avec une porosité totalement interconnectée après extraction des PEIs. De plus, les propriétés mécaniques en tension révèlent qu'ajouter 20 à 30 vol% de PEI, associé à une augmentation de la cristallinité par recuit thermique, augmente le module d'Young du matériau final en comparaison au PEEK pur. Enfin, le type de PEI utilisé a peu d'impact sur les valeurs des augmentations mécaniques observées.

Dans la deuxième partie, l'étude est étendue aux systèmes ternaires de PEEK, *m*-PEI, et *p*-PEI. En faisant varier la composition, le traitement thermique et le procédé, la miscibilité et la taille des phases peuvent être ajustées finement et de manière continue, de quelques nanomètres à plusieurs dizaines de micromètres, sans recourir à des compatibilisants interfaciaux. Des morphologies miscibles induites par cisaillement, rarement rapportées, sont observées, lesquelles se séparent ensuite lors d'un recuit thermique. Les paramètres d'interaction polymère-polymère de Flory-Huggins ont été calculés à partir de données calorimétriques pour toutes les paires binaires, y compris pour les systèmes PEEK/*p*-PEI et *m*-PEI/*p*-PEI non rapportés auparavant. Ces paramètres ont permis de calculer une courbe spinodale théorique, délimitant la région de séparation de phase spinodale, qui concorde bien avec les observations expérimentales. Le diagramme ternaire résultant offre un visuel prédictif du développement des morphologies. L'extraction sélective des deux phases de PEI conduit à des monolithes de PEEK poreux avec des tailles de pores finement ajustables, pertinents pour de potentielles applications avancées telles que la filtration ou le biomédical.

Enfin, trois nouveaux systèmes ternaires à base de PEEK et de polycarbonate (PC), contenant également du *m*-PEI, du *p*-PEI, ou du poly(phényl sulfone) (PPSU) sont développés. La morphologie résultante dépend fortement de la miscibilité des paires constitutives : des morphologies biphasiques apparaissent lorsque PEEK/*m*-PEI est présent, tandis que les paires partiellement miscibles (PEEK/*p*-PEI et PEEK/PPSU) mènent à des morphologies triphasiques. Les tensions interfaciales et l'analyse des coefficients d'étalement prédisent correctement l'agencement des phases, le PEEK séparant systématiquement le PC du troisième composant. Ces résultats sont exploités pour préparer des monolithes de PEEK poreux bimodaux (taille de pores nm et µm) et ultraporeux avec seulement 5 % vol de PEEK, offrant une densité extrêmement faible

et une porosité ajustable. Ces matériaux poreux sont prometteurs pour la fabrication de pièces légères, la gestion thermique et la filtration avancée.

Cette thèse explore la préparation de systèmes binaires et ternaires à base de PEEK, en étudiant leur miscibilité, leur morphologie et leur comportement thermique en fonction de leur historique de préparation. Ce travail fournit des connaissances fondamentales sur la manière dont le contrôle morphologique, de l'échelle nanométrique à micrométrique, peut être réalisé sans compatibilisant dans des systèmes multiphasiques à base de PEEK. Ces résultats ouvrent de nouvelles opportunités pour le développement de matériaux haute performance destinés à des environnements extrêmes, tels que les composites thermoplastiques, les composants structurels légers, l'isolation thermique ou acoustique, les membranes de filtration, les membranes pour piles à combustible, etc.

Grammarly et des outils basés sur l'IA ont été utilisés pendant la rédaction de cette thèse, en particulier pour la relecture et la structuration du plan d'écriture.

ABSTRACT

The exploration of the Moon brings unique challenges for material design, particularly for components exposed to extreme thermal variations, abrasive lunar regolith, vacuum, and radiation. High-performance thermoplastics, such as poly(ether ether ketone) (PEEK) and poly(ether imide) (PEI), offer an attractive combination of properties, including high thermal resistance, excellent chemical stability, and good mechanical strength. Thus, blending them to prepare PEEK/PEI-based systems is of special interest because they combine the crystalline nature and solvent resistance of PEEK, with the amorphous character and high glass transition temperature of PEI. Blending PEEK with *meta*-PEI (*m*-PEI) or *para*-PEI (*p*-PEI) provides opportunities to tailor morphology, thermal behavior, and mechanical properties. These multiphase systems could provide an excellent matrix for the development of thermoplastic composites to reach the higher mechanical performance needed for structural parts. These polymer blends also present the potential to generate porous PEEK microstructures after selective PEI extraction, which could reduce weight and open new applications. Understanding the influence of composition, miscibility, crystallization, and post-processing treatments on these systems is therefore crucial to optimize their properties and develop new materials for demanding lunar applications.

The main objective of this work is to develop multiphase polymer materials based on poly(ether ether ketone) (PEEK), with highly controlled morphologies, and capable of withstanding the lunar environment as part of the structure of a lunar rover.

In the first part, the PEEK/*m*-PEI and PEEK/*p*-PEI binary systems are investigated, highlighting their distinct miscibility and morphological behaviors. PEEK/*m*-PEI is confirmed to be fully miscible in the amorphous state, whereas PEEK/*p*-PEI is proven partially miscible, forming sub-µm co-continuous or dispersed morphologies in the melt. The PEEK/*p*-PEI interfacial tension was measured to be very low (0.14 mN/m), enabling morphology control through quiescent annealing over PEEK's melting point. For PEEK/*m*-PEI, PEEK crystallization was controlled through thermal treatments, which induced *m*-PEI segregation from nm to µm scales. The two binary systems combined, this work demonstrates morphological control over nearly four orders of magnitude (~5 nm to over 15 µm), allowing the preparation of porous PEEK monoliths with fully interconnected pores after PEIs extraction. Furthermore, the tensile mechanical properties reveal that adding 20 to 30 vol% of PEI, combined with an increase in crystallinity through thermal

annealing, increases the Young's modulus of the final material compared to pure PEEK. Finally, the type of PEI used has little impact on the value of the observed mechanical enhancements.

In the second part, the research is extended to ternary blends of PEEK, *m*-PEI, and *p*-PEI. By varying the composition, thermal treatment, and processing, the miscibility and phase size can be finely and continually tuned, from a few nm to tens of µm, without the need for interfacial compatibilizers. Rare shear-induced miscible morphologies are observed, which later phase-separate upon annealing. Flory-Huggins' polymer-polymer interaction parameters were calculated from calorimetric data for all binary pairs, including those of unreported PEEK/*p*-PEI and *m*-PEI/*p*-PEI. The parameters enabled the calculation of a theoretical spinodal curve, delimitating the spinodal phase separation region, that matches well with experimental observations. The resulting ternary phase diagram provides predictive insight into morphology development. Selective extraction of both PEIs phases yields porous PEEK monoliths with finely tunable pore sizes, relevant for potential advanced applications, such as filtration or biomedical domains.

Finally, three new ternary systems based on PEEK and polycarbonate (PC), also containing *m*-PEI, *p*-PEI, or poly(phenyl sulfone) (PPSU), are developed. The resulting morphology is shown to depend strongly on the miscibility of the constitutive pairs: biphasic morphologies form when PEEK/*m*-PEI is present, while partially miscible pairs (PEEK/*p*-PEI and PEEK/PPSU) lead to triphasic morphologies. Interfacial tensions and spreading coefficient analysis correctly predict phase localization, with PEEK consistently separating PC from the third component. These insights are leveraged to prepare bimodal porous (nm and µm pore sizes) and ultraporous PEEK monoliths with as little as 5 vol% PEEK, offering extremely low density and tunable porosity. Such porous materials are promising for preparing lightweight parts, thermal management, and advanced filtration.

This thesis explored the preparation of binary and ternary PEEK-based systems, investigating their miscibility, morphology, and thermal behavior based on their processing history. This research provides fundamental knowledge on how morphological control, from nanoscale to micron-scale, can be achieved without compatibilizers in PEEK-based multiphase systems. These findings open new opportunities for high-performance materials development for extreme environments, such as thermoplastics composites, lightweight structural components, thermal or acoustic insulation, filtration membranes, fuel cell membranes, etc.

Grammarly and AI-based tools were used during the writing of this thesis, particularly for proofreading and writing plan structuring.

TABLE OF CONTENTS

LIST OF TABLES

LIST OF FIGURES

LIST OF SYMBOLS AND ABBREVIATIONS

This list presents, in alphabetical order, the acronyms and abbreviations used in the thesis and their meaning.

AFM	Atomic force microscopy
χ_{ij}	Binary segmental polymers interaction parameter
CLTE	Coefficient of linear thermal expansion
DMA	Dynamic mechanical analysis
DSC	Differential scanning calorimetry
FTIR	Fourier transform infrared spectroscopy
γ	Interfacial tension
h-BN	Hexagonal boron nitride
HDT	Heat deflection temperature
LCP	Liquid crystalline polymer
MWCNT	Multi-walled carbon nanotubes
NMP	1-methyl-2-pyrrolidone
ω	Weight fraction
PC	poly(bisphenol A carbonate)
PEDEK	poly(ether diphenyl ether ketone)
PEEK	poly(ether ether ketone)
PEI	poly(ether imide)
m-PEI	*meta*-poly(ether imide)
p-PEI	*para*-poly(ether imide)
PEN	poly(ethylene naphthalate)
PES	poly(ether sulfone)

PPSU	poly(phenyl sulfone)
SEM	Scanning electron microscopy
SPEEK	Sulfonated poly(ether ether ketone)
TEM	Transmission electron microscopy
T_c	Crystallization temperature from the melt state
T_{cc}	Cold-crystallization temperature from the glassy state
T_g	Glass transition temperature
T_m	Melting temperature
TGA	Thermogravimetric analysis
X_c	Material crystallinity based on its total mass
XRD	X-ray diffraction

CHAPTER 1 INTRODUCTION

With 1/6th of Earth's gravity and an atmosphere so thin that it is considered quasi-inexistent, the lunar surface undergoes drastic variations in temperatures between day and night, with the mean surface temperature ranging from -153 °C to 107 °C, and extremes beyond -200 °C and 123 °C [1]. Without any magnetic field, coupled with a thin atmosphere, the moon is defenseless against space radiation [1]. Solar particle events originate from the sun's activity and produce a high number of charged particles in a short amount of time, mainly protons, with high energy [2]. Galactic cosmic radiation is constantly produced in the rest of the universe and strikes the lunar surface from every direction. It is composed of fully ionized atoms, from hydrogen to high atomic number atoms, that can present high energy (E > 100 GeV) [3, 4]. The first layer of the lunar soil is composed of lunar regolith, which consists of particles with a mean size of 45 to 100 μm, sometimes reaching a nanometric scale. Due to low electrical conductivity and dielectric losses, lunar dust is electrostatically charged when exposed to the ultraviolet radiation (UV) coming from the sun [1], causing it to adhere easily to the surfaces of every object. Furthermore, as lunar dust grains are often compared to crushed glass (with Al_2O_3 and SiO_2 being on the high end of the hardness scale of Mohs), their power of abrasion makes it one of the biggest challenges that exploration missions have to face on the lunar surface. Another critical constraint of the lunar environment is the impact of roughly 1 mm micrometeorites, not so rare on the moon [1].

All the aforementioned constraints generate demanding specifications for a structural material designed for lunar applications: resistance to extreme temperature changes, resistance to radiation, low accumulation of electrical charges within the material, mechanical properties that withstand the impacts of micrometeorites, absence of volatile compounds in the material that could lead to vacuum outgassing, and resistance to the erosion caused by the lunar dust.

Aluminum (Al) has always played a key role in the development of the aerospace industry, not least because of its reproducible and easily predictable properties, but also because of its relatively low density (2.7 g/cm^3). Commonly used Al alloys for aerospace applications include: 1100, 2024, 2195, 2219, 6061, and 7075 [5-9]. Although this metal presents outstanding mechanical properties, it still possesses important flaws, particularly when applied for lunar use. Indeed, the aluminum on-site repairability remains a challenge yet to be overcome. Moreover, its specific gravity, although lower than that of a vast majority of metals, is still significantly higher than high-

performance polymers and their reinforced composites. Finally, regarding the precise application aim of this project, *i.e.* manufacture the chassis of a lunar rover, thermal conductivity is a critical parameter to be taken into account to protect the scientific payload of the rover from extreme temperatures and maintain the equipment fully functional. While the thermal conductivity of aluminum is higher than 200 $W.m^{-1}.K^{-1}$ [10], high-performance polymers possess thermal conductivities of roughly 0.3 $W.m^{-1}.K^{-1}$ [11, 12]. Owing to these inherent flaws, a need has arisen for new lighter, and repairable materials capable of resisting the lunar environment and potentially replacing aluminum for some extra atmospheric applications.

This work aims to investigate the miscibility behavior of different complex high-performance polymer blends to leverage their advantages over aluminum in the formulation of new materials for lunar exploration. Precisely controlling the melt processing of polymer blends is important for their morphology development and their following mechanical properties, allowing their use as (nano)composites matrices, for example.

The main objective of this research is to develop multiphase polymer materials based on poly(ether ether ketone) (PEEK), with highly controlled morphologies, and capable of withstanding the lunar environment as part of the structure of a lunar rover.

In this thesis, the morphological, thermal, and mechanical properties of two different binary PEEK/PEI blends are explored in detail. Based on the miscibility behaviors of the two previous binary blends, a novel ternary system is developed and characterized, in part by using a theoretical framework based on the polymers' interaction parameters and the spinodal decomposition curve. Finally, three new ternary systems, with varying levels of (im)miscibility in one of the constitutive pairs, are developed and compared through their morphology development behavior.

This thesis comprises three articles published in or submitted to peer-reviewed journals and consists of the following chapters:

- Chapter 2: Literature review

- Chapter 3: Objectives and organization of the articles

- Chapters 4 to 6: The three articles reporting and discussing the results from this work

- Chapter 7: General discussion

- Chapter 8: Conclusions and recommendations

CHAPTER 2 LITERATURE REVIEW

2.1 High-performance thermoplastics

2.1.1 Overview and key properties

High-performance thermoplastics are a class of polymers with enhanced thermal, chemical, and mechanical properties when compared to other common and engineering polymers. This allows high-performance thermoplastics to compete against thermosets or even metals, once under their composites' form, in certain applications where low density and high specific strength are required. Figure 2.1 summarizes some of the high-performance polymers and other commodity polymers, which are divided into two subgroups: semi-crystalline or amorphous polymers. When compared to the latter, materials from the semi-crystalline subgroup present higher stiffness and chemical resistance thanks to their crystalline domains that act as reinforcements and barriers against the attack of solvents or crack propagation. Usually, due to an aromatic backbone structure, materials composing the class of high-performance thermoplastics present "in use" thermal stability above 200 °C, thanks to a glass transition temperature higher than this value or a melting temperature higher than 300 °C. Furthermore, polymers belonging to this category display degradation temperatures superior to 450 °C, while engineering plastics start to degrade in the range of 300 to 400 °C [13]. Additionally, this aromatic backbone often comes with high molecular rigidity and high melt viscosities. However, such high thermal resistances and melt viscosities are limitations to their ease of processing since specific pieces of equipment are then needed to operate at such high temperatures. Moreover, high-performance polymers exhibit an extended resistance to solvent attack, being susceptible to dissolution only in strong acid/base or specific organic solvents. As the volume production of high-performance thermoplastics is very low compared to other commodity plastics, their final prices are in return higher than average. Regarding the three main materials considered in this research project, prices range from 140 to 180 CAD/kg for PEEK, 55 to 75 CAD/kg for PEI, and 55 to 75 CAD/kg for PPSU based on internal purchase orders for 25 kg bags.

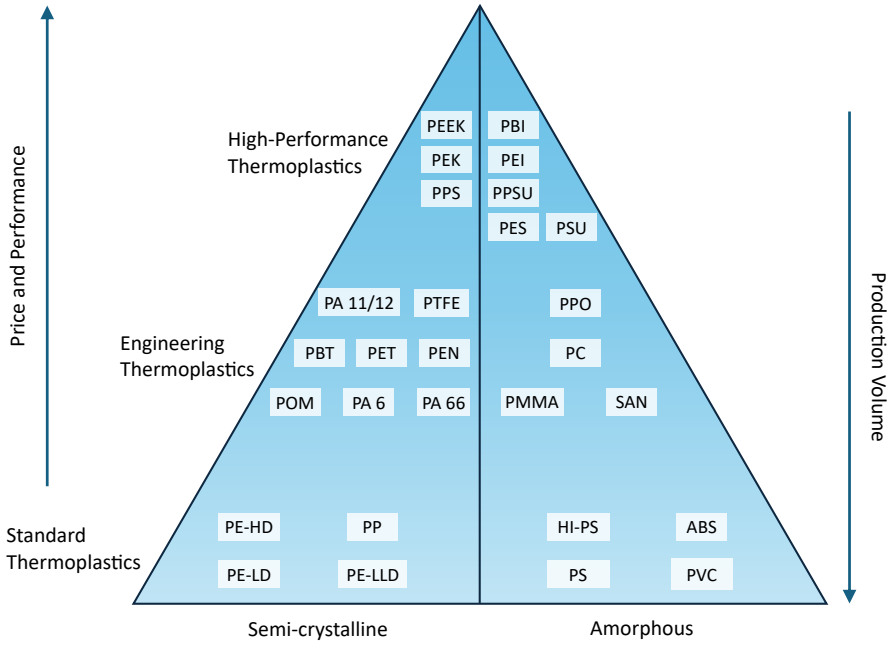

Figure 2.1 The three classical categories and two subgroups for the main polymers available on the market.

2.1.2 Poly(ether ether ketone) (PEEK)

PEEK is a semi-crystalline high-performance thermoplastic, employed for a broad range of applications such as industrial gears, biomedical implants [14], and aeronautical parts [15]. Figure 2.2 presents its chemical structure, mainly aromatic, where two ether links and one ketone group constitute the base of the PEEK's monomer repeating unit.

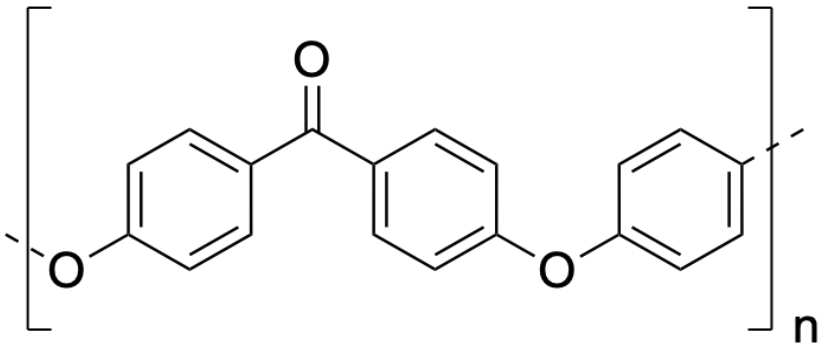

Figure 2.2 Chemical structure of poly(ether ether ketone) (PEEK).

The potential of PEEK for aerospace applications derives from some of its characteristics: *i)* the semi-crystalline nature of PEEK provides it with good stiffness when compared to its fully amorphous counterparts, with a Young's modulus of around 4.1 GPa [12]; *ii)* because it is semi-crystalline, PEEK presents an outstanding chemical resistance, being susceptible to degradation only in extremely harsh environments, such as super-concentrated acidic medium [16]; *iii)* depending on the application, different grades of PEEK can be selected to obtain the desired melt viscosity; *iv)* PEEK is a robust polymer, with a yield strength of 105 MPa and an elongation at break of 20 % at 23 °C. Moreover, its notched Izod impact strength can reach 4.5 $kJ.m^{-2}$ at room temperature; *v)* from the thermal point of view, PEEK has a heat deflection temperature of 156 °C, close to lunar extremes. Its glass transition temperature (T_g) is between 140 °C and 147 °C, and its melting temperature (T_m) is between 343 °C and 345 °C, depending on its level of crystallinity. PEEK is also a proper thermal insulator with an average thermal conductivity of 0.29 $W.m^{-1}.K^{-1}$ [12, 17]; *vi)* PEEK respects the NASA outgassing standard for materials to be used in space [18]; *vii)* finally, its aromatic molecular structure ensures high stability against radiation, avoiding the accumulation of free radicals due to an easy delocalization of electrons along the entire backbone by resonance [14].

2.1.3 Poly(ether imide) (PEI)

Poly(ether imide) is a family of amorphous high-performance thermoplastics, with backbones composed of ether and imide links. Figure 2.3 presents the chemical structures of ULTEM™ resins 1000 and CRS 5001 (from Sabic), two common PEIs found on the market and used in this thesis work. As a *meta*-PEI and a *para*-PEI, respectively, the two imide functions are either linked in a *meta*- or a *para*- position onto a specific aromatic cycle, as shown in Figure 2.3. Besides, these PEIs are also composed of a bisphenol A-type unit, present between the two ether links, composing the remaining monomer repeating unit. The molecular structure of this family of polymers may vary with different backbone structures between the two ether links, such as bisphenol AF, bisphenol S, bisphenol F, 4,4'-biphenol, or 4,4'-dihydroxybenzophenone, resulting in materials with distinct properties.

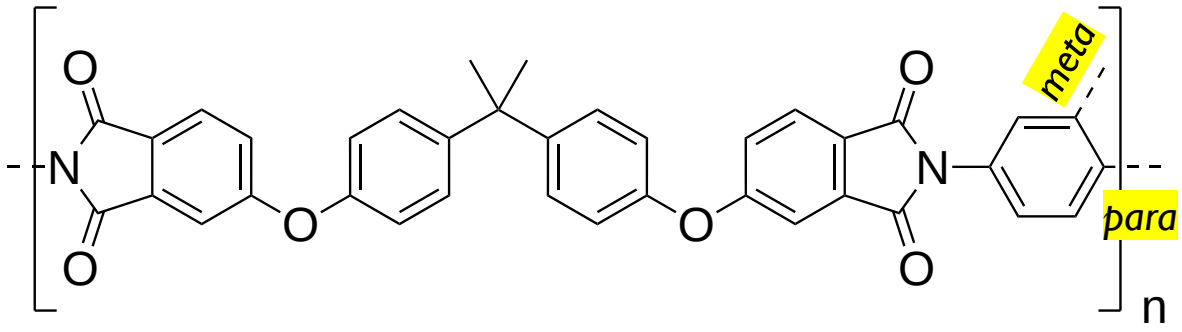

Figure 2.3 Chemical structures of the ULTEM™ resins 1000 and CRS 5001, respectively a *meta*-PEI and a *para*-PEI from Sabic.

This family of polymers possesses several advantages: *i)* they are approximately three times cheaper than the semi-crystalline PEEK; *ii)* from a mechanical point of view, they can present higher elongation at break (roughly 60%), comparable yield strength, but lower tensile modulus (3.2 GPa) than PEEK. Additionally, PEI polymers present a high impact resistance, ranging from 5 to 8 $kJ.m^{-2}$ depending on the chosen PEI grade. It is noteworthy to mention that these notched Izod impact values are the same when measured at -30 °C or 23 °C, demonstrating some of the cryogenic resistance of these thermoplastics; *iii)* regarding the thermal properties, PEI polymers usually possess T_g's from 210 °C to 230 °C. They are good thermal insulators with low thermal conductivities ranging from 0.21 to 0.29 $W.m^{-1}.K^{-1}$; *iv)* because of their high glass-transition temperature, PEI present heat deflection temperatures of at least 190°C, demonstrating their high-temperature mechanical performance [11]; *v)* finally, many PEI grades are found in NASA's list of low outgassing materials that can be safely used in space [18].

2.1.4 Poly(phenyl sulfone) (PPSU)

The molecular structure of poly(phenyl sulfone) (PPSU), another amorphous high-performance thermoplastic, is presented in Figure 2.4. Similar to the previously discussed PEEK and PEI, this thermoplastic possesses an extensive aromatic structure linked by ether bonds, only this time sulfonyl and biphenol groups are also present.

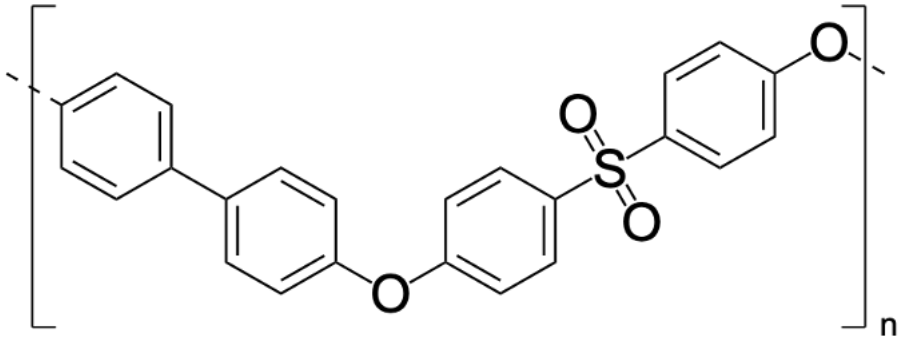

Figure 2.4 Chemical structure of poly(phenyl sulfone) (PPSU).

As an amorphous thermoplastic, PPSU shares some of the advantages listed for PEI polymers. While PPSU is a cheap and good insulator thermoplastic, its general mechanical properties, with the exception of impact resistance, are inferior to those of the two previously discussed polymers [19]. Finally, although neat PPSU does not respect NASA's outgassing standard for safe use in space, some of its composites can be safely employed for aerospace applications [18].

2.1.5 Poly(bisphenol A carbonate) (PC)

Poly(bisphenol A carbonate) (PC) is not considered a high-performance thermoplastic but an engineering polymer (see Figure 2.1). Even though it possesses a partly aromatic backbone, presented in Figure 2.5, the carbonate link that follows is prone to hydrolysis, which makes the polymer globally less resistant to its environment.

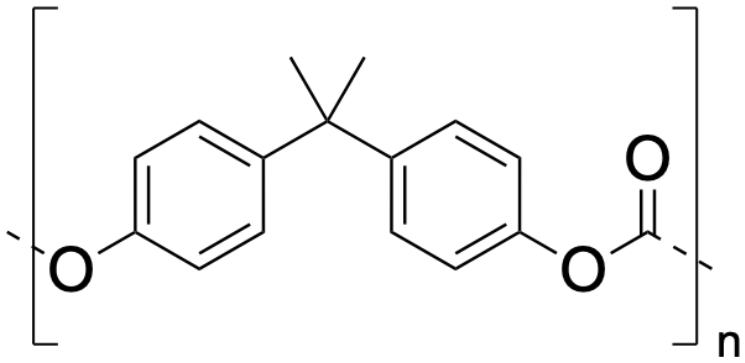

Figure 2.5 Chemical structure of poly(bisphenol A carbonate) (PC).

As an amorphous thermoplastic, PC shares a lot of mechanical properties similar to the previously presented PPSU; notably, PC possesses similar tensile behavior alongside an important impact

resistance, which makes it a tough engineering polymer [20]. However, PC displays a T_g of approximately 150 °C, which is quite lower than the other amorphous high-performance thermoplastics used in this work. Furthermore, some PC grades respect the outgassing standard for materials to be safely used in space [18].

2.1.6 Performance in extreme conditions

Table 2.1 summarizes the main properties of the thermoplastics previously discussed, as well as those of an aerospace-grade aluminum alloy and a commercially available 40 % carbon fiber PEEK composite. It is worth mentioning that a direct comparison between the mechanical properties of thermoplastics and aluminum alloys is unnecessary, as high-performance thermoplastics cannot be used in their pure form to directly replace aluminum in demanding applications. However, composite materials use the addition of particles or fibers to enhance their mechanical, physical, and chemical properties, and should be taken into account for comparison. As such, a commercially available 40 % carbon fiber PEEK composite is given for comparison purposes to show what range of properties can be obtained by adding such high-performance fillers to thermoplastic-based matrices.

Table 2.1 Main properties of an aluminum alloy (2195-T8 Al), a carbon fiber/PEEK composite (Victrex 90HMF40), and some high-performance thermoplastics

	Tensile Modulus (GPa)	Yield Strength (MPa)	Elongation at break (%)	Notched Izod impact (kJ/m²)	HDT [a] (°C)	Thermal Conductivity ($W.m^{-1}.K^{-1}$)	CLTE [b] (10^{-6} cm/cm/°C)
2195-T8 Al alloy	75	540	16	/	>400	~200	~21 - 24
PEEK Victrex 90HMF40	43	330	1.2	10.5	349	~2 - 4.3	35
PEEK Victrex 90G	4.1	105	20	4.5	156	0.29	55
m-PEI Ultem 1000	3.2	105	60	6	190	0.24	52

Table 2.1 Main properties of an aluminum alloy (2195-T8 Al), a carbon fiber/PEEK composite (Victrex 90HMF40), and some high-performance thermoplastics (cont'd)

m-PEI Ultem 1010	3.2	105	60	5	190	0.21	/
p-PEI Ultem CRS 5001	3.2	100	50	8	200	0.29	54
PPSU Radel 5000	2.3	70	60 to 120	690 **J/m***	207	0.30	56
PC Lexan 101	2.3	62	135	70	132	0.29	68

Values provided by suppliers.

[a] HDT = Heat Deflection Temperature.

[b] CLTE = Coefficient of Linear Thermal Expansion.

* This value is given with the ASTM D256 standard, which differs from the norm ISO 180/A given in this column. It corresponds roughly to 10 times the value of p-PEI Ultem CRS 5001, but is inferior to the value obtained for PC Lexan 101 when all polymers are measured with the same ASTM D256 norm.

Tensile mechanical properties are only one aspect of the requirements that materials need to fulfill to be part of the chassis of a lunar rover. As briefly presented in CHAPTER 1, the lunar environment is associated with extreme conditions that materials developed for such applications need to account for. The continuous cycles of extreme temperatures, from -200 °C to 123 °C (which is already a large window for any polymer to resist), are another key aspect to consider. Indeed, the changes from one extreme to another are fast and depend mainly on the direct exposure of the rover to either the sun's rays or deep space. Furthermore, since a lunar daytime is equivalent to approximately 14 Earth days, the materials need to resist the previously mentioned temperatures for this long [1].

Additionally, the presence of different sources of radiations that strike the lunar surface further complicates the environment for the materials. These radiations comprise ultraviolets (UV), protons and electrons of medium energy (a few keV to hundreds of MeV) coming mainly from the solar wind and solar cosmic rays, but also more energetic and heavy nuclei (~GeV) coming from galactic cosmic rays [1]. In the long term, some of these radiations can cause damage or changes

to the molecular structures of the different polymers, for example, by chain scission, radical formation, or cross-linking [21-23]. Additionally, the charged particles present in some of these radiations can create an accumulation of electrical charges at the surface of the materials, which in turn can create dangerous electric arcs, potentially damaging the electronics present inside the rover. Since laboratory testing cannot perfectly reproduce the temperature and radiation conditions found in space, some materials have been brought just outside of the International Space Station (ISS) to expose them to the real space environment of low Earth orbit. In this specific environment, atomic oxygen is the main compound provoking erosion of the exposed materials [24]. Although not present at the lunar surface, it gives additional information about the polymers' resistance to such extreme environments. PEEK displays an erosion yield similar to poly(imide) Kapton H (often used in space missions); poly(sulfone) materials perform a bit better in general, and PEI and PC are more susceptible to erosion [25]. Bending mechanical tests were also performed on materials in order to characterize their embrittlement due to this harsh space environment. In this case, PEEK was found to be more brittle than PEI or poly(sulfones) since it was the only one to present some surface cracks after the test, as revealed by optical microscopy [26].

The intense vacuum of space poses its own set of challenges, notably in the form of outgassing – *e.g.* the lower pressure induces any volatile compounds present inside the materials to diffuse from the bulk toward the outside. This outgassing of the materials is known to be a source of pollution for any instruments onboard the mission vehicle because the outgassed volatile compounds will then tend to condense on any optical lens or similar colder surfaces. To avoid such complications, a standard laboratory test was developed (ASTM E 595-77) to screen in advance the materials with low outgassing properties at 125 °C, *i.e.* a total mass loss inferior to 1 % combined with less than 0.1 % of condensable materials [27]. All the materials used in this work, except for the PPSU that was just outside the limits, were found to respect this standard and are present in the freely available NASA database [18].

Finally, the lunar regolith found on the Moon's surface poses a real threat to any moving mechanism because of its nm to µm size and abrasion properties [1]. The small particles can enter the moving parts and slowly crumble them if the materials composing the parts display lower hardness than the regolith. Hence, the polymers' tribological properties are important if these materials are used in the design of moving parts such as the rover wheels or the wheels' shaft, for example. It was shown that PEEK performs better and presents a lower specific wear rate when exposed to either

cryogenic or higher temperatures than its T_g during the test [28, 29]. However, prolonged exposure for several months to cryogenic temperatures or thermal cycling between this cryogenic regime and 40 °C increased the wear rate while the coefficient of friction was reduced [30, 31]. The rest of the polymers studied in this work are all amorphous, and it is known that this polymer category exhibits a higher wear rate in general compared to semi-crystalline ones [32-34]. Between the three amorphous polymers, PC and PEI display similar wear rates, two orders of magnitude higher than PPSU [32, 35].

Hence, to be relevant for lunar exploration, the materials should possess the following general properties: high mechanical properties, low density, some on-site repair capability, low thermal conductivity, good thermal resistance (cycles and extremes), good radiation resistance, sufficient electrical conductivity, low outgassing, and good tribological properties.

2.2 Binary polymer blends

2.2.1 Generalities of polymer blending

The development of polymer blends relies on the mixing of multiple polymers that can be either miscible, partially miscible, or immiscible, giving rise to complex morphologies in some cases [36]. Like composite materials, polymer systems are a tool to tailor specific properties by combining the advantages of several polymers, *e.g.* processability for one and strength from the other, or also cost saving, density, temperature resistance, crystallinity, solvent resistance, etc. Blending of polymers can be done using different methods. Melt-blending, for example, is performed at temperatures higher than the melting points of the polymers (or higher than the glass temperature for amorphous polymers) so they have sufficient flow properties and low viscosities to be efficiently mixed and easily processed. It is the main industrial process used to produce commercial blends, notably through extrusion [37]. Solvent casting is another method, requiring finding a common solvent for the polymers to be dissolved into and homogeneously mixed, and then the solvent is slowly evaporated to obtain the polymer blend. The design and control of the morphological and interfacial properties are essential to obtain the right characteristics for the targeted applications. For example, it is usual to aim for strong adhesion between the mixed polymers, or similar coefficients of thermal expansion, all in order to avoid stress concentration at

a weak interface. Therefore, interfacial compatibilizers are often used in the industry to control the polymer-polymer interactions at the interface, usually to increase their mechanical properties and/or limit undesired morphology evolutions [38]. To achieve the same result and level of control, more complex methods involve the reactive mixing of different compounds directly during the extrusion process, in order to form *in situ* favorable compatibilizers or chemical interactions between the polymers [39].

2.2.2 Miscibility and morphology

As previously mentioned, polymer blends can belong to three distinct categories: fully miscible, partially miscible, or immiscible [36]. Fully miscible binary polymer blends are rare since the necessary condition to obtain them is to have a favorable Gibbs free energy of mixing (< 0), which depends directly on the enthalpy of mixing, temperature, and entropy of mixing as follows:

$$\Delta G_{mix} = \Delta H_{mix} - T\Delta S_{mix} \tag{2.1}$$

The long molecular chains of polymers are associated with a low number of molecular arrangements (or configurations), which in turn does not promote high combinatorial entropy of mixing (favorable for miscibility). Moreover, the enthalpy of mixing is usually unfavorable (> 0) due to non-specific molecular interactions between the polymers, which leads in the end to generally immiscible polymer blends. When binary polymer blends demonstrate full miscibility, they typically display favorable specific interactions at the molecular level, resulting in a homogeneous morphology at the macroscopic level – *e.g* PMMA/PLA [40, 41] and PMMA/PVDF [42, 43]. The binary blends of this category usually display properties such as the T_g, the mechanical properties, and viscoelastic behavior, which follow an additivity rule of mixing based on the volume or weight fraction of each polymer present in the blend (*e.g.* Fox equation).

In opposition, binary immiscible blends do not mix at the molecular level, and each component forms its own phase separated from the other. This behavior automatically creates an interface between the two polymers, and with it, an interfacial tension. This reversible work, needed to create one unit of interfacial area, represents the level of affinity between the two polymers: the more immiscible, the higher the interfacial tension. Two classical morphologies arising in this case are the dispersed phase and co-continuous morphologies represented in Figure 2.6:

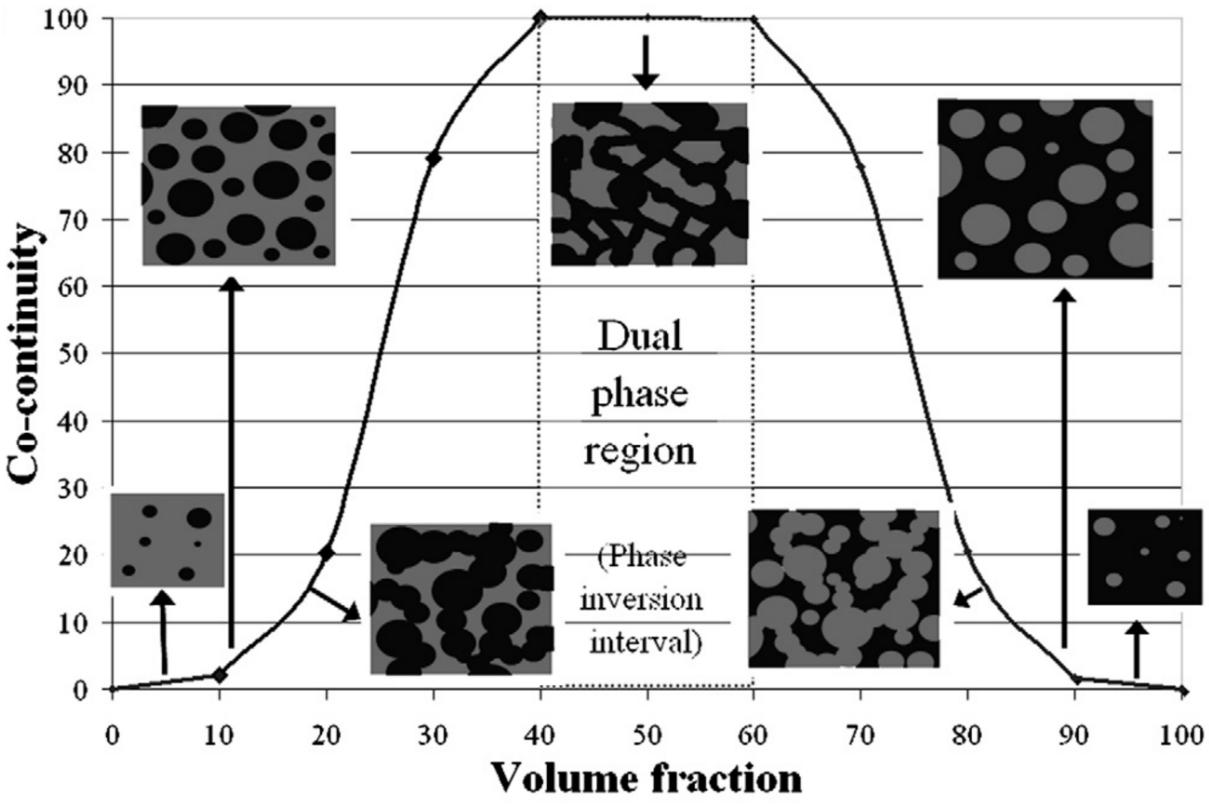

Figure 2.6 Classical dispersed phase and co-continuous morphologies observed in binary immiscible polymer blends. Figure adapted from Ravati and Favis [44]. Copyright © 2010 Elsevier Ltd. All rights reserved.

Figure 2.6 clearly depicts the transition between different morphologies in immiscible polymer blends. By adding a small amount of the second polymer (in black) into the major polymer matrix (in grey), the dispersed phase morphology is the first to appear. By slowly increasing the volume fraction of the second polymer, the dispersed phase starts to percolate, reaching the critical volume fraction at which the co-continuity increases dramatically (around 20%). Continuing to increase the second polymer volume fraction, the co-continuous morphology is reached when both polymers are fully interconnected and continuous with themselves (40-60%). Due to this full continuity of the polymer domains, such morphology is prone to coarsening during processing in the molten state. This well-known behavior can be leveraged to control the size of the polymer phases by maintaining the polymer blend in the molten state for various durations [45-47]. Passing the previous co-continuity region, a phase inversion occurs, where the second polymer (in black) becomes the newly formed matrix and the first polymer now becomes the dispersed phase (in grey).

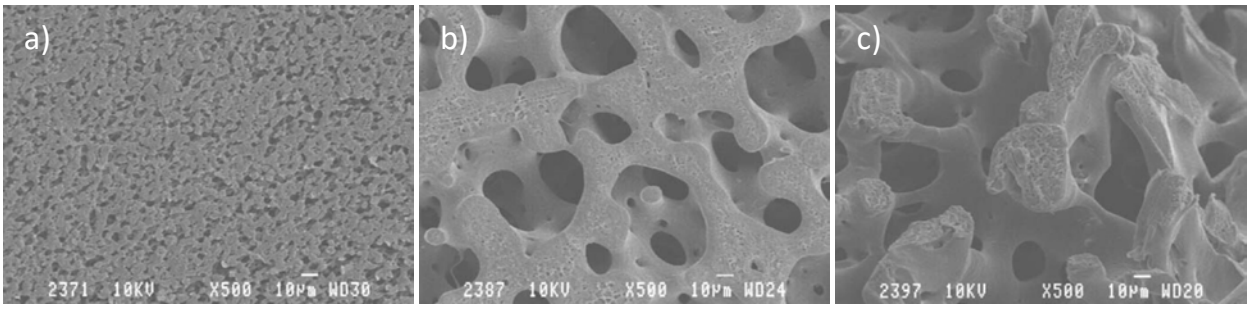

Figure 2.7 Controlled coarsening effect observed for a PLLA/PCL 40/60 blend annealed at 200 °C for: a) non-annealed, b) 2h, and c) 4h. Figure adapted from Sarazin, et al. [48].

Figure 2.7 presents the controlled coarsening effect observed for immiscible polymer blends. In this experiment, the PLLA/PCL blend was subjected to an annealing step in the molten state to increase the polymer domains' size and hence the resulting pores' size after PCL solvent extraction. This simple method relies on the existence of an interfacial tension between the two immiscible polymers and allows the control of domain size over several order of magnitude [49, 50]. The interfacial tension is responsible for the existence of a capillary pressure inside the polymer network, which is higher in the thinner channels of the network resulting in their flow towards larger connected channels, creating the observed coarsening effect [49].

The two types of immiscible morphologies can lead to very different mechanical properties for the material. Commonly, these properties are inferior to those of miscible blends, because of the poor interfacial adhesion that provokes stress concentrations at interfaces, and easier rupture of the material. However, when interfacial compatibilizers are used to increase adhesion at interfaces, these immiscible morphologies can display synergistic properties that result in enhanced mechanical properties compared to an additive rule, *e.g.* impact properties [38]. Such interfacial compatibilizers generally include diblock, triblock, tapered, starblock, or grafted copolymers [51]. When these copolymers are placed at the interface, they separate the two immiscible homopolymers resulting in a decrease of their interaction energy. In addition, the separation of each block of the copolymer, which penetrate in each homopolymer phases, also decreases their interaction energies. These two effects taken altogether lead to a decrease of the free energy of the system and to a compatibilization between the immiscible phases [52, 53]. Symmetrical diblock copolymers with high molecular weights proved to be better compatibilizers than tapered or unsymmetrical molecular structures [54, 55].

Finally, binary partially miscible blends present characteristics associated with both miscible and immiscible blends. They tend to form two separate phases that contain the two polymers in different proportions, and these phases can reach thermodynamic equilibrium given enough time and temperature to rearrange their compositions. Hence, these blends present the morphological attributes of immiscible blends, but since the two phases behave as two separate miscible blends, their intrinsic properties and the shared interface display behaviors closer to those of miscible blends. Because of these specific characteristics, this category of blends might not require interfacial compatibilizers to achieve good mechanical behavior because of sufficient interfacial interactions.

Overall, one must consider the competition between thermodynamic and kinetic control when blending polymers. The chosen method of mixing, cooling rate, mixing time, or the viscosity ratio between the blended polymers will all have an impact on the resulting morphology. A clear example of this competition is phase separation due to the crystallization of one of the polymer components. In this specific case, the two polymers can be thermodynamically miscible in the melt or amorphous state, but upon cooling from the melt (or heating from the glassy state), one of the polymers can crystallize and separate itself from the homogeneous amorphous phase by forming pure crystalline domains, which in turn create amorphous domains rich in the second polymer [56, 57]. Finally, controlling the morphology of blends is primordial for different applications, such as barrier films, where lamellar morphologies are of great interest, or porous monoliths for which co-continuous morphologies are relevant.

2.2.3 Theory of χ_{ij} polymers' interaction parameters

The Flory-Huggins theory on dilute polymer solutions developed a theoretical framework for the thermodynamics of mixing and the interactions between a molecule of solvent and a polymer molecular chain, based on a lattice theory [58]. From this theory, an interaction parameter χ is defined, describing the enthalpic interactions between the solvent molecules and the polymer chains. The Gibbs free energy change due to mixing is then described as:

$$\Delta G_{mix} = RT\,(n_1 \ln \phi_1 + n_2 \ln \phi_2 + n_1 \phi_2 \chi) \tag{2.2}$$

where R is the gas constant, T is the temperature, n_i the number of moles of component "i", ϕ_i the volume fraction of component "i", and χ the Flory-Huggins interaction parameter for the whole polymer molecule interacting with the solvent.

The theory can be extended to binary polymer blends by taking into account the change in molecular size from a low molecular weight solvent to a macromolecule of polymer with N repeating units.

$$\Delta G_{mix} = RT\,[n_1 \ln \phi_1 + n_2 \ln \phi_2 + \chi_{12}\phi_1\phi_2(m_1 n_1 + m_2 n_2) \tag{2.3}$$

$$m_i = \frac{V_i}{V_0} \tag{2.4}$$

where ϕ_i is the volume fraction of component "i", n_i is the number of moles of component "i", m_i is a kind of degree of polymerization relating the molar volume of polymer "i" (V_i) to a chosen reference molar volume of one repeating unit of one of the component polymers (V_0), and χ_{ij} is the segmental Flory-Huggins interaction parameter defining the enthalpic interaction between two segments of the blended polymers (note that this interaction parameter can also comprise non-combinatorial entropy effects).

Once the theory is developed, different experimental methods exist to obtain the Flory-Huggins interaction parameter. One of the most accurate methods is the neutron scattering technique, which gives access to motional mechanisms and structures in polymer blends [59-61]. Others include cloud point curves determination [62, 63] or inverse gas chromatography [64], which will not be discussed in further detail since they were not used during this work. More easily accessible methods are those based on the thermal characteristics of polymer blends obtained through DSC analysis, such as the melting temperature, or glass transition temperature (T_g). The first one, developed for miscible blends, uses the melting point depression observed when a crystalline polymer is blended with a miscible amorphous one [65]. It assumes that at the melting point of the blend (T_m), an equality should exist for the chemical potentials of the crystalline polymer between the crystalline and liquid phases, such as:

$$\frac{1}{T_m} - \frac{1}{T_m{}^0} = -\frac{RV_{2u}}{\Delta H_{2u} V_{1u}}\left[\frac{\ln \phi_2}{m_2} + \left(\frac{1}{m_2} - \frac{1}{m_1}\right) \times (1 - \phi_2) + \chi_{12}(1 - \phi_2)^2\right] \tag{2.5}$$

where the subscripts 1 and 2 are assigned to the amorphous and crystalline polymers, respectively, T_m^0 is the equilibrium melting temperature, V_{iu} is the molar volume of the repeating unit of polymer "i", and ΔH_{2u} is the enthalpy of fusion per mole of repeating unit. The rest of the symbols were described previously. Furthermore, by assuming the interaction parameter to be independent of entropy and composition effects, the following equation is derived:

$$\frac{1}{\phi_1}\left[\frac{1}{T_m}-\frac{1}{T_m{}^0}\right]=-\frac{BV_{2u}}{\Delta H_{2u}}\frac{\phi_1}{T_m} \tag{2.6}$$

$$\chi_{12}=\frac{BV_{1u}}{RT} \tag{2.7}$$

By plotting the left side of Equation 2.6 as a function of ϕ_1/T_m, a linear relationship is obtained that allows for the calculation of B, the interaction energy density, which in turn permits the obtention of χ_{ij}. The rest of the symbols are defined as previously.

The second method relies on the measurement of the miscible blends' glass transition temperature (T_{gm}) and was developed by Lu and Weiss [66], taking the enthalpy as the varying thermodynamic parameter as a result of mixing. The Flory-Huggins interaction parameter χ between two miscible polymers "*i*" and "*j*" is then calculated using the following set of equations:

$$T_{gm}=\frac{\omega_i T_{gi}+k\omega_j T_{gj}}{\omega_i+k\omega_j}+\frac{A\omega_i\omega_j}{(\omega_i+k\omega_j)(\omega_i+b\omega_j)(\omega_i+c\omega_j)^2} \tag{2.8}$$

With:

$$A=\frac{\chi R\left(T_{gi}-T_{gj}\right)c}{M_i\Delta C_{pi}} \tag{2.9}$$

$$k=\frac{\Delta C_{pj}-\omega_i\delta C_p^l}{\Delta C_{pi}-\omega_j\delta C_p^g} \tag{2.10}$$

$$b=\frac{M_{0j}}{M_{0i}} \tag{2.11}$$

$$c=\frac{\rho_i}{\rho_j} \tag{2.12}$$

The weight fraction of polymer "*i*" in the blend is denoted ω_i, and its glass transition temperature is T_{gi}. The repeat unit molar mass is expressed as M_{0i}, while ρ_i refers to its density. The thermal contribution ΔC_{pi} corresponds to the difference in specific heat at constant pressure between the melt and glassy states of polymer "*i*". Any change in specific heat due to mixing (δC_p) is generally considered negligible and set to zero [66]. *R* represents the universal gas constant. Identical definitions apply to polymer "*j*".

Finally, the last method was developed for partially miscible blends and considers the chemical potential of each component to be equal in each of the phases in equilibrium [67]. The composition of the phases in equilibrium is thus needed to calculate the resulting segmental interaction parameter and is usually obtained by treating each phase as its own miscible blend and applying the Fox formalism to their T_g to calculate their compositions:

$$\chi_{ij} = \frac{\ln\frac{\phi_i''}{\phi_i'} + (1 - \frac{m_i}{m_j})(\phi_j'' - \phi_j')}{m_i(\phi_j'^2 - \phi_j''^2)} \tag{2.13}$$

where $'$ and $''$ denote the two phases in equilibrium, and the other symbols were previously defined.

2.2.4 PEEK/*meta*- or *para*-PEI systems

The miscibility of PEEK with *m*-PEI in the melt/amorphous state has been widely established, and this compatibility influences the resulting phase morphology. Differential scanning calorimetry (DSC) [68-74] and dynamic mechanical analysis (DMA) [68, 69, 71, 75] consistently show only one T_g for PEEK/*m*-PEI blends, in agreement with the additivity rule in function of the blend composition. Dielectric spectroscopy has further confirmed this miscibility [73, 76]. Infrared spectroscopy indicates that the interaction between the ether functionalities in the PEEK backbone and the imide groups in *m*-PEI [77] leads to a favorable binary interaction parameter (χ_{12} = -0.058 to -0.196) [78]. This melt miscibility results in a homogeneous amorphous phase that can be preserved by quenching the material directly after its melt processing, thus hindering the PEEK crystallization.

In contrast, PEEK blended with *p*-PEI exhibits a very different behavior. The literature reports immiscibility in the melt, as evidenced by TEM observation of sub-µm phase-separated

morphology (Figure 2.8) and DMA profiles showing two distinct T_g values [79]. However, these transitions are shifted from those of the neat polymers: +10 °C for the lower T_g (PEEK-related) and -15 °C for the higher T_g (*p*-PEI-related), suggesting some level of interaction between the two polymers, but not enough to achieve complete miscibility. This apparent immiscibility in the melt presents an initially phase-separated microstructure before crystallization occurs.

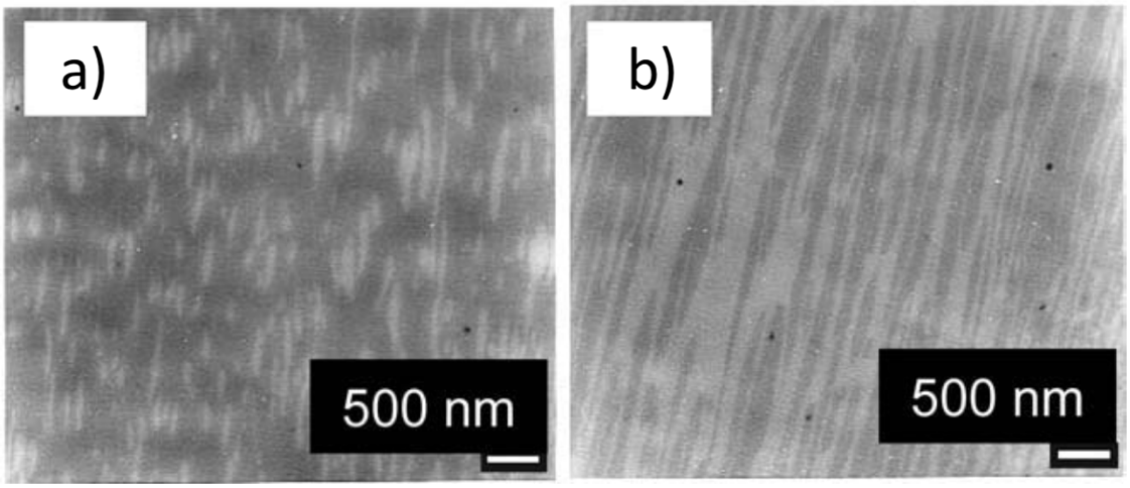

Figure 2.8 TEM micrographs of PEEK/*p*-PEI binary blend morphologies with the following compositions (wt%): a) 60/40 and b) 40/60. Figure adapted from Nemoto, et al. [79]. Copyright © 2010 Society of Plastics Engineers.

These fundamental differences in melt behavior have a direct impact on the morphology after processing. PEEK/*m*-PEI blends can develop very fine microstructures upon crystallization. As PEEK crystallizes, the *m*-PEI is expelled from the crystalline lamellae and accumulates in the interlamellar, interfibrillar, or interspherulitic regions – creating phase-separated domains (see Figure 2.9) [69, 72, 73, 80]. The characteristic size of the *m*-PEI-rich domains typically ranges from a few nanometers to ~1 μm [72], depending on crystallization conditions. Parameters such as molecular weight, thermal history, processing conditions (*e.g.* mixing temperature, cooling rate, etc.), and post-thermal treatments all display a direct impact on the PEEK crystallization behavior and thus on the *m*-PEI segregation. This interplay between crystallization kinetics and phase segregation enables fine morphology control, which has been exploited to prepare high-performance mesoporous PEEK membranes [81-87]. Thanks to the development of a specific solvent capable of depolymerizing and extracting even the interlamellar portion of *m*-PEI, pores with an average size of 11 nm could be obtained in such membranes [83]. Subsequent studies confirmed similar pore size distributions (10 to 40 nm) under varied blend compositions and

crystallization conditions [81, 84]. These membranes exhibit tailored pore structures, making them suitable for demanding filtration and separation applications.

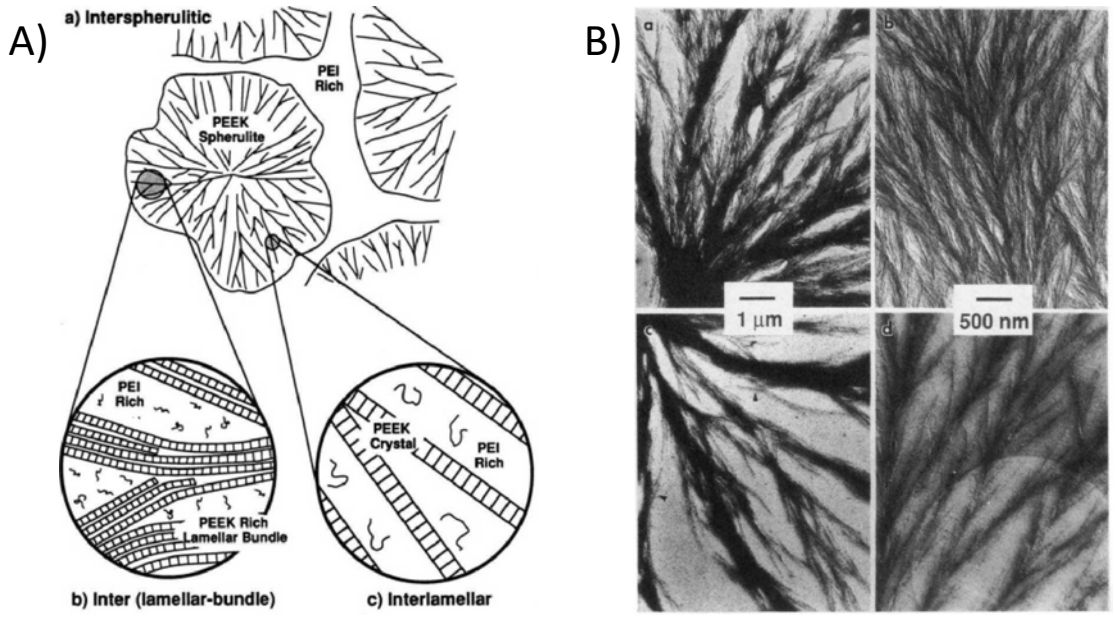

Figure 2.9 A) Diagram showing the different modes of segregation of *m*-PEI during PEEK crystallization. B) TEM micrographs displaying the characteristic interlamellar mode of *m*-PEI segregation. Reprinted with permission from Hudson, et al. [72]. Copyright © 1992, American Chemical Society.

By contrast, the morphology of PEEK/*p*-PEI blends is already phase-separated on a scale of hundreds of nm, consistent with polymer pairs displaying very low interfacial tension. The absence of a homogeneous amorphous phase before crystallization means that PEEK will tend to predominantly crystallize in the PEEK-rich phase rather than in the *p*-PEI-rich one. Hence, the morphology is less influenced by the PEEK crystallization process than in PEEK/*m*-PEI blends, being determined more by the initial melt structure.

These distinctions are expected to impact the mechanical properties. PEEK/*m*-PEI blends are expected to display good mechanical properties due to their finer and more homogeneous morphology. These blends can exhibit mechanical performances that are competitive with, or superior to, the neat polymers due to the favorable distribution and interactions between the two polymers [68, 88]. In PEEK/*p*-PEI blends, the larger, more distinct domains could result in less efficient stress transfer if their interfacial adhesion is limited. If so, this interfacial weakness could lead to lower toughness compared to the miscible blend counterpart. Furthermore, the presence of

two separated phases could lead to heterogeneous thermal expansion and property changes across the material. However, no studies on this subject could be found in the literature.

These contrasting behaviors underscore the importance of understanding blend composition and processing conditions when designing PEEK/PEI-based materials with targeted performance. It also underlines how subtly changing the position of one covalent bond, from *meta* to *para* position in the PEI backbone, can have a profound impact on the molecular interactions, and resulting phase behavior, between PEEK and the two PEIs. No work in the literature has addressed the cause of this difference.

2.3 Ternary polymer blends

2.3.1 Phase behavior and morphology

Ternary polymer blends significantly increase the level of complexity compared to the previously described binary systems. Composed of three different polymers, they possess many variable parameters (composition, polymer pair (im)miscibility, molecular weights, etc.) to tailor their morphological, thermal, and/or mechanical properties. Consequently, the level of control over their main properties is even more extended than for binary blends, but also comes with great opportunities and challenges to obtain the maximum benefit out of it.

In the previous sections, it was shown that obtaining miscible polymer blends is not an easy task, and this is even truer for ternary polymer blends. With three components possibly interacting with each other, any differences in the strength of their binary interactions can promote phase separation. Zeman and Patterson [89] first investigated this "$\Delta\chi$ effect" in detail for ternary systems composed of two polymers and one solvent. In such systems, even if all of the pairs' interaction parameters (solvent-polymers, and polymer-polymer) promote miscibility for each binary system, a slight difference in the value of these interaction parameters results in phase separation of the whole ternary system. Thus, bi-phasic or tri-phasic ternary polymer blends can be obtained instead, depending on the miscibility or partial miscibility of the interacting polymers.

When three distinct phases are observed in such systems, a variety of possible equilibrium morphologies may result, ranging from core-shell (Figure 2.10a and c) or double-emulsion (Figure 2.10b) dispersed phases in a third component matrix, to fully co-continuous morphologies where

all three components are interconnected and continuous with themselves (Figure 2.10a-c, when the three components are present in comparable amount in the blend). As discussed previously, many factors influence the resulting morphology of a blend, and it is a competition between thermodynamics and kinetics. In the kinetic category, factors such as the applied shear rate, the viscosity ratio between the dispersed phase and the matrix, the cooling rate of the melt material, or, in other methods, the solvent evaporation rate, all impact the blend morphology and therefore its subsequent control.

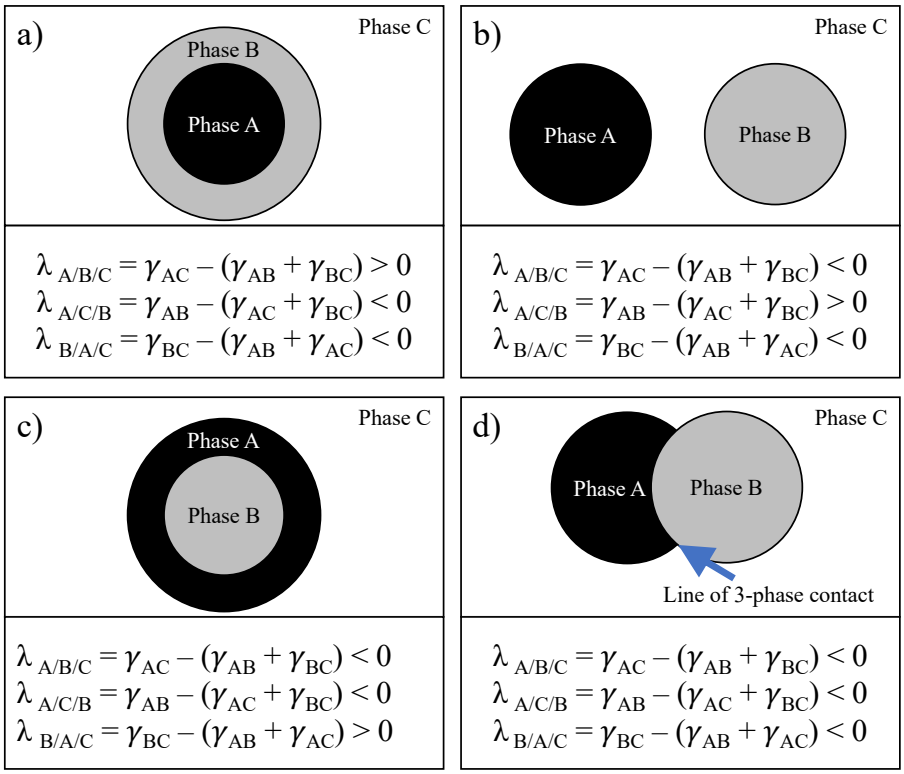

Figure 2.10 The four different morphologies predicted by the spreading coefficients' signs for a ternary blend composed of two minor phases A and B (in black and gray) and one major phase C (in white). From (a) to (c), a complete wetting behavior is reached, while in (d), only partial wetting is observed.

However, given enough time and energy, all polymer systems will tend towards an equilibrium state for which their free energy will be minimized. Consequently, theoretical tools have been developed to help predict these final morphologies based on parameters such as the interfacial tension or the Flory-Huggins interaction parameters.

2.3.2 Theoretical tools

2.3.2.1 Spreading coefficients to predict equilibrium morphology in fully immiscible ternary systems

Torza and Mason [90] used the spreading coefficients theory to describe and predict the resulting morphology in emulsions of three immiscible components. They extended the thermodynamic theory developed earlier by Harkins, which studied the tendency of a liquid drop to spread onto a solid or liquid surface [91, 92]. A spreading coefficient (λ) basically compares the values of the interfacial tensions (γ) between the different components:

$$\lambda_{ikj} = \gamma_{ij} - (\gamma_{ik} + \gamma_{kj}) \tag{2.14}$$

This theory can be applied to ternary polymer systems. It predicts four resulting types of morphologies, depending on the signs of three spreading coefficients. If λ_{ikj} is positive while the two others (λ_{ijk} and λ_{kij}) are negative, then the theory predicts that the component "k" will tend to spread and separate components "i" and "j"; these morphologies are called "complete wetting" (see Figure 2.10a-c). In the last case, when all three spreading coefficients are negative, none of the constituents spreading at the interface between the other two represents a thermodynamic advantage for the system. Thus, the resulting morphology is called "partial wetting", and all three components are in contact along a three-phase line of contact, as described in Figure 2.10d. This approach has been mainly applied so far to fully immiscible ternary polymer systems – there are no reports in the literature for ternary systems with partially miscible or fully miscible pairs.

2.3.2.2 Ternary systems with partially miscible or miscible pairs: phase diagram and spinodal frontier line

Scott [93] and Tompa [94] built on the theoretical framework developed by Flory [58] and extended the mathematical description of phase equilibria in multicomponent systems, especially for mixtures containing two polymers and one solvent. Their work extended classical thermodynamics of mixing to more complex ternary systems, taking into account how enthalpy and entropy contributions determine whether a single phase or multiple phases are thermodynamically stable. In polymer/polymer/solvent mixtures, the entropy term is small because of the high molecular

weights of the polymers, while the enthalpy of mixing depends strongly on the specific interactions between each component pair, where the solvent's main role is to decrease the polymer/polymer interaction by separating them.

Zeman and Patterson [89] work clearly showed how a solvent can shift the position of the phase separation boundary depending on its relative affinity for each polymer, acting either as a compatibilizer or a destabilizer. The authors reformulated the spinodal condition into a more practical form for ternary polymer systems. This version of the equation allowed easier modeling of the spinodal boundary, which marks the limit where the homogeneous phase becomes unstable and composition fluctuations lead to spontaneous spinodal phase separation.

Afterwards, Su and Fried [95] investigated how the interaction parameters between each binary pair influence the shape of the spinodal curve in ternary blend diagrams. They showed that when all three binary pairs have a similar level of incompatibility, the ternary system can remain miscible over a large composition range. On the other hand, strong asymmetry, where one pair is much more (im)miscible than the others, tends to reduce the miscibility range.

In practice, the results from these analyses are commonly represented in ternary phase diagrams. These diagrams use a triangular plot where each corner corresponds to one pure component, and any point inside represents a specific composition of the three. The spinodal and binodal curves drawn inside the triangle separate stable (monophasic), metastable (binodal region), and unstable (spinodal region) areas (see Figure 2.11). For ternary polymer blends, these diagrams are useful tools to visualize how changing the composition or interaction parameters can shift the system from a single-phase morphology to phase-separated microstructures, which is key for tailoring the properties of high-performance blends.

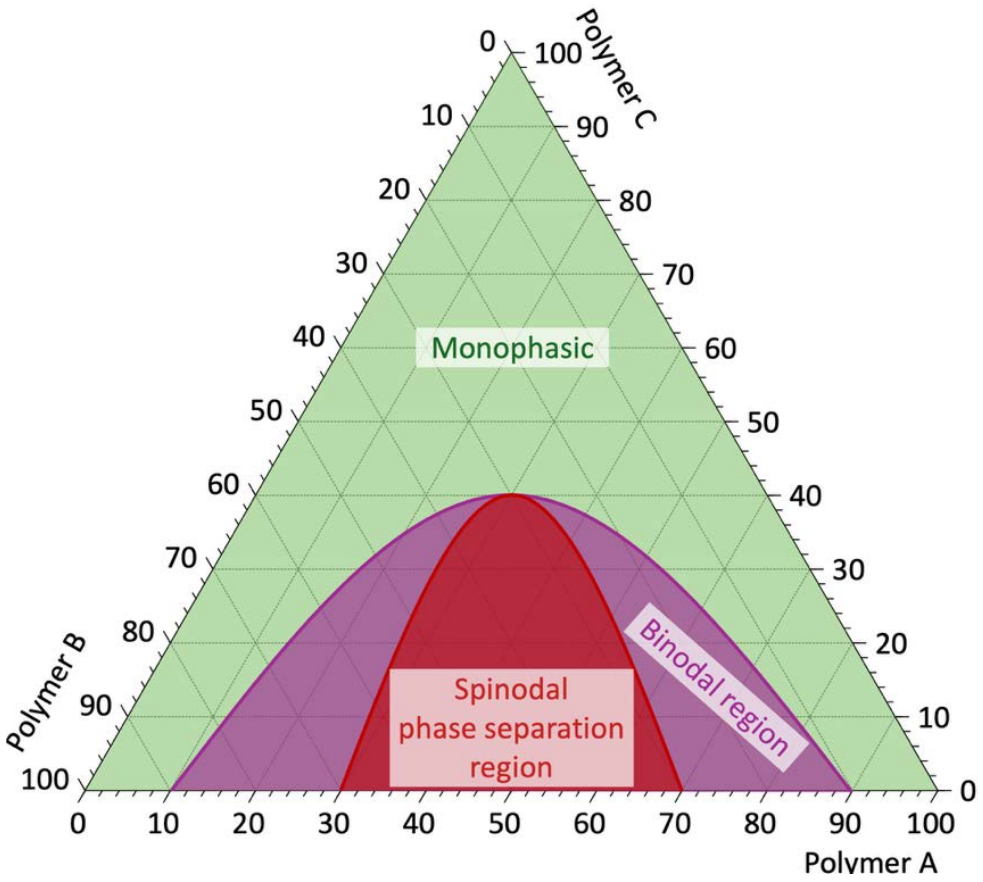

Figure 2.11 Ternary phase diagram with classical representations of the monophasic, binodal, and spinodal regions.

2.3.3 Ternary systems with PEEK and PEI

In the literature on polymer blends, ternary systems only represent a small fraction of the global published research (~5%), and among that small fraction, ternary blends incorporating PEEK represent an even smaller proportion of publications (~1%). Figure 2.12 displays this observation graphically, clearly showing the rapid expansion of polymer blends research, while the number of publications on more complex ternary systems tends to plateau since the early 2000s due to the difficulties associated with complex miscibility behavior, multi-length scales morphology, crystallization, etc. Thus, only a few published scientific papers are directly relevant to this literature review. In the vast majority of these studies, PEEK and *m*-PEI were combined with a third polymer in order to investigate their phase behavior and/or improve their general properties.

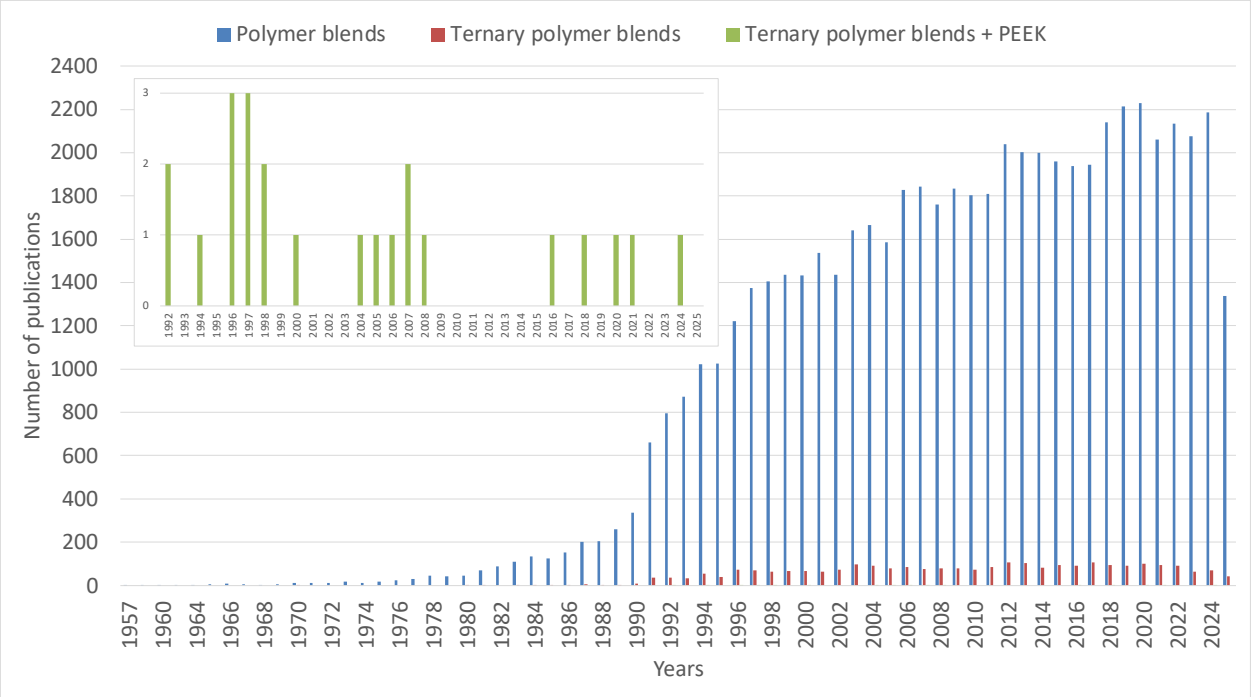

Figure 2.12 Number of publications per year containing the terms “polymer blends”, “ternary polymer blends”, or “ternary polymer blends and PEEK”.

One of these studies investigated solvent-cast films composed of sulfonated PEEK (SPEEK, often considered for the fabrication of ion conductive membranes) with *m*-PEI and PC [96]. Using DSC analysis, they reported the SPEEK/*m*-PEI pair to be fully miscible, while the SPEEK/PC and *m*-PEI/PC were estimated to be partially miscible. In this mostly theoretical work, without any morphological investigation, binary interaction parameters were calculated for each pair and used to generate a spinodal curve, which predicted a wide two-phase region on the phase diagram, in accordance with the experimental calorimetric data.

Another fundamental work, based on calorimetric measurements with a note of morphological and FTIR analyses, focused on the ternary system consisting of PEEK, *m*-PEI, and a second high-performance semi-crystalline polymer: poly(ether diphenyl ether ketone) (PEDEK) [97]. This system was one of the rare ones to be characterized as fully miscible in the amorphous state over the complete composition range. The authors reported this miscibility as stemming from the comparable values of the binary interaction parameter between the three constitutive pairs, limiting the “$\Delta\chi$ effect” described previously in section 2.3.1.

A ternary blend prepared from PEEK, *m*-PEI, and a liquid crystalline polymer (LCP) was also explored to enhance mechanical performance through synergistic effects among the components [98-100]. While the PEEK/*m*-PEI pair is now well-known to be fully miscible in the amorphous state, the addition of LCP introduced a more complex phase behavior. Partial miscibility was observed between LCP and *m*-PEI, whereas the PEEK/LCP interaction behavior was strongly dependent on composition and the crystallization state of each polymer. As a result, the system could display a morphology combining phase-separated crystalline domains from PEEK and LCP with an amorphous, miscible matrix [99, 100]. These complex morphologies contributed to tensile mechanical improvements, with certain compositions yielding higher modulus or ultimate strength than the individual neat polymers. Morphological analysis revealed that such enhancements were always associated with phase-separated morphologies displaying partial miscibility behavior [98].

In a series of studies, Cakmak investigated a ternary system of PEEK/*m*-PEI/poly(ethylene naphthalate) (PEN) to prepare transparent films with good mechanical properties and a high glass transition temperature [101-103]. In this system, the PEEK/*m*-PEI and PEN/*m*-PEI pairs were found to be fully miscible, while the PEEK/PEN pair is immiscible. Depending on the composition, the system displayed either homogeneous or biphasic morphologies. Bicakci and Cakmak [101] employed the presence of a single T_g as an indicator of miscibility and used experimental data to extract interaction parameters for all binary pairs, based on a spinodal curve fitting model. The addition of *m*-PEI not only raised the blend's glass transition temperature, but also disrupted PEN crystallization. To compensate for the loss of crystallization-induced strain hardening, small amounts of PEEK were introduced to restore this property while preserving the desired transparency and toughness in the final self-leveling films [102, 103].

More recently, ternary blends of PEEK, *m*-PEI, and poly(ether sulfone) (PES) have been developed to prepare hierarchical porous membranes (HPMs) with tunable porosity and water permeation properties [104]. In these systems, both PEEK/PES and *m*-PEI/PES pairs are immiscible, leading to the formation of a dispersed PES phase within a PEEK/*m*-PEI matrix. The inclusion of PES aims to create larger pores (~μm), which helps lower the pressure drop and increase the flux through the membrane. Upon inducing crystallization of the PEEK phase, a second phase separation occurs between PEEK and *m*-PEI, producing a nm-sized co-continuous structure. This finer morphology allows the membrane to stay component-selective, especially for applications such as water-in-oil emulsion separation. The final PEEK filtration membrane was obtained by extracting the PES and

m-PEI phases, with its resulting performance being tunable by varying the proportions of each component.

In all cases, detailed morphological investigations in such complex systems remain scarce, in part due to the difficulty in finding selective solvents to provide sufficient contrast between the phases. The intricate, complex morphologies with multiple length scales, ranging from a few nanometers to several microns, resulting from combinations of miscible, partially miscible, and immiscible pairs, combined with the semi-crystalline character of some polymers (*i.e.* PEEK), also poses significant challenges. Considering the significant impact of morphology and interfacial properties on multicomponent/multiphase polymer systems, there is a need to develop more elaborate tools and techniques.

2.4 Summary

Extreme environments such as the lunar surface impose severe constraints on materials design, including exposure to intense thermal cycling, mechanical stresses, and chemically aggressive conditions. These challenges, associated with new requirements, highlight the urgent need to develop new high-performance materials that not only offer excellent thermal and mechanical stability but also lightness, ease of repair, and good thermal insulation. High-performance multiphase polymer systems offer an attractive route to meet these demands by combining the strengths of different thermoplastics phases. Binary blends of PEEK with *m*-PEI have been widely studied and are considered a reference system due to their complete miscibility. On the other hand, PEEK/*p*-PEI blends, while similar chemically, remain largely unexplored despite offering the potential for new morphological features. Ternary polymer systems further expand the material design space, but bring additional challenges in terms of phase compatibility, kinetic control of morphology, and prediction of macroscopic properties. Only a few studies have explored ternary blends involving PEEK, and these often lack in-depth morphological analysis.

The development and control of complex morphologies in multiphase polymer systems remain only partially understood, especially for high-performance thermoplastics. In particular, extensive morphological analysis across different length scales is scarce in the literature, despite its importance in linking formulation, processing, and final properties. Another limitation lies in the absence of a tunable and reproducible ternary system that can serve as a reference model for investigating phase separation behavior and morphology development without interfacial compatibilizers. The limited understanding of how the level of miscibility, composition, and crystallization impacts morphology during processing hinders the development of such materials. Therefore, a deeper and systematic investigation of the morphology-property relationships in multiphase PEEK-based systems is essential to unlock their full potential, whether as matrices for (nano)composites, as processable precursors for porous architectures, or as model systems for fundamental studies in polymer blends physics.

CHAPTER 3 OUTLINE OF DISSERTATION

3.1 Research objectives

The literature review of CHAPTER 2 illustrated that new materials are needed to push forward the exploration of extreme environments, such as the lunar surface, and that challenges remain in using multiphase polymer systems as a tool to design and control the physical properties of new high-performance materials to answer this need. **The main objective** of this work is to develop multiphase polymer materials based on poly(ether ether ketone) (PEEK), with highly controlled morphologies, and capable of withstanding the lunar environment as part of the structure of a lunar rover.

The associated specific objectives are:

1. Determine and prioritize the main underlying factors controlling phase separation and morphology development in binary PEEK/*m*-PEI and PEEK/*p*-PEI blends, and correlate with tensile mechanical properties.
2. Define and control the conditions for miscibility in PEEK/*m*-PEI/*p*-PEI ternary systems.
3. Establish key interrelationships between miscibility, morphology, interface, and physical properties for PEEK-based multiphase systems.

3.2 Organization of the articles

To achieve the preceding objectives, three scientific papers were either submitted or published during the completion of this research work. CHAPTER 4 to CHAPTER 6 present the main scientific findings of this thesis.

CHAPTER 4 presents the first scientific paper of this thesis, entitled "*Tailoring the morphology in partially and fully miscible mixtures of PEEK and PEI*" and published in the journal "*Polymer*" on May 9th, 2025. This work focuses on the properties of binary blends of PEEK/*m*-PEI and PEEK/*p*-PEI. The complete miscibility in the melt/amorphous state for PEEK/*m*-PEI was

confirmed, while a partial miscibility behavior was demonstrated for the PEEK/*p*-PEI system. Then, extensive thermal and morphological analyses were performed on the blends, revealing in unprecedented detail the thermal-related morphology evolution of these binary systems. Finally, some of their tensile mechanical properties were also obtained.

CHAPTER 5 presents the second article of this research work, entitled "*Controlling and modeling phase separation behavior in ternary systems of PEEK with meta- and para-PEI*" and submitted to the journal "*Macromolecules*" on August 8th, 2025. In this work, newly prepared PEEK/*m*-PEI/*p*-PEI ternary systems are thermally and morphologically characterized, and their phase separation behavior is theoretically modeled. Polymer-polymer interaction parameters are obtained for the three constitutive pairs based on the results from thermal analysis. Furthermore, by playing on the composition, the system can change from monophasic to bi-phasic morphology, agreeing well with theoretical predictions and providing a tool to prepare highly controlled mesoporous PEEK-based materials.

CHAPTER 6 presents the third publication entitled "*Designing PEEK-based High-Performance Ternary Systems Displaying Highly Controlled Hierarchical Morphologies*" and submitted to the journal "*Polymer*" on September 3rd, 2025. In this last work, three new PEEK-based ternary systems also comprising PC, *m*-PEI, *p*-PEI, and PPSU are analyzed by morphological and thermal characterization. For the first time, the impact of polymer pair miscibility on the resulting blend's morphology is correctly predicted with spreading coefficients, which are based on the interfacial tensions of the constitutive pairs. This level of prediction and control over the blend's morphology allows the preparation of ultraporous and bimodal mesoporous PEEK monoliths.

CHAPTER 4 ARTICLE 1: TAILORING THE MORPHOLOGY IN PARTIALLY AND FULLY MISCIBLE MIXTURES OF PEEK AND PEI

*Arthur Lassus [a], Daniel Therriault [b], Basil D. Favis [a], and Nick Virgilio [a,]**

[a]CREPEC, Department of Chemical Engineering, Polytechnique Montréal, Montréal, Québec H3T 1J4, Canada

[b]CREPEC, Department of Mechanical Engineering, Polytechnique Montréal, Montréal, Québec H3T 1J4, Canada

*Corresponding author's E-mail: nick.virgilio@polymtl.ca

Published in: *Polymer*, 27th March 2025, Volume 326, 128315

Abstract

Over the last three decades, the vast body of work related to the control of the morphology of multiphase polymers has concentrated on systems that are inherently immiscible. On the other hand, detailed morphological studies of phase separation in miscible blends have been limited by the highly unstable nature of the structures generated as a function of time and temperature. In this work, we present one basic polymer system, with a slight variation in chemical structure, that allows for a high level of morphological tailoring and control in the miscible to partially miscible region. Two close isomeric forms of poly(ether imides) (PEI) yield fundamentally different types of morphologies in poly(ether ether ketone) (PEEK)/PEI melt-processed multiphase systems: a partially miscible, phase-separated microstructure for the barely studied PEEK/*para*-PEI (*p*-PEI) system, and the typically reported fully miscible PEEK/*meta*-PEI system (*m*-PEI). The PEEK/*p*-PEI system displays sub-µm, matrix/dispersed phase or co-continuous types of morphologies, with the latter quickly coarsening over tens of µm in length scale under quiescent annealing conditions

due to the PEEK/*p*-PEI interfacial tension, which was measured by the breaking thread method at 0.14 mN/m, one of the lowest values ever reported for a polymer pair. On the other hand, for the PEEK/*m*-PEI system, controlling the thermal annealing temperature promotes PEEK recrystallization and the formation of a nanostructured PEI-rich phase. Considering both types of blends, it is then possible to control the morphological length scale of PEEK and PEI domains over nearly 4 orders of magnitude, from ≈ 5 nm to over 15 µm. This is the smallest domain size ever reported for co-continuous systems. The selective extraction of the PEI phase then results in porous PEEK monoliths with full pore interconnectivity, with an average pore size spanning the same considerable range – without any interfacial modifier or block copolymer.

4.1 Introduction

Poly(ether ether ketone) (PEEK) is a high-performance semi-crystalline polymer well known for its superior thermal and mechanical properties, high solvent resistance, and hence for its use in demanding environments and fields of applications such as biomedical implants or parts in the aeronautics sector. Poly(ether imide) (PEI) is also a high-performance polymer displaying a significantly higher glass transition temperature and lower costs than PEEK. However, its amorphous character results in lower chemical resistance and mechanical properties. PEI can also be added to PEEK via melt-processing to improve both its processability and thermal properties, while at the same time maintaining high solvent resistance and mechanical properties, with lower material costs.

The miscibility of PEEK/*meta*-poly(ether imide) (*m*-PEI) systems in their amorphous (melt) state has been confirmed by many authors using differential scanning calorimetry (DSC) [68-74, 105, 106] or dynamic mechanical analysis (DMA) [68, 69, 71, 75] by the observation of a single glass transition temperature (T_g) following the additivity rule – a relatively rare feature in melt-processed polymer blends. Dielectric spectroscopy has also been used to confirm the miscibility of these polymers [73, 76]. When analyzed via infrared spectroscopy, the miscibility of this system has been explained, in part, by a specific interaction between the electron-rich ether functional groups in the PEEK repeating unit, and the electron-deficient imide ring in the *m*-PEI backbone [77], resulting in an interaction parameter (χ_{12}) ranging from -0.058 to -0.196, promoting miscibility [78]. However, phase separation occurs when PEEK crystallizes – either from the melt state during cooling, or via cold crystallization – and provokes the expulsion and segregation of *m*-PEI. The

crystallization of PEEK in this binary system is highly dependent on its molecular weight and the conditions applied, i.e., temperature, isothermal or dynamic crystallization from the melt or solid state, blend composition, blending technique, etc. The segregation of PEI has been reported, by small-angle X-ray scattering (SAXS) and transmission electron microscopy (TEM), to occur between PEEK crystalline lamellae, fibrils, and/or spherulites – respectively designated as interlamellar, interfibrillar, and interspherulitic segregation, as illustrated in **Scheme S1** [69, 72, 73, 80]. The characteristic length scale of the resulting PEI-rich domains increases accordingly to the segregation mode, from a few nm to ≈ 1 μm [72]. As a result, the morphology is quite fine, even without the addition of an interfacial compatibilizing agent such as a block copolymer.

High-performance PEEK-based microporous membranes successfully capitalized on the finely tuned crystallization-induced phase separation process in PEEK/*m*-PEI blends [81-87] – a quite unique feature in melt-processed polymer blends. Ding and Bikson [83] were the first to report the use of a novel composite solvent (80 vol% 1-methyl-2-pyrrolidinone (NMP), 10 vol% ethanolamine, 10 vol% water) able to remove all of the *m*-PEI present in PEEK/*m*-PEI blends, via PEI depolymerization. Even interlamellar *m*-PEI could be removed, resulting in a very low average pore size of 11 nm. This range of pore sizes (10 to 40 nm) was further confirmed by several authors using the same composite solvent, at various blend compositions and crystallization temperatures [81, 84]. To the best of our knowledge, there is however no systematic analysis on how blend composition and post-processing thermal treatment impact the resulting morphology, thermal and mechanical properties of bulk PEEK/*m*-PEI blends, and the resulting porosity once the PEI is extracted.

On the other hand, Nemoto, et al. [79] reported relatively recently a novel binary system composed of PEEK and *para*-PEI (with a covalent link in *para*- position instead of *meta*- on its aromatic imide ring, see Supporting Information **Scheme S2**), which they qualified as immiscible in part because of the development of a phase-separated microstructure. DMA analysis revealed two peaks in the loss tangent curve, which the authors associated with immiscibility. However, the two peaks were shifted from the characteristic curves of the pure components (an increase of 10 °C for the PEEK-related T_g, and a decrease of 15 °C for the *p*-PEI-related T_g), suggesting a certain affinity between the two polymers – a feature that was not linked to potential partial miscibility by the authors however. TEM observations also revealed a fine sub-μm phase-separated microstructure quite reminiscent of immiscible polymer pairs displaying a very low interfacial tension. However,

no additional data or work could be found in the literature on this particular system, and no attempts were made to extract the PEI phase to obtain porous PEEK materials, and to control the morphology by post-processing heat treatments, such as quiescent annealing.

It remains unclear for now why *p*-PEI behaves fundamentally differently when blended with PEEK, compared to *m*-PEI. In addition, the effects of blend composition and thermal treatment, both during and after melt processing, on the resulting microstructure, thermal and mechanical properties, are only partly understood in PEEK/*m*-PEI blends and remain mostly unknown for PEEK/*p*-PEI blends.

p-PEI offers a significant yet unexplored potential to generate entirely new morphological structures when melt-processed with PEEK, while preserving the fundamental characteristics of a PEEK/PEI system. The main objective of this work is to understand the impacts of composition and post-processing thermal treatment (both T and time) on the morphology, the thermal properties including the glass transition temperature, and the resulting mechanical properties of melt-processed blends of PEEK with either *meta*-PEI or *para*-PEI. Finally, this work assesses the possibility of preparing porous PEEK materials over an extended porosity range, from a few nm in average pore size to tens of μm, by controlling the morphology via composition and post-processing thermal treatments, followed by the selective extraction of both *m*-PEI and *p*-PEI.

4.2 Materials and methods

4.2.1 Materials

Poly(ether ether ketone) (PEEK) 90G under pellet form was obtained from Victrex. Poly(ether imides) (pellet form) Ultem 1010 (*meta*-PEI or *m*-PEI), Ultem CRS 5001 (*para*-PEI or *p*-PEI) and Ultem CRS 5011 (*p*-PEI_2) were obtained from SABIC, the last two being sold as copolymers of PEI. Note that *p*-PEI was used for most of this work except for the breaking thread experiments (Section 4.2.9) for which *p*-PEI_2 was used. The *para*-diamine composition of Ultem CRS 5001 was first reported by Nemoto, et al. [79] and then by l'Abee, et al. [107]. **Table 4.1** summarizes some of their main properties.

Table 4.1 PEEK and PEI main properties

	Density ρ at room temperature (g/cm^3) [a]	M_w (g/mol)	Melt viscosity at 400 °C (Pa.s) [a]	MFI at 337 °C (g) [a]	Torque at plateau in internal mixer at 370 °C and 50 rpm (N·m)	T_g (°C) [c]
PEEK	1.30	5.97×10^4 [a]	90	-	0.77	147
m-PEI	1.27	4.75×10^4 [b]	-	17.8	1.48	216
p-PEI	1.28	-	-	4.2	3.80	225
p-PEI_2	1.28	-	-	11	-	226

[a] Provided by the supplier.

[b] Measured by GPC in chloroform at 35 °C.

[c] Measured by DSC.

4.2.2 Blend preparation

PEEK/*m*-PEI and PEEK/*p*-PEI binary blends were prepared over the full composition range. Prior to melt blending, all polymers were dried for 24 h under vacuum at 100 °C. In a typical mixing experiment, the materials were fed to a micro-compounder (DSM Xplore, mixing volume = 5 cc), with temperature and screw speed preset at 370 °C and 50 rpm, respectively. Based on previous experiments, once all the polymer pellets were added to the micro extruder, the mixing time was set at 6 min in recirculation mode. After blending completion, a ≈ 30 cm long filament was extruded and either quenched in an icy water bath or allowed to cool at room temperature (these samples are respectively designated as Q and N).

4.2.3 Quiescent annealing

Before a typical quiescent annealing experiment, ≈ 1 cm long pieces of quenched binary blend filaments were dried 24 h under vacuum at 100 °C. The pieces were then wrapped up in aluminum foil initially coated with a boron nitride-based releasing agent (Momentive, United States). Annealing was performed with a Carver high-temperature hydraulic press at temperatures ranging from 190 °C to 380 °C. Annealing protocols, specifically aiming at either increasing the crystallinity of PEEK and/or investigating the resulting nano- and microstructure due to phase

separation in the PEEK/*m*- PEI binary blends, were performed for 5 min at different temperatures all inferior to the melting T of PEEK (345 °C). The samples were next cooled down in air until they reached room T, and are denoted as R (temperature value) °C. As for quiescent annealing protocols aiming at measuring the level of coarsening in PEEK/*p*-PEI binary blends, they were performed for different durations at 380 °C, over the melting T of PEEK. In this case, the samples were directly quenched in an icy water bath right after annealing to freeze in the morphology.

4.2.4 Thermal analysis

The neat polymers and their binary blends were analyzed by differential scanning calorimetry (DSC, TA instruments Q2000). The protocol consisted of two heat/isotherm/cool cycles: (1) heating from 50 °C to 380 °C at 10 °C/min, an isotherm of 5 min at 380 °C, cooling to 50 °C at 10 °C/min; (2) heating again to 380 °C at 10 °C/min, an isotherm of 1 min at 380 °C, and finally cooling to 50 °C at 10 °C/min. Glass transition temperatures (T_g) were measured as the inflection points of the baseline during the first and second heating ramps. The crystallinity based on the mass of the blend sample was calculated with **Equation 4.1**:

$$X_c = \frac{(\Delta H_m - \Delta H_{cc})}{\Delta H_f} \tag{4.1}$$

where ΔH_m is the specific melting enthalpy, ΔH_{cc} is the specific enthalpy of cold-crystallization upon heating, and ΔH_f is the theoretical heat of fusion of 100% crystalline PEEK, taken as 130 J/g [108]. Alternatively, PEEK crystallinity based only on the PEEK mass present in each blend was obtained from **Equation 4.2**:

$$X_{PEEK} = \frac{(\Delta H_m - \Delta H_{cc})}{\Delta H_f \times \omega_{PEEK}} \tag{4.2}$$

where ω_{PEEK} is the mass fraction of PEEK in the blend.

From the DSC analysis and based on Marin and Favis [109] work on partially miscible polymer systems, the compositions ω_i of the two separate $PEEK_{rich}$ and *p*-PEI_{rich} domains can be calculated (**Equations 4.3 & 4.4**). The $PEEK_{rich}$ phase is designated as ‘ and the *p*-PEI_{rich} phase as “. PEEK is designated as 1 and *p*-PEI as 2:

$$\omega'_2 = \frac{Tg_2(Tg_1 - Tg')}{Tg'(Tg_1 - Tg_2)} \tag{4.3}$$

$$\omega''_1 = \frac{Tg_1(Tg_2 - Tg'')}{Tg''(Tg_2 - Tg_1)} \quad (4.4)$$

where ω'_1 is the PEEK weight fraction in the $PEEK_{rich}$ phase, ω'_2 is the *p*-PEI weight fraction in the $PEEK_{rich}$ phase, ω''_1 is the PEEK weight fraction in the *p*-PEI_{rich} phase, ω''_2 is the *p*-PEI weight fraction in the *p*-PEI_{rich} phase, T_{g1} is the glass transition temperature of pure PEEK, T_{g2} is the glass transition temperature of pure *p*-PEI, T_g' is the glass transition temperature of the $PEEK_{rich}$ phase and T_g'' is the glass transition temperature of the *p*-PEI_{rich} phase.

Furthermore, **Equations 4.5 and 4.6** have been adapted from the previously cited work by subtracting the proportion of crystallized PEEK, providing corrected global weight fractions of both $PEEK_{rich}$ and *p*-PEI_{rich} domains:

$$\omega' = \frac{\omega_2 - \omega''_2(1 - X_c)}{\omega'_2 - \omega''_2} \quad (4.5)$$

$$\omega'' = \frac{\omega_2 - \omega'_2(1 - X_c)}{\omega''_2 - \omega'_2} \quad (4.6)$$

where X_c is the level of PEEK crystallinity from Equation 4.1. ω' is the $PEEK_{rich}$ phase weight fraction in the blend, ω'' is the *p*-PEI_{rich} phase weight fraction in the blend, ω_1 is the PEEK weight fraction in the blend and ω_2 is the *p*-PEI weight fraction in the blend. It is assumed that the PEEK crystalline domains are pure and therefore are not considered in the partial miscibility phenomenon.

4.2.5 Gravimetric analysis

The continuity of the PEI in the blends was measured by gravimetric analysis, by extracting the PEI with a selective solvent. Typically, three ≈ 1 cm long pieces of blend filaments (≈ 100 mg total) were dried 24 h under vacuum at 100 °C and then weighed. The samples were subsequently deposited in a composite solvent (80 vol% 1-methyl-2-pyrrolidone, 10 vol% ethanolamine, 10 vol% deionized water) at 120 °C for 1 h [83]. The samples were then cleaned with ultrasounds three times for 1 min, first while immersed in their extraction solvent (1 min), then in 95% ethanol (1 min), and finally in deionized water (1 min). The samples were then dried again for 24 h under vacuum at 100 °C and weighed. For the most delicate samples (generally when the PEI volume fraction > 50 vol%), ultrasounds were not used during the cleaning process, which was instead repeated two times. Post-drying was also replaced with a 3-days freeze-drying step.

The continuity of the PEI was next calculated using **Equation 4.7**:

$$PEI\ continuity\ (\%) = \frac{m_i - m_f}{m_i} \times \frac{m_{blend}}{m_{PEI\ in\ blend}} \times 100 \quad (4.7)$$

where m_i is the mass of the sample before extraction, m_f is the mass after extraction, m_{blend} is the mass of the original blend, and $m_{PEI\ in\ blend}$ is the mass of PEI in the original blend. It was noticed that PEEK absorbed some solvent during the extraction procedure, corresponding to ≈ 1 wt% for recrystallized PEEK, and 3.3 wt% for amorphous PEEK. Hence, a minor correction of sample mass loss was applied depending on the crystallinity and amount of PEEK in the samples.

4.2.6 Morphological analysis

Scanning electron microscopy (SEM, HITACHI Regulus 8220) was used to characterize the microstructure of the binary blends. Sample surface was prepared at room temperature using a Leica RM2165 microtome equipped with a glass knife. The observed surfaces were always at the center of the cross-sections of the filaments to limit the impact of the skin effect. The PEI phase was selectively extracted following the previous protocol (see Section 4.2.5) to improve contrast during observation. Finally, the samples were covered with ≈ 8 nm of carbon with a Leica EM ACE600 instrument, and observed at a 2 kV accelerating voltage and a 10 µA current.

ImageJ 1.53 was used for image analysis to directly measure the diameter of the dispersed phase droplets, whereas the interfacial perimeter was measured for co-continuous phases. For co-continuous morphologies, the specific interfacial area was calculated with **Equation 4.8** [110]:

$$S = \frac{P}{A} \quad (4.8)$$

where P is the interfacial perimeter and A the total area of the micrograph. Finally, the average strut thickness (or domain size) of the PEI co-continuous phases was calculated with **Equation 4.9**:

$$d = \frac{4 \times \Phi}{S} \quad (4.9)$$

where Φ is the PEI volume fraction in the blend. For dispersed phase morphologies, an average of the maximum and minimum Ferret diameters for at least 200 particles was calculated.

4.2.7 Gas sorption

For gas sorption analysis, binary blends samples (a total of ≈ 400 mg) were first subjected to the solvent extraction protocol to obtain porous PEEK samples (see Section 4.2.5). The samples were then dried and degassed for 24 h under vacuum at 100 °C and weighed. The measurements of adsorbed nitrogen inside the porous PEEK samples were performed with a TriStar 3000 gas sorption apparatus (Micromeritics), which allows the calculation of the specific surface area, the distribution in pore width, pore area, and pore volume.

4.2.8 Rheological measurements

Disks of PEEK and PEI (25 mm in diameter and 2 mm thick) were obtained by pressing dried pellets at 380 °C and 300 °C, respectively, using a Carver high-temperature hydraulic press. Amplitude, time, and frequency sweeps were performed at 375 °C under a nitrogen blanket to limit degradation on an MCR 302 rheometer (Anton Paar), equipped with a CTD 450 oven and a 25 mm diameter parallel plate geometry. The validity of the Cox-Merz rule was assumed for all tested polymers [111-113]. Zero-shear rate viscosity values were obtained by performing at least three frequency-sweep tests at $\gamma_0 = 5\%$ and by extrapolating the Newtonian plateau value with a Carreau-Yasuda model.

4.2.9 Breaking thread method

Filaments of PEEK, with diameters ranging from 20 to 40 µm, were drawn by hand from pellets molten on a hot plate. Films of *p*-PEI_2 (Ultem CRS 5011) were pressed at 380 °C to perform the experiment, since *p*-PEI (Ultem CRS 5001) was too viscous to achieve acceptable experimental times. Typically, a 2 cm-long PEEK thread was sandwiched in between two 1 x 2 cm films of *p*-PEI, which was then placed on a microscope glass slide with a glass cover. The whole setup was inserted inside a Mettler FP-82HT hot stage controlled by a Mettler FP-90 Central Processor. Observations of the samples were carried out at 375 °C on a Nikon optical microscope. Digitalized images from the microscope were captured with a computer equipped with a Coreco Oculus image analysis system driven by the Visilog 4.1.3 image analysis software. From these acquired images, ImageJ 1.53 was used to measure the diameters and the wavelength of the observed distortions in relation to time.

According to theory, the interfacial tension (γ) can be calculated from **Equations 4.10 and 4.11**:

$$\gamma = \frac{q\eta_m D_0}{\Omega(p,\lambda)} \tag{4.10}$$

$$q = \frac{\ln\left(\frac{\alpha(t)}{\alpha_0}\right)}{t} \tag{4.11}$$

where $\frac{\alpha(t)}{\alpha_0} = \frac{D_{max}(t) - D_{min}(t)}{D_{max}(t_0) - D_{min}(t_0)}$

with q the growth rate of the distortions (α), η_m the zero-shear viscosity of the polymer films used in the experiment (see Section 4.2.8), D_0 the initial thread diameter, $\Omega(p,\lambda)$ is a reported function in Chappelear's 1964 article [114], α_0 the distortion amplitude at the beginning of the measurements, α(t) the distortion amplitude at time t, D_{max} is the maximum thread diameter during deformation, D_{min} is the minimum thread diameter during deformation. The average of three maximum and two minimum successive diameters were used in the calculations of the distortion for a total of 6 performed experiments.

4.2.10 Tensile mechanical properties

The tensile mechanical properties were evaluated on a 3365 universal testing system (Instron) at a speed of 50 mm/min. Since the different compositions were not produced in sufficient quantity to manufacture tensile dogbone specimens to follow the ASTM D638 standard, 3 cm long pieces of the filaments cooled in ambient air during extrusion were used to perform the tensile tests. For each composition, at least 5 specimens were evaluated and their mechanical properties were averaged. To evaluate the impact of PEEK crystallinity on the mechanical properties, each composition was also mechanically tested after a thermal treatment of 30 min at 200 °C, which was performed to increase PEEK crystallinity to its maximum without deforming the specimens.

4.3 Results and discussion

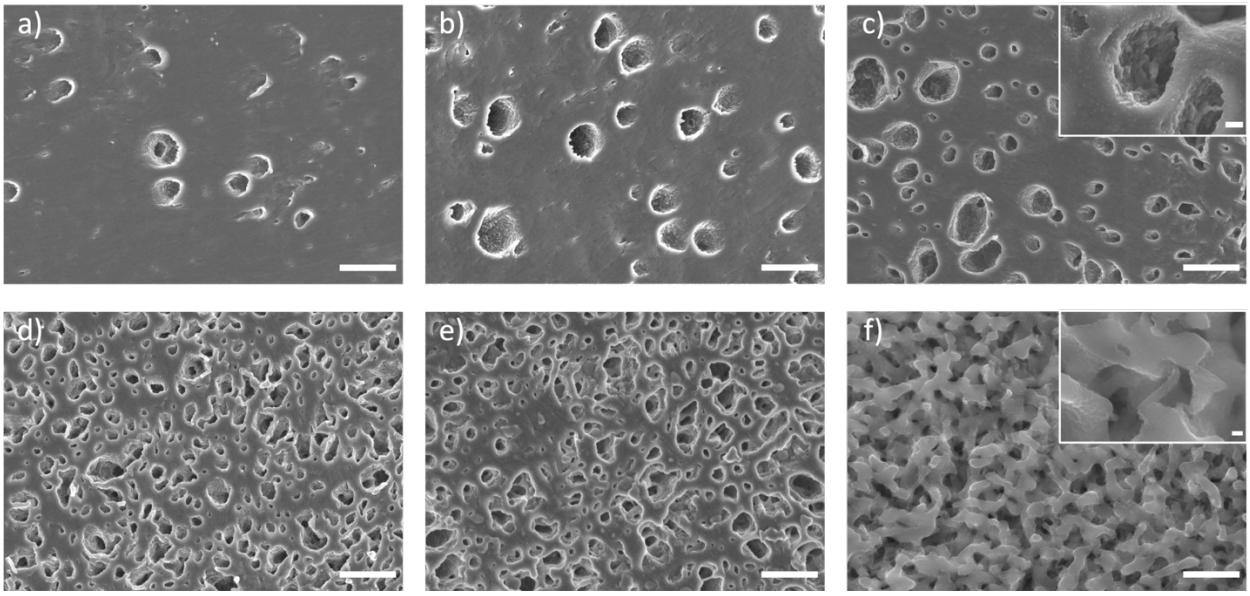

Figure 4.1 Microstructure of PEEK/*p*-PEI N blends as revealed after the selective extraction of *p*-PEI. Compositions in vol%: a) 90/10 ; b) 80/20 ; c) 70/30 ; d) 60/40 ; e) 50/50 ; f) 40/60. White scale bars represent 1 µm for main magnification and 100 nm for the close-up inset micrographs.

Figure 4.1 shows the morphology of melt-processed PEEK/*p*-PEI blends cooled at room temperature (N) after exiting the micro-compounder, for compositions ranging from 90/10 vol% to 40/60 vol%, after the selective extraction of *p*-PEI (note that no obvious difference was observed for blends quenched in ice-cold water). The PEEK/*p*-PEI system displays the microstructure of a classical immiscible blend with two distinct phases clearly observable – quite different from the fully miscible PEEK/*m*-PEI system typically reported in the literature and presented below as a point of comparison [68-74, 105, 106]. There is an increase in the visual connectivity of the *p*-PEI phase when its volume fraction in the blend increases. From 60/40 vol% to 40/60 vol% (Figure 4.1d-f), the *p*-PEI phase appears continuous. Since PEEK is the major component in Figure 1 d) and e), the two compositions display similar features. Close-up micrographs reveal a rather rough texture at the interface, which could be the result of solvent-induced crystallization of PEEK at high temperature (based on [84] and confirmed by DSC analysis of PEEK/*m*-PEI performed before and after extraction). The *p*-PEI dispersed phase shows a constant size of approximately 300 nm independently of the blend composition, which is quite fine compared to what is usually observed for fully immiscible polymer blends. Regarding PEEK domains, based on the 40/60 vol%

composition (Figure 4.1f), the domain size is closer to 150 nm. To the authors' knowledge, this is the first time that such porous PEEK monoliths are obtained from binary melt-processed blends.

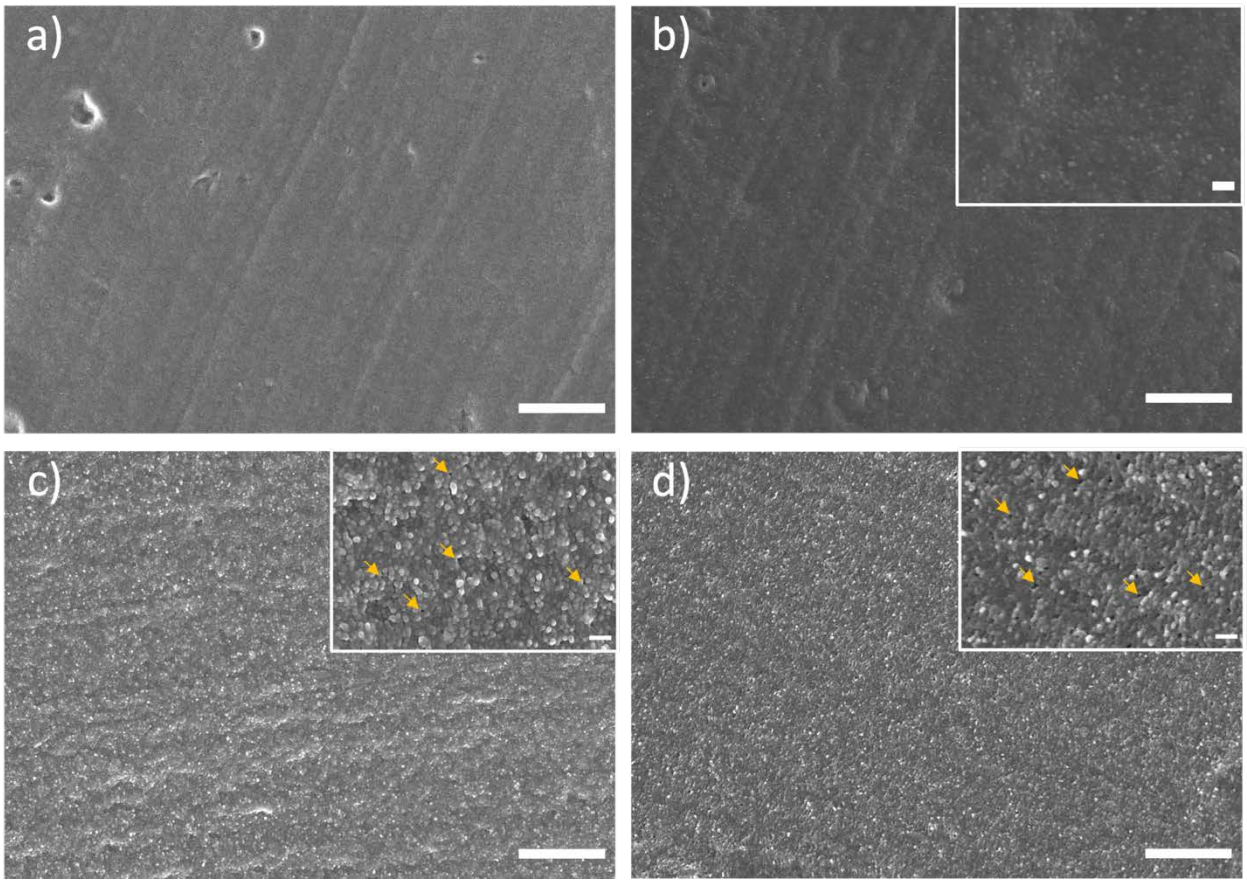

Figure 4.2 Microstructure of PEEK/*m*-PEI blends quenched in cold water at the exit of the micro-compounder, as revealed after the selective extraction of *m*-PEI. Compositions in vol%: a) 70/30 ; b) 50/50 ; c) 40/60 ; d) 30/70. White scale bars represent 1 µm for main magnification and 100 nm for the close-up inset micrographs. Yellow arrows indicate mesopores resulting from the extraction of *m*-PEI.

In comparison, **Figure 4.2** presents the morphology of melt-processed PEEK/*m*-PEI blends quenched in an icy water bath after exiting the micro-compounder, for compositions ranging from 70/30 vol% to 30/70 vol%, and after the selective extraction of the *m*-PEI material. For all compositions, the samples appear homogeneous with no distinctive features or evolution of the apparent microstructure, which is consistent with the full miscibility reported for this binary pair over the years [68-74, 105, 106]. Closer inspection reveals small pores of 7-8 nm in diameter for the 40/60 vol% blend, and 8-15 nm for the 30/70 vol% compositions, as higher magnifications illustrate (Figure 4.2c-d).

The scale of the nano/microstructure is then completely dependent on the type of PEI melt-blended with PEEK: a sub-µm morphology is obtained with *p*-PEI, whereas *m*-PEI gives rise to a nanoscale/molecular scale structure. Note that nodules of PEEK of 15 to 30 nm in size are also visible on the surface, which is again the result of solvent-induced PEEK crystallization, where the nodules are composed of crystalline and amorphous PEEK (Huang, et al. [84] reported 6.3 nm from XRD, and Olley, et al. [115] reported 15.9 nm from etching). However, the characteristic length scale of the nano/microstructure is not impacted by the extraction procedure.

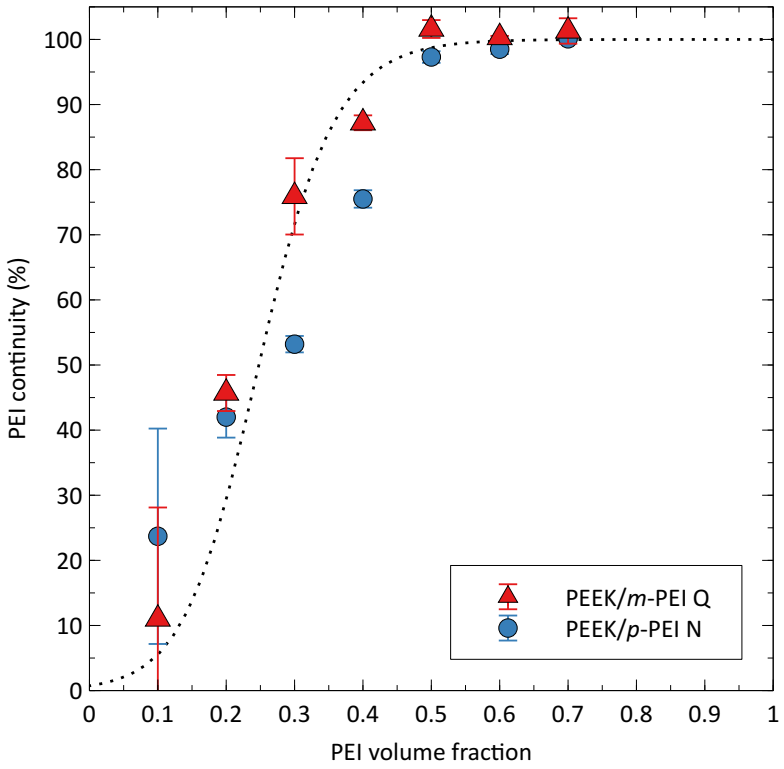

Figure 4.3 PEEK/(*m*- or *p*-)PEI co-continuous morphology development curves based on gravimetric results by solvent extraction. The dotted line is a guide for the eye.

Figure 4.3 quantifies the development of the co-continuous morphology for the two systems, by measuring the amount of extracted PEI, as a function of composition. The percolation threshold is quite low for both systems, as low as 10 vol% of PEI, whereas full co-continuity is reached at about 50 vol% in both cases. Both *m*-PEI and *p*-PEI already form highly continuous networks at 30 vol% (see Figure 4.1c-f for *p*-PEI, and Figure 4.2 for *m*-PEI). Over 70 vol% of PEI, the samples either collapsed (for *m*-PEI as the PEEK network was too tenuous) or lost their integrity, indicating the formation of a dispersed PEEK phase in a *p*-PEI matrix (phase inversion).

Due to the miscibility of *m*-PEI in PEEK, the PEEK monoliths obtained after *m*-PEI reactive solvent extraction display one of the finest continuous porosity reported in the literature – without any interfacial modifier or block copolymer [83]. Whereas *m*-PEI forms a continuous network at the molecular level in the blend or forms a network during the extraction process due to local PEEK recrystallization remains unclear at this point.

For *p*-PEI, such a low value of the percolation threshold, combined with its sub-µm microstructure, again points to a partially miscible system displaying a low interfacial tension [109, 116]. The capacity to extract PEI at such fine scales comes from the solvent composition, which depolymerizes the PEIs and allows a more efficient and complete extraction.

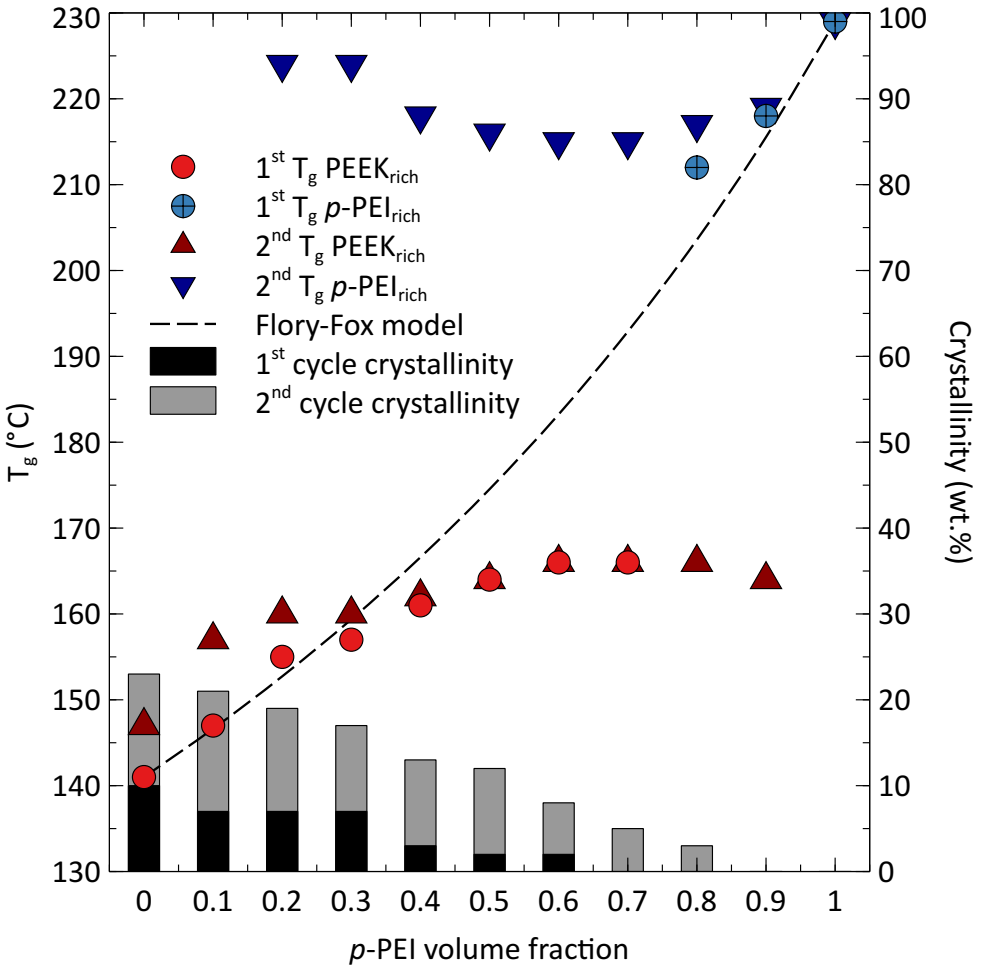

Figure 4.4 Glass transition temperatures and total material crystallinity for the 1st and 2nd DSC cycles as a function of *p*-PEI volume fraction for PEEK/*p*-PEI quenched system.

Figure 4.4 presents the glass transition temperatures and total material crystallinity for PEEK/*p*-PEI blends initially quenched in cold water (results of the 1st DSC cycle) and after a second run (2nd DSC cycle) - see also Supporting Information **Figure S4.1** for the complete thermograms. First, both 1st and 2nd heating cycles show composition-dependent T_g's, confirming a certain level of interaction between PEEK and *p*-PEI. However, these T_g's present a strong deviation from the Fox equation for fully miscible blends (dotted curve): they are shifted compared to the values of the pure components and form two distinct sets with one closer to the T_g of pure PEEK (141 °C or 147 °C), and the second closer to the value of pure *p*-PEI (229 °C) which, combined with the fine sub-µm morphology (Figure 4.1), confirm partial miscibility for this pair. This behavior is also reported for a few other polymer pairs, such as poly(methyl methacrylate) and polycarbonate [109, 117]. As a result, two phases of mixed compositions are formed: a PEEK rich (denoted $PEEK_{rich}$) and a *p*-PEI rich (denoted *p*-PEI_{rich}) phases.

For the 1st heating cycle, the T_g of the $PEEK_{rich}$ phase gradually increases with the composition in *p*-PEI, due to the increased composition of *p*-PEI in the $PEEK_{rich}$ phase – until it could not be detected over 70% of *p*-PEI. For the *p*-PEI_{rich} phase, the T_g decreases as PEEK is added to the blend, as expected. Note however that the T_g of the *p*-PEI_{rich} phase could not be measured during the 1st heating cycle, from 10 vol% to 70 vol% *p*-PEI, because of the PEEK cold-crystallization exothermic peak masking the *p*-PEI_{rich} T_g on the DSC thermograms.

Two T_g's can also be observed during the 2nd heating cycle, one associated with $PEEK_{rich}$ domains around 160 °C, and the other related to *p*-PEI_{rich} domains around 217 °C. We also note the higher crystallinity of PEEK after the 1st cycle, and the increased range of measurable T_g's (especially for the *p*-PEI_{rich} phase). Subtle differences also appear compared to the 1st heating cycle: (1) the T_g of pure PEEK increases due to recrystallization, as reported in other publications [69, 118], whereas it remains constant for pure *p*-PEI (an amorphous polymer); (2) the $PEEK_{rich}$ T_g's slightly increase for *p*-PEI compositions between 10% and 40 vol%, then stabilizes; (3) the *p*-PEI_{rich} T_g's also slightly increase, for the two compositions that could be analyzed (10% and 20% PEEK); (4) the T_g of the *p*-PEI_{rich} phase also reaches a minimum around 60%-70% *p*-PEI overall, and increases again as the composition in PEEK increases. Finally, note that PEEK crystallinity and recrystallization become negligible over 80% *p*-PEI. A PEEK-rich dispersed phase is also detected at a content as low as 10 vol%, indicating a phase-separated morphology. However, selectively

extracting the PEEK phase to observe the morphology was impossible due to the lack of a selective solvent.

These differences between the 1st and 2nd cycles are mainly due to PEEK recrystallization and *p*-PEI expulsion from the PEEK crystalline domains. For the $PEEK_{rich}$ domains at high overall PEEK content, the T_g increases both due to PEEK recrystallization, as mentioned earlier, and enrichment of the amorphous PEEK domains with the expelled *p*-PEI. Over 40% of *p*-PEI, the T_g's of the 1st and 2nd cycles become practically identical, suggesting that both crystallization of PEEK and expulsion of *p*-PEI are less important compared to the effect of the already initially present *p*-PEI in the PEEK-rich phase. For the *p*-PEI_{rich} domains, the differences in T_g between the 1st and 2nd cycles are more difficult to interpret since the data for the 1st cycle are only available at 80% and 90% *p*-PEI.

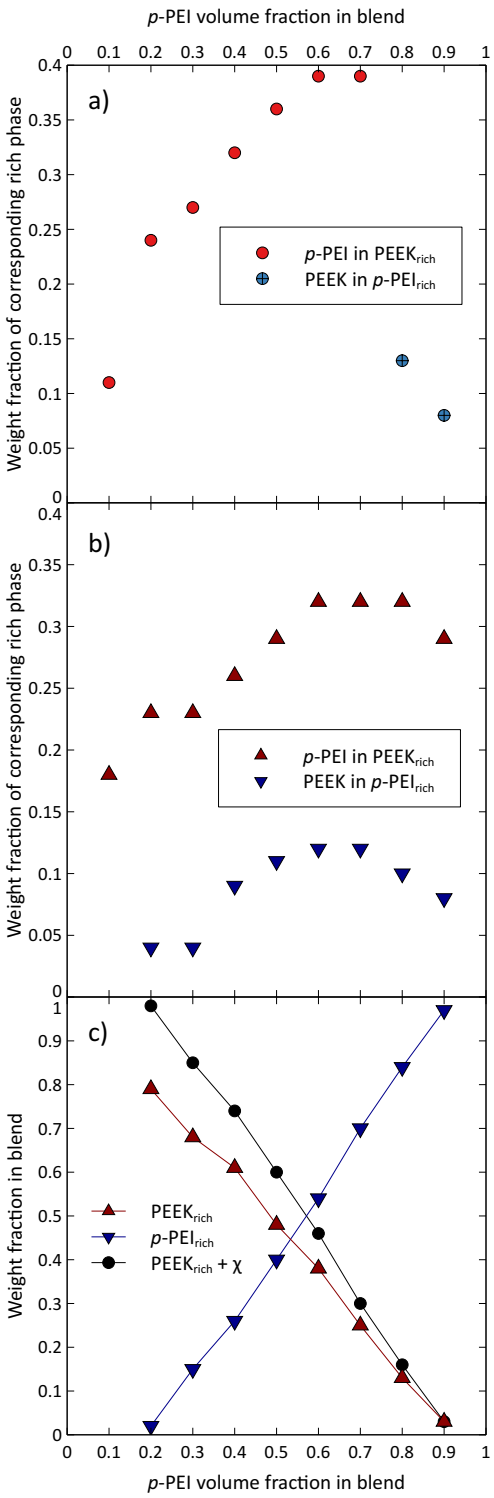

Figure 4.5 Weight fraction compositions of the PEEK$_{rich}$ and *p*-PEI$_{rich}$ phases calculated from a) T_g's from the 1st DSC heating cycle; b) T_g's from the 2nd DSC heating cycle. c) Weight fractions of the PEEK$_{rich}$ and *p*-PEI$_{rich}$ phases in the total blend, with or without the addition of PEEK crystallinity, calculated from the 2nd DSC heating cycle melting peak and rich phases compositions.

Figure 4.5a-b presents the compositions of the $PEEK_{rich}$ and *p*-PEI_{rich} phases, as a function of the overall *p*-PEI composition. These compositions were calculated based on the T_g's measured by DSC, following Equations 4.3 and 4.4 presented in Section 4.2.4. Since in the first heating cycle of DSC measurements (Figure 4.4), the T_g of the *p*-PEI_{rich} phase is only measurable for 10% and 20% of *p*-PEI, determining the PEEK weight fraction in this phase is limited to these two compositions. The results show that there is always more *p*-PEI dispersed in the $PEEK_{rich}$ phase than PEEK dispersed in the *p*-PEI_{rich} phase. For both phases, the minor component's composition reaches a maximum between 60% and 70% of *p*-PEI in the blend. Note also that between 10% and 70% of *p*-PEI, the increase and maximum weight fraction of *p*-PEI in the $PEEK_{rich}$ phase is more pronounced for the first DSC heating cycle compared to the second heating cycle. This arises from the larger differences between the blends' T_g's and T_g of pure PEEK in the first heating cycle, compared to the second heating cycle. Indeed, during the second heating cycle, PEEK has recrystallized, increasing its T_g, which in turn decreases the calculated amount of *p*-PEI in the $PEEK_{rich}$ phase (Equations 4.3 and 4.4).

Figure 4.5c presents the weight fractions of the $PEEK_{rich}$ and *p*-PEI_{rich} phases in the blends. These results were obtained from Equations 4.5 and 4.6 presented in Section 4.2.4, which subtract the amount of crystallized PEEK from the $PEEK_{rich}$ and *p*-PEI_{rich} phases. A third curve is thus added where the PEEK's crystallinity is fully attributed to the $PEEK_{rich}$ domain, since the PEEK composition in the *p*-PEI_{rich} phase is always inferior to 15 wt% (≈ 15 vol%), and because PEEK does not recrystallize in *p*-PEI at such compositions (see Figure 4.4). From the results, it can be observed that above 55 vol% of *p*-PEI in the blend, the $PEEK_{rich}$ domain becomes the minor one, which is corroborated by the SEM observations made in Figure 4.1f and the fact that at higher *p*-PEI volume fractions it is impossible to obtain a porous PEEK monolith via extraction. Values lacking at 10 vol% *p*-PEI is due to the difficulty in measuring the T_g of the *p*-PEI_{rich} phase at this composition.

An apparent discrepancy is also observed at low *p*-PEI compositions (≤ 20 vol%), suggesting the absence of a *p*-PEI_{rich} phase, and nearly full blend miscibility. This is indeed not the case, as the SEM micrographs of Figure 4.1 show. Further analysis of Equations 4.3 and 4.4, based on the Flory-Fox equation predicting the T_g of miscible homopolymers, and Equations 4.5 and 4.6, are probably required in this case and will be addressed in a future work.

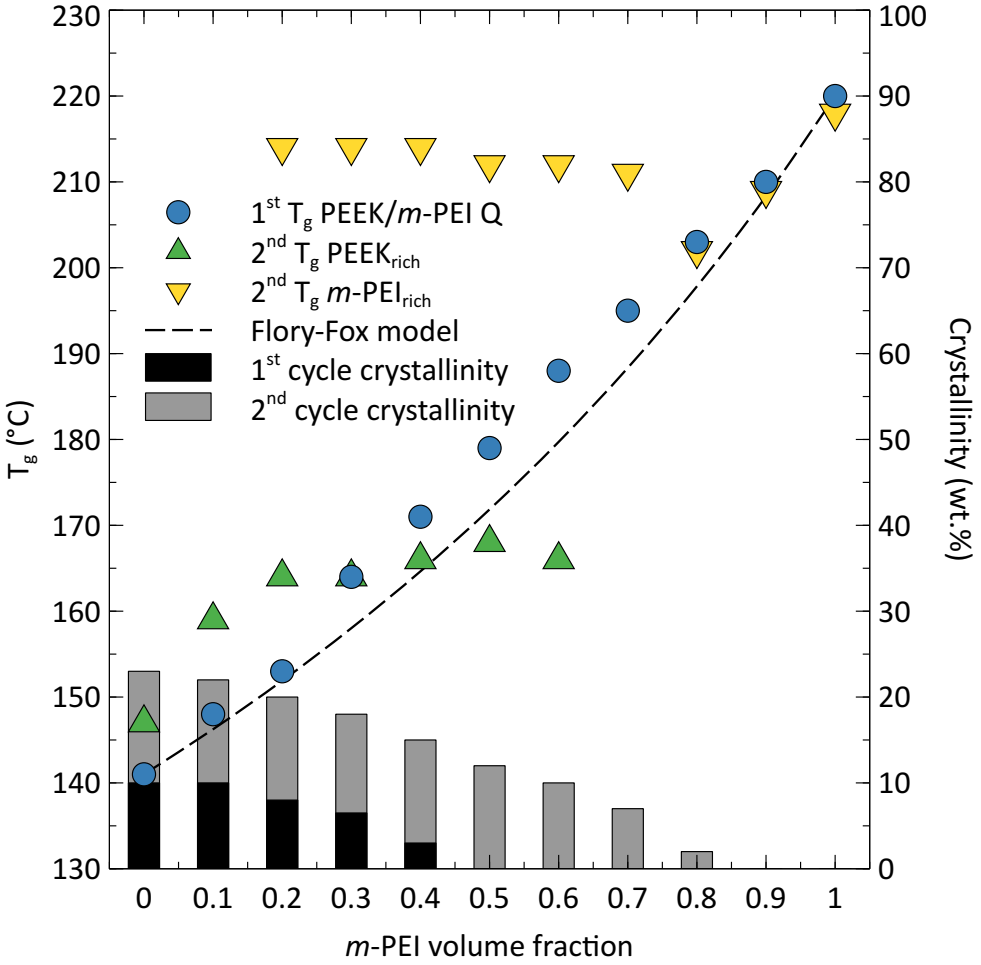

Figure 4.6 Glass transition temperatures and total material crystallinity for 1st and 2nd DSC cycles as a function of *m*-PEI volume fraction for PEEK/*m*-PEI quenched system.

In **Figure 4.6**, the T_g's and total crystallinity for PEEK/*m*-PEI quenched blends are presented (see Supporting Information **Figure S4.2** for the thermograms). On the 1st cycle, only one T_g is observed for all compositions, and it nearly follows the Fox equation (with a slight positive deviation), which confirms that PEEK/*m*-PEI systems are miscible in the melt state over the full composition spectrum. This agrees with previously published works [68-74, 105, 106]. The initial crystallinity is also relatively low (with a maximum of 10% for pure PEEK), and the blends are fully amorphous above 40 vol% of *m*-PEI, which differs from the PEEK/*p*-PEI system presented in Figure 4.4 which shows crystallinity up to 60 vol% of *p*-PEI.

During the 2nd cycle, two sets of T_g's are observed. They are also shifted compared to the pure components: up for the $PEEK_{rich}$ phase and down for *m*-PEI_{rich} phase, compared respectively to

pure PEEK and *m*-PEI, with each phase containing minor amounts of *m*-PEI and PEEK, respectively. This phase separation is the result of PEEK crystallization, as demonstrated previously [69, 72, 73] and as observed also for the PEEK/*p*-PEI system. This crystallization creates interlamellar regions rich in PEEK but containing a small amount of *m*-PEI, responsible for the lower T_g, and interfibrillar/interspherulitic regions rich in *m*-PEI but containing small amounts of PEEK, responsible for the higher T_g (Scheme S1) [56]. The T_g's reach plateau values between 20 vol% and 70 vol% of *m*-PEI. No *m*-PEI_{rich} T_g is observed at 10 vol% of *m*-PEI either because it is too faint to be detected or because all of the *m*-PEI is present in the $PEEK_{rich}$ phase and only contributes to the $PEEK_{rich}$ T_g (similar observation for the $PEEK_{rich}$ T_g above 70 vol% of *m*-PEI).

The T_g of the *m*-PEI_{rich} phase decreases between 70 vol% and 80 vol% of *m*-PEI, and increases again at 90 vol%. Two potential contributions are that PEEK does not crystallize sufficiently anymore, remaining mainly amorphous and enriching the *m*-PEI_{rich} phase, lowering its T_g. However, as the *m*-PEI content keeps increasing, the PEEK content decreases and the *m*-PEI_{rich} T_g increases towards the value of pure *m*-PEI, explaining the minima observed at 80 vol% *m*-PEI.

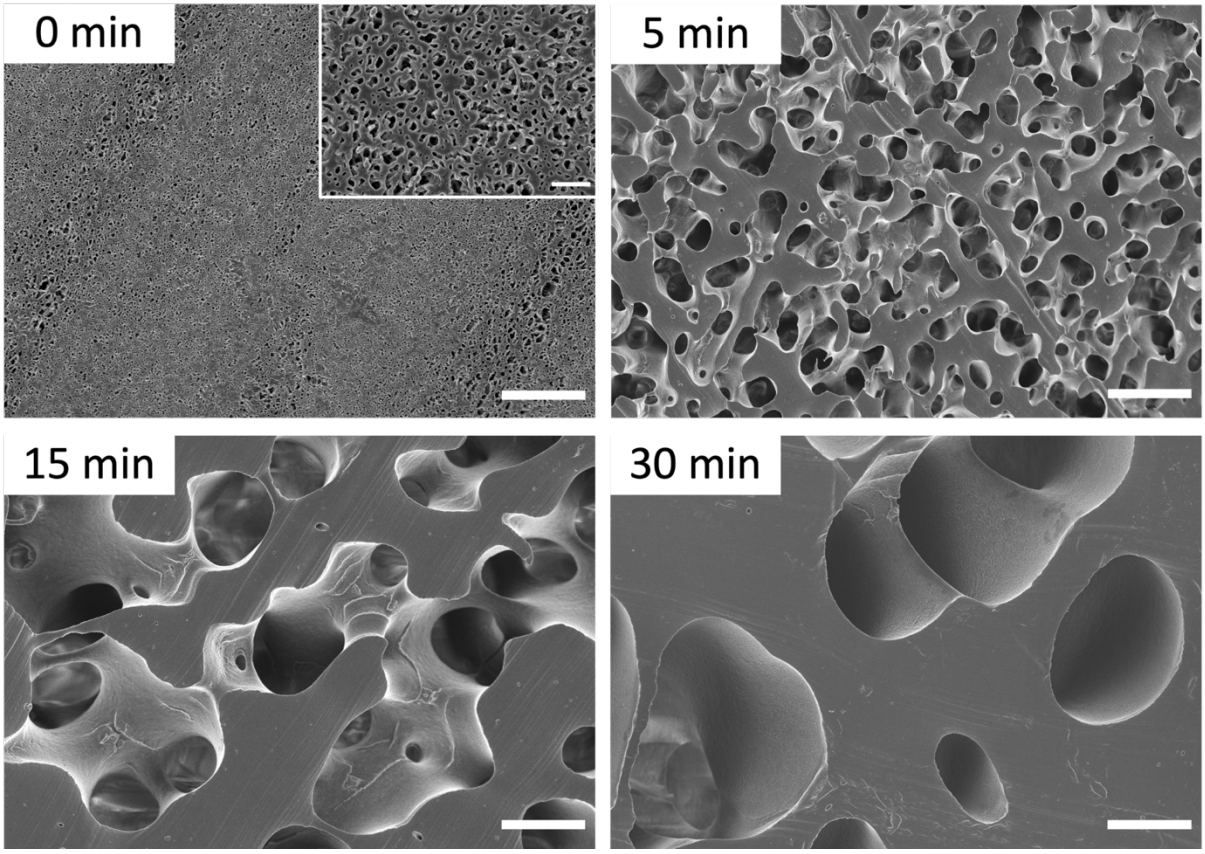

Figure 4.7 Microstructure of PEEK/*p*-PEI 50/50 blend, initially quenched, for different times spent under quiescent annealing at 380 °C. White scale bars represent 10 μm for main magnification and 1 μm for the close-up inset micrograph.

Figure 4.7 shows the coarsening of the co-continuous PEEK/*p*-PEI 50/50 vol% blend microstructure, as a function of quiescent annealing time at 380 °C (blend initially quenched). Even if the system is partially miscible, it significantly coarsens, from sub-μm to over 15 μm domains after 30 min of annealing time. The rate of coarsening appears surprisingly fast considering the expected low interfacial tension, which is the coarsening driving force. Furthermore, **Figure 4.8** confirms that the continuity of the *p*-PEI phase is maintained during the coarsening process for the 50/50 blend and remains quite high (and even increases) for 30% and 20% *p*-PEI. To the authors' knowledge, this is the first time that the coarsening process in partially miscible bulk polymer blends has been reported in the literature.

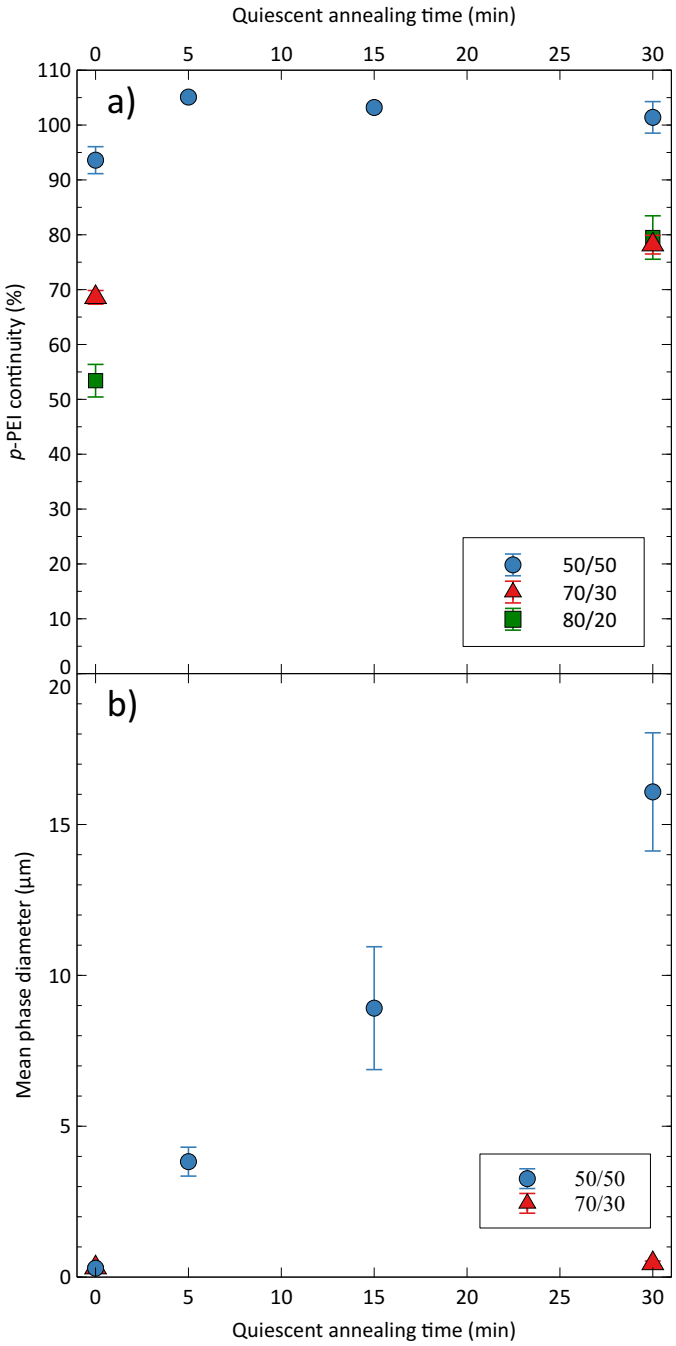

Figure 4.8 a) *p*-PEI continuity and b) its average phase diameter, as a function of quiescent annealing time, at 380 °C for three PEEK/*p*-PEI compositions initially quenched.

Figure 4.8 presents the evolution of *p*-PEI continuity and the average phase diameter as a function of quiescent annealing time, at 380 °C, starting from blends initially quenched in cold water. As the results show, the *p*-PEI phase in the 50/50 blend remains fully continuous even after 30 min of annealing time (results slightly higher than 100% are caused by the removal of PEEK present in

the *p*-PEI$_{rich}$ phase during the solvent extraction protocol). The maintained continuity is accompanied by a quasi-linear increase in the *p*-PEI phase diameter, from 0.29 ± 0.08 µm in the quenched state to 16 ± 2 µm after 30 min of annealing time [48, 49]. For the 70/30 composition, a slight increase in continuity is observed for the *p*-PEI phase after 30 min of annealing, with the *p*-PEI dispersed phase diameter only increasing marginally from 0.31 ± 0.06 µm to 0.45 ± 0.08 µm. Such high continuity results, even at low *p*-PEI contents, could be explained by a certain level of connectivity between the *p*-PEI$_{rich}$ dispersed phase droplets, via the miscible fraction of *p*-PEI present in the PEEK$_{rich}$ matrix phase – indeed, the solvent can extract the *p*-PEI at a molecular level present in the PEEK$_{rich}$ phase, which could link the droplets together in a network. To the best of the authors' knowledge, this is the first time that such porous PEEK monoliths, with precise control over pore size - over an extended range, from 300 nm to 15 µm and more for longer annealing times - and pore interconnectivity, have been reported in the literature.

The breaking thread (BT) method was then employed to measure the PEEK/*p*-PEI interfacial tension (following the procedure explained in Section 4.2.9) and a value of 0.14 ± 0.04 mN/m was obtained for the PEEK/*p*-PEI_2 system. This value is especially low compared to classical immiscible polymer blends but can be expected for the partially miscible behavior of this system. In comparison, Lee and Kim [117] reported a value of 1.02 mN/m for a PC/PMMA system, which is a well-known partially miscible polymer blend. Although the thermal stability of the *p*-PEI posed some problems during the BT experiments, complementary experiments demonstrated that the overall impact on the interfacial tension value was relatively minor and did not affect the main conclusions (see Supporting Information, Section 4.5.4).

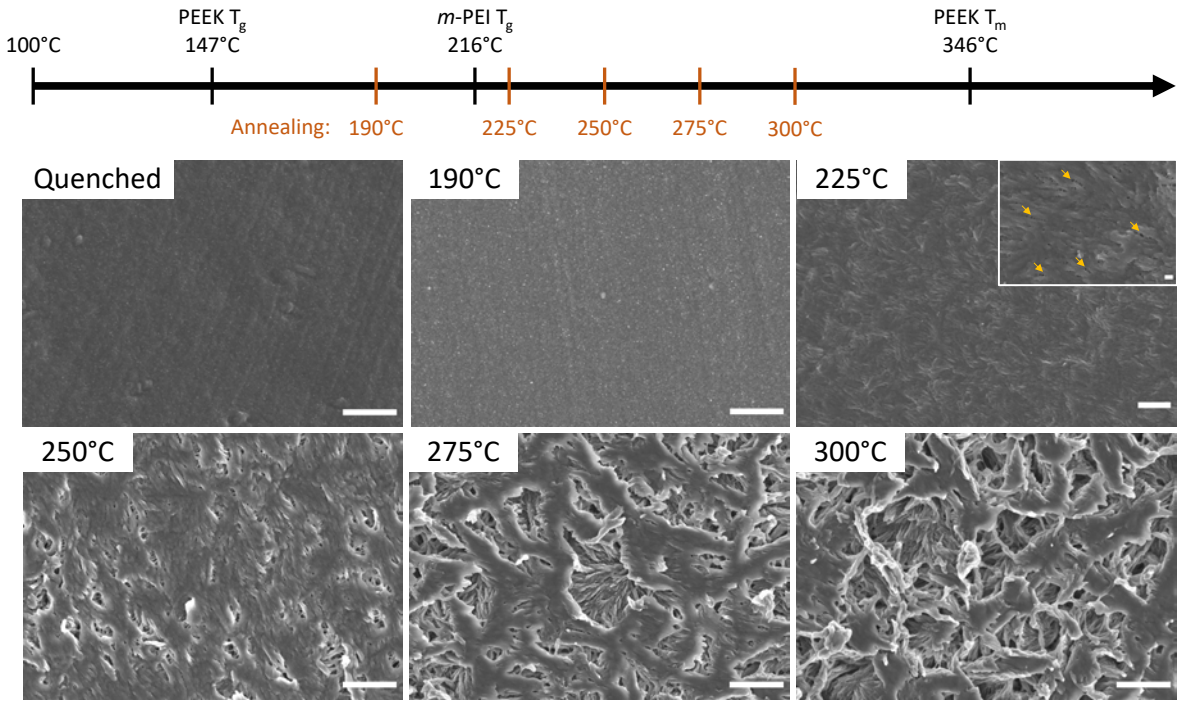

Figure 4.9 Microstructure of PEEK/*m*-PEI 50/50 blend as a function of annealing temperature, compared to the initially quenched blend at the exit of the micro-compounder. White scale bars represent 1 µm for main magnification and 100 nm for the close-up micrograph. Yellow arrows indicate mesopores. Note that the *m*-PEI was selectively extracted to enhance contrast.

In comparison, **Figure 4.9** presents the microstructure evolution for the PEEK/*m*-PEI 50/50 composition for five different annealing temperatures (all below the melting T of PEEK), compared to the initially quenched blend at the exit of the micro-compounder: 190 °C (above the T_g of PEEK but below the T_g of *m*-PEI), 225 °C (slightly over the T_g of *m*-PEI), 250 °C, 275°C, and 300 °C. At 190 °C, PEEK can crystallize but chain mobility remains very limited for the *m*-PEI phase – no significant difference is noticed compared to the quenched blends after *m*-PEI extraction. PEEK can only form crystalline lamellae with *m*-PEI trapped in between because of the very limited chain mobility.

Above the T_g of *m*-PEI at 216 °C, both PEEK crystallization and increased *m*-PEI molecular chain mobility occur. At 10 °C above the *m*-PEI T_g, e.g. 225 °C, differences between the annealed and initially quenched samples start to appear. The PEEK crystalline microstructure is now easier to distinguish and mesopore formation becomes apparent, left by the *m*-PEI extracted from PEEK interfibrillar spaces (≈ 20 nm, see inset showing a magnified view in Figure 4.9 at 225 °C) (Mehta,

et al. [87] and Ding and Bikson [83] observed 11 nm pores after annealing at 250 °C). *m*-PEI now has sufficient molecular mobility to move out of PEEK during fibrillae growth.

By increasing the temperature again, both *m*-PEI and PEEK continue to gain in mobility, which promotes the formation of PEEK spherulites and the progressive expulsion of *m*-PEI in the newly formed interspherulitic spaces, increasing the size of *m*-PEI_{rich} domains – this is especially apparent at 275°C and 300°C. The shape of the pores changes at this point, from circular mesopores, to larger but still narrow pores, as observed for example in crystallized PVDF templates prepared from miscible polymer systems [57, 119]. The characteristic domain sizes of both $PEEK_{rich}$ and *m*-PEI_{rich} phases significantly increase as the annealing temperature increases, from the nm scale, up to the μm scale. This means that the microstructural length scale can be controlled over three orders of magnitude with simple heat treatments.

These structural features are supported by the DSC data (Figure 4.6), which show that PEEK recrystallization drives phase separation and results in the formation of a crystalline PEEK phase, an amorphous interlamellar $PEEK_{rich}$ phase containing *m*-PEI, and an amorphous interfibrillar/interspherulitic *m*-PEI_{rich} phase containing PEEK (probably mostly amorphous also).

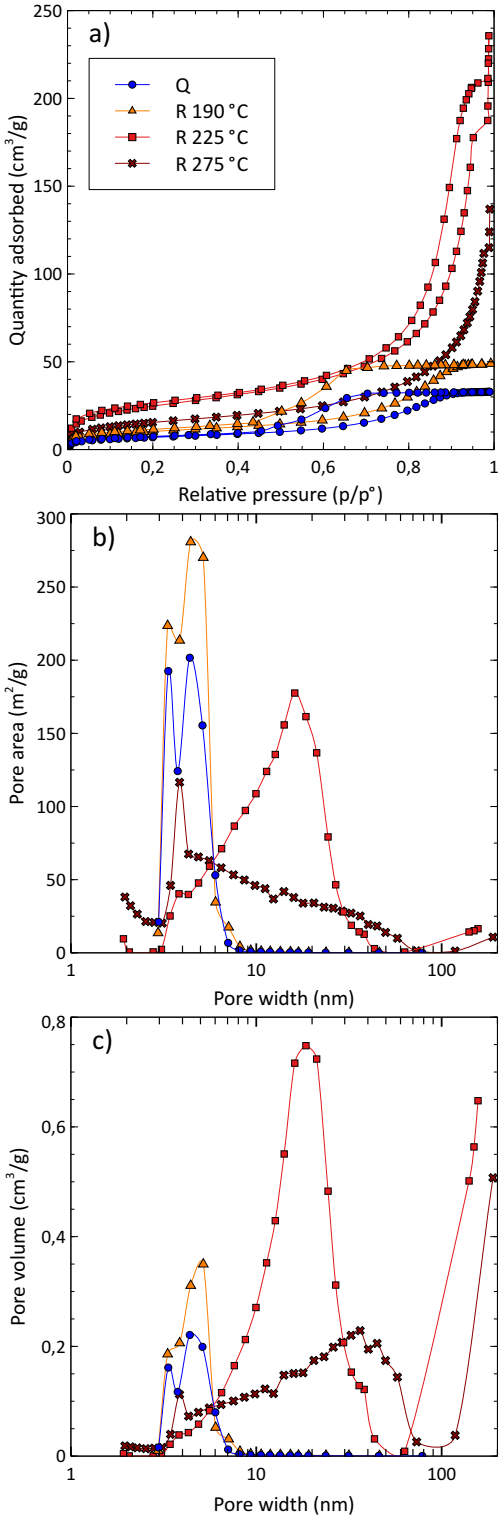

Figure 4.10 a) Quantity of adsorbed nitrogen as a function of relative pressure, b) pore area as a function of pore width, and c) pore volume as a function of pore width, obtained from gas sorption experiments on porous PEEK monoliths prepared from PEEK/*m*-PEI 50/50 blend, from the initial quenched state or annealed at different temperatures.

Figure 4.10 presents the results of gas sorption experiments on porous PEEK monoliths prepared from the PEEK/*m*-PEI 50/50 blend by *m*-PEI extraction, in the quenched state and after annealing at different temperatures. According to IUPAC, the isotherm curves obtained for the quenched sample and the sample annealed at 190 °C (R 190 °C) are of type IV(a), with H1 or H2(a) hysteresis, which corresponds to mesoporous adsorbents. The R 225 °C and R 275 °C samples present composite type IV and type II isotherms, revealing the presence of macropores [120]. These qualitative features are in agreement with the morphological features displayed in Figure 4.9.

The pore size distributions - Pore area vs Pore width (Figure 4.10b) and Pore volume vs Pore width (Figure 4.10c) - were calculated from the desorption isotherm curves using the Barrett, Joyner and Halenda (BJH) method. The results reveal the presence of mesopores of 2 to 4 nm for the quenched and R 190 °C samples, with similar quantities of adsorbed nitrogen, supporting the similar, homogeneous appearances observed in Figure 4.9. The R 225 °C sample shows a higher quantity of adsorbed nitrogen and a wider pore width distribution, centered around 20 nm and extending up to 40-50 nm, and even over 100 nm, in accordance again with SEM observation. The last sample (R 275 °C) adsorbs less nitrogen than R 225 °C. It shows an even broader pore width distribution, with a maximum arising around 3 nm (in Figure 4.10b) and another one centered around 35 nm (in Figure 4.10c), extending well over 100 nm in both cases – the morphology is now quite open and shows the presence of macropores. However, it was not possible to extend the measurements over 100 nm.

Table 4.2 Gas sorption analysis summary

	Q	R 190 °C	R 190 °C freeze dried	R 225 °C	R 275 °C
Surface Area BET (m^2/g)	25	38	154	90	57
Surface Area BJH Desorption (m^2/g)	46	69	276	94	61
Cumulative pore volume (cm^3/g)	0.05	0.08	0.38	0.37	0.21
Average pore width (nm)	4.5	4.4	6.7	15.5	14.1

Table 4.2 summarizes the main results of the gas sorption experiments performed on the PEEK/*m*-PEI 50/50 blend. An estimation of the expected cumulative pore volume, based on the PEEK and *m*-PEI densities at room temperature (see Table 4.1), gives a value of approx. 0.39 cm^3/g, which is close to the result obtained for the R 225 °C sample (0.37 cm^3/g). However, the R 275 °C sample presented a lower value of 0.21 cm^3/g, which is explained by unaccounted macropores over 100 nm (as Figure 4.9 shows).

However, the cumulative pore volume is quite lower for the quenched and R 190 °C samples, compared to the expected calculated value. Apart from pore tortuosity that might restrict nitrogen diffusion, another reason could be the reduction of sample dimensions during drying, i.e. pore collapsing, which was observed after the final drying step in the oven – estimated in between 25% and 40% of the total volume for the quenched blend. Such collapsing is thought to come from the capillary forces exerted by the solvent during evaporation in the oven, combined with the more fragile and fine nanostructure of the quenched and R 190 °C blends (compared to the coarser and more solid microstructure of blends annealed at 225 °C and 275 °C). The effect was significantly reduced when using freeze-drying, with only 7% to 13% of volume reduction. Indeed, after freeze-drying, the cumulative pore volume of the R 190 °C sample increases from 0.08 cm^3/g to 0.38 cm^3/g, almost matching the theoretical value – with a surface area reaching a maximum of 154 m^2/g, amongst the highest values reported for microporous polymer monoliths prepared from melt-processed polymer blend. In comparison, Mehta and Kalika [86] performed mercury porosimetry experiments on similar materials and obtained an equivalent value of 0.28 cm^3/g.

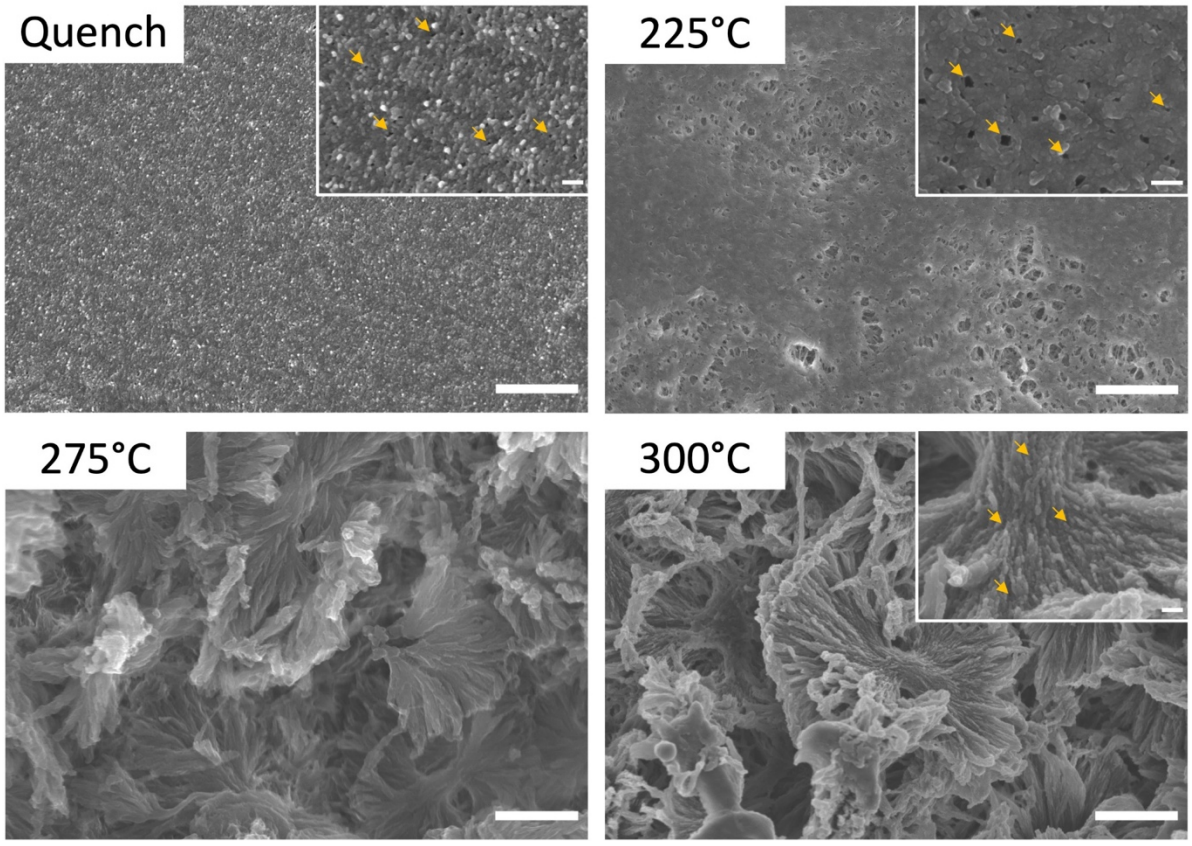

Figure 4.11 Microstructure of PEEK/*m*-PEI 30/70 blend as a function of annealing temperature. White scale bars represent 1 µm for main magnification and 100 nm for the close-up inset micrographs. Yellow arrows indicate mesopores.

Thermal annealing of a PEEK/*m*-PEI 30/70 blend exacerbates the previous morphological features, as **Figure 4.11** illustrates. After full *m*-PEI extraction and freeze-drying, for example, mesopores of roughly ≈ 12 nm are already apparent in the quenched sample, as indicated by the yellow arrows in the close-up micrograph. At 10 °C above the T_g of *m*-PEI, e.g. 225 °C, the mesopores left by extracting the *m*-PEI from PEEK interfibrillar spaces (Mehta, et al. [87] and Ding and Bikson [83] observed 33 nm pores after annealing at 250 °C) are larger, ≈ 25 nm, following the hypothesis of higher chain mobility. At even higher temperatures (275 °C and 300 °C), both *m*-PEI and PEEK further gain in mobility, which promotes the formation of PEEK spherulites and *m*-PEI rich interspherulitic regions. Since the volume fraction of PEEK is lower at this composition, PEEK possesses a larger available volume for its spherulites to grow without impingement, resulting in a very high porosity after *m*-PEI extraction, large pores, and the formation of "farfalle"-looking PEEK crystalline domains (see also Supporting Information Section 6). Additionally, the *m*-PEI

interfibrillar domains are also distinguishable inside the spherulitic microstructure (e.g. close-up micrograph for the 300 °C annealing temperature).

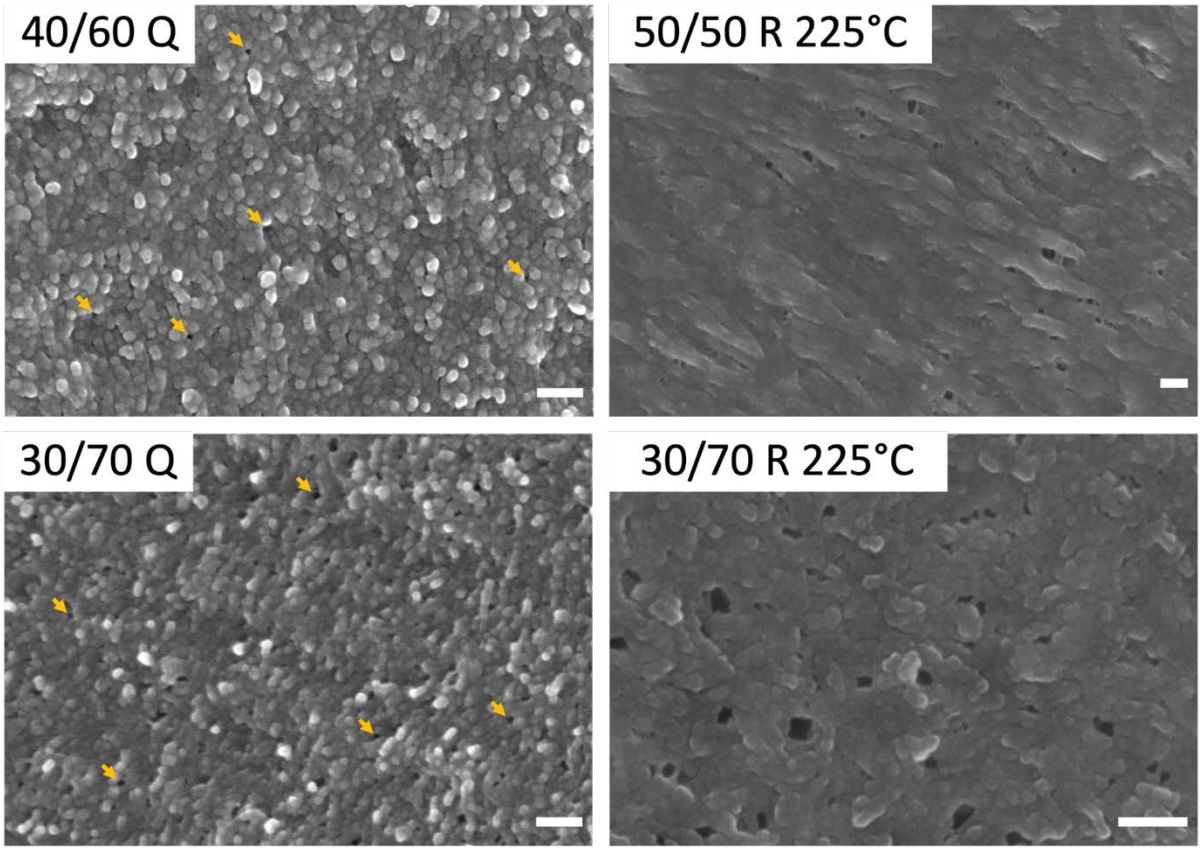

Figure 4.12 Mesoporous structures obtained at different compositions and thermal treatments for the PEEK/*m*-PEI system. White scale bars represent 100 nm. Yellow arrows indicate mesopores.

Figure 4.12 illustrates some of the mesoporous structures observed in this work, ranging from ≈ 7 nm to ≈ 25 nm, obtained from the PEEK/*m*-PEI system at different compositions or thermal treatments. According to gravimetric analysis, the *m*-PEI originally present was completely removed during solvent extraction. Hence the mesopores are fully continuous throughout the materials. What truly stands out is the range of attainable porosities and average pore size, combined with full pore interconnectivity, and the possibility of independently controlling these features by simply adjusting blend composition and thermal treatment. It is also quite pertinent to note that the range of porosities and pore architectures reported in this work are quite complementary, for example, to PEEK aerogels and foams prepared by temperature-induced phase separation (TIPS) [121, 122]. However, the samples decrease in size during the final drying step

(although the effect is much less severe when freeze-drying is employed), resulting in a decrease in volume that can be accompanied by either a reduction in pore size and/or pore collapse, thus potentially affecting the continuity. It can also explain why 30 vol% of PEEK apparently occupies so much surface area on the micrographs. Solving this last issue would provide a way to prepare porous PEEK materials over a wide range of porosities and average pore sizes – from nearly 2-3 nm to tens of μm.

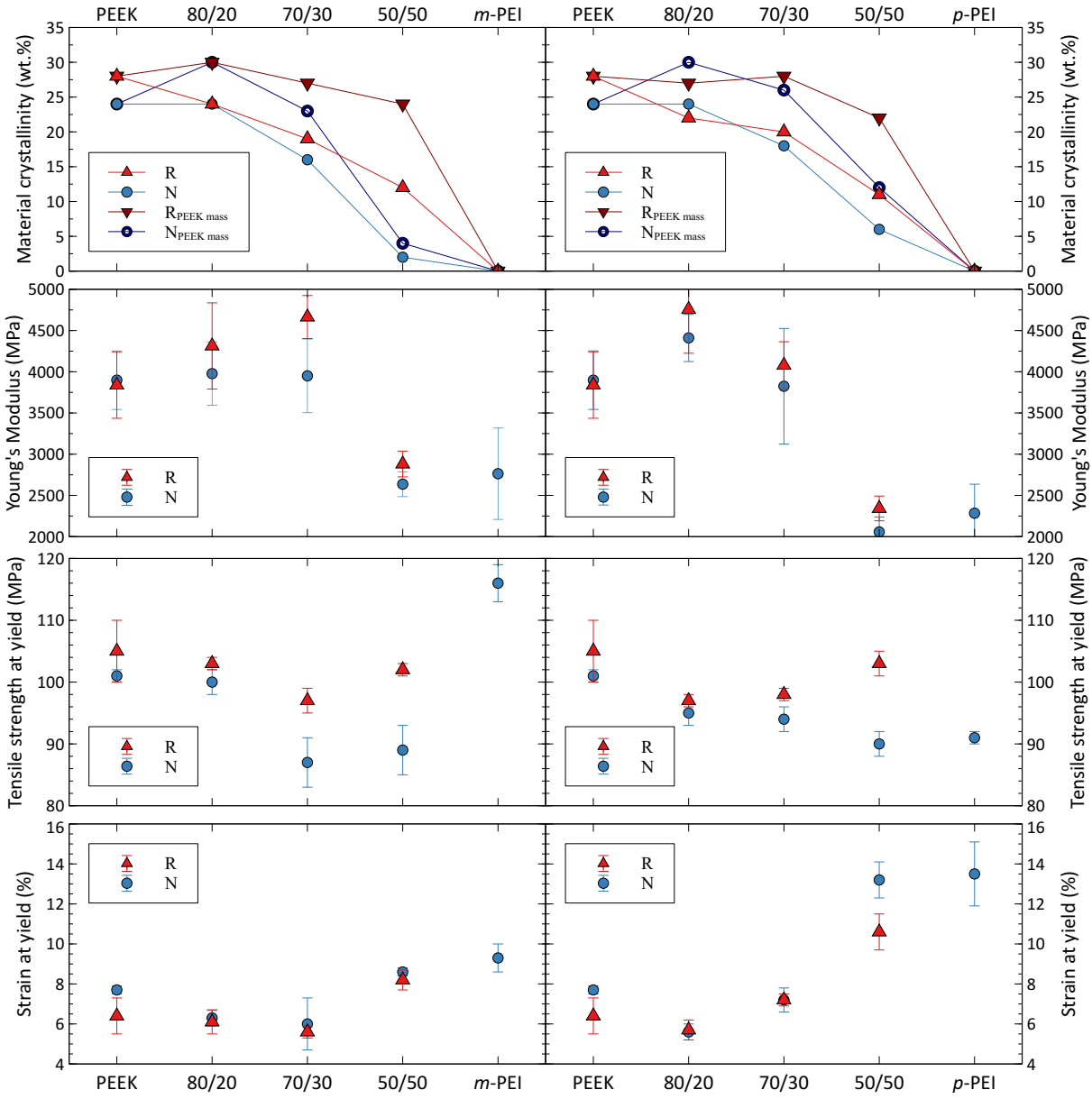

Figure 4.13 Tensile properties of both PEEK/*m*-PEI and PEEK/*p*-PEI systems as a function of composition (80/20, 70/30, and 50/50) and thermal treatment (with or without annealing for 30 min at 200 °C, denoted as R and N samples respectively).

Figure 4.13 summarizes the tensile properties obtained as a function of composition, for the two different systems of PEEK/*m*-PEI (left) and PEEK/*p*-PEI (right), with or without a thermal annealing treatment (30 min at 200 °C). The total crystallinity of the material, the crystallinity based on the PEEK mass present in the blend, Young's modulus, the tensile strength at yield, and the strain at yield are reported. Note also that the results obtained in this work for the neat polymers are comparable to the data provided by the suppliers.

Apart from the PEEK/*p*-PEI 80/20 composition, all materials present higher total crystallinity after the annealing step. Since only one specimen for each composition was analyzed by DSC to obtain the crystallinity, it could explain why there is a slight discrepancy for the PEEK/*p*-PEI 80/20. Interestingly, for non-annealed (N) samples, the PEEK/*m*-PEI 80/20, PEEK/*p*-PEI 80/20 and 70/30 compositions all present higher crystallinity, based on the PEEK mass present in the blend, compared to pure PEEK.

All the compositions tested show higher Young's modulus and tensile strength at yield after the annealing step, confirming the relevance of such post-extrusion thermal treatment. Regarding Young's modulus, the highest increases after annealing were observed for the PEEK/*m*-PEI 70/30 and PEEK/*p*-PEI 80/20 blends, with 18% and 8% improvement respectively. For the tensile strength at yield, the highest increases reported were 14 % for both the PEEK/*m*-PEI 50/50 and PEEK/*p*-PEI 50/50 compositions.

Comparing pure PEEK with the blends, an increase in Young's modulus of 21% was observed for the PEEK/*m*-PEI 70/30, and of almost 24% for the PEEK/*p*-PEI 80/20, after annealing. Regarding the tensile strength at yield, neat PEEK always displays a higher value than the blends. As expected for the two systems, the compositions with the highest moduli in each case also present the lowest tensile strain at yield. Arzak, et al. [68] and, Harris and Robeson [88] also evaluated the tensile properties of PEEK/*m*-PEI blends produced by injection molding, with some of the amorphous as-molded blends later annealed at 185 °C and 250°C, respectively, to increase their crystallinity. While the samples with less than 50 wt.% of PEEK showed only marginal improvements in Young's modulus after annealing, annealed PEEK-rich samples possessed the highest stiffness, reaching 3.2 GPa for the 85/15 blend [68] and 3.6 GPa for the 80/20 composition [88]. However, the authors did not report the same positive deviation in Young's modulus observed in this work for the 80/20 and 70/30 compositions compared to pure PEEK. It is worth mentioning that the processing of the tensile samples and their annealing temperature are different in this work

compared to the cited literature which could explain the discrepancies. Regarding ductility, a higher deformation was reported for amorphous samples than for annealed ones.

Another interesting observation is that the type of PEI blended with PEEK does not result in significant differences (with a few exceptions) in mechanical properties between PEEK/*m*-PEI and PEEK/*p*-PEI blends. Hence, adding a small amount of PEI to PEEK maintains (and in some cases significantly improves) the material's properties, while at the same time reducing the costs, as PEI is less expensive. PEI is also known to facilitate the processing of PEEK, particularly for 3D printing processes. Future work will aim at characterizing the mechanical properties of porous PEEK monoliths (*e.g.* in compression) prepared with both types of PEI's, for applications requiring such materials, including PEEK-based scaffolds for bone tissue regeneration, and porous monoliths for heterogeneous catalysis.

By simply changing the position of a linkage in the chemical structure of PEI, we go from a fully miscible system for the PEEK/*m*-PEI pair, to a partially miscible one, displaying a very low interfacial tension of 0.1 mN/m for the PEEK/*p*-PEI system. The resulting blend morphologies right after melt processing (Figures 1 and 2), and the subsequent morphology control strategies, contrast sharply: (1) for the miscible PEEK/*m*-PEI system, the nm to sub-µm scale morphology is mainly controlled by the composition, but also by the annealing temperature, with relatively sharp transitions at the polymers' T_g's, over which the significant increases in chain mobility gradually lead to coarser domains, driven by PEEK recrystallization and *m*-PEI expulsion from PEEK-rich domains (Figures 6, 9, 11 and 12) ; (2) for the partially miscible PEEK/*p*-PEI system, the sub-µm to µm scale morphology is also controlled by composition, but also by annealing over the melting temperature of PEEK, which is much higher than the components T_g's (Figures 7 and 8b). The resulting coarsening rate is driven by the interfacial tension and modulated by the components' viscosities – a fundamentally different mechanism compared to the PEEK/*m*-PEI system, which does not coarsen since PEEK and *m*-PEI are miscible – there is no interfacial tension ; (3) combined together, it is possible to generate morphologies with a characteristic length scale ranging over nearly 4 orders of magnitude, from nearly ≈ 5 nm, to ten's of µm, and which, after the selective removal of the PEI phase, generate porous PEEK monoliths with an average porosity ranging over the same extensive range – probably the widest reported to date in the literature for PEEK monoliths, and polymer monoliths in general. While similar types of intermolecular interactions between PEEK and both PEIs are expected since both PEIs comprise the exact same functional

groups, the exact reasons behind these contrasting behaviors are not fundamentally clear. However, *p*-PEI possesses a higher T_g compared to *m*-PEI – nearly 10 °C – suggesting differences in chain flexibility, intra-chains interactions and conformations, leading then to subtle differences in inter-chains interactions with PEEK - sufficient to promote either full miscibility for *m*-PEI, or partial miscibility for *p*-PEI.

Chen, et al. [77] have studied the miscibility of the PEEK/*m*-PEI system by FTIR, and have shown that a specific interaction forms between the electron-rich ether functional groups in PEEK, and the electron-deficient imide rings in the *m*-PEI backbone. Recent work has also shown that the presence of interacting functional groups is not by itself sufficient – the chains must also have sufficient mobility in order for these functional groups to orient properly [123, 124]. For example, Heshmati and Favis [123] have shown that a PEO plasticizer located in polylactide (PLA) increases the mobility of the PLA chains (PLA is a relatively stiff polymer), and promotes interfacial interactions between the complementary functional groups of PLA and polyamide11 in that immiscible system. In another work, Bhadane, et al. [124] have shown that the addition of a plasticizer to an immiscible blend of brominated poly(isobutylene-*co*-*p*-methylstyrene) and polyamide promotes the formation of a graft copolymer at the interface, by enhancing chain mobility. In the present case, *p*-PEI demonstrates a glass transition temperature almost 10 °C higher than *m*-PEI, a clear indication of lower *p*-PEI chain mobility. Figure 4.1 and Figure 4.2 clearly demonstrate that *p*-PEI possesses a lower level of miscibility compared to *m*-PEI, which could be due to lower chain mobility and, ultimately, differences regarding the level of specific interactions with PEEK. The investigation and understanding of such subtle changes at the molecular level is beyond the scope of this work but would constitute an interesting topic for future work.

A number of novel contributions are observed for the PEEK/*m*-PEI blend. The *m*-PEI phase in the miscible PEEK/*m*-PEI system displays a low percolation threshold in-between 10 to 15% (Figure 4.3), with a microstructural characteristic length scale close to molecular dimensions (Figure 4.2 and Figure 4.12) – amongst the finest structures for a co-continuous system reported to date in the literature, and constituting the first investigation related to the development of co-continuity in the limit of a fully miscible binary polymer system. The quiescent annealing temperature impacts the crystallization process of PEEK, the subsequent PEEK/*m*-PEI phase separation process and blend morphology, and ultimately its impact on co-continuity development (Figure 4.9, S5, and S6), revealing that co-continuity is indeed maintained, whereas the microstructure length scale

gradually increases from a few nm, to a sub-µm value. Ultimately, it allows the preparation of porous PEEK monoliths when the *m*-PEI is selectively extracted, resulting in some of the finest porous networks, in the nanoscale range, reported to date in the literature when prepared with co-continuous polymer systems, with very high specific surfaces (Figure 4.12 and Table 4.2).

Finally, viscosity does not have a significant impact since using the lower viscosity *p*-PEI_2 also yields a phase-separated blend with similar morphological features (**Figure S4.8**). Supposing that *m*-PEI and *p*-PEI are miscible (yet to be verified), this opens the way to explore a unique ternary system where two pairs are fully miscible, and the third pair is only partially miscible - potentially offering the opportunity, for example, to control the miscibility of PEEK with *p*-PEI by the addition of *m*-PEI.

4.4 Conclusion

This work demonstrates that two close isomeric forms of poly(ether imides) result in fundamentally different types of morphologies when blended with PEEK: a new partially miscible and phase-separated system for the PEEK/*p*-PEI system, and the typically reported fully miscible PEEK/*m*-PEI system. The PEEK/*p*-PEI system displays sub-µm, matrix/dispersed phase or co-continuous types of morphologies, with the latter quickly coarsening over tens of µm in length scale under quiescent annealing conditions due to the PEEK/*p*-PEI interfacial tension, which was measured by the breaking thread method at 0.14 mN/m, a very low value. On the other hand, the PEEK/*m*-PEI system displays full miscibility over the whole composition spectrum. Then, controlling the thermal annealing temperature promotes PEEK recrystallization and the formation of a nanostructured *m*-PEI-rich phase. Taken altogether, it is then possible to control the morphological length scale of both PEEK and PEI domains over nearly 4 orders of magnitude, from ≈ 5 nm to over 15 µm. The selective extraction of the PEI phase then results in porous PEEK monoliths with full pore interconnectivity, with an average pore size spanning the same considerable range, without the addition of interfacial modifiers – a unique feature in the field of binary melt-processed polymer blends. Considering the extensive range of average pore size, from approx. 5 nm to over ten's of microns, this work opens the way to a variety of applications, including PEEK-based porous materials for nanofiltration and separation processes in general, monoliths for heterogeneous catalysis in continuous flow systems, and 3D porous PEEK scaffolds for regenerative medicine applications, for example.

4.5 Supporting information

4.5.1 Segregation modes of PEI in PEEK/PEI blends

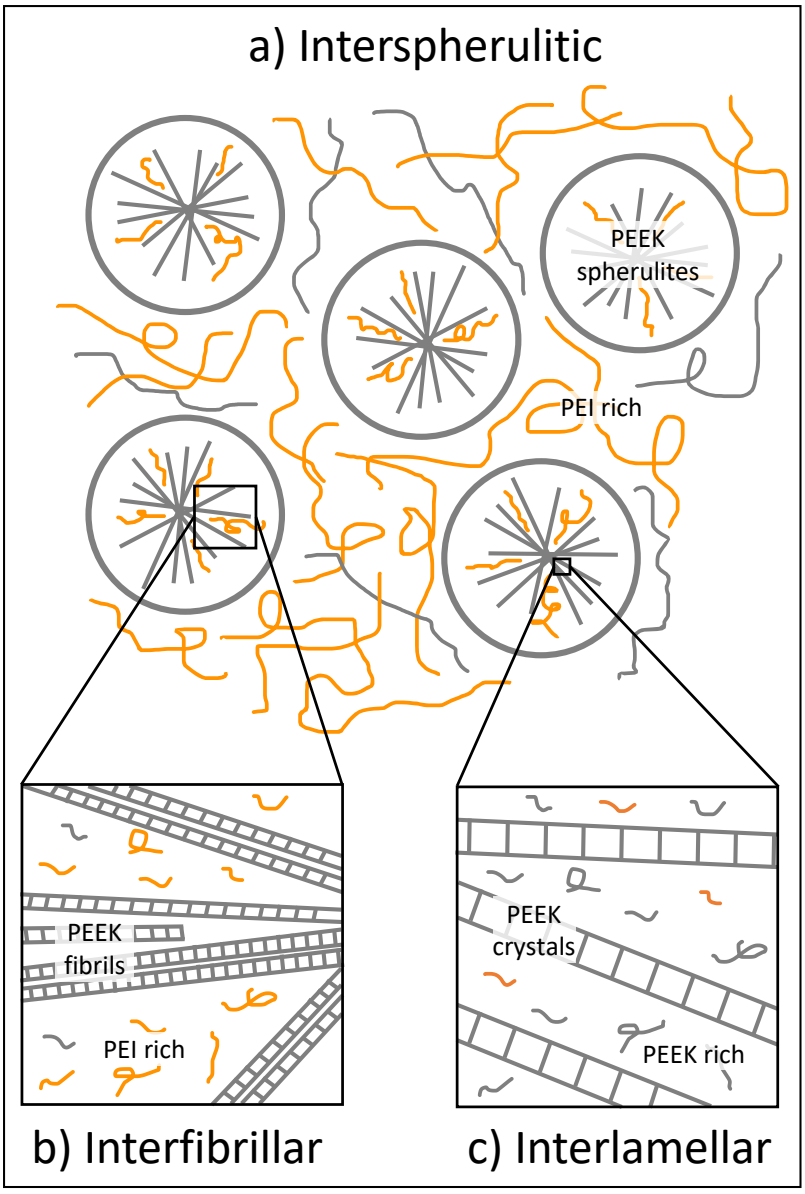

Scheme S4.1: The different possible segregation modes of PEI concerning PEEK's crystallization.

The segregation of PEI has been reported to occur between PEEK crystalline lamellae, and/or fibrils, and/or spherulites – respectively designated as interlamellar, interfibrillar, and interspherulitic segregation, as illustrated in **Scheme S4.1**.

4.5.2 Molecular structures

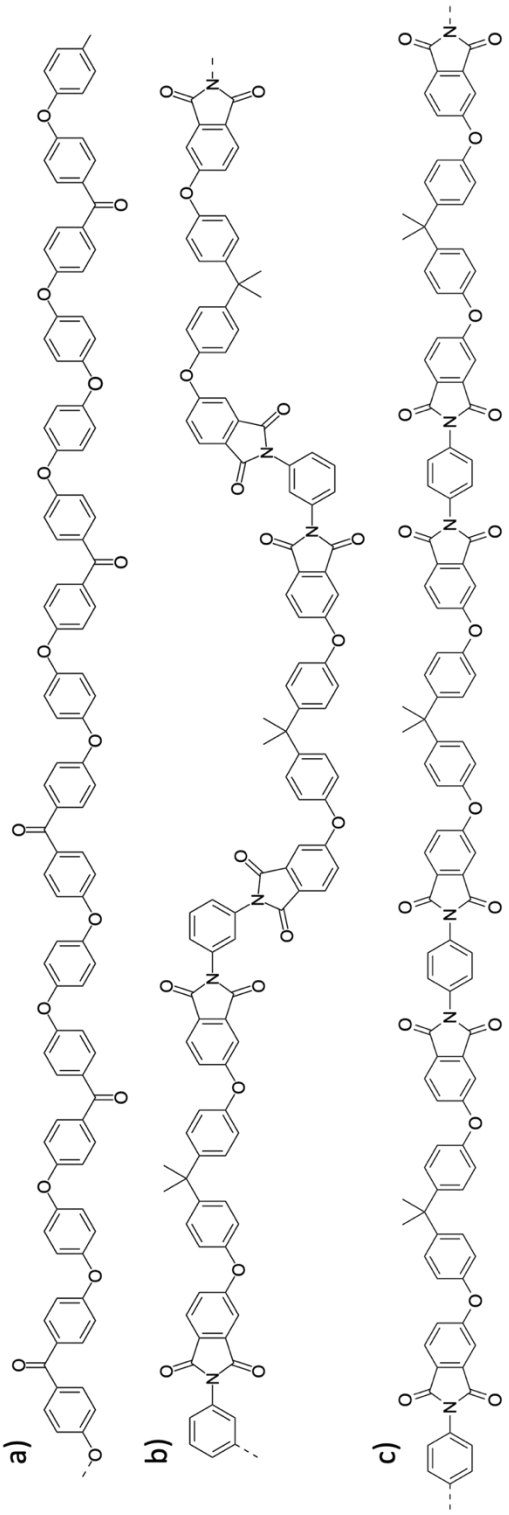

Scheme S4.2: Molecular structures of a) PEEK; b) *meta*-PEI; and c) *para*-PEI

4.5.3 DSC thermograms

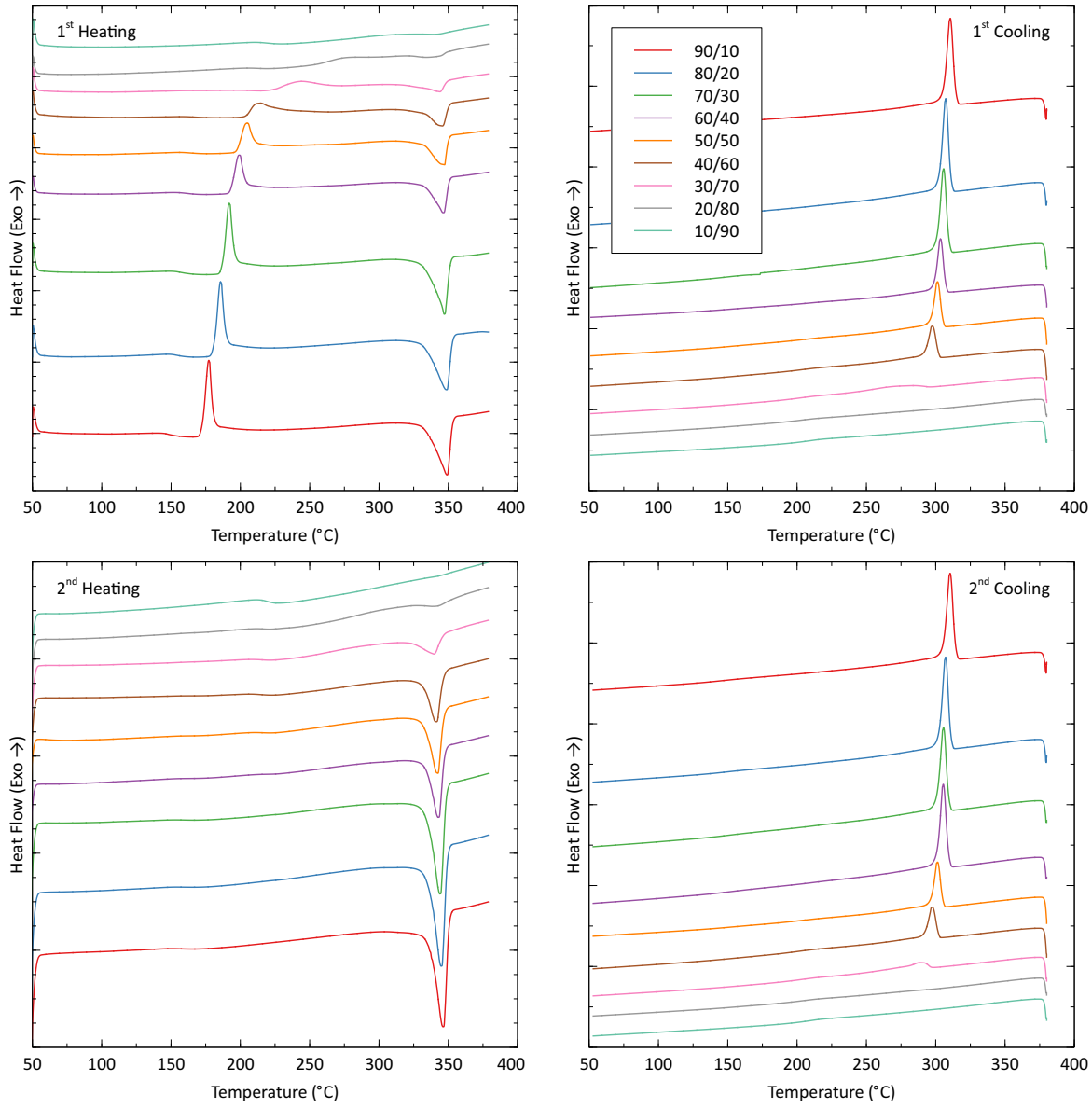

Figure S4.1: DSC thermograms (10°C/min) for the whole composition range for the PEEK/*p*-PEI quenched system.

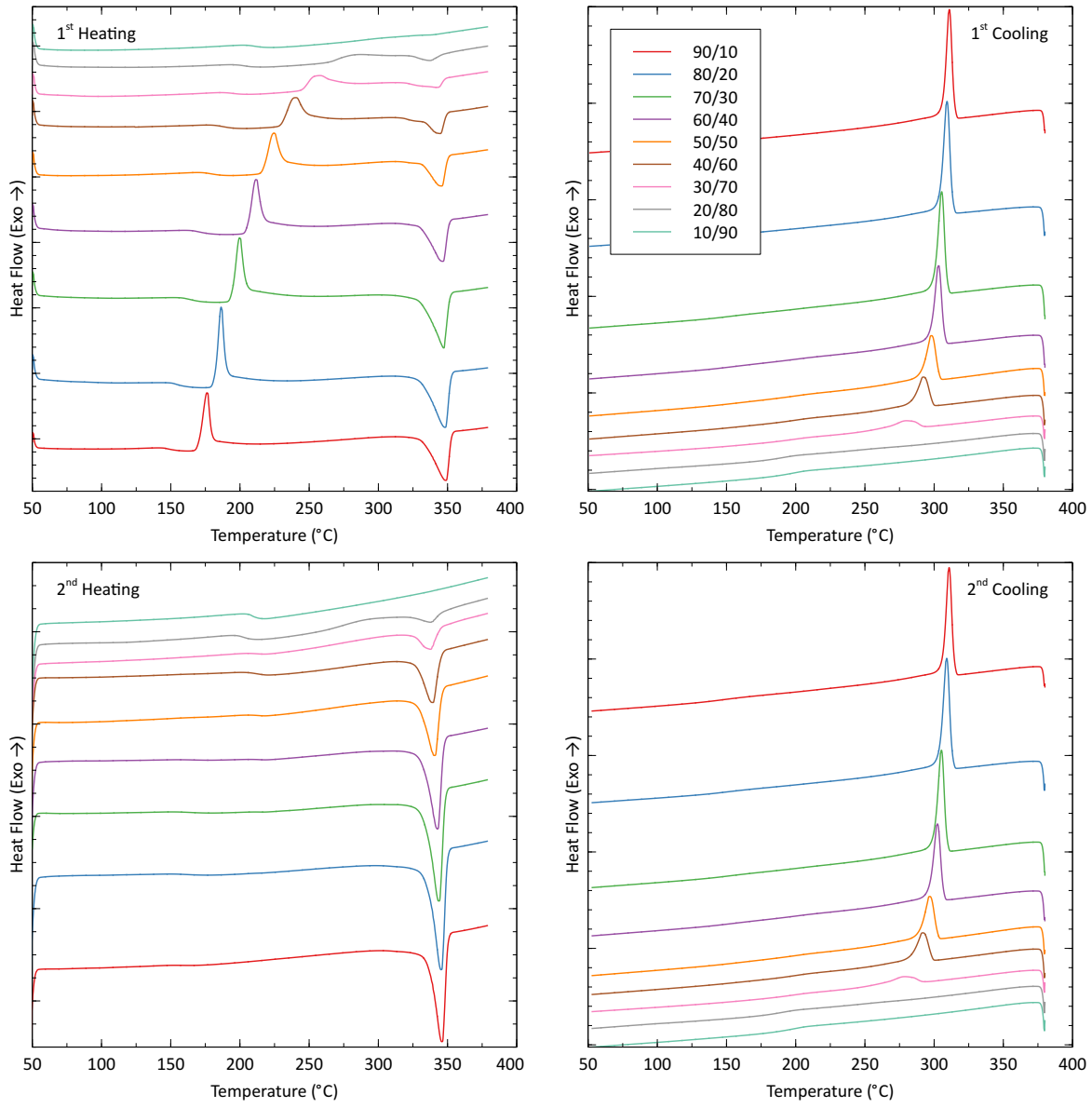

Figure S4.2: DSC thermograms (10°C/min) for the whole composition range for the PEEK/*m*-PEI quenched system.

4.5.4 Breaking thread method

The zero-shear rate viscosities (η_0) of 210 ± 60 Pa.s for PEEK, and 432 ± 55 Pa.s for *p*-PEI_2 (Ultem CRS 5011), were obtained at 375 °C following the procedure described in section 4.2.8 of the Materials and methods of the article. However, because of the apparition at low frequencies of a sharp increase in complex viscosity, the identification of a zero-shear rate viscosity from the Newtonian plateau for the *p*-PEI_2 proved difficult. Hence, some complementary frequency sweep

tests were performed at different temperatures (300, 320, 340, and 360 °C) to monitor the evolution in the Newtonian plateau for the complex viscosity. This work led to two primary conclusions: (1) First, deviations from the plateau value at low frequencies were observed for test temperatures exceeding 320 °C (see **Figure S4.3**). This phenomenon is attributed to the partial thermal degradation of the *p*-PEI_2 samples during the experiments at high temperatures; (2) Secondly, an empirical power-law relationship was identified and links the plateau value of the complex viscosity with the test temperature (see **Figure S4.4**).

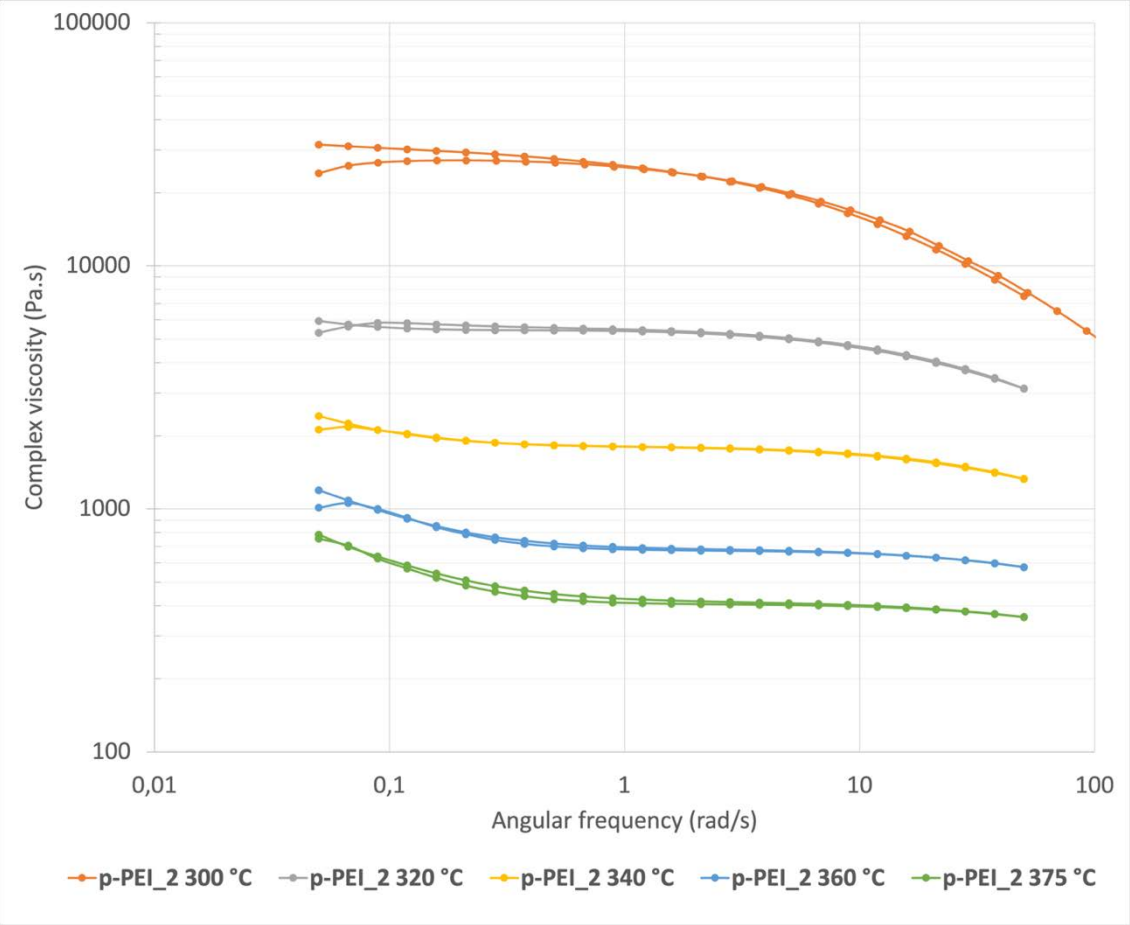

Figure S4.3: Frequency sweep tests performed at different temperatures (300, 320, 340, 360, and 375 °C) for the *p*-PEI_2 (Ultem CRS 5011).

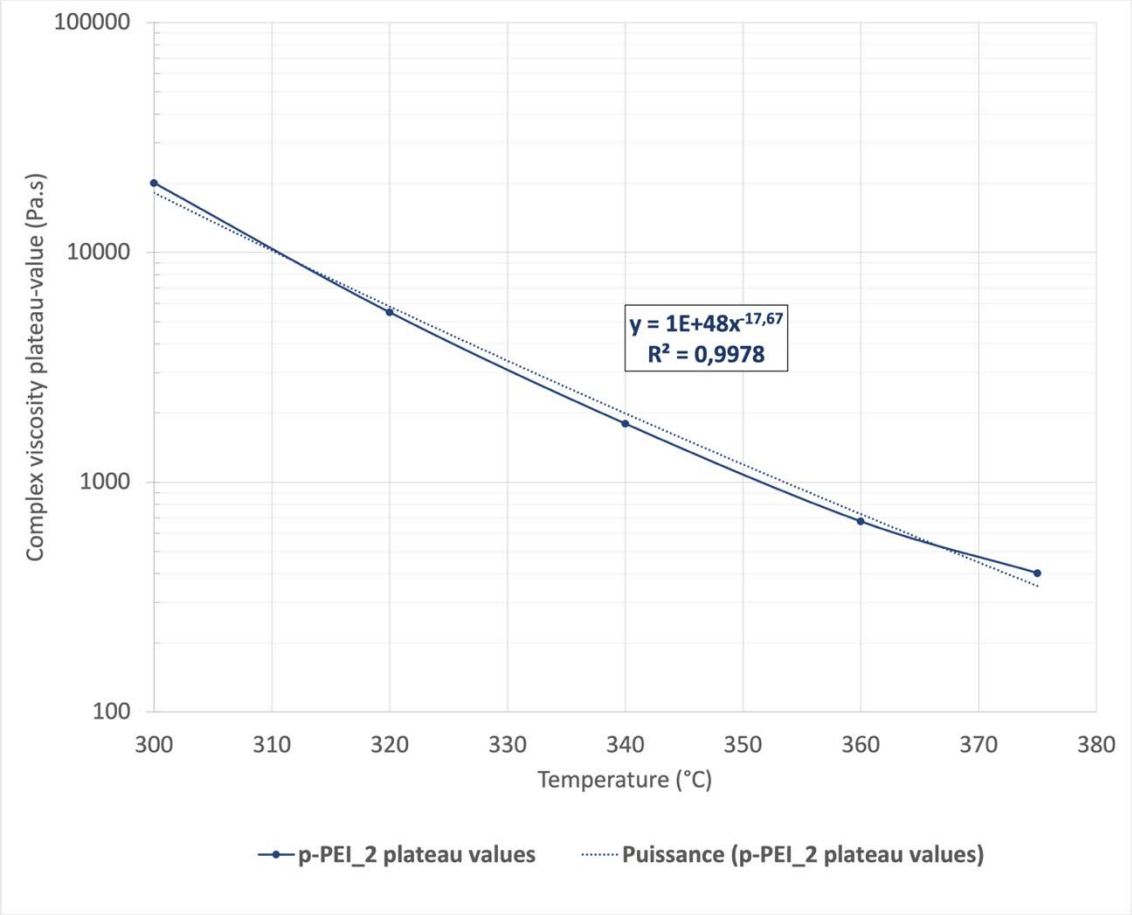

Figure S4.4: Empirical power-law relationship between the plateau value of the complex viscosity and the test temperature for *p*-PEI_2.

Furthermore, at 375 °C, the difference in the value of complex viscosity between the maximum observed at low frequencies (at 0.05 rad/s = 800 Pa.s) and the Newtonian plateau (at 3.75 rad/s = 404 Pa.s) corresponds to roughly 400 Pa.s. However, doubling the *p*-PEI_2 η_0 value does not affect the interfacial tension value much. This is because the omega (Ω) parameter in Equation 4.10, which depends on the viscosity ratio between the two polymers, partly compensates for the increase in η_0 of *p*-PEI_2, resulting only in a small increase in the calculated interfacial tension, from 0.14 ± 0.04 mN/m to 0.18 ± 0.05 mN/m.

4.5.5 Gravimetric analysis

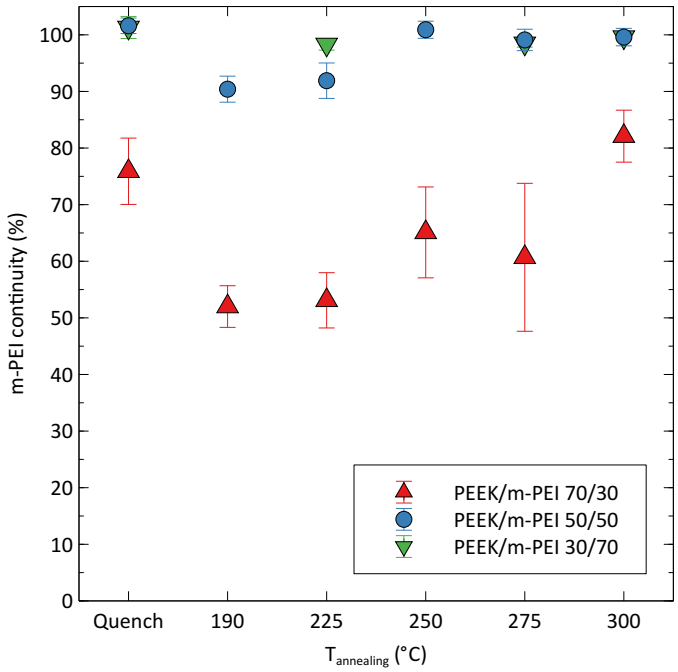

Figure S4.5: *m*-PEI continuity measured by gravimetric analysis as a function of annealing temperature for three PEEK/*m*-PEI compositions.

Figure S4.5 presents the continuity of the *m*-PEI phase for three different PEEK/*m*-PEI compositions, annealed at five different temperatures. As already observed in Figure 4.3 of the article, by increasing the amount of *m*-PEI in the blend we can observe that its continuity is increased too. Interestingly, for each composition under study, the first two temperatures of annealing (190°C and 225°C) always result in lower extraction yields (e.g. *m*-PEI continuity) compared to the quenched blend and annealed blends at higher temperatures. Since these two temperatures are well under and just above the T_g of *m*-PEI, one hypothesis is that the *m*-PEI does not possess enough molecular mobility and gets trapped in between PEEK lamellae or fibrillae when the latter crystallizes. Because crystalline PEEK is less permeable to the solvent than amorphous PEEK, *m*-PEI is hence less accessible to the follow-up attack by the solvent. Above those temperatures, *m*-PEI displays higher chain mobility and gets expelled in between PEEK spherulites which allows for a higher extraction yield compared to the two previous temperatures. Finally, the quenched state seems to always present nearly equal *m*-PEI continuity compared to the three higher annealing temperatures, suggesting a subtle balance between *m*-PEI expulsion from PEEK crystals and the protection to solvent attack/diffusion offered by these same crystals.

4.5.6 PEEK/*m*-PEI 30/70 annealed at 275 and 300 °C

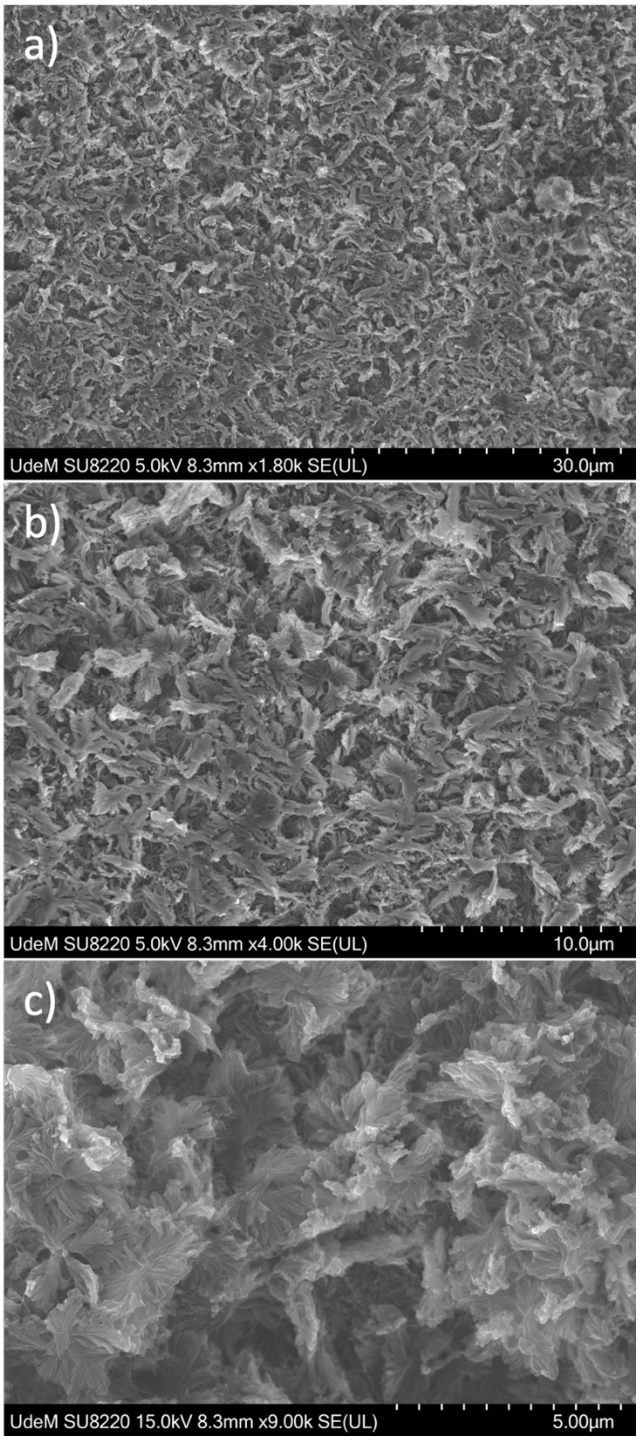

Figure S4.6: SEM micrographs of PEEK/*m*-PEI 30/70 annealed at 275 °C for 5 min. a) magnification 1 800x; b) magnification 4 000x; c) magnification 9 000x.

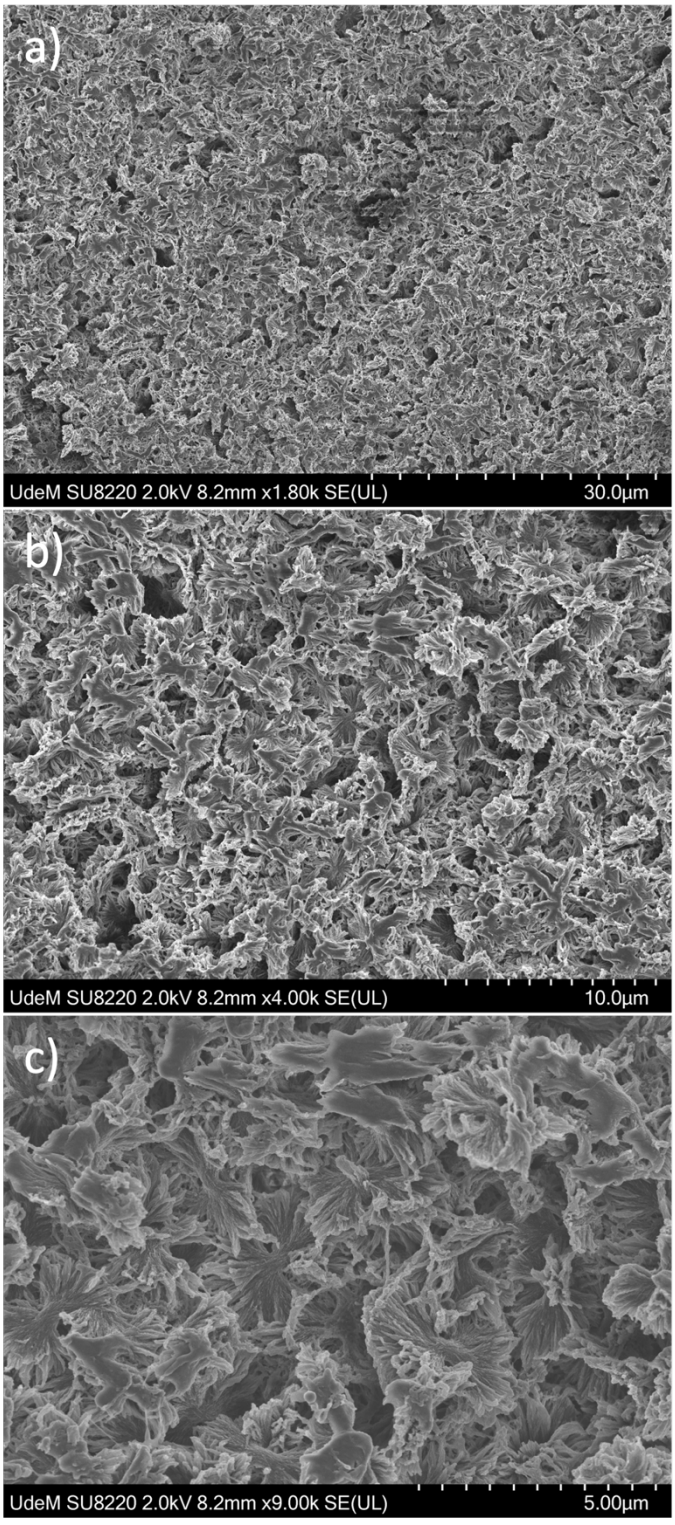

Figure S4.7: SEM micrographs of PEEK/*m*-PEI 30/70 annealed at 300 °C for 5 min. a) magnification 1 800x; b) magnification 4 000x; c) magnification 9 000x.

4.5.7 PEEK/*p*-PEI_2 50/50 blend

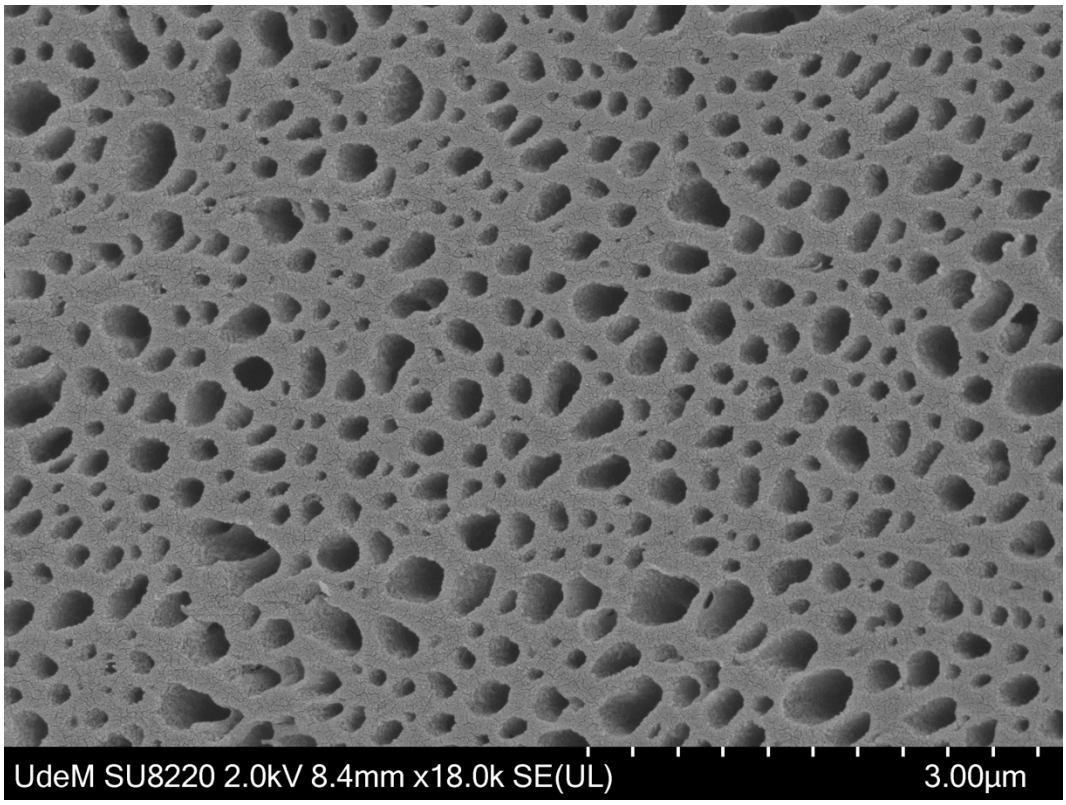

Figure S4.8: SEM micrograph of PEEK/*p*-PEI_2 50/50 quenched blend, displaying a phase-separated microstructure similar to the PEEK/*p*-PEI system.

CHAPTER 5 ARTICLE 2: CONTROLLING AND MODELING PHASE SEPARATION BEHAVIOR IN TERNARY SYSTEMS OF PEEK WITH *META*- AND *PARA*-PEI

*Arthur Lassus, Basil D. Favis, and Nick Virgilio**

CREPEC, Department of Chemical Engineering, Polytechnique Montréal, Montréal, Québec H3T 1J4, Canada

*Corresponding author's E-mail: nick.virgilio@polymtl.ca

Submitted to: *Macromolecules*, 8th August 2025

Abstract

This work presents a novel approach to finely tune the miscibility and morphological features of ternary high-performance polymer systems composed of poly(ether ether ketone) (PEEK) and two isomeric forms of poly(ether imide) (PEI), *meta*-PEI (*m*-PEI) and *para*-PEI (*p*-PEI). By controlling the PEEK, *m*-PEI (miscible with PEEK) and *p*-PEI (partially miscible with PEEK) compositions, processing parameters and thermal history, it is possible to control the level of miscibility of the system, and the resulting microstructural length scale over nearly 4 orders of magnitude - from the nm scale for fully homogeneous systems, to tens of μm's for phase-separated co-continuous networks, without relying on any interfacial compatibilizer. Interestingly, the morphologies of shear-induced miscible states are observed and undergo phase separation upon thermal annealing – a phenomenon seldom reported. To understand and model the thermodynamic interactions and resulting phase diagram, binary Flory-Huggins segmental interaction parameters (χ_{ij}) were calculated from experimental calorimetric data for all three polymer pairs, including two new systems not reported previously in the literature, *i.e.* PEEK/*p*-PEI and *m*-PEI/*p*-PEI. Based on these parameters, a spinodal decomposition curve was computed, which compares relatively well to the

experimental ternary phase diagram. The resulting phase diagram not only offers predictive power for material design but also provides valuable insights into the subtle interplay between structural isomerism and blend miscibility in these high-performance polymer systems. Finally, by selectively extracting both PEIs, porous PEEK monolithic materials can be generated displaying fully interconnected porosities, tunable from a few nm to several μm's in size. This could potentially impact fields encompassing filtration and separation processes, to biomedical material design.

5.1 Introduction

Poly(ether ether ketone) (PEEK) and poly(ether imide) (PEI) are two high-performance polymers with complementary characteristics. PEEK is a semi-crystalline polymer offering excellent chemical resistance and mechanical strength, while amorphous PEI provides a higher glass transition temperature (T_g) and lower cost. Blending PEEK with PEI via melt processing enhances both the thermal behavior and processability, without compromising on mechanical performance [68].

The miscibility of PEEK with *meta*-PEI (*m*-PEI) in the melt state has been confirmed by DSC and DMA [68-75, 106], based on the detection of a single T_g. This behavior is attributed to specific interactions between the PEEK's ether groups and *m*-PEI's imide rings [77], supported by a Flory-Huggins segmental interaction parameter (χ_{ij}) ranging from -0.058 to -0.196 [78]. PEEK crystallization induces *m*-PEI phase separation and segregation into interlamellar, interfibrillar and interspherulitic domains, which vary from nanometer to micrometer length scales depending on processing conditions and thermal treatments [69, 72, 73, 80].

In contrast, PEEK/*para*-PEI (*p*-PEI) blends show partial miscibility and phase-separated morphologies, ranging from sub-μm matrix/dispersed phase to co-continuous morphologies [79, 125]. The very low interfacial tension (0.14 mN/m) still drives coarsening under annealing, with domain sizes reaching tens of micrometers [125]. These morphologies, especially the sub-μm co-continuous networks, reflect a distinct thermodynamic behavior and underscore their promise for tailored material design. However, no work to date has explored the binary combination of *meta*-PEI and *para*-PEI, and their ternary combinations with PEEK.

Ternary polymer blends offer a range of phase behaviors, depending on the miscibility of their constituent binary pairs. Ternary systems can, in theory, range from fully miscible systems (all three polymers are miscible at the molecular level) [97], to fully immiscible [126, 127], with a variety of intermediate behaviors also encompassing partial miscibility [96, 128]. This diversity makes ternary blends an important and quite interesting subject of study in understanding phase separation mechanisms and morphology development, but also for practical applications as it provides a variety of levers, including composition and processing parameters, to tune the mechanical and functional properties. For example, even when all binary pairs are miscible, a ternary blend may phase-separate due to $\Delta\chi$ effects, such as in the poly(methyl methacrylate) (PMMA), poly(ethylene oxide) (PEO) and poly(hydroxy ether of bisphenol-A) (phenoxy) system. The phenomenon in this case arises from subtle differences in interaction parameters, leading to a closed-loop immiscibility region within the ternary phase diagram [129]. Other ternary systems show that replacing a miscible binary pair with a partially miscible one can result in an extended miscibility region, going against what might be intuitively expected at first. This is the case when poly(hexamethylene sebacate) is replaced by poly(hexamethylene adipate) in ternary systems also composed of poly(propylene oxide) and poly(methyl methacrylate-co-*n*-butyl methacrylate) [128]. These examples illustrate the rich morphological landscapes and associated complex physics offered by ternary systems.

In the category of high-performance polymer systems, Chun, et al. [96] investigated solution-cast films of sulfonated PEEK (SPEEK), *m*-PEI, and polycarbonate (PC). SPEEK/*m*-PEI was found to be fully miscible, while SPEEK/PC and *m*-PEI/PC were partially miscible as confirmed by DSC analysis. In this ternary system, phase separation dominated, resulting in a wide two-phases region covering most of the phase diagram. This result was consistent with spinodal predictions based on the calculated binary interaction parameters. Another high-performance ternary system composed of PEEK, *m*-PEI, and a liquid crystalline polymer (LCP) was studied for its synergistic mechanical properties, displaying higher elastic modulus, and ultimate tensile strength, compared to the pure components [98]. This ternary system demonstrated a complex phase behavior originating mainly from the phase-separated domains of crystallized PEEK and LCP fractions, complemented with a fully miscible amorphous fraction [99, 100].

Bicakci and Cakmak [101] conducted a comprehensive investigation on the phase behavior of a melt-processed high-performance ternary system composed of PEEK, *m*-PEI, and poly(ethylene

naphthalate) (PEN) to develop transparent materials displaying a high glass transition temperature. The ternary system exhibited two fully miscible binary pairs (PEEK/*m*-PEI and *m*-PEI/PEN) and one immiscible pair (PEEK/PEN). The authors systematically explored a broad range of compositions across the ternary phase diagram and adopted the presence of a single T_g as a criterion for blend miscibility. By applying this criterion and assuming a known segmental interaction parameter (χ_{ij}) for the PEEK/*m*-PEI binary system, they were able to extract χ_{ij} values for the remaining binary pairs by fitting a spinodal curve model [89] to their experimental results, yielding $\chi_{PEEK/PEN} \approx 0.048$ and $\chi_{PEI/PEN} \approx -0.001$.

PEEK/*m*-PEI/poly(ether sulfone) (PES) ternary blends were also developed to produce hierarchical porous membranes (HPMs) with controllable pore size by varying the overall blend composition. Modifying the content in either PEI or PES allowed tuning of the water flux through the membranes, while retaining high selectivity for water-in-oil emulsion [104].

Despite the few theoretical and experimental studies on ternary polymer blends displaying complex phase diagrams that include miscible and phase-separated domains, gaps remain in understanding systems involving such complex phase behaviors. In addition, detailed morphological investigations remain scarce. This work aims to bridge these gaps in part by analyzing the phase and morphological behavior, and thermal properties, of ternary systems composed of PEEK, *m*-PEI, and *p*-PEI. A theoretical framework is used to calculate all three binary segmental interaction parameters, and the calculated spinodal decomposition line (frontier) is compared with experimental results. Finally, this work assesses the potential of these ternary systems to prepare highly controlled porous PEEK monolithic materials, with an extended range of porosity features in terms of average pore size – from a few nm to several μm – and full pore interconnectivity. Such highly controlled porous PEEK materials could find applications in fields ranging from separation processes (membranes) to biomedical engineering, by selectively extracting both PEIs.

5.2 Materials and methods

5.2.1 Materials

Pellets of poly(ether ether ketone) (PEEK) 90G, poly(ether imides) Ultem 1010 (*meta*-PEI or *m*-PEI), and Ultem CRS 5001 (*para*-PEI or *p*-PEI) were obtained from Victrex and SABIC, respectively, the latter material being sold as a copolymer of PEI. The *para*-diamine nature of

Ultem CRS 5001 was reported by several authors [79, 107]. **Table 5.1** summarizes some of their main properties.

Table 5.1 PEEK and PEIs main properties

	Density ρ_0 Room T (g/cm^3) [a]	Density ρ_m extrapolated at 375 °C (g/cm^3) [b]	M_0 [d] (g/mol)	M_n (g/mol)	M_w (g/mol)	Torque at plateau (N·m)[f]	T_g (°C) [g]	ΔC_p (J/g°C) [g]
PEEK	1.30	1.09	288.30	22 380 [a]	59 680 [a]	0.77	141/ 147	0.313
m-PEI	1.27	1.18	592.61	20 100 [e]	47 500 [e]	1.48	215/ 217	0.226
p-PEI	1.28	1.18 [c]	592.61	15 657 [c]	37 000 [b]	3.80	225/ 227	0.217

[a] Provided by the supplier.

[b] Based on references [79, 130, 131].

[c] Based on the hypothesis that *p*-PEI has similar properties to *m*-PEI (*i.e.* density & PDI = 2.36).

[d] Molar mass of the polymer repeating unit.

[e] Measured by GPC in chloroform at 35 °C.

[f] In internal mixer at 370 °C and 50 rpm.

[g] Measured by DSC on the 1st/2nd heating cycles.

5.2.2 Blend preparation

Ternary blends of PEEK/*m*-PEI/*p*-PEI were melt-processed over nearly the full composition spectrum. The blends are denoted as PEEK vol%/*m*-PEI vol%/*p*-PEI vol% throughout this work. Before melt processing, all polymers were dried under vacuum at 100 °C for 24 h. Blends were prepared with a micro-compounder (DSM Xplore, mixing volume of 5 cc), in which the temperature and screw speed were set at 370 °C and 50 rpm, respectively. Drawing on previous experiments, once all of the polymer pellets were loaded into the micro-extruder, the mixing time

was set at 6 min in recirculation mode. After mixing, a ≈ 30 cm filament was extruded and immediately quenched in an ice water bath to preserve the morphology from the melt state. **Figure S5.1** indicates the ternary systems that were prepared on the corresponding triangular composition diagram.

5.2.3 Quiescent annealing

Prior to a standard quiescent annealing experiment, ≈ 1 cm long segments of quenched ternary blend filaments were dried under vacuum at 100 °C for 24 h. The filaments were then wrapped in aluminum foil pre-coated with a boron nitride-based release agent (Momentive, United States). Annealing was conducted using a Carver high-temperature hydraulic press at 380 °C, exceeding the melting temperature of PEEK (> 345 °C), for various periods of time ranging from 5 to 30 min. Immediately after annealing, the samples were quenched in an ice water bath to preserve the resulting morphology.

5.2.4 Morphological analysis

To examine the microstructure of the ternary blends, scanning electron microscopy (SEM, HITACHI Regulus 8220) was employed. The sample surfaces were prepared at ambient temperature using a Leica RM2165 microtome equipped with a glass knife. Imaging was consistently conducted at the center of the filament cross-section to reduce potential skin effect influence. For enhanced contrast, the PEIs (*m*-PEI and *p*-PEI) were selectively extracted with a solvent composed of 80 vol% 1-methyl-2-pyrrolidone, 10 vol% ethanolamine, and 10 vol% deionized water [83].

After extraction, the continuity of the PEIs within the blends was assessed by gravimetric analysis. Typically, three filament segments of ≈ 1 cm in length (around 100 mg total) were dried under vacuum at 100 °C for 24 h and then weighed. The samples were then immersed in the selective solvent at 120 °C for 1 h [83]. They were next rinsed and immersed for 5 min twice in ethanol and twice in deionized water, followed by freeze-drying for two days, after which they were weighed again.

The continuity of the PEIs was calculated using **Equation 5.1**:

$$PEIs\ continuity\ (\%) = \frac{m_i - m_f}{m_i} \times \frac{m_{blend}}{m_{PEIs\ in\ blend}} \times 100 \tag{5.1}$$

where m_i is the initial sample mass before extraction, m_f is the mass after extraction, m_{blend} is the mass of the original blend, and $m_{PEIs\ in\ blend}$ is the mass of PEIs in the original blend. It was noted that PEEK absorbed a small amount of solvent during extraction, approximately 1 wt% for recrystallized PEEK and 3.3 wt% for amorphous PEEK. Consequently, a minor correction was applied to account for this in the sample mass loss calculation, depending on the crystallinity and PEEK content in the samples.

Finally, prior to SEM analysis, an approx. 8 nm carbon layer was deposited on the samples using a Leica EM ACE600, and imaging was performed at an accelerating voltage of 2 kV with a 10 µA current.

5.2.5 Thermal analysis

The neat polymers, binary, and ternary blends were analyzed by differential scanning calorimetry (DSC, TA instruments Q2000). The protocol consisted in two heat/isotherm/cool cycles: (1) heating from 50 °C to 380 °C at 10 °C/min, an isotherm of 3 min at 380 °C, cooling to 50 °C at 10 °C/min; (2) heating again to 380 °C at 10 °C/min, an isotherm of 3 min at 380 °C, and finally cooling to 50 °C at 10 °C/min. Glass transition temperatures (T_g) were measured as the inflection points of the baseline during the first and second heating ramps. The ΔC_p*'s* were calculated from the difference between the heat capacities C_p^l (over the glass transition temperature) and C_p^g (under the glass transition temperature), measured 5 °C after the end and 5 °C before the onset of the T_g transition, respectively. All DSC data are provided in **Table S1**.

5.2.6 Calculations of χ_{ij} parameters for the binary systems

5.2.6.1 Monophasic (miscible) binary systems: PEEK/*m*-PEI and *m*-PEI/*p*-PEI

The Gordon-Taylor model was used to fit the T_g data from the first DSC heating cycle, for quenched miscible binary mixtures. With this method, each system, e.g. PEEK/*m*-PEI and *m*-PEI/*p*-PEI, demonstrates a specific fitting parameter K_{ij}.

For the PEEK/*m*-PEI system:

$$T_{g12} = \frac{\omega_1 T_{g1} + K_{12}\omega_2 T_{g2}}{\omega_1 + K_{12}\omega_2} \tag{5.2}$$

where "1" denotes PEEK and "2" the *m*-PEI for the rest of this work. T_{g12} is the T_g of the mixture, ω_i is the weight fraction of polymer *"i"* in the binary blend, T_{gi} is the T_g of neat polymer *"i"*, and K_{12} is a fitting parameter.

For the *m*-PEI/*p*-PEI system:

$$T_{g23} = \frac{\omega_2 T_{g2} + K_{23}\omega_3 T_{g3}}{\omega_2 + K_{23}\omega_3} \tag{5.3}$$

where "2" denotes the *m*-PEI and "3" the *p*-PEI for the rest of this work. T_{g23} is the T_g of the mixture, ω_i is the weight fraction of polymer *"i"* in the binary blend, T_{gi} is the T_g of neat polymer *"i"*, and K_{23} is a fitting parameter.

Based on the work of Lu and Weiss [66], the interaction parameter χ between two miscible polymers *"i"* and *"j"* can be directly related to the T_g of their blend (T_{gm}) with **Equation 5.4:**

$$T_{gm} = \frac{\omega_i T_{gi} + k\omega_j T_{gj}}{\omega_i + k\omega_j} + \frac{A\omega_i\omega_j}{(\omega_i + k\omega_j)(\omega_i + b\omega_j)(\omega_i + c\omega_j)^2} \tag{5.4}$$

with

$$A = \frac{\chi R(T_{gi} - T_{gj})c}{M_i \Delta C_{pi}} \tag{5.5}$$

$$k = \frac{\Delta C_{pj} - \omega_i \delta C_p^l}{\Delta C_{pi} - \omega_j \delta C_p^g} \tag{5.6}$$

$$b = \frac{M_{0j}}{M_{0i}} \tag{5.7}$$

$$c = \frac{\rho_i}{\rho_j} \tag{5.8}$$

where ω_i is the weight fraction of polymer *"i"* in the binary blend, T_{gi} is the T_g of neat polymer *"i"*, χ is the binary interaction parameter between the two polymers, R is the ideal gas constant, ΔC_{pi} is the difference in specific heat at constant pressure for polymer *"i"* between its liquid and glassy states, δC_p are the specific heat changes resulting from blending and are generally

considered negligible [66], M_{0i} is the molar mass of the monomer of polymer *"i"*, and ρ_i is the density of polymer *"i"*. The same notations hold true for polymer *"j"*.

χ can also be calculated from K_{ij} from the Gordon-Taylor fit, based on Equations 23 & 17 from the work of Lu and Weiss [66], from which the following **Equation 5.9** is derived:

$$\chi = \frac{(K_{ij} - k)(T_{gj} - 1)(M_i \Delta C_{pi})}{R(T_{gi} - T_{gj})c} \tag{5.9}$$

where the terminology is the same as defined for Equations 5.4 to 5.8.

To obtain the segmental binary interaction parameter χ_{ij}, the χ parameter obtained from Equations 5.4 & 5.9 needs to be divided by the number of lattice sites present in the PEEK and PEIs molecules with reference to the monomer molar volume of PEEK (V_0), chosen as the reference in this work. V_0 was calculated using the values from Table 4.1 ($V_0 = M_0/\rho_{m,PEEK}$ = 265.24 cm^3/mol), which is similar to a value found in the literature [101]. χ_{ij} is then obtained from **Equation 5.10**:

$$\chi_{ij} = \frac{2.V_0.\chi}{\frac{M_{ni}}{\rho_{0i}} + \frac{M_{nj}}{\rho_{0j}}} \tag{5.10}$$

where M_{ni} is the number average molecular weight of polymer *"i"*, and ρ_{0i} is its density at room temperature. Their ratio provides an estimate of the molar volume of one macromolecule of polymer *"i"*. The same notations are used for polymer *"j"*.

5.2.6.2 Biphasic binary systems: PEEK/*p*-PEI

Based on the work of Kim and Burns [67], the interaction parameter between two partially miscible polymers can be evaluated from the T_g of the phases in equilibrium, considering that at equilibrium the chemical potential of each component is identical in the coexisting phases. From our previous work, the compositions of the phases at equilibrium in the PEEK/*p*-PEI blends are known (see also **Table S2**, with the crystallinity of PEEK associated entirely to the $PEEK_{rich}$ phase) [125]. Then:

$$\chi_{13} = \frac{\ln\left(\frac{\phi_1''}{\phi_1'}\right) + \left(1 - \frac{m_1}{m_3}\right)(\phi_3'' - \phi_3')}{m_1\left(\phi_3'^2 - \phi_3''^2\right)} \tag{5.11}$$

$$\chi_{31} = \frac{\ln\left(\frac{\phi_3''}{\phi_3'}\right) + \left(1 - \frac{m_3}{m_1}\right)(\phi_1'' - \phi_1')}{m_3\left(\phi_1'^2 - \phi_1''^2\right)} \tag{5.12}$$

where ' denotes the $PEEK_{rich}$ phase, and '' the PEI_{rich} phase. ϕ_i is the volume fraction of polymer *"i"* in the denoted phase. For example, ϕ'_3 is the volume fraction of *p*-PEI in the $PEEK_{rich}$ phase. m_i is the number of lattice sites considered per molecule, comparing the molar volumes V_1 and V_3 of the polymers to the molar volume V_0 of one monomer of PEEK, so $m_i = (M_{ni}/\rho_{0i})/V_0$ (equivalent to the approach in **Equation 5.10**). The results from **Equations 5.11 & 5.12** have then been averaged (in theory, $\chi_{13} = \chi_{31}$).

5.2.6.3 Spinodal curve calculation

Based on the work of Zeman and Patterson [89], **Equation 5.13** represents the spinodal curve in the Flory-Huggins formalism:

$$m_1\phi_1 + m_2\phi_2 + m_3\phi_3 - 2[m_1m_2(\chi_1 + \chi_2)\phi_1\phi_2 + m_2m_3(\chi_2 + \chi_3)\phi_2\phi_3 + m_1m_3(\chi_1 + \chi_3)\phi_1\phi_3] + 4m_1m_2m_3(\chi_1\chi_2 + \chi_2\chi_3 + \chi_1\chi_3)\phi_1\phi_2\phi_3 = 0 \tag{5.13}$$

with

$$\chi_1 = \frac{\chi_{12} + \chi_{13} - \chi_{23}}{2} \tag{5.14a}$$

$$\chi_2 = \frac{\chi_{23} + \chi_{12} - \chi_{13}}{2} \tag{5.14b}$$

$$\chi_3 = \frac{\chi_{13} + \chi_{23} - \chi_{12}}{2} \tag{5.14c}$$

where ϕ_i is the volume fraction of polymer *"i"* in the ternary blend, m_i is the degree of polymerization of polymer *"i"*, and χ_{ij} is the segmental binary interaction parameter between polymer *"i"* and *"j"* calculated from Equations 5.10, 5.11, and 5.12.

To plot the spinodal curve, ternary blend compositions were varied by increments of 0.1 vol% of each component, and the result of Equation 5.13 was then calculated for each increment. Only compositions giving an equation result equal to 0 ± 0.1 were used to plot the spinodal curve on the triangular composition diagram.

5.3 Results and Discussion

5.3.1 Morphology of binary and ternary systems

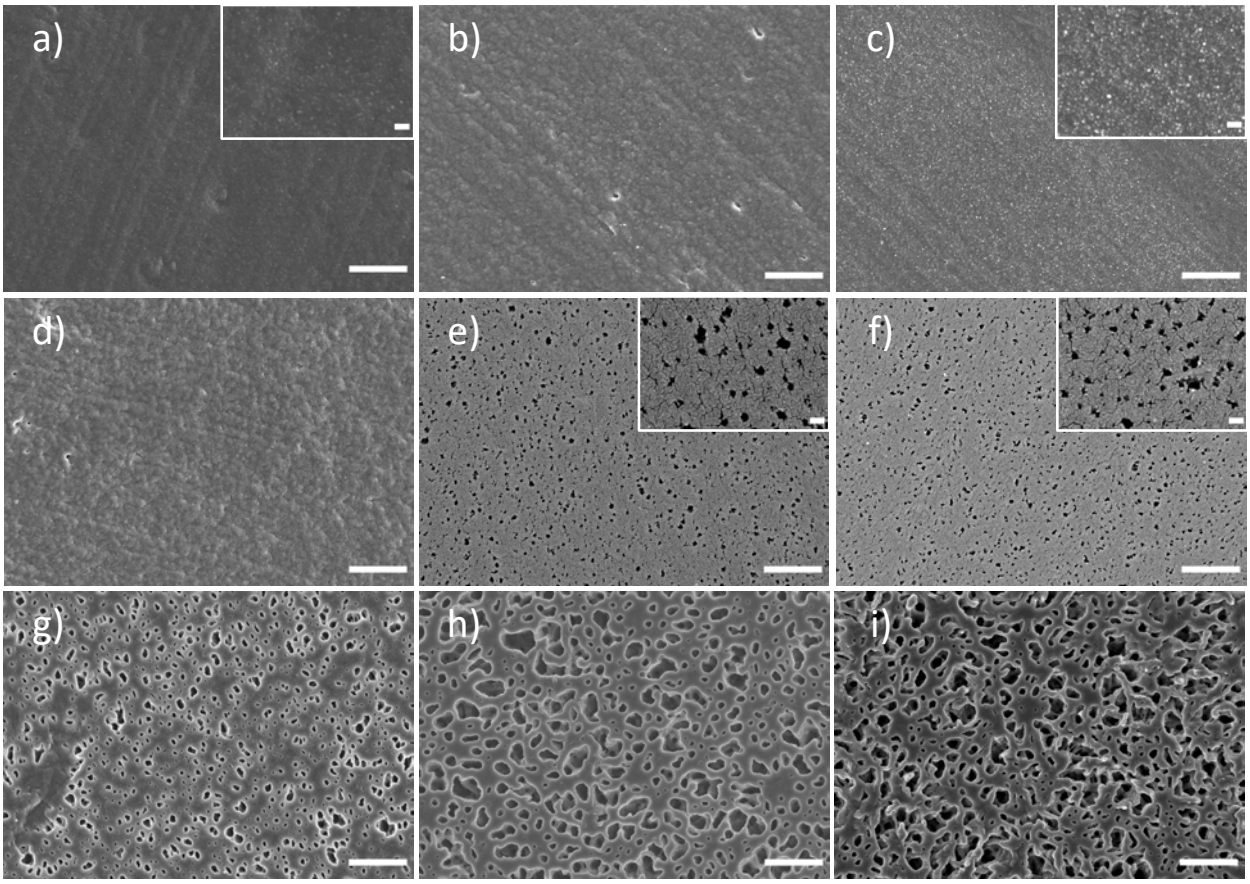

Figure 5.1 Morphology of quenched binary and ternary PEEK/*m*-PEI/*p*-PEI blends as revealed after the selective extraction of both PEIs. Compositions in vol%: a) PEEK/*m*-PEI 50/50; b) 50/37.5/12.5; c) 50/25/25; d) 50/20/30; e) 50/17.5/32.5; f) 50/15/35; g) 50/12.5/37.5; h) 50/5/45; i) PEEK/*p*-PEI 50/50. The white scale bars represent 1 µm for main magnification and 100 nm for the close-up inset micrographs.

Figure 5.1 presents the morphology of melt-processed ternary PEEK/*m*-PEI/*p*-PEI blends quenched in ice-cold water after exiting the micro-compounder, and after the selective extraction of both PEIs to increase contrast. In this series of micrographs, the volume fraction of PEEK is held constant at 50 vol%, while *m*-PEI is progressively substituted for *p*-PEI, thereby covering a significant portion of the 50 vol% PEEK isopleth in the ternary composition diagram (see blue arrow in Figure S5.1).

Figure 5.1a to c reveal homogeneous blends after PEI extraction. Figure 5.1a corresponds to the PEEK/*m*-PEI 50/50 system, which is fully miscible in the melt state [69, 71, 125]. Substituting a small amount of *m*-PEI by *p*-PEI still results in full blend miscibility, as no phase-separated domains are observed (or they are smaller than the SEM detection limit of a few nm). The transition from Figure 5.1c to d reveals a first noticeable morphological change: the surface appears rougher in Figure 5.1d, suggesting the onset of a miscibility transition, although no distinct phase-separated domains are yet resolved. A small increase in *p*-PEI content (by 2.5 vol%) leads to the emergence of visibly phase-separated PEI_{rich} domains, as seen in Figure 5.1e. This morphology is characterized by what appears to be interconnected mesopores with an average size of ~ 32 nm. As the *p*-PEI fraction increases further, the microstructure gradually becomes coarser, until the maximum domain size is reached when all *m*-PEI has been substituted by *p*-PEI. The PEIs extraction yield is also nearly complete in all cases at approx. 100%. This indicates the formation of a fully percolated network of PEI in all cases. Overall, the morphology transitions from a fully miscible system (PEEK/*m*-PEI) to a partially miscible system (PEEK/*p*-PEI) by the gradual substitution of *m*-PEI by *p*-PEI, accompanied by a transition from mesopores (a-f) to macropores (g-i). By selectively extracting the PEIs, porous PEEK monoliths with a high level of control over the porosity features can be prepared. To the best of our knowledge, this is the first time that such a range of PEEK monoliths are reported.

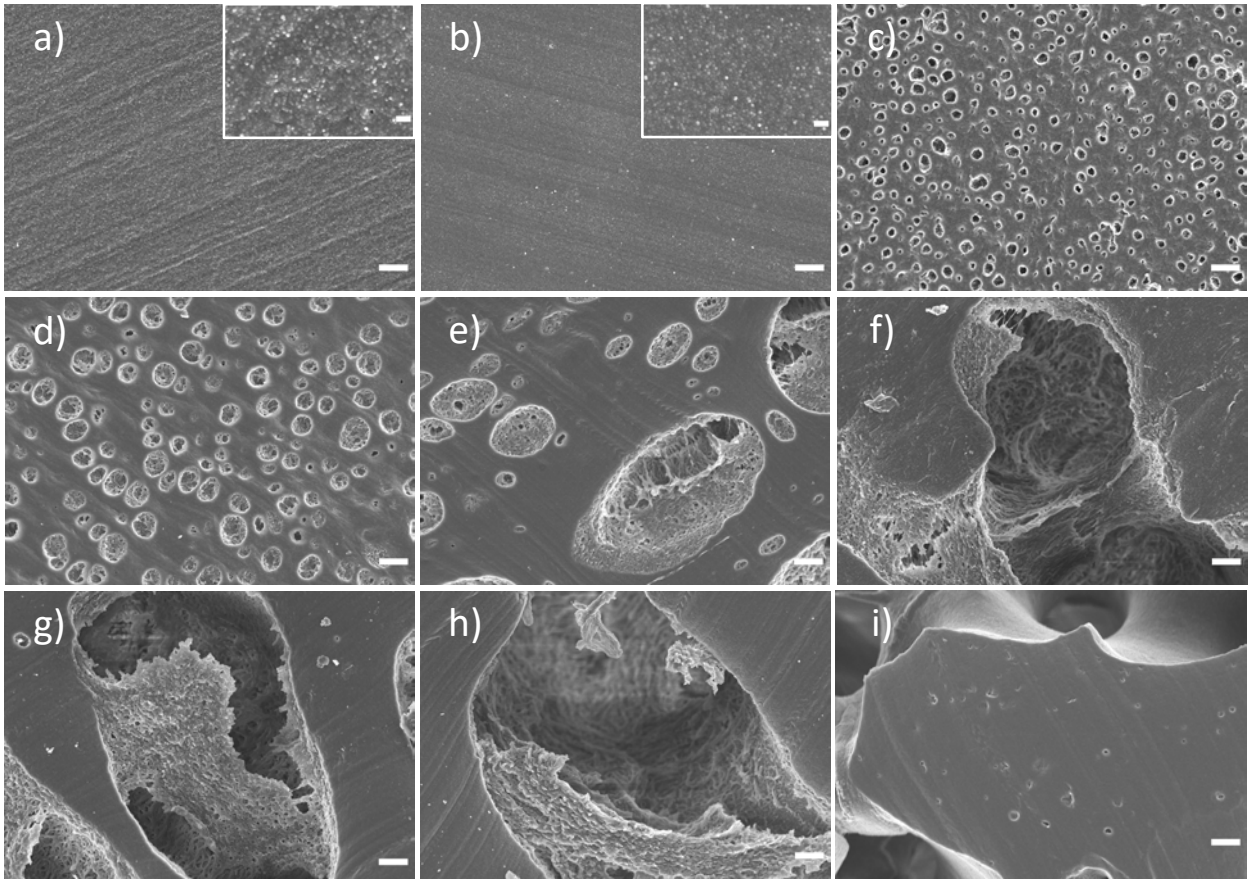

Figure 5.2 Morphology of binary and ternary PEEK/*m*-PEI/*p*-PEI blends, obtained after 15 min of quiescent annealing time at 380 °C and followed by the selective extraction of both PEIs. Compositions in vol%: a) PEEK/*m*-PEI 50/50; b) 50/37.5/12.5; c) 50/25/25; d) 50/20/30; e) 50/17.5/32.5; f) 50/15/35; g) 50/12.5/37.5; h) 50/5/45; i) PEEK/*p*-PEI 50/50. The white scale bars represent 1 µm for main magnification and 100 nm for the close-up inset micrographs.

To further differentiate miscible systems from immiscible ones, and identify the miscibility limit, Figure 5.2 shows the morphological evolution of the same melt-processed PEEK/*m*-PEI/*p*-PEI ternary blends as in Figure 5.1, following 15 min of quiescent annealing at 380 °C (micrographs at lower magnifications are also presented in **Figure S5.2**).

In Figure 5.2b, the 50/37.5/12.5 blend exhibits no discernible phase separation after annealing, similar to the fully miscible binary 50/50 PEEK/*m*-PEI system (Figure 5.2a, as reported previously) [125]. This morphological homogeneity after annealing confirms that the substitution of 12.5 vol% of *m*-PEI by *p*-PEI does not disrupt the miscibility of the blend, indicating a composition still within the single-phase region.

In contrast, the compositions in Figure 5.2c and d (50/25/25 and 50/20/30, respectively) display morphologies characterized by discrete, dispersed spherical domains embedded within a continuous $PEEK_{rich}$ matrix, after annealing. Such droplet-like structures are reminiscent of a nucleation-and-growth phase separation mechanism, suggesting that these blends could reside within the binodal region of the phase diagram. It also demonstrates the importance of annealing under quiescent conditions to allow these systems to relax towards their thermodynamic equilibrium state to avoid misinterpretations: the apparently homogeneous, miscible systems in Figure 5.1c and d are in fact unstable and phase separate. Then, intermediate morphologies are observed in Figure 5.2e and f (50/17.5/32.5 and 50/15/35), where both dispersed droplets and emerging interconnected domains coexist, potentially indicating a transition between binodal decomposition and the onset of spinodal-like features (see also Figure S5.2e and f).

Finally, Figure 5.2g-i, including the binary PEEK/*p*-PEI 50/50 blend, reveal a well-developed co-continuous phase morphology with clear signs of domain coalescence and coarsening compared to features observed in Figure 5.2a-d, and Figure 5.1. These morphological variations indicate that gradually substituting *m*-PEI by *p*-PEI (at 50 vol% PEEK) maintains full miscibility up until 12.5 vol% of *p*-PEI, followed by phase separation by what looks like a nucleation-and-growth mechanism (binodal decomposition) up until approx. 32.5 vol% of *p*-PEI, and then followed by spinodal decomposition at even higher *p*-PEI compositions.

We can also note the presence of residual PEEK within the PEI_{rich} phase in Figure 5.2e-h (see also Figure S5.2e-h) (in this case, no ultrasonic cleaning treatment was applied after the solvent extraction process), confirming that each phase indeed contains all three polymers. In contrast, the binary PEEK/*p*-PEI 50/50 blend shown in Figure 5.2i (and Figure S5.2i) was cleaned in an ultrasonic bath following extraction, rendering the surface of the pores completely smooth.

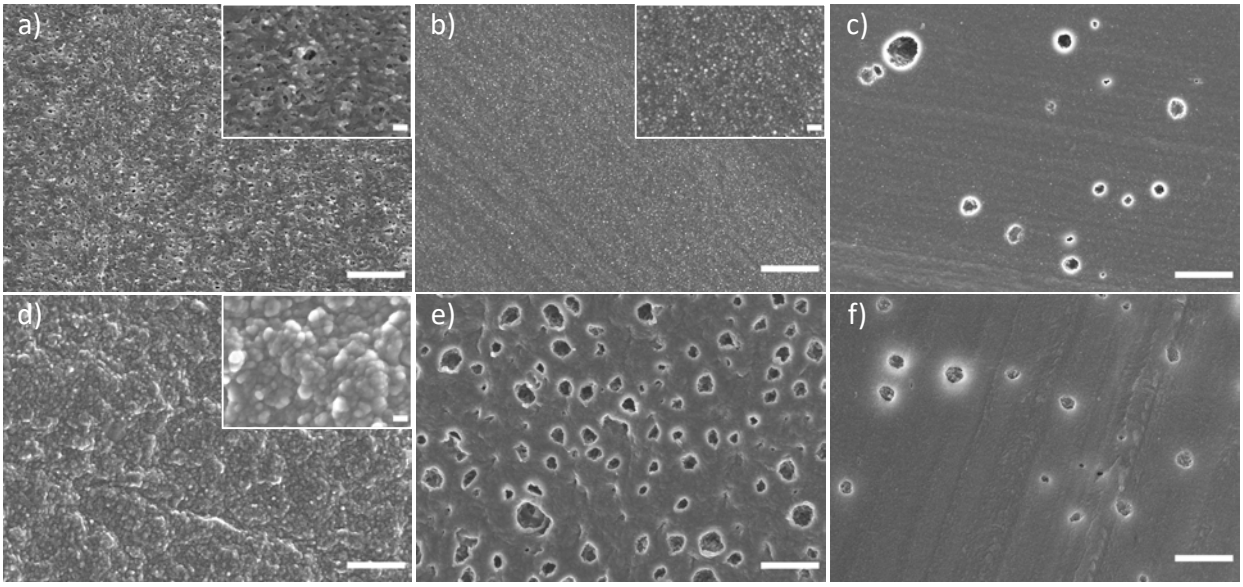

Figure 5.3 Morphology of ternary PEEK/*m*-PEI/*p*-PEI quenched blends right after melt-processing (Q), or following 15 min of quiescent annealing time at 380 °C (C15), after the selective extraction of both PEIs. Compositions in vol%: a) 20/40/40 Q; b) 50/25/25 Q; c) 70/15/15 Q; d) 20/40/40 C15; e) 50/25/25 C15; f) 70/15/15 C15. The white scale bars represent 1 μm for main magnification and 100 nm for the close-up inset micrographs.

Figure 5.3 displays the morphology of three ternary PEEK/*m*-PEI/*p*-PEI compositions, both in the quenched state (Q) and after 15 minutes (C15) of quiescent annealing at 380 °C. Unlike the blends shown in Figure 5.1 and 5.2, these compositions are located along a distinct isopleth in which the *m*-PEI/*p*-PEI ratio is held constant at 1:1, while the volume fraction of PEEK is systematically varied (see red arrow in Figure S5.1).

The 20/40/40 blend, shown in Figure 5.3a and d, displays no apparent phase separation, even after thermal annealing, which is consistent with a miscible system at the molecular level. Interestingly, the quenched sample in Figure 5.3a exhibits the presence of mesopores, which arises from the low volume fraction of diluted PEEK in the blend, combined with the solvent-induced, PEEK crystallization-induced phase segregation, in which PEI_{rich} regions are excluded during the growth of PEEK crystalline domains. The presence of a single glass transition temperature in the second DSC heating cycle, equal to the one measured on the first cycle (see Table S1), supports the hypothesis of full miscibility or at least highly intimate mixing at the nanoscale. Both PEIs are extracted at 100%, yielding a highly porous, mesoporous PEEK monolith.

Figure 5.3b and e correspond to the 50/25/25 composition, previously discussed in Figure 5.1 and 5.2, and serves here as a comparative reference point within this second isopleth – the system appears homogeneous right after processing, and undergoes phase separation during annealing. The 70/15/15 blend, shown in Figure 5.3c and f, reveals a morphology consisting of discrete dispersed domains even in the quenched state, which persists after annealing with little evidence of domain coalescence or growth. The high PEEK content likely promotes a dominant continuous phase, limiting the coalescence of the PEI_{rich} domains during annealing. The frontier between monophasic and biphasic systems is then located between the 50/25/25 and 70/15/15 compositions.

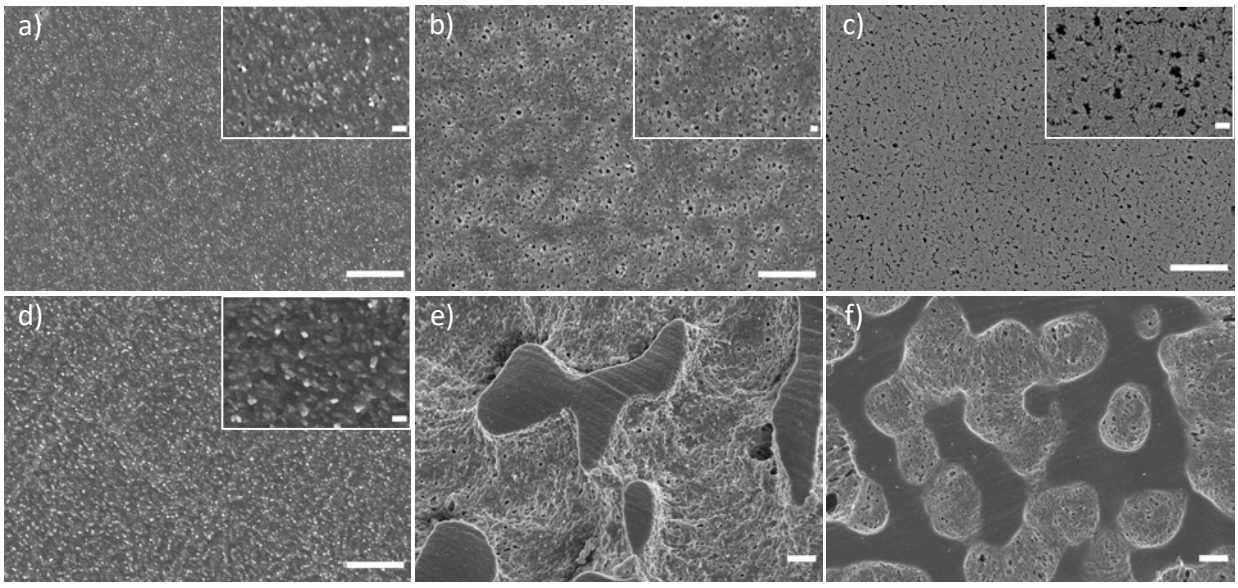

Figure 5.4 Morphology of ternary PEEK/*m*-PEI/*p*-PEI blends quenched (Q) or following 15 min of quiescent annealing at 380 °C (C15) obtained after the selective extraction of both PEIs. Compositions in vol%: a) 30/60/10 Q; b) 30/20/50 Q; c) 40/24/36 Q; d) 30/60/10 C15; e) 30/20/50 C15; f) 40/24/36 C15. The white scale bars represent 1 µm for main magnification and 100 nm for the close-up inset micrographs.

Figure 5.4 displays the morphology of three additional ternary PEEK/*m*-PEI/*p*-PEI blends, in both their quenched state (Q) and after 15 minutes of quiescent annealing at 380 °C (C15) (see higher magnifications in **Figure S5.3**). These compositions were selected to complement the morphological exploration of the ternary composition diagram. The 30/60/10 composition, shown in Figure 5.4a and d, exhibits a homogeneous morphology before and after annealing, consistent with a miscible blend. The presence of sub-micrometric pores in the quenched sample is attributed again to the solvent-induced crystallization of PEEK, which locally excludes the PEI phase -

similar to what was previously observed for the 20/40/40 blend in Figure 5.3. In that case, a highly porous, mesoporous PEEK monolith is also obtained, with more robust mechanical properties considering the higher composition in PEEK.

In contrast, the two remaining compositions clearly exhibit phase-separated morphologies and coarsening upon annealing. The 30/20/50 (Figure 5.4b and e) and 40/24/36 (Figure 5.4c and f) systems both display co-continuous structures that further coarsen upon annealing, consistent with the behavior observed in the binary PEEK/*p*-PEI system, but with a much finer morphology. It is worth noting that the 40/24/36 composition shares the same *m*-PEI/*p*-PEI ratio as in the 50/20/30 blend presented in Figure 5.1 and 5.2. The lower PEEK content in the former enhances the visibility of the co-continuous morphology under SEM, resulting in a more open and resolvable phase-separated morphology. Consistent with the observations in Figure 5.2, the PEI_{rich} phase in Figure 5.4e and f exhibits a distinct fibrous/porous PEEK network after quiescent annealing and PEIs extraction, supporting the notion that PEEK is distributed within both coexisting phases at equilibrium. After ultrasonication, this fibrous PEEK network is disrupted, revealing a very rough and textured interface with the $PEEK_{rich}$ phase (Figure S5.3c and d). This is an interesting feature: keeping the fibrous PEEK structure yields a very fine network of interconnected pores, whereas removing it yields relatively large macropores, which could prove useful for separation applications, for example.

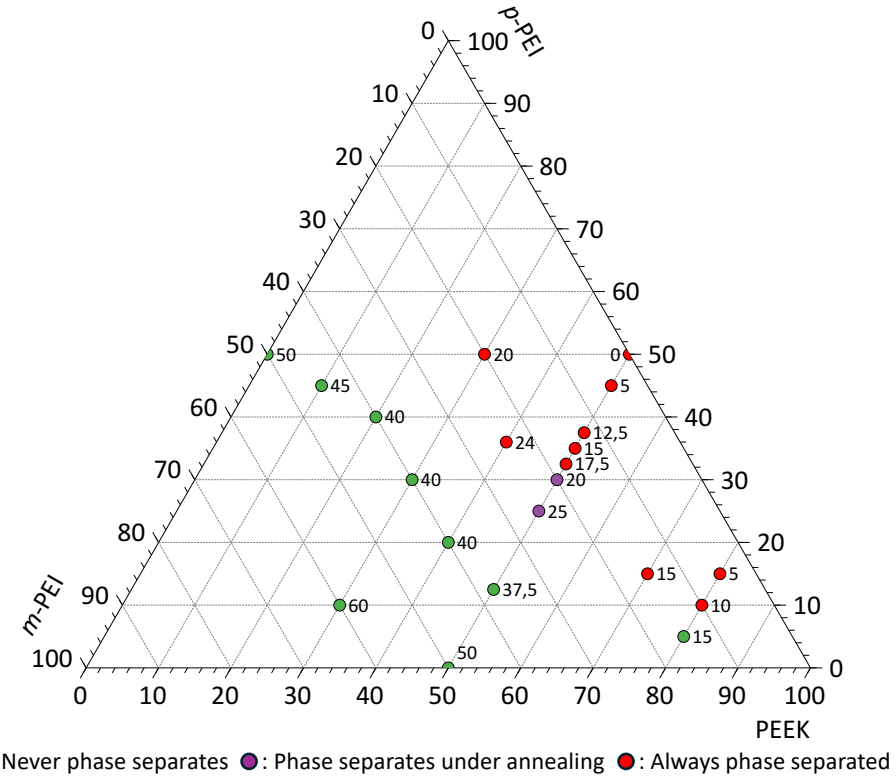

Figure 5.5 Ternary diagram for the PEEK/*m*-PEI/*p*-PEI system indicating homogeneous (miscible) compositions (in green), homogeneous after processing and transitioning to biphasic morphology upon annealing (in purple), and phase-separated biphasic compositions (in red).

Figure 5.5 synthesizes the morphological data on a ternary diagram. The color of the markers denote the morphological behavior of the blends based on SEM micrographs (Figure 5.1 to 5.4 and **Figures S4** & **S5**). Note that for the binary *m*-PEI/*p*-PEI 50/50 and the ternary 10/45/45 systems, miscibility is confirmed by DSC, see Table S1). Compositions represented by green dots are considered fully miscible, as no evidence of phase separation was detected - even after quiescent annealing at 380 °C. Purple dots correspond to compositions that appear homogeneous in the quenched state, but exhibit phase-separated domains upon annealing, indicating latent thermodynamic instability. Red dots identify compositions that are already phase-separated in the melt state, as observed directly after quenching.

It is worth noting that experimental data are sparse in the region containing less than 20 vol% of PEEK – *i.e. m*-PEI and/or *p*-PEI rich regions. This is due to practical limitations: below this threshold, the structural integrity of the blends becomes insufficient to withstand the solvent extraction process, leading to brittle fragmentation and limiting reliable SEM observation (no

selective solvent for PEEK could be found). For this reason, the binary *m*-PEI/*p*-PEI 50/50 and the ternary 10/45/45 were the only blends not characterized by SEM. Additionally, in this low PEEK content region, the glass transition signal associated with the $PEEK_{rich}$ phase becomes weak on the DSC thermograms, making its accurate detection and interpretation difficult.

5.3.2 Calorimetric analysis and determination of χ_{ij} coefficients

Following morphology analysis, calorimetric (DSC) experiments were conducted to evaluate the binary pairs segmental interaction parameters χ_{ij}. The PEEK/*m*-PEI system was selected first since it is already documented in the literature and constitutes an adequate reference. This system is miscible in the melt state and displays a single T_g at all compositions, varying from pure PEEK to pure *m*-PEI (**Figure 5.6a**). For each composition, the formalism of Lu and Weiss [66] (Equations 5.4 to 5.8) was employed to calculate the associated interaction parameter χ. Then, according to the work of Chun, et al. [78], the segmental interaction parameter was calculated (Equation 5.10). A similar approach was employed for the *m*-PEI/*p*-PEI blends, which also displayed a unique T_g associated with a miscible system (**Figure 5.6b**). However, for this particular system, no data were previously reported in the literature.

Table 5.2 Segmental χ_{ij} calculated from the DSC data for binary miscible systems

	PEEK/*m*-PEI									*m*-PEI/*p*-PEI		
Component 1 vol%	90	80	70	60	50	40	30	20	10	75	50	25
Component 2 vol%	10	20	30	40	50	60	70	80	90	25	50	75
Segmental χ_{ij}	-0.071	-0.029	-0.088	-0.086	-0.097	-0.124	-0.129	-0.159	-0.196	-0.008	0.088	0.006
Mean value	-0.109 ± 0.050									0.029 ± 0.052		
Coefficient of variation	46%									182%		

Table 5.3 Segmental χ_{ij} calculated from the DSC data for binary partially miscible blends

	PEEK/*p*-PEI							
PEEK vol%	80	70	60	50	40	30	20	10
p-PEI vol%	20	30	40	50	60	70	80	90
Segmental χ_{13}	0.049	0.049	0.042	0.040	0.039	0.039	0.040	0.042
Segmental χ_{31}	0.042	0.042	0.040	0.039	0.038	0.038	0.038	0.038
Mean value	0.041 ± 0.004							
Coefficient of variation	9%							

Table 5.2 summarizes the values of segmental interaction parameters calculated with Equations 5.4-5.8 & 5.10 for the full range of compositions for the miscible PEEK/*m*-PEI and *m*-PEI/*p*-PEI systems. In complement, **Table 5.3** summarizes the values of segmental interaction parameters calculated with Equations 5.11 & 5.12 for the full range of compositions for the partially miscible PEEK/*p*-PEI binary system.

First, the average PEEK/*m*-PEI segmental interaction parameter (χ_{12}) obtained in this work (-0.109 ± 0.050) closely matches the result of Chun, et al. [78] (-0.115 ± 0.054), who used the same equation. Moreover, it is similar to the value reported by Chen and Porter [132] who used the melting point depression approach. Overall, the value obtained in this work compares well with previously reported values in the literature.

For the *m*-PEI/*p*-PEI system, $\chi_{23} = 0.029 \pm 0.052$. The coefficient of variation associated with the calculation of the *m*-PEI/*p*-PEI interaction parameter is quite high, making it difficult to conclude whether χ_{23} is negative or positive. The value is expected to be close to 0 since the *m*-PEI and the *p*-PEI are two isomeric forms of PEI and should not intuitively present strong specific intermolecular interactions. This uncertainty is explained by the fact that the averaged χ_{23} value is only based on three different compositions, and because the 10 °C difference in T_g between the *m*-PEI and the *p*-PEI is quite small, considering the difficulty in making very precise measurements

by DSC. Additionally, the number average molecular weight of the *p*-PEI was only approximated – the magnitude of χ_{23} would gradually tend towards 0 by increasing the molecular weight.

Finally, for the PEEK/*p*-PEI system, the formalism of Kim and Burns [67] developed for partially miscible systems was employed, based on the equality of the chemical potentials for each species distributed in the two phases (see Table S2), and yields a value of $\chi_{13} = 0.041 \pm 0.004$. This approach demonstrates great reproducibility, with a slightly positive result, as would be expected for a partially miscible system.

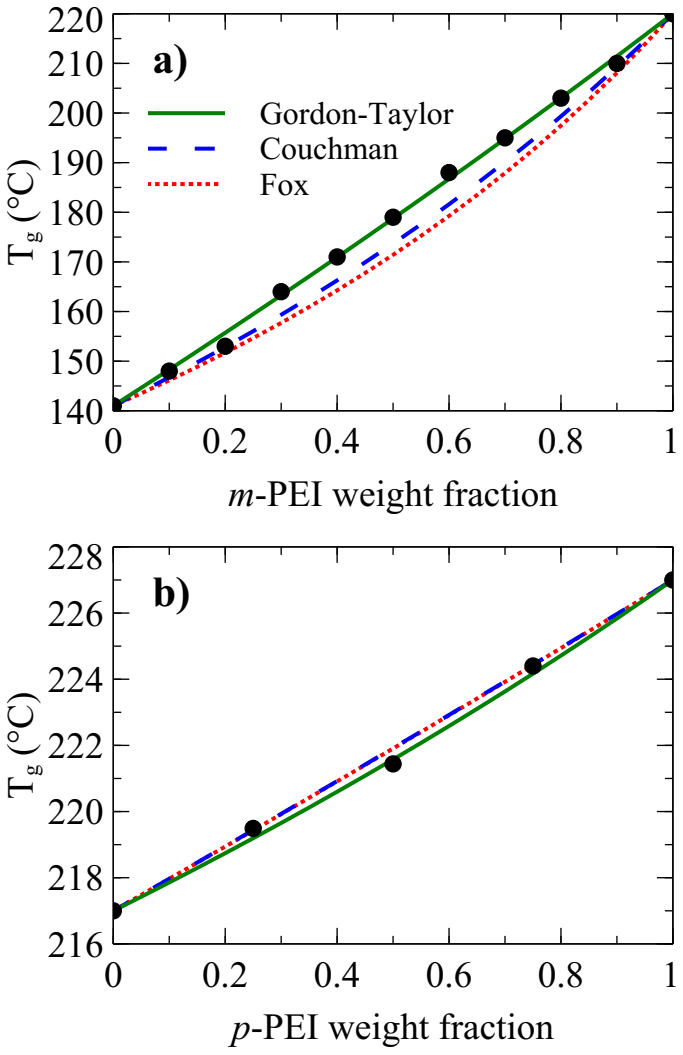

Figure 5.6 T_g experimentally measured (•), compared with the corresponding Gordon-Taylor, Couchman, and Fox fitting curves for: a) PEEK/*m*-PEI ($K_{12} = 0.937$), and b) *m*-PEI/*p*-PEI ($K_{23} = 0.837$).

Figure 5.6 presents the experimental values of T_g for the PEEK/*m*-PEI and the *m*-PEI/*p*-PEI systems, along with the associated fitting models from the Fox, Couchman, and Gordon-Taylor equations, which are used to model miscible systems. In **Figure 5.6a**, for the PEEK/*m*-PEI system, the Gordon-Taylor equation best fits the experimental T_g data with a K_{12} fitting parameter equal to 0.937. The model presents a positive deviation compared to the Fox and Couchman curves, which can be described as specific cases of the Gordon-Taylor model. Indeed, when the fitting parameter K_{12} is equal to the T_g's ratio (T_{g1}/T_{g2} = 0.641 for the PEEK/*m*-PEI system), the equation simplifies to the Fox equation, whereas when K_{12} is equal to $\Delta C_{p2}/\Delta C_{p1}$ (= 0.722 for PEEK/*m*-PEI), it simplifies to the Couchman equation. This positive deviation, in contrast to the two weak-interaction models (Fox, Couchman), supports that PEEK and *m*-PEI display relatively strong intermolecular interactions [66]. Furthermore, based on the work of Lu and Weiss [66], an average χ_{12} can be obtained from the K_{12} fitting parameter of Gordon-Taylor (see Equation 9). The calculations for the PEEK/*m*-PEI system yield an average χ_{12} value of -0.101, which matches quasi-perfectly with the one obtained based on the individual composition calculations from Table 5.2.

In **Figure 5.6b**, the opposite is observed for the *m*-PEI/*p*-PEI system, which displays a Gordon-Taylor fit with a slight negative deviation compared to the Fox and Couchman models. In this case, however, caution is necessary due to the small difference between the T_g's of the two pure polymers (10 °C). Hence, only a 1 °C difference in the measurement of any composition's T_g has a great impact on the value of the associated K_{23} fitting parameter and the following average χ_{23}. This is why the latter interaction parameter was not estimated by this method but only based on the individual composition calculations reported in Table 5.2.

5.3.3 Modeling the spinodal curve of PEEK/*m*-PEI/*p*-PEI systems

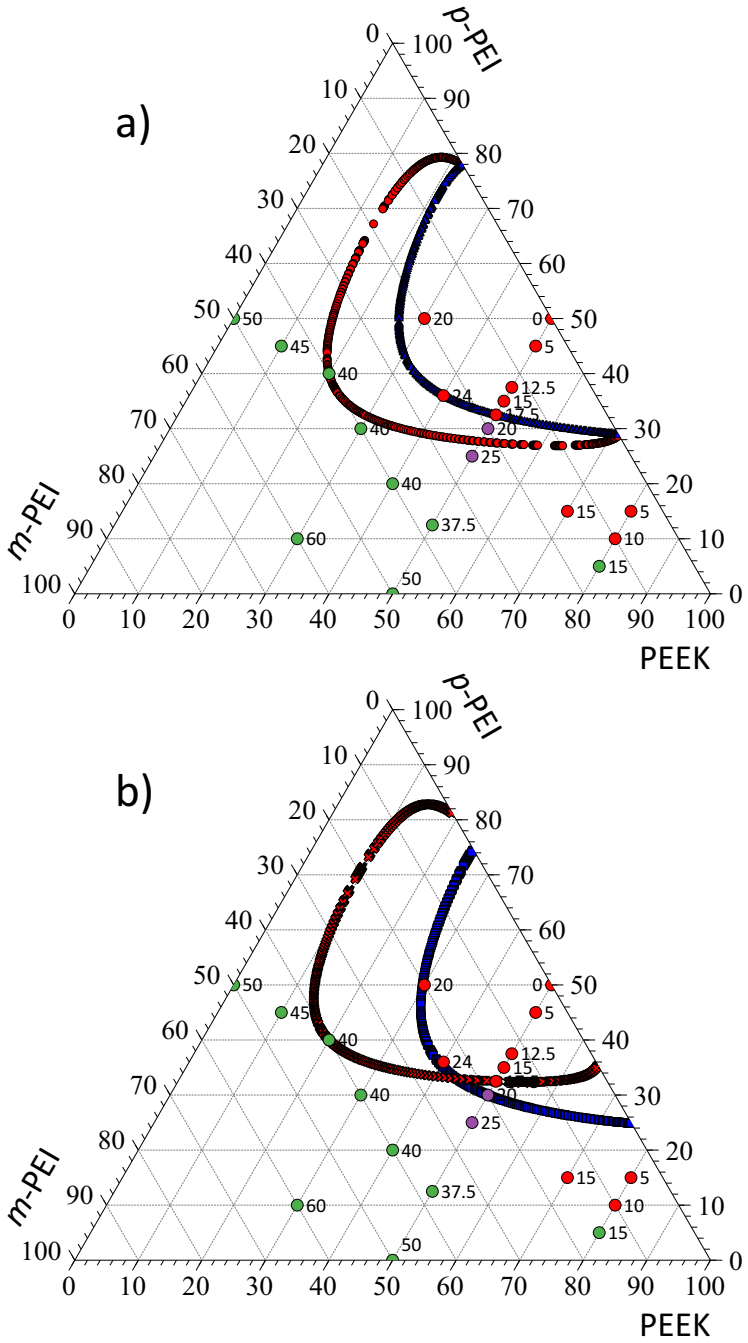

Figure 5.7 Theoretical spinodal curves modeled using Equation 5.13, compared to experimental data points (in green, red and purple, see Figure 5.5), for the PEEK/*m*-PEI/*p*-PEI system with different values of *p*-PEI's M_n, and χ_{23}: a) *p*-PEI's M_n fixed at 15 657 g/mol and χ_{23} = -0.079 (blue triangles curve) or -0.037 (red circles curve); b) *p*-PEI's M_n and χ_{23} as variables: 9 518 g/mol and -0.015 (red crosses curve), 23 041 g/mol and -0.101 (blue squares curve). The numbers associated with the experimental points represent the vol% of *m*-PEI contained in the ternary blend.

Having obtained the average segmental parameters χ_{ij} (χ_{12} = -0.109, χ_{23} = 0.029, and χ_{13} = 0.041), the spinodal decomposition curve and region were modeled using Equations 5.13 to 5.14c. In that case, the spinodal region is much too wide compared to the experimental data, as illustrated in **Figure S5.6**.

Figure 5.7 illustrates possible spinodal curves, depending on different values of *p*-PEI's M_n, and χ_{23}. The segmental interaction parameter χ_{23} was first allowed to vary (more or less negative value), in order for the spinodal curve to better fit the experimentally determined phase-separated and fully miscible domains, respectively (note that the phase-separated blends containing 70% or 80% PEEK were considered within the binodal region). In **Figure 5.7a**, the *p*-PEI's M_n was fixed at 15 657 g/mol, a value obtained by assuming a polydispersity index (PDI) equal to 2.36 (similar to the PDI of *m*-PEI), and a M_w of 37 000 g/mol [79]. Then, χ_{23} was minimized at -0.079 (blue triangles), or maximized at -0.037 (red circles), by constraining the spinodal curve to respect the experimental observations of phase-separated and fully miscible regions, respectively. With these assumptions, a slightly negative χ_{23} value is deduced from morphology observations, compared to the slightly positive value obtained from DSC experiments (note that the DSC value could be both negative or positive considering the experimental error). This is also consistent with a system displaying relatively weak interactions.

In **Figure 5.7b**, both the *p*-PEI's M_n and χ_{23} were allowed to vary in order to explore different hypotheses. The constraints associated with the experimental data points are fixed in a way that the spinodal region only includes the immiscible compositions observed right after melt processing (and with no more than 50 vol% of PEEK), and excludes the initially homogeneous compositions undergoing phase separation upon annealing (reminiscent of binodal decomposition after annealing, see Figure 5.1c and d, Figure 5.2c and d), and miscible ones. This scenario either minimized the *p*-PEI's M_n at 9 518 g/mol (resulting PDI of 3.89) with an associated χ_{23} of -0.015 (red crosses), or maximized it at 23 041 g/mol (resulting PDI of 1.6) with a χ_{23} of -0.101 (blue squares). Considering the reported M_w of *p*-PEI at 37 000 g/mol [79], these results appear reasonable (again note the significant variation of χ_{23}), and the correct values most probably lie within these intervals. Another scenario that included all of the immiscible blends (including the ones containing more than 70 vol% of PEEK) was also considered (see **Figure S5.7**) but was

deemed much less plausible since it yielded *p*-PEI's M_n values either relatively equal or higher than the reported M_w, which is not possible.

Overall, the potential range for the *p*-PEI's M_n spans from 9 518 to 23 041 g/mol, representing roughly 16 to 39 repeating units of *p*-PEI monomers and a PDI ranging from 1.6 to 3.89, respectively. For χ_{23}, the range spans from -0.101 to -0.015, with the first value corresponding to moderate to strong interactions between the two isomeric forms of PEI, promoting miscibility. In contrast, the second would only represent a weak interaction, yet still promoting miscibility between the two types of PEI.

5.3.4 Discussion

Our results demonstrate that PEEK/*m*-PEI/*p*-PEI ternary systems are fully tunable in terms of miscibility by controlling the volume fractions of all three materials. As Figure 5.1 shows, when the PEEK volume fraction is fixed at 50 vol%, the system transitions from fully miscible to metastable, and then to immiscible morphologies when the *p*-PEI becomes the major component over *m*-PEI in the PEI_{rich} phase. Once control over the miscibility of the system is achieved, the selective extraction of the PEIs produces porous PEEK materials with highly tunable porosity features. The resulting average pore size can be controlled over a continuous range, from a few nm to several µm, corresponding to the PEI_{rich} phase domains. To the best of our knowledge, this is the most extensive range of available pore sizes reported for porous polymer monoliths prepared from melt-processed systems, without the use of any interfacial modifier typically used to obtain sub-µm domains.

In addition, from our previous work [125], mesopores are also obtained by the extraction of the PEIs miscible fraction present within the $PEEK_{rich}$ phase. Overall, bimodal pore size distributions can also be obtained, with mesopores under 15 nm in size present in the $PEEK_{rich}$ phase, associated with mesopores/macropores from 15 nm to a few µm resulting from the extraction of the PEI_{rich} phase. This is demonstrated by slowly replacing *m*-PEI with *p*-PEI in the quenched compositions, starting from the homogeneous binary 50/50 PEEK/*m*-PEI blend (Figure 5.1a) solely displaying mesopores once the *m*-PEI is extracted, with a specific surface area of 154 m^2/g and pore size distribution peaks at 10 nm and 15 nm, as measured by BET analysis (**Figure S5.8a**). By gradually substituting *m*-PEI with *p*-PEI, *e.g.* PEEK/*m*-PEI/*p*-PEI 50/17.5/32.5 and 50/12.5/37.5 (Figure 5.1e and g), secondary peaks gradually appear between 25 nm and 35 nm on the pore size distributions

(**Figure S5.8b and c**). This observation supports the progressive nano-scale phase separation in the ternary systems when *m*-PEI is substituted by *p*-PEI (Figure 5.1e and g). In all cases, the specific surface area is very high, with values >135 m^2/g. Overall, this high level of tunability allows the preparation of ultraporous PEEK materials with a variable PEEK content and with the possibility of maintaining high mechanical properties. Using higher melt viscosity polymer grades could then provide further experimental levers to control the resulting morphology, first for the quenched state right after processing, and then by slowing down the subsequent coarsening during annealing, or PEEK recrystallization process.

Another interesting aspect of this ternary system is the observation of shear-induced miscibility for compositions located in the metastable region (*e.g.* 50/25/25 and 50/20/30). For these two compositions, the resulting blends are homogeneous after melt-processing and quenching, then phase separate during quiescent annealing, as seen in Figure 5.1 and 5.2. This behavior was reported in a few past publications, in which it was demonstrated that increasing the shear rate, over a certain threshold, promoted miscibility for binary LCST systems. It was also shown that this shear-induced miscibility is dependent on blend composition and molecular weight of the components [133-135]. Complementary tests on shear-induced miscibility were also performed on the 50/15/35 composition – this system is very finely phase-separated in the quenched state when processed at 50 rpm, as Figure 5.1f illustrates. When processed at 150 rpm, instead of 50 rpm, a more homogeneous, nearly miscible morphology is obtained, following a similar behavior previously reported in the literature (see **Figure S5.9**). Regarding the scarcity of morphological data for compositions with less than 20 vol% of PEEK, atomic force microscopy (AFM) could be used to elucidate the phase separation behavior in this missing data region.

This work also demonstrates that calorimetry data can present some limitations when used to support the experimental morphological data. The calorimetry approach works well for systems where the T_g's of the pure components are sufficiently different from each other (at least 20 °C), and when relatively precise values of the molecular weights are available. For the limiting case of the *m*-PEI/*p*-PEI binary system in this work, for which the T_g's are close and M_n of *p*-PEI is only estimated, **Table S3** presents an initial analysis showing how sensitive χ_{23} is to the measured T_g values. We started from χ_{23} values equal to either -0.079 or -0.037, obtained by fitting the spinodal curve on the morphology results (see Figure 5.7a); a M_n value of 15 657 g/mol (*i.e.* similar PDI

between *m*-PEI and *p*-PEI); the additional imposed constraint of equal uncertainties on the T_g's for the 75/25 and 25/75 compositions, to simplify the initial assessment. Solving numerically, the differences between the calculated T_g values and experimental values are all inferior to 1 °C, which is well within the experimental error when determining the T_g by DSC – demonstrating how delicate this calculation is for this particular case. The semi-crystalline nature of PEEK adds another layer of complexity, which masks the presence of a possible PEI_{rich} T_g in quenched materials due to PEEK recrystallization (*i.e.* 1st DSC heating cycle) – it also subsequently provokes phase separation on a very fine scale (< 5 nm), only visible by DSC analysis and difficult to detect by SEM.

However, this semi-crystalline nature can be leveraged by using the melting point depression technique to obtain the segmental χ_{ij} parameter for miscible binary polymer blends containing one crystallizable component [65]. This method, relying on the equality of the polymer's chemical potential between the crystalline and liquid phases, is based on the earlier work of Scott [93] on phase equilibria for systems of two polymers diluted in a common solvent. Chen and Porter [132] then applied this technique to the PEEK/*m*-PEI system and obtained a χ_{ij} parameter equal to -0.4 at 400 °C. The apparent discrepancy between their value, compared to the average values in our work (-0.109) and the work of Chun, et al. [78] (-0.115), mainly stems from the monomer molar volume Chen and Porter [132] chose as a reference, *i.e.* the value of *m*-PEI (459.31 cm^3/mol). In comparison, we chose PEEK as the reference value (265.24 cm^3/mol), like Chun, et al. [78]. This difference accounts for the approximate factor of 2 between the values. Selecting PEEK as a reference, the value of Chen and Porter [132] would give a segmental interaction parameter of (-0.198) between PEEK and *m*-PEI. The remaining difference could originate from the polymer molecular weights, the inherent uncertainty of the melting point depression method, as mentioned by the authors, or from the difference in the chosen temperature for analysis. Finally, for partially miscible systems (PEEK/*p*-PEI), the calorimetric approach developed by Kim and Burns [67], which uses the compositions of the phases in equilibrium to calculate the segmental interaction parameter, proved to be useful and accurate for different polymeric systems [96, 128, 136-139].

Scott [93] and Tompa [94] were among the first to develop the mathematical framework of the thermodynamics of phase equilibria in multicomponent systems, specifically for systems composed of two polymers and one solvent. Later, Zeman and Patterson [89] expressed the spinodal equation under a more convenient form for ternary systems to understand the influence of

the solvent on the polymers' incompatibility in solution. Finally, building on this framework, Su and Fried [95] were the first to explore the effect of the interaction parameters on computed spinodal curves (frontiers) for ternary polymer blend diagrams. Their results showed that miscibility is improved when all pairs are slightly miscible or immiscible but is limited in cases of strong asymmetry, such as systems with one highly miscible or one highly immiscible pair. Based on this formalism for ternary polymer systems, one practical and interesting result is the possibility of calculating (at least approximately) the segmental interaction parameter of a binary system, knowing the values of the complementary pairs. This approach also requires experimental phase equilibrium data identifying the frontier between the miscible, and biphasic states, on the ternary diagram, which can be obtained by SEM analysis (or complementary methods). Then, it is also necessary to have relatively precise values of the polymers' molecular weights to perform the calculations. Finally, the value of the unknown interaction parameter is allowed to vary in order to fit the experimental miscibility data until a range of values is obtained.

In our work, differences are observed between the segmental χ_{23} parameter (between *m*-PEI and *p*-PEI) obtained from calorimetric data, compared to the value obtained by fitting the spinodal curve based on the ternary blends' morphological data. This discrepancy can stem from multiple reasons: 1) the close values between the two T_g's of the *m*-PEI and *p*-PEI, 2) the approximate *p*-PEI's M_n, which is required to calculate the segmental χ_{23} parameter, 3) the limit of phase separation detection by SEM for compositions close to the frontier between miscible and biphasic states (binodal or spinodal frontiers), 4) the restrictive approximation in each model that considers the segmental χ_{23} parameter independent of blend composition, which is not the case in reality. Hence, to better predict the value of segmental interaction parameters, especially in ternary polymer systems, all of these limitations would need to be alleviated.

5.4 Conclusion

This work employs, for the first time, a three-component composition-driven strategy to precisely tune the (im)miscibility and morphological features in high-performance ternary PEEK-based polymer systems containing *meta*- and *para*-PEI. *Meta*-PEI and *para*-PEI are respectively fully and partially miscible with PEEK, whereas both PEIs are mutually miscible. By controlling the compositions and ratio of PEEK, *m*-PEI, and *p*-PEI, processing parameters, and thermal history, a rich morphological landscape becomes accessible. This work demonstrates the most extended

range of microstructural length scales reported in the literature so far in multiphase polymer systems: from a few nm for fully miscible compositions, to several μm for phase-separated systems, without the need for any additional compatibilizer. Next, by selectively extracting both PEIs, porous PEEK-based monolithic materials can be prepared with the same extended range of porosity features. Interestingly, shear-induced miscibility, followed by controlled phase separation by thermal treatment, a phenomenon seldom reported and rarely investigated from a morphological perspective, becomes relatively accessible with this ternary system.

The phase behavior is quantitatively related to Flory-Huggins segmental interaction parameters (χ_{ij}) calculated from calorimetry measurements, for the PEEK/*m*-PEI (-0.109), PEEK/*p*-PEI (0.041), and *m*-PEI/*p*-PEI (from -0.101 to -0.015) binary systems – the last two never reported before in the literature. These thermodynamic parameters serve as a basis for computing the spinodal curve, which is then plotted onto the ternary diagram to identify compositions at which spinodal decomposition is expected as a phase-separation mechanism. This representation provides a practical framework for predicting phase separation and guides the formulation of blends with targeted morphologies. Alternatively, it can also be used to estimate an unknown χ_{ij}, as we demonstrate, provided that the other two parameters and the molecular weights are known. Overall, the ternary PEEK/*m*-PEI/*p*-PEI system emerges as a flexible and predictive system to investigate a variety of fundamental phenomena from the fully miscible to immiscible state in multicomponent/multiphase polymer systems and allows for material design where microstructural control is critical, potentially impacting applications such as filtration processes or biomedical material design.

5.5 Supporting information

5.5.1 Complete set of studied compositions and DSC data

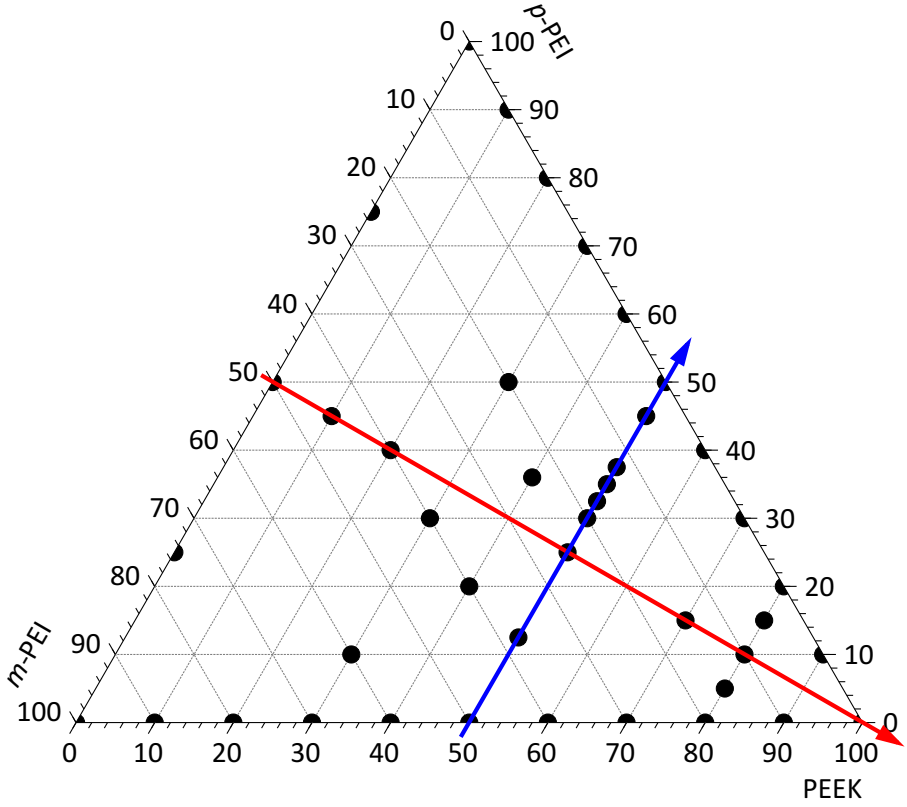

Figure S5.1: Ternary diagram representing all of the binary and ternary compositions prepared in this work. Isopleth with PEEK volume fraction fixed at 50 vol% (blue arrow). Isopleth with constant *m*-PEI/*p*-PEI ratio fixed at 50/50 (red arrow).

Table S5.1. Main DSC data

N°	PEEK (vol%)	*m*-PEI (vol%)	*p*-PEI (vol%)	*m*-PEI/*p*-PEI ratio	1st T_g (°C)		2nd T_g (°C)	
					$PEEK_{rich}$	PEI_{rich}	$PEEK_{rich}$	PEI_{rich}
1	100	0	0	-	141	-	145	-
2	0	100	0	-	-	215	-	217
3	0	0	100	-	-	225	-	227
4	10	90	0	-	210		-	209
5	20	80	0	-	203		-	202
6	30	70	0	-	195		-	211
7	40	60	0	-	188		166	212

Table S5.1. Main DSC data (cont'd)

8	50	50	0	-	179		168	212
9	60	40	0	-	171		166	214
10	70	30	0	-	164		164	214
11	80	20	0	-	153		164	214
12	90	10	0	-	148		159	-
13	10	0	90	-	-	218	164	219
14	20	0	80	-	-	212	166	217
15	30	0	70	-	166	/	166	215
16	40	0	60	-	166	/	166	215
17	50	0	50	-	164	/	164	216
18	60	0	40	-	161	/	162	218
19	70	0	30	-	157	/	160	224
20	80	0	20	-	155	/	160	224
21	90	0	10	-	147	/	157	-
22	0	25	75	25/75	-	-	-	219.49
23	0	50	50	50/50	-	220.28	-	221.18
24	0	75	25	75/25	-	-	-	224.40
25	80	15	5	75/25	153	/	162	212?
26	80	10	10	50/50	153	/	162	-
27	80	5	15	25/75	153	/	162	222?
28	70	15	15	50/50	162	/	164	218
29	50	37.5	12.5	75/25	177	/	172	216
30	50	25	25	50/50	180	/	174	219
31	50	20	30	40/60	177	/	168	219
32	50	17.5	32.5	35/65	178	/	170	220
33	50	15	35	30/70	176	/	169	219
34	50	12.5	37.5	25/75	172	/	170	217
35	50	5	45	10/90	165	/	165	218
36	40	40	20	67/33	-	187	168	213
37	40	24	36	40/60	-	187	178	219
38	30	60	10	86/14	-	195	-	211

Table S5.1. Main DSC data (cont'd)

39	30	40	30	57/43	-	194	180?	213
40	30	20	50	29/71	-	196	178?	214
41	20	40	40	50/50	-	205	-	205
42	10	45	45	50/50	-	211	-	212

"/": cold-crystallization of PEEK blocking the measurement of any PEI_{rich} T_g.

5.5.2 Annealing of ternary PEEK/*m*-PEI/*p*-PEI blends

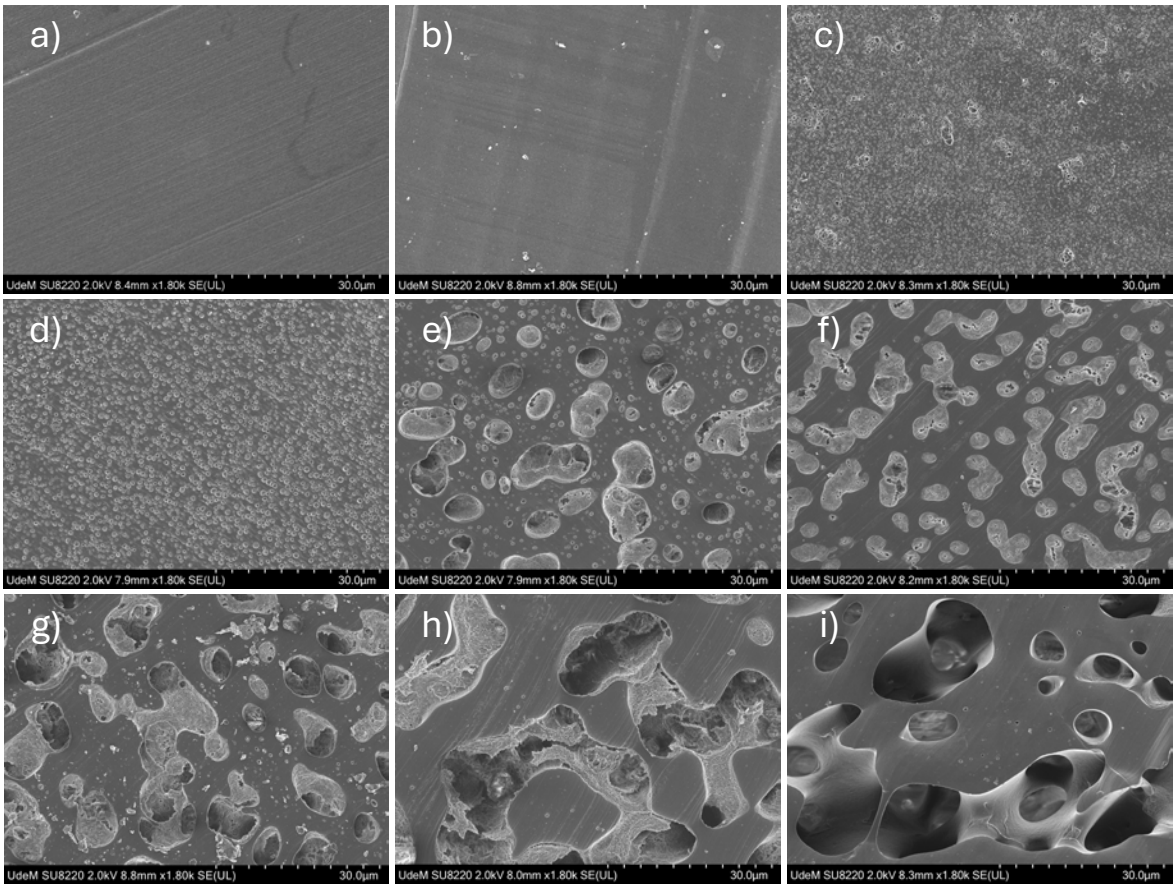

Figure S5.2: Low-magnification micrographs of the microstructures of binary and ternary PEEK/m-PEI/p-PEI blends, obtained after 15 min of quiescent annealing time at 380 °C and after the selective extraction of PEIs. Compositions in vol%: a) PEEK/m-PEI 50/50; b) 50/37.5/12.5; c) 50/25/25; d) 50/20/30; e) 50/17.5/32.5; f) 50/15/35; g) 50/12.5/37.5; h) 50/5/45; i) PEEK/p-PEI 50/50.

Figure S5.2 presents low-magnification SEM micrographs of the ternary PEEK/*m*-PEI/*p*-PEI blends after 15 min of quiescent annealing time at 380 °C, followed by selective solvent extraction of the PEIs. The results clearly illustrate the composition-dependent evolution of phase separation

and coarsening scales. Blends shown in a) and b) exhibit fully homogeneous morphologies, consistent with complete miscibility under these conditions. In contrast, compositions c) and d) display a finely dispersed droplet-like microstructure, indicative of phase separation via a potential nucleation and growth mechanism. Composition e) reveals an intermediate morphology, where isolated fine droplets coexist with larger, partially interconnected domains, suggesting the early stages of co-continuous structure development. From composition f) through i), the microstructure progressively evolves into a well-developed co-continuous network, with increasing domain size due to coarsening. Notably, in these latter compositions, a web-like network of PEEK is observed within the PEI_{rich} phase, confirming the presence of PEEK in both phases at equilibrium. In Figure S5.2i, this network is absent as it was effectively removed during the cleaning process of the solvent extraction via an ultrasonic bath, resulting in a cleaner, more distinct co-continuous morphology.

5.5.3 Additional compositions completing the ternary phase diagram

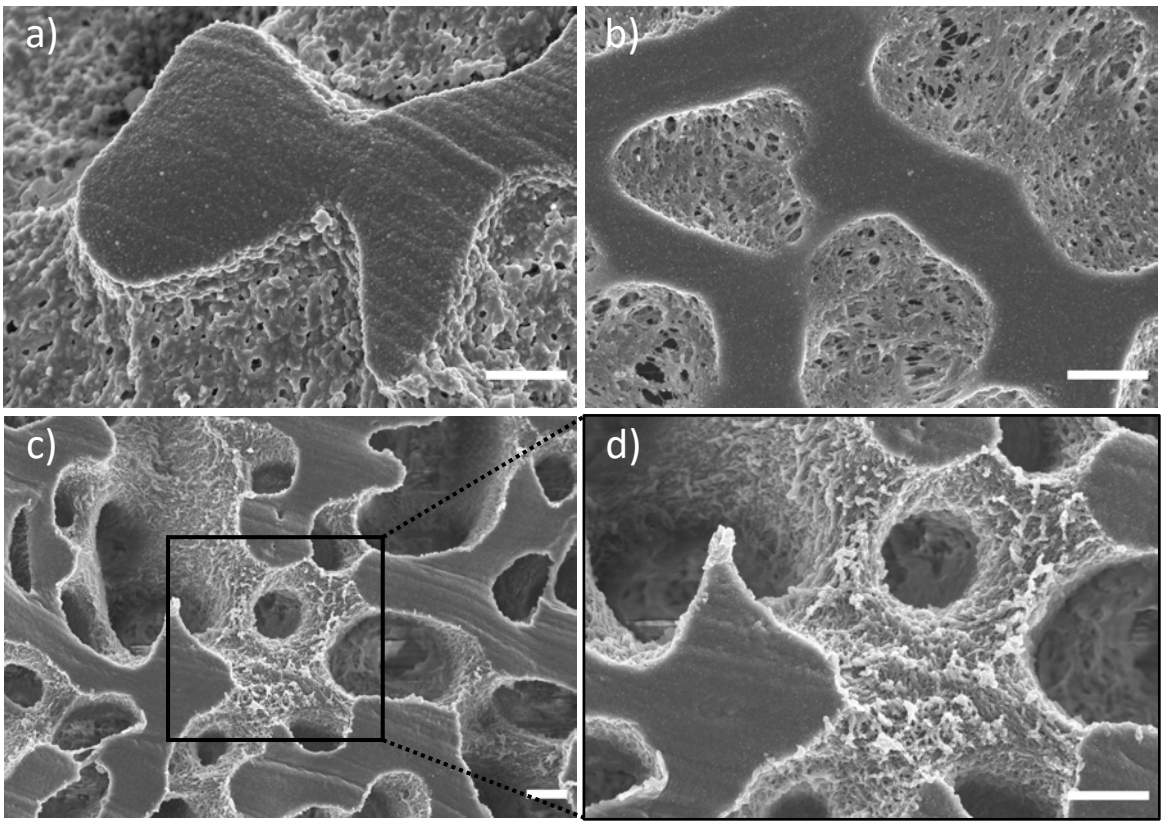

Figure S5.3: Microstructure of ternary PEEK/*m*-PEI/*p*-PEI blends, after 15 min of quiescent annealing at 380 °C (C15) and the selective extraction of PEIs. Compositions in vol%: a) 30/20/50 C15; b) 40/24/36 C15; c) and d) 40/24/36 C15 with an ultrasonic bath treatment during the cleaning step. White scale bars represent 1 µm.

Figure S5.3 highlights two compositions exhibiting particularly insightful morphological features. After 15 min of quiescent annealing, the 30/20/50 blend displays a clear co-continuous morphology at low magnification. At higher magnification shown in Figure S5.3a, the network of PEEK embedded within the PEI_{rich} phase becomes clearly visible, along with its interfacial contact with the $PEEK_{rich}$ domains. A similar observation applies to the 40/24/36 composition after 15 min of quiescent annealing, presented in Figure S5.3b. In contrast, the micrograph in Figure S5.3c and its corresponding magnification in Figure S5.3d illustrate the removal of this PEEK network, achieved by ultrasonication. Together, these images demonstrate that the PEEK network is not a superficial layer covering extraction-induced pores, but rather forms an interconnected structure that permeates the entire PEI_{rich} phase and that is connected at the interface with the $PEEK_{rich}$ phase.

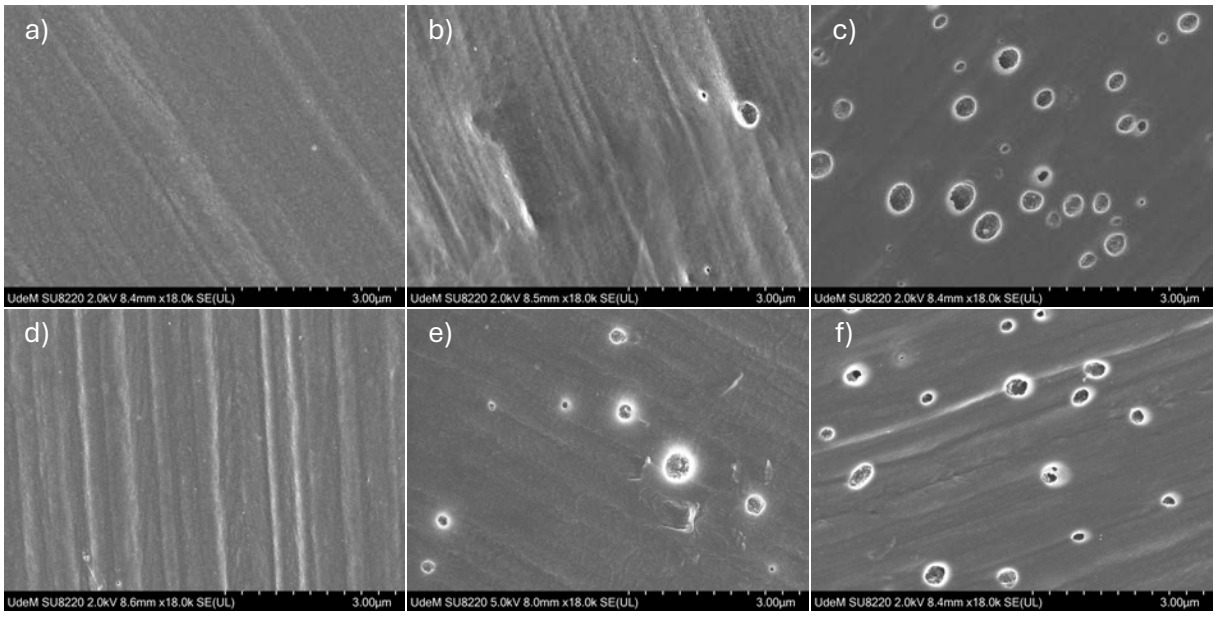

Figure S5.4: Microstructure of ternary PEEK/m-PEI/p-PEI blends, either quenched (Q) or after 15 min of quiescent annealing at 380 °C (C15) and the selective extraction of PEIs. Compositions in vol%: a) 80/15/5 Q; b) 80/10/10 Q; c) 80/5/15 Q; d) 80/15/5 C15; e) 80/10/10 C15; f) 80/5/15 C15.

Figure S5.4 compares three ternary compositions, rich in PEEK, in their quenched state and after 15 min of quiescent annealing at 380 °C. The 80/15/5 blend remains fully miscible in both conditions, as evidenced by its homogeneous morphology. In contrast, the 80/10/10 composition exhibits clear phase separation following annealing. Although its quenched morphology is less definitive, the presence of a small number of droplet-like domains suggests that phase separation

may have already been present from the start. The 80/5/15 composition is phase-separated in both the quenched and annealed states, with pronounced morphological contrast confirming its immiscibility under all conditions examined.

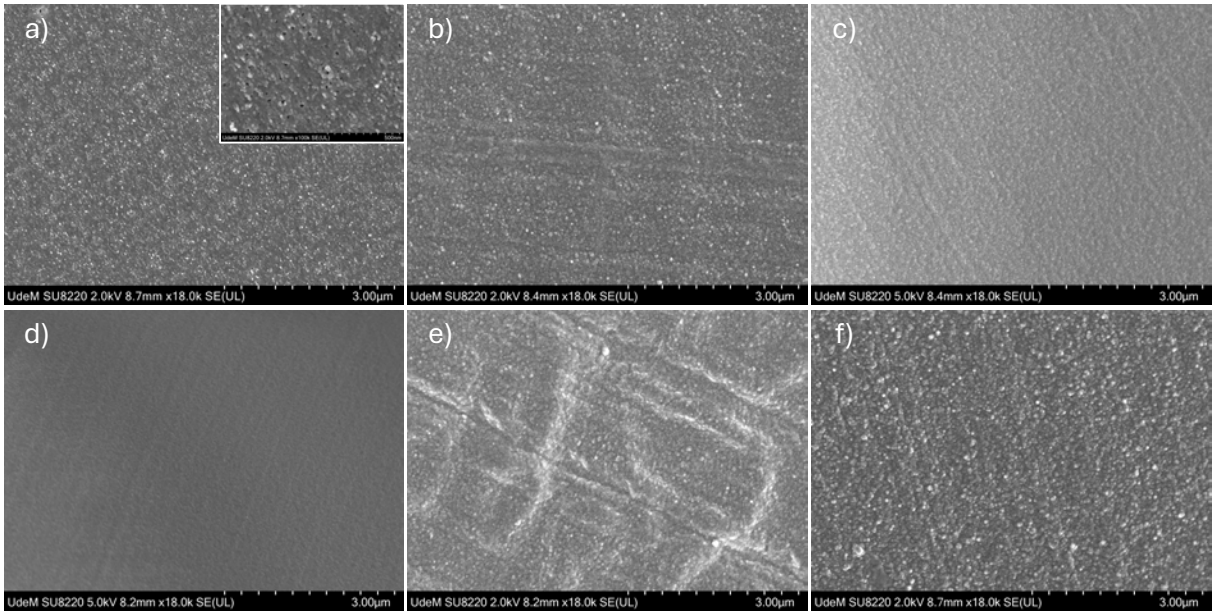

Figure S5.5: Microstructure of ternary PEEK/*m*-PEI/*p*-PEI blends, either quenched (Q) or after 15 min of quiescent annealing at 380 °C (C15) and the selective extraction of PEIs. Compositions in vol%: a) 30/60/10 Q; b) 40/40/20 Q; c) 30/40/30 Q; d) 30/60/10 C15; e) 40/40/20 C15; and f) 30/40/30 C15.

Figure S5.5 presents three additional compositions that complete the mapping of the ternary diagram. All are considered fully miscible in the quenched state and remain so after 15 min of quiescent annealing, as no signs of domain coarsening are observed. At higher magnification, the inset of the micrograph in Figure S5.5a reveals the presence of mesopores, which can be attributed in part to solvent-induced crystallization of PEEK. This phenomenon leads to the exclusion of PEI into PEI_{rich} regions that are subsequently removed during solvent extraction. The relatively low PEEK content (30 vol%) in this blend may also contribute to this microstructure. Interestingly, similar mesopores are not observed in Figure S5.5c, despite an identical PEEK volume fraction.

5.5.4 Binary interaction parameter and spinodal region

Table S5.2. Volume fractions of PEEK and *p*-PEI distributed in the two phases in equilibrium ($PEEK_{rich}$ and *p*-PEI_{rich}), for various global compositions of the partially miscible PEEK/*p*-PEI system, and with the crystallinity of PEEK associated entirely to the $PEEK_{rich}$ phase.

Blends global compositions		PEEK$_{rich}$		*p*-PEI$_{rich}$	
PEEK (vol%)	*p*-PEI (vol%)	PEEK (vol%) ϕ'_1	*p*-PEI (vol%) ϕ'_3	PEEK (vol%) ϕ''_1	*p*-PEI (vol%) ϕ''_3
80	20	83	17	4	96
70	30	83	17	4	96
60	40	80	20	10	90
50	50	78	22	12	88
40	60	76	24	13	87
30	70	78	22	13	87
20	80	76	24	11	89
10	90	73	27	9	91

Table S5.3. Sensitivity analysis of the calculated binary interaction parameter for the *m*-PEI/*p*-PEI system with respect to measured T_g (for a *p*-PEI's M_n = 15 657 g/mol).

	Experimental data			Test 1			Test 2		
m-PEI/*p*-PEI (vol%)	75/25	50/50	25/75	75/25	50/50	25/75	75/25	50/50	25/75
T_g (°C)	219.49	221.18	224.4	220.28	221.77	225.19	219.97	221.54	224.88
Deviation from experimental T_g (°C)	/	/	/	0.79	0.59	0.79	0.48	0.36	0.48
χ	-0.434	4.660	0.317	-7.166	0.911	-6.281	-4.539	2.374	-3.706
Segmental χ_{23}	-0.008	0.088	0.006	-0.135	0.017	-0.119	-0.086	0.045	-0.070
Mean value	0.029 ± 0.052			-0.079 ± 0.084			-0.037 ± 0.071		

Table S5.3 presents the impact of the measured T_g on the calculated value of the binary interaction parameter χ_{23} for the *m*-PEI/*p*-PEI system. It is observed that a hypothetical variation of 0.8 °C or less on the measured T_g dramatically changes the mean value of χ_{23}, from 0.029 to -0.079 (Test 1). This change in the value of χ_{23} has a great impact on the following generated spinodal curve (*i.e.* **Figure S5.6** compared to **Figure 5.7a**).

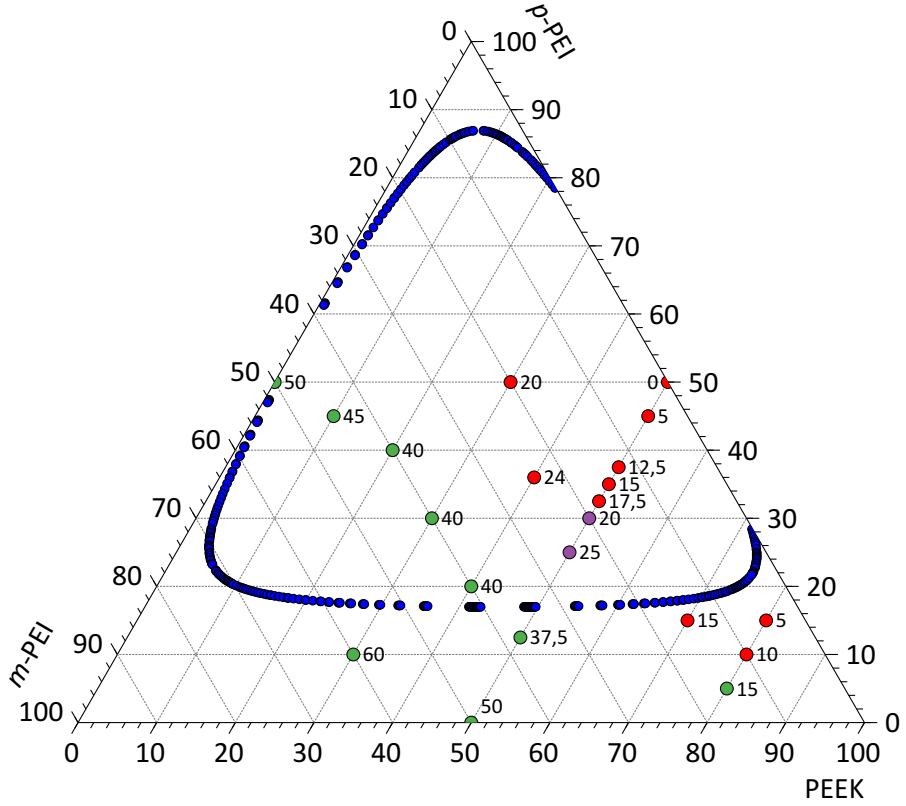

Figure S5.6: Spinodal curve calculated from the raw DSC data of all the binary systems: the number averaged molecular weight (M_n) of *p*-PEI was fixed at 15 657 g/mol, $\chi_{12} = -0.109$; $\chi_{23} = 0.029$; $\chi_{13} = 0.041$. The numbers associated with the experimental points represent the vol% of *m*-PEI contained in the ternary blend.

Figure S5.6 shows the spinodal curve constructed using interaction parameters derived from raw DSC measurements. This includes the less reliable χ_{23} value (between *m*-PEI and *p*-PEI), which exhibits a high coefficient of variation (see the Discussion section of the main article). With this limitation, the resulting spinodal curve spans a broad region of the ternary diagram and significantly overlaps with the compositions identified as miscible based on SEM and DSC analyses. This discrepancy highlights the considerable uncertainty associated with the χ_{23}

estimation and underscores the necessity of considering multiple scenarios with a variable χ_{23} value to better align with experimental observations.

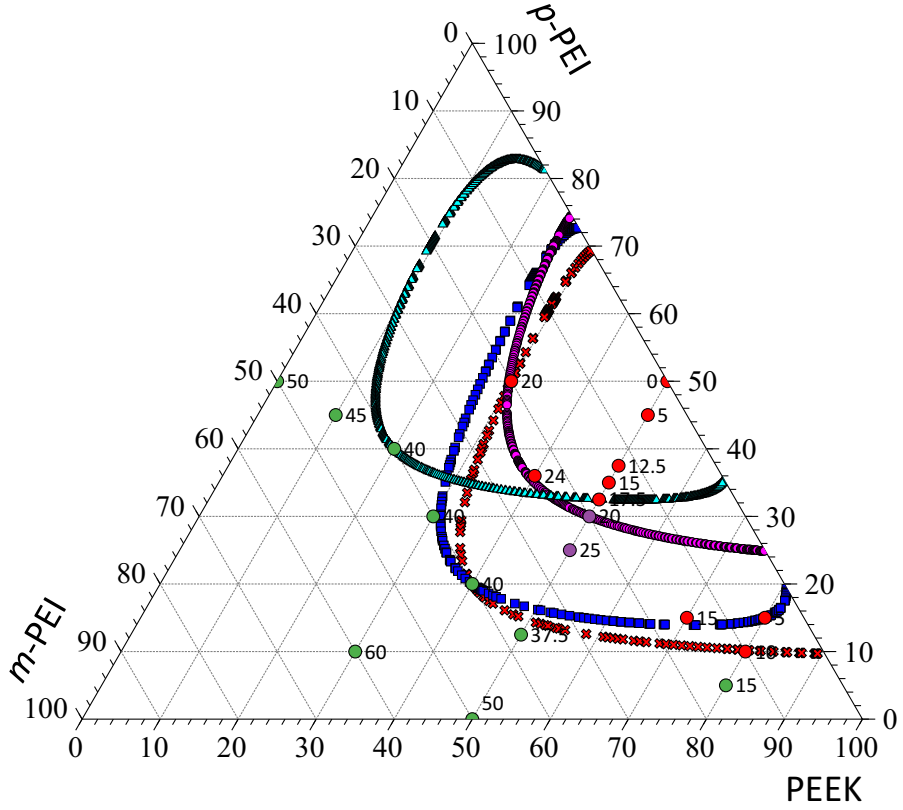

Figure S5.7. Spinodal curves for the PEEK/*m*-PEI/*p*-PEI system with different values of *p*-PEI's M_n and χ_{23}: 9 518 g/mol and -0.015 (cyan triangles), 23 041 g/mol and -0.101 (magenta circles), 34 711 g/mol and -0.177 (blue squares), 92 320 g/mol and -0.099 (red crosses). The numbers associated with the experimental points represent the vol% of *m*-PEI contained in the ternary blend.

In **Figure S5.7**, both the *p*-PEI's M_n and χ_{23} were allowed to vary in order to explore different hypotheses. In the first scenario, the constraints associated with the experimental data points are fixed in a way that the spinodal region only includes the immiscible compositions observed right after melt processing (with no more than 50 vol% of PEEK) and excludes the shear-induced miscible (reminiscent of binodal decomposition after annealing), and miscible ones. This scenario either minimized the *p*-PEI's M_n at 9 518 g/mol, with an associated χ_{23} of -0.015 (cyan triangles), or maximized it at 23 041 g/mol with a χ_{23} of -0.101 (magenta circles). Considering the reported M_w of *p*-PEI at 37 000 g/mol in the literature, these results appear reasonable.

The second scenario forced the spinodal region to include all of the immiscible compositions, which included the shear-induced miscible ones while excluding the miscible compositions. This scenario either minimized the *p*-PEI's M_n to 34 711 g/mol with a χ_{23} of -0.177 (blue squares), or maximized it at 92 320 g/mol, with an associated χ_{23} of -0.099 (red crosses). Considering the reported M_w of *p*-PEI, this scenario appears less plausible.

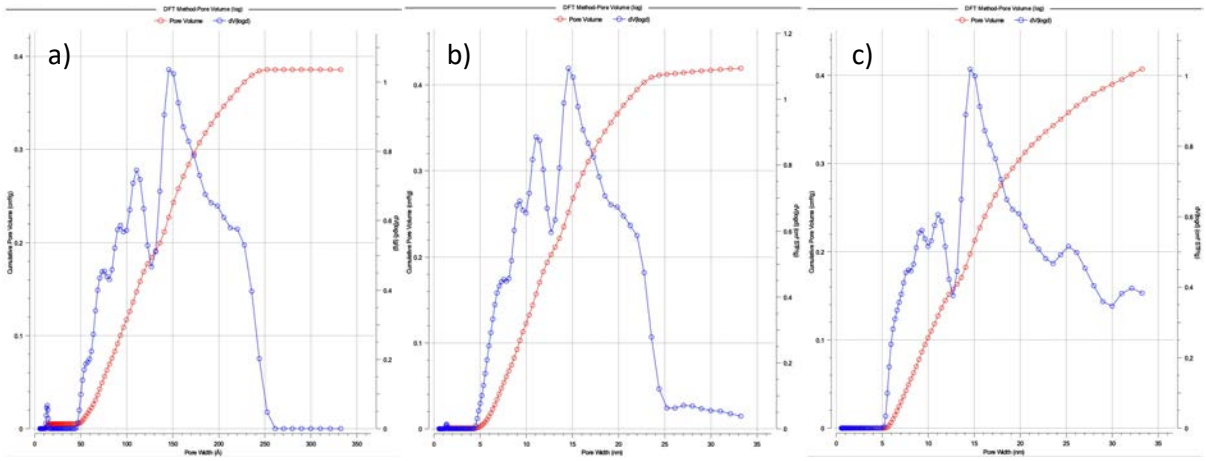

	a)	b)	c)
BET surface (m^2/g):	154	158	136
DFT surface (m^2/g):	137	143	124
BJH surface (m^2/g):	276	252	219

Figure S5.8. Pore size distribution and associated specific surface area from gas sorption analysis for: a) PEEK/*m*-PEI 50/50 Q, b) PEEK/*m*-PEI/*p*-PEI 50/17.5/32.5 Q, and c) PEEK/*m*-PEI/*p*-PEI 50/12.5/37.5 Q.

In **Figure S5.8**, the pore size distributions are obtained for the quenched compositions of PEEK/*m*-PEI 50/50, PEEK/*m*-PEI/*p*-PEI 50/17.5/32.5, and PEEK/*m*-PEI/*p*-PEI 50/12.5/37.5. Note that the pore width is given in angstroms for panel a), whereas it is in nm for the two other panels b) and c). The associated specific surface areas, calculated with different models (BET, DFT, and BJH), are also reported. The pore size distributions of the quenched compositions provide a clear and direct comparison between the different systems. Upon increasing the *p*-PEI content in the blend, a change in the distributions is observed: the peak around ~1.5 nm (a and b) progressively diminishes, while new features appear beyond ~25 nm (b and c), consistent with the formation of larger mesopores associated with the extraction of the PEI_{rich} phase. According to the BET and DFT models, all three compositions display high specific surface areas higher than 100 m^2/g. Only the BJH method, performed in the range of p/p_0 from 0.39 to 0.96, seems to overestimate this same property.

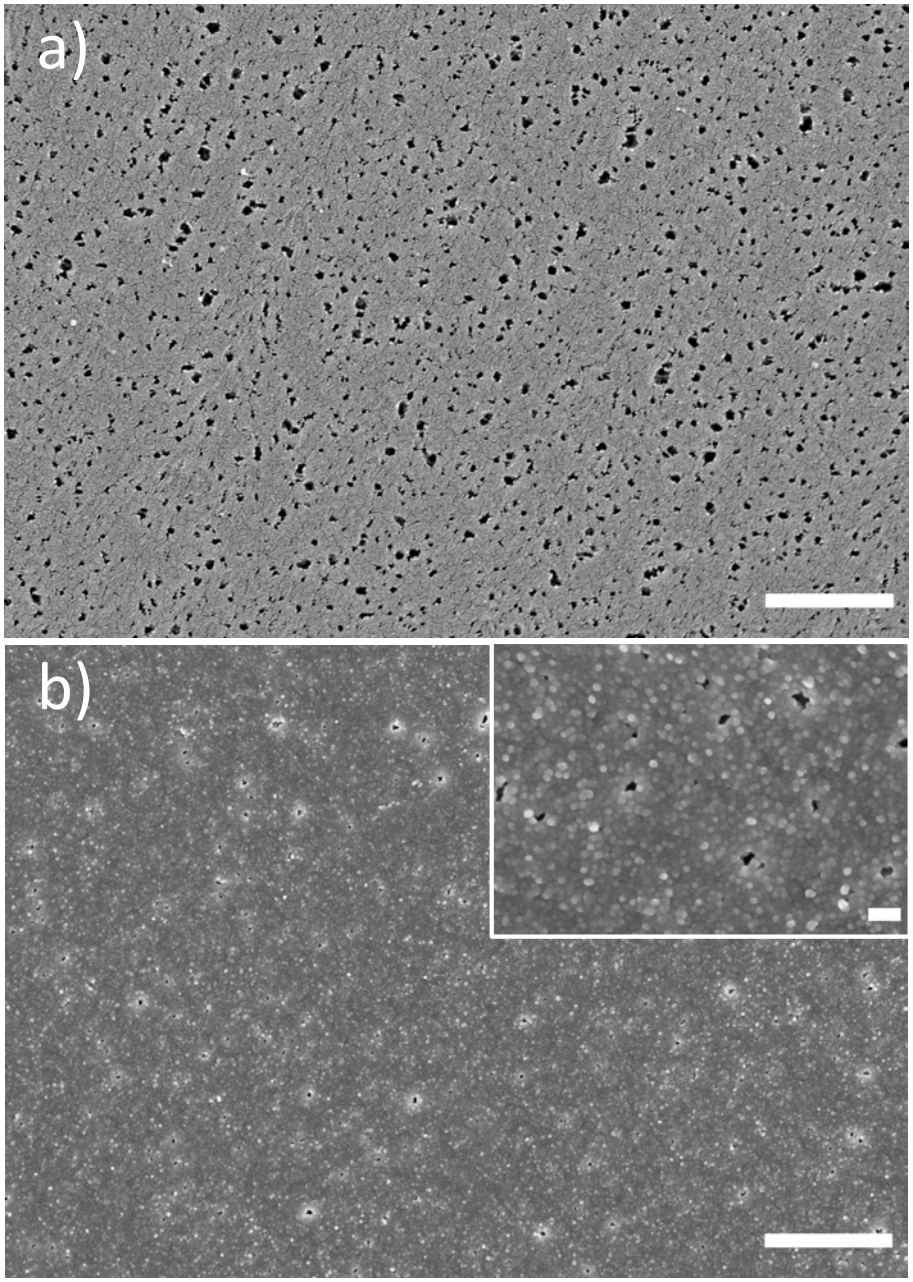

Figure S5.9. Morphology of ternary PEEK/*m*-PEI/*p*-PEI 50/15/35 composition, obtained after the selective extraction of both PEIs. Melt-processed for 6 min at 370 °C and at: a) 50 rpm; b) 150 rpm. The white scale bars represent 1 μm for the main magnification and 100 nm for the close-up inset micrograph.

In **Figure S5.9**, the effect of shear-induced miscibility is also observed for the 50/15/35 composition, where the system, melt-processed at a higher speed (150 rpm) in **Figure S5.9b,** is more homogeneous and nearly miscible compared to the one processed at a lower speed (50 rpm) in **Figure S5.9a.**

CHAPTER 6 ARTICLE 3: DESIGNING PEEK-BASED HIGH-PERFORMANCE TERNARY SYSTEMS DISPLAYING HIGHLY CONTROLLED HIERARCHICAL MORPHOLOGIES

*Arthur Lassus, Basil D. Favis, and Nick Virgilio**

CREPEC, Department of Chemical Engineering, Polytechnique Montréal, Montréal, Québec H3T 1J4, Canada

*Corresponding author's E-mail: nick.virgilio@polymtl.ca

Submitted to: *Macromolecules*, 18th August 2025

Abstract

In this work, ternary systems of melt-processed poly(ether ether ketone) (PEEK) combined with various combinations of *meta*-poly(ether imide) (*m*-PEI), *para*-poly(ether imide) (*p*-PEI), polycarbonate (PC), or poly(phenyl sulfone) (PPSU) are shown to result in uniquely sophisticated and tunable hierarchical morphologies. The highly controlled morphologies shown here, for the first time in the literature for any ternary-based system, span the entire range of miscible to partially miscible to fully immiscible. The structure evolves from a biphasic system, as observed when PEEK is combined with PC and *m*-PEI, to fully triphasic systems when PEEK is instead combined with PC and *p*-PEI or PPSU. In all cases, PEEK systematically and fully separates the other two components, as predicted by the spreading coefficients, a unique result for ternary systems displaying low interfacial tensions involving miscible or partially miscible polymer pairs. These insights then enabled the preparation of hierarchically porous PEEK monoliths comprised simultaneously of both macro and meso-porous network structures with tunable pore sizes, and even ultraporous materials containing as little as 5 vol% PEEK. The average pore sizes span a considerable range of nearly 4 orders of magnitude, from a few nanometers to several microns.

These results underscore the potential of such blends for designing PEEK porous monoliths for very lightweight, high-temperature applications.

6.1 Introduction

Blending *meta*-poly(ether imide) (*m*-PEI) with poly(ether ether ketone) (PEEK) is a well-known approach to improve the processability and thermal properties of PEEK-based high-performance materials. It increases the glass transition temperature (T_g), thereby yielding better thermal resistance, slows down PEEK crystallization, and decreases costs as PEI is less expensive. These binary blends have been extensively characterized in terms of thermal properties and crystallization kinetics [68-74, 106], mechanical properties [68, 88], or as templates to create mesoporous filtration membranes [81-87].

More complex PEEK-based ternary systems, usually containing *m*-PEI (miscible with PEEK) as one of the components, have also been reported in the literature. For example, a PEEK/*m*-PEI/poly(ether diphenyl ether ketone) (PEDEK) ternary system was reported and mainly characterized in terms of thermal properties, without, however, extensive morphological characterization. This ternary system was reported to be fully miscible in the amorphous/melt state, not because of strong specific interactions between its components, but rather due to the similar binary pairs' interaction parameter values that promote miscibility, a rare feature in ternary polymer blends [97].

In order to improve the mechanical properties of PEEK, a PEEK/*m*-PEI/liquid crystalline polymer (LCP) system was prepared, and its morphological features and phase diagram were analyzed [98-100]. The PEEK/*m*-PEI pair is known to be fully miscible in the amorphous state at all compositions. Meanwhile, the LCP/*m*-PEI pair was found to be only partially miscible, whereas the PEEK/LCP pair displayed complex miscibility/immiscibility behavior depending on the composition and crystallinity of the PEEK and LCP. The system displayed a higher tensile modulus or higher ultimate tensile strength, depending on the compositions, compared to the pure polymers [98]. In each case, the compositions displaying better mechanical properties were partially miscible with complex phase-separated morphologies [98].

For the preparation of filtration membranes, a PEEK/*m*-PEI/poly(ether sulfone) (PES) ternary system was developed, and its morphology was characterized by SEM [104]. The PEEK/PES and *m*-PEI/PES pairs were found to be immiscible, resulting in PES forming micron-size droplets in a

PEEK/*m*-PEI matrix. The addition of PES was intended to generate micron-size pores, thereby reducing pressure drop and enhancing permeation flux across the membrane. Thermally controlled phase separation was next induced between PEEK and *m*-PEI by further crystallizing the PEEK, resulting in an additional nanoscale co-continuous morphology which contributes to the membrane's selectivity. Finally, hierarchically porous PEEK membranes were obtained by selectively extracting both the PES and *m*-PEI phases, respectively generating micron-scale and sub-micrometer-scale pores.

Another ternary system combined PEEK with *m*-PEI and poly(ethylene naphthalate) (PEN). PEEK/*m*-PEI and PEN/*m*-PEI are miscible pairs, whereas the PEEK/PEN pair is immiscible. It displays fully miscible (homogeneous) and biphasic states, depending on composition, with the biphasic region extending towards the binary PEEK/PEN system on the phase diagram [101]. This ternary system was developed to obtain high T_g materials that can still be strain-hardened under a tensile force to obtain self-leveling films with good mechanical properties [102, 103]. Since the addition of *m*-PEI to PEN hinders its crystallization, while increasing the blend T_g, PEEK is thus added in a small amount to the blend to regain the crystallization-based strain-hardening effect.

Although multicomponent/multiphase systems of high-performance polymers, with highly controlled morphologies, can offer clear application advantages and opportunities – *i.e.* hierarchical porosity or enhanced mechanical properties as demonstrated previously – predicting the resulting type of morphology and how the phases are organized for a given system has not been addressed so far, to the best of our knowledge. To predict the complex morphologies obtainable in immiscible ternary polymer systems, theoretical tools, such as spreading coefficients calculated from the binary pairs' interfacial tensions, can be used. These coefficients proved efficient in predicting the equilibrium morphologies observed in more classical and fully immiscible ternary systems of commodity thermoplastics, such as HDPE/PS/PMMA [126, 140], or HDPE/PP/PS [141]. However, to the authors' knowledge, they have never been employed for high-performance polymer systems, for which several miscible and partially miscible pairs are reported [142-145].

In our previous work, we investigated the morphological behavior of melt-processed PEEK/*m*-PEI/*p*-PEI ternary systems composed of two miscible pairs, *i.e.* PEEK/*m*-PEI and *m*-PEI/*p*-PEI, and the partially miscible PEEK/*p*-PEI [146]. This system presents either monophasic or biphasic phase-separated morphologies, depending on the chosen composition, and allows for the

preparation of porous PEEK materials with one of the broadest ranges of achievable average pore diameter, from a few nm to several μm, by carefully tuning the composition, and by selectively extracting both PEIs.

Following this study, the main objective of the present work is to assess and understand how melt-processed PEEK-based high-performance ternary polymer systems, with highly controlled hierarchical morphologies, can be comprehensively designed and prepared. Starting from the nearly immiscible mixture of PEEK and polycarbonate (PC), a third component is added to the system: (1) *meta*-PEI, fully miscible and typically generating a nanoscale morphology with PEEK; (2) *para*-PEI, partially miscible and generating a sub-μm morphology with PEEK; (3) poly(phenyl sulfone) (PPSU), a material comparable to PEI, with superior impact properties, but barely investigated in combination with PEEK.

The level of compatibility for each polymer pair is evaluated both by calorimetric analysis (via the shift in T_g's) and by measuring the interfacial tensions by the breaking thread method. We then evaluate if spreading coefficients, based on the polymer pairs' interfacial tensions, can be used to accurately predict the morphologies observed by SEM, in the limiting cases when partially miscible and/or fully miscible binary pairs are involved. Finally, the possibility of preparing hierarchically porous PEEK monoliths is evaluated by selectively extracting the other two complementary polymers.

6.2 Materials and methods

6.2.1 Materials

All high-performance thermoplastics used in this work were in pellet form. Polycarbonate (PC) Lexan 101, poly(ether imides) Ultem 1010 (*m*-PEI), Ultem CRS 5001 (*p*-PEI), and Ultem CRS 5011 (*p*-PEI_2) were all obtained from Sabic. Two past publications supported the *para*-diamine nature of Ultem CRS 5001 [79, 107]. Poly(phenyl sulfone) (PPSU) Radel 5000 was obtained from Solvay. Poly(ether ether ketone) (PEEK) 90G was obtained from Victrex. **Table 6.1** presents their main properties.

Table 6.1 High-performance thermoplastics' main properties

	Density ρ_0 Room T (g/cm^3) [a]	M_0 (g/mol) [b]	M_n (g/mol)	M_w (g/mol)	η_0 at 375 °C (Pa.s)	Torque at plateau (N·m) [e]	T_g (°C) [f]
PEEK	1.30	288.30	22 380 [a]	59 680 [a]	210	0.77	141/147
m-PEI	1.27	592.61	20 100 [c]	47 500 [c]	381	1.48	215/217
p-PEI	1.28	592.61	-	37 000 [d]	2190	3.80	225/227
p-PEI_2	1.28	592.61	-	-	440	-	223/226
PPSU	1.29	400.45	42 000 [d]	50 000 [d]	1044	-	221/221
PC	1.20	254.28	11 600 [d]	30 500 [d]	133	-	150/150

[a] Provided by the supplier.

[b] Molar mass of the polymer repeating unit.

[c] Measured by GPC in chloroform at 35 °C.

[d] Based on references [79, 147, 148]

[e] In internal mixer at 370 °C and 50 rpm.

[f] Measured by DSC on the 1st/2nd heating cycles.

6.2.2 Blend preparation

Three different ternary systems were investigated: PC/PEEK/*m*-PEI, PC/PEEK/*p*-PEI, and PC/PEEK/PPSU. The 7 associated binary pairs were also prepared at a composition of 50/50 vol%. The ternary systems are denoted as "PC vol%/PEEK vol%/X vol%" for the rest of this work, where X = *m*-PEI, *p*-PEI, or PPSU. All materials were dried under vacuum at 100 °C for 24 h before extrusion. Blends were melt-processed for 6 min in a micro-compounder (DSM Xplore, 5 cc), at 370 °C and 50 rpm. The resulting ≈ 30 cm extruded filaments were plunged in an ice-water bath right after processing to freeze the morphology.

6.2.3 Quiescent annealing

Before conducting quiescent annealing experiments, quenched ternary blend filaments were cut into ≈ 1 cm pieces and vacuum-dried at 100 °C for 24 h to eliminate residual moisture. Each piece

was then individually wrapped in aluminum foil coated with a boron nitride-based release agent (Momentive, USA) to prevent adhesion during thermal treatment. Annealing was carried out using a Carver high-temperature hydraulic press at either 200 °C or 380 °C, depending on the intended thermal protocol. To increase the crystallinity of PEEK, samples were annealed at 200 °C for 30 min and subsequently air-cooled to ambient conditions. These samples are referred to as "R 200 °C". To investigate morphological coarsening, separate sets of samples were annealed at 380 °C, a temperature exceeding the melting point of PEEK, for durations of 1 or 3 min. In order to preserve the morphology and prevent post-annealing crystallization of PEEK, these samples were rapidly quenched in an ice-water bath immediately after treatment.

6.2.4 Morphological analysis

The morphology of the binary and ternary polymer blends was investigated by scanning electron microscopy (SEM, HITACHI Regulus 8220). Prior to imaging, filaments' cross-sections were prepared at room temperature using a Leica RM2165 microtome equipped with a glass knife to obtain flat and uniform surfaces. To minimize potential artifacts associated with surface skin effects, imaging was systematically carried out in the central region of the filament cross-sections.

Phase contrast was enhanced by selectively extracting the amorphous polymers (PC, PEI, and PPSU) following a solvent-based extraction protocol. Three pieces of blend filaments (≈ 1 cm each, total mass ≈ 100 mg) were first vacuum-dried at 100 °C for 24 h and weighed. For the three binary blends containing two amorphous polymers (*i.e.* PC/*m*-PEI, PC/*p*-PEI, and PC/PPSU), room-temperature benzene was used for 30 min to etch the PC present at the surface of the samples. All other samples were immersed in a composite solvent composed of 80 vol% of 1-methyl-2-pyrrolidone, 10 vol% ethanolamine, and 10 vol% deionized water, which extracts all of the amorphous polymers. In this latter case, the extraction was conducted at 120 °C for 1 h [83].

For samples containing more than 20 vol% of PEEK, a cleaning procedure was applied using an ultrasonic bath: first in the extraction solvent (1 min), then in 95% ethanol (1 min), and finally in deionized water (1 min). For more delicate compositions (notably 45/10/45 and 47.5/5/47.5), the ultrasonic treatment was omitted, and the cleaning sequence in ethanol and water was instead repeated twice. After the solvent extraction and cleaning sequences, all samples were freeze-dried for 3 days and reweighed to assess the extraction efficiency.

Before SEM observation, a conductive carbon coating (≈ 12 nm) was deposited using a Leica EM ACE600 coater. Imaging was performed at an accelerating voltage of 2 kV with an emission current of 10 µA.

6.2.5 Rheological measurements

Disks of PEEK, *m*-PEI, *p*-PEI, PC, and PPSU, each 25 mm in diameter and 2 mm thick, were prepared by compression molding of pre-dried pellets at processing temperatures of 380 °C, 300 °C, 300 °C, 280 °C, and 280 °C, respectively. Molding was carried out using a Carver hydraulic hot press under a nitrogen atmosphere to prevent oxidative degradation. Rheological characterization was conducted on an MCR 302 rheometer (Anton Paar) equipped with a CTD 450 convection oven and a 25 mm parallel plate geometry. All measurements were performed at 375 °C under nitrogen. The validity of the Cox-Merz equivalence was assumed [111-113]. Zero-shear viscosity values were obtained by fitting the data of at least three independent frequency sweep experiments (performed at a constant strain amplitude of $\gamma_0 = 5\%$) using the Carreau–Yasuda model to approximate the Newtonian plateau.

6.2.6 Breaking thread method

For the interfacial tension measurements, *p*-PEI_2 (Ultem CRS 5011) was selected in place of *p*-PEI (Ultem CRS 5001), whose high melt viscosity prevented practical observation times. Filaments of PEEK, *p*-PEI_2, and PPSU, with diameters ranging between 20 and 40 µm, were manually drawn from molten pellets using a hot plate. Films of PC, *p*-PEI_2, and PPSU, approximately 150 µm thick, were prepared by compression molding at 280 °C under a nitrogen atmosphere. A typical sample configuration consisted of a 2 cm long filament of the higher-melting/softening polymer positioned between two films (1 x 2 cm) of the lower-melting/softening component. This layered assembly was placed on a microscope glass slide and covered with a glass coverslip. Observations were conducted using a Mettler FP-82HT hot stage, controlled by a Mettler FP-90 processor, and maintained at 375 °C. Real-time observation was performed with a Nikon optical microscope, while image acquisition was handled by a Coreco Oculus acquisition system coupled with Visilog 4.1.3 software. The evolution of interfacial instabilities was analyzed using ImageJ (version 1.53), enabling quantification of filament diameters and distortion wavelengths over time.

The interfacial tension (γ) is calculated from **Equations 6.1 to 6.3**:

$$\gamma = \frac{q\eta_m D_0}{\Omega(p,\lambda)} \tag{6.1}$$

$$q = \frac{\ln\left(\frac{\alpha(t)}{\alpha_0}\right)}{t} \tag{6.2}$$

where

$$\frac{\alpha(t)}{\alpha_0} = \frac{D_{max}(t) - D_{min}(t)}{D_{max}(t_0) - D_{min}(t_0)} \tag{6.3}$$

with q the growth rate of the distortions (α), η_m the zero-shear viscosity of the polymer films, D_0 the initial filament diameter, the function $\Omega(p,\lambda)$ reported in Chappelear's work [114], α_0 the distortion amplitude at the start of the observation, $\alpha(t)$ the distortion amplitude at time t, D_{max} and D_{min} respectively the maximum and minimum filament diameters during deformation. For each polymer pair investigated, the quantification of $\alpha(t)$ was based on the average of three successive maxima and two successive minima in the filament diameter, with all measurements repeated for three independent experiments.

6.3 Results and Discussion

6.3.1 Phase behavior of binary systems

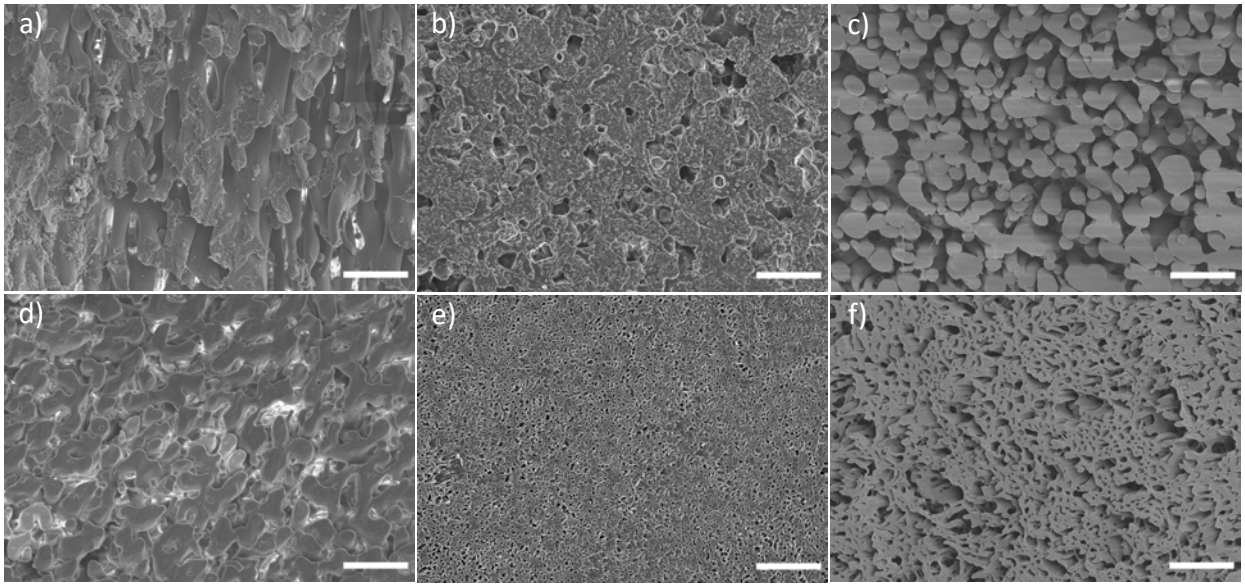

Figure 6.1 Morphology of the quenched binary systems at a 50/50 composition, as revealed after the selective extraction of either PC, *p*-PEI, or PPSU. a) PC/*m*-PEI; b) PC/*p*-PEI; c) PC/PPSU; d) PC/PEEK; e) PEEK/*p*-PEI; f) PEEK/PPSU. White scale bars represent 5 µm.

Figure 6.1 displays the morphology of six binary systems used in this work. The remaining PEEK/*m*-PEI pair is not represented, since it is known to be fully miscible in the melt state [69, 71, 72, 125]. All six binary blends in Figure 6.1 exhibit phase-separated morphologies, with a clearly discernable co-continuous microstructure with percolated domains typically observed around a 50/50 composition – indicating a certain level of immiscibility between the materials. The domain sizes are approx. 2 to 3 µm for the PC/*m*-PEI (a), PC/*p*-PEI (b), PC/PPSU (c), and PC/PEEK (d) systems. The PEEK/PPSU (f) system displays a finer morphology ranging from 0.5 to 1 µm which suggests a higher affinity between these two polymers compared to the previous binary pairs. Finally, the PEEK/*p*-PEI (e) system, exhibits the finest morphology of all at only 0.3 µm because of its partial miscibility nature [125]. In all cases, the morphology is quite fine and suggests a certain level of affinity between the materials, even though phase separation is observed.

Table 6.2 Glass transition temperatures (T_g) and interfacial tension values for binary systems

		PC/ *m*-PEI	PC/ *p*-PEI	PC/ PPSU	PC/ PEEK	PEEK/ *m*-PEI	PEEK/ *p*-PEI	PEEK/ PPSU
1st DSC cycle	T_{g1}	151	150	154	143	179	164	149
	T_{g2}	216	227	222	/		/ [c]	/ [c]
2nd DSC cycle	T_{g1}	150	151	153	148	168	164	161
	T_{g2}	216	227	220	/	212	216	215
Interfacial tension at 375 °C (mN/m)		1.76 ± 0.14 [a]	1.70 ± 0.13	2.75 ± 0.33	0.70 ± 0.12	0 [b]	0.18 ± 0.05	0.32 ± 0.04

[a] Measured at 340 °C.

[b] Set to 0 since the pair is fully miscible.

[c] PEEK cold-crystallization masks T_g measurement.

To better evaluate the level of miscibility between the various pairs, **Table 6.2** presents the T_g values for the 1st and 2nd cycles of calorimetric (DSC) analysis, and the interfacial tension values obtained at 375 °C. In relation to the observations made in Figure 6.1, three categories of polymer pairs are distinguishable. The first one includes the PC/*m*-PEI, PC/*p*-PEI, and PC/PPSU systems. For this category, two T_g's are observed on the DSC heating cycles, and these are very close to the values of the pure polymers (± 1-2 °C), suggesting nearly full immiscibility between the polymers (except for PPSU in PC, where the slightly higher T_g of the PC-rich phase compared to pure PC (154 °C vs 150 °C) might indicate a small amount of PPSU miscible with PC). Furthermore, the interfacial tensions measured for these systems are relatively high (compared to the other pairs), indicating lower affinity between the polymers, which supports the DSC data.

The second category comprises PEEK/*p*-PEI and PEEK/PPSU systems for which two T_g's, shifted inward compared to the values of the pure polymers, are always measured on the 2nd heating cycle, supporting a partial miscibility behavior [109, 125]. Only one T_g is observed on the 1st heating cycle because the PEEK's exothermic cold-crystallization masks the presence of a potentially higher value T_g. For these two systems, the interfacial tensions are quite low (nearly an order of magnitude lower compared to the three previous nearly immiscible binary pairs), as expected for partially miscible pairs. However, it should be noted that the interfacial tension value of PEEK/PPSU is almost twice the value of PEEK/*p*-PEI, a noticeable difference that will impact the morphology of the following ternary blends.

The third category only contains the PEEK/*m*-PEI system, which is miscible in the melt state and hence only presents one T_g in the 1st DSC cycle [69, 71, 72, 125]. This system undergoes phase separation once the PEEK crystallization starts, resulting in two T_g on the 2nd heating cycle. For this system, an interfacial tension value could not be measured because of its full miscibility, hence a value of 0 was attributed.

Finally, at first glance, the PC/PEEK system does not fit perfectly in either of the categories. Indeed, for this polymer pair only one T_g is observed on the two DSC cycles, indicating a miscible system – this is not compatible however with the observed phase separation, *i.e.* the partial miscibility or immiscibility behavior clearly observed in Figure 6.1d. The intermediate interfacial tension value also supports a certain level of immiscibility. The conflicting thermal analysis result comes from the fact that the PEEK's and PC's T_g values are very close to each other (< 10 °C on

the 1st cycle, < 5 °C on the 2nd cycle), and this prevents the accurate measurement of potentially two T_g's on this small temperature interval. Whether PC and PEEK are partially miscible or fully immiscible is not clear at this point.

6.3.2 Phase behavior of ternary systems

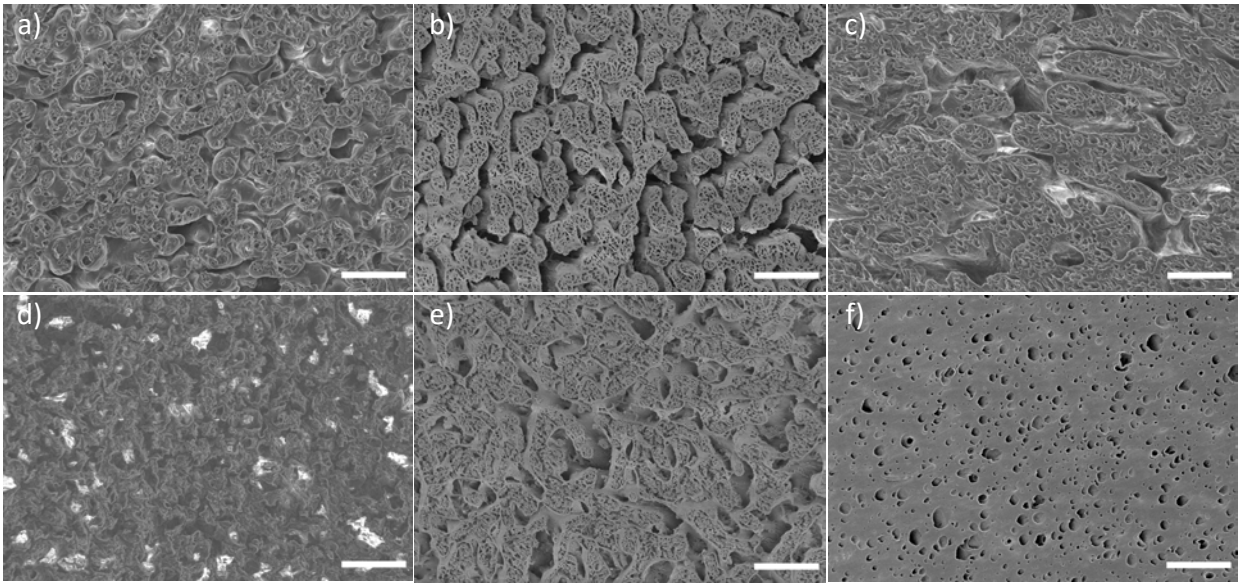

Figure 6.2 Morphology of quenched ternary PC/PEEK/*p*-PEI blends as revealed after the selective extraction of PC and *p*-PEI. Compositions in vol%: a) 50/25/25; b) 40/30/30; c) 33/33/33; d) 45/10/45; e) 40/20/40; f) 15/70/15. White scale bars represent 5 μm.

Figure 6.2 presents the morphology for the ternary PC/PEEK/*p*-PEI system at different compositions. This system was the most studied in this work and serves as a reference for comparison for the rest of the ternary systems. The three top micrographs represent compositions that are on the same isopleth on the ternary phase diagram, by progressively decreasing the amount of PC in the blend while maintaining the ratio of PEEK/*p*-PEI equal to 1 (see **Figure S6.1,** blue arrow). The three bottom micrographs represent compositions also present on a common isopleth (see Figure S6.1, red arrow), this time by increasing the amount of PEEK while maintaining the ratio PC/*p*-PEI equal to 1. In all cases (except for Figure 6.2f), both PC and *p*-PEI were completely extracted, confirming that all three materials, including PEEK, form percolated networks.

Looking at the morphology in Figure 6.2a-c, varying the amount of PC while maintaining the PEEK/*p*-PEI ratio constant reveals two distinct, separate networks of pores following PC and *p*-PEI

extractions: (1) a fine network within the residual PEEK phase associated to the extraction of *p*-PEI (compatible with the low interfacial tension between PEEK and *p*-PEI), and (2) a separate, coarser network following PC extraction (see **Figure S6.2** for morphologies after selectively extracting PC only). Both networks are completely separated by a fully formed layer of PEEK, which is especially apparent at the PC/PEEK interface (see **Figure S6.3** for higher magnification micrographs). This result is compatible with the morphologies of the binary systems in Figure 6.1d-e, and with the relative magnitudes of the interfacial tensions (PC and *p*-PEI have the highest interfacial tension), which should promote their separation by PEEK. Hence, the porous PEEK monoliths obtained after the extraction process possess a bimodal pore size distribution, with PC domains around 2 μm and *p*-PEI domains roughly 0.2-0.3 μm wide.

In Figure 6.2d, the amount of PEEK is decreased down to 10 vol% (at symmetric compositions of PC and *p*-PEI). Such a small volume fraction results in a delicate PEEK thin-film type of microstructure after the complete extraction of both PC and *p*-PEI. This thin PEEK film (herein on the micrograph collapsed over itself and forming veil-like walls outlining the network of pores) forms in fact a thin layer at the interface of the PC and *p*-PEI materials (see Figure S6.3d). By increasing the amount of PEEK to 20 vol% (Figure 6.2e), a morphology comparable to Figure 6.2b and c is recovered.

In Figure 6.2f, PEEK is now the main component of the blend and acts as the matrix for PC and *p*-PEI dispersed droplet phases. According to the previous morphological observations, the PEEK phase should separate the PC from the *p*-PEI droplets, which seems to be the case as no composite droplets of PC and *p*-PEI were observed [126].

Overall, many of these features are comparable to those observed in more classical and fully immiscible ternary systems reported in the literature.

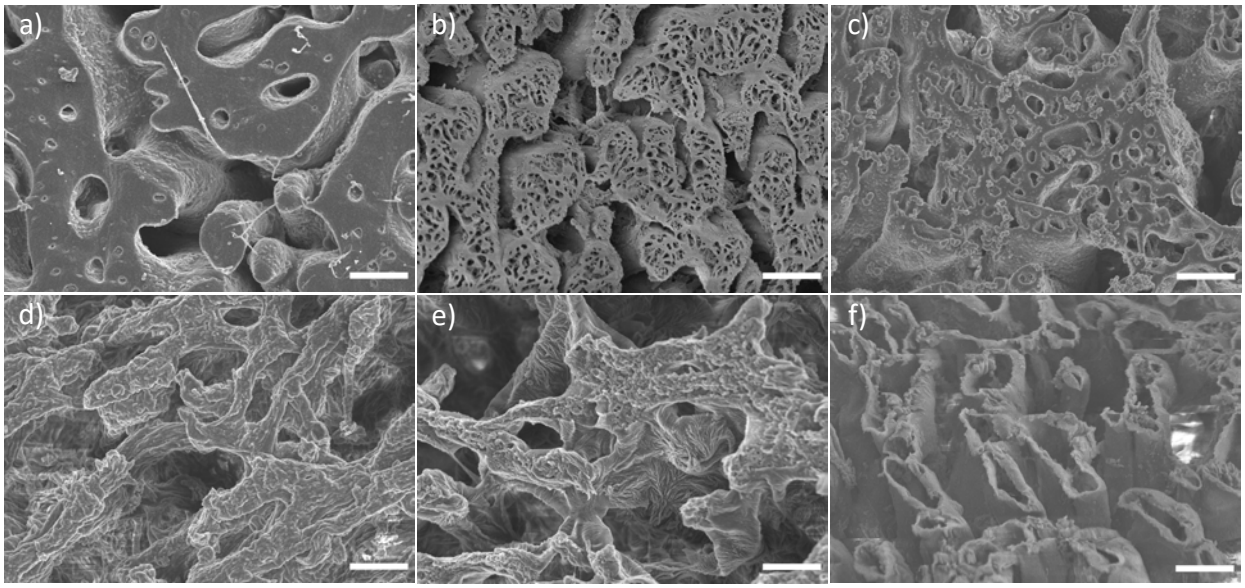

Figure 6.3 Morphology of the three ternary systems for two different compositions, as revealed after the selective extraction of PC, *p*-PEI, and PPSU. Compositions in vol%: a) PC/PEEK/*m*-PEI 40/30/30; b) PC/PEEK/*p*-PEI 40/30/30; c) PC/PEEK/PPSU 40/30/30; d) PC/PEEK/*m*-PEI 45/10/45 R 200 °C; e) PC/PEEK/*p*-PEI 45/10/45 R 200 °C; f) PC/PEEK/PPSU 45/10/45. White scale bars represent 2 μm.

Figure 6.3 displays a direct comparison between the three different ternary systems studied in this work (PC and PEEK are always present; the third material changes). From the left column to the right, the overall level of miscibility decreases, from a miscible pair (PEEK/*m*-PEI, (a) & (d)), to a partially miscible pair with a low interfacial tension (PEEK/*p*-PEI, (b) & (e)), to a partially miscible pair with higher interfacial tension (PEEK/PPSU, (c) & (f)). In all cases, PC is nearly immiscible with both PEIs and PPSU, as the T_g's of Table 6.2 indicate, with the highest interfacial tension values.

In Figure 6.3a to c, the morphology transitions from what looks like a classical binary immiscible blend with a co-continuous microstructure, to a more complex tri-continuous morphology. In Figure 6.3a, the *m*-PEI is fully miscible in the PEEK phase, and this miscible homogeneous phase interacts with the PC phase like a classical binary blend would. In Figure 6.3b, the partial miscibility between PEEK and *p*-PEI results in two distinct networks (as Figure 6.2 also illustrates), with *p*-PEI forming the finer network (~ 0.3 μm) within the PEEK domains. Finally, as the level of miscibility decreases again by substituting *p*-PEI with PPSU in Figure 6.3c, there are still two distinct networks, including a PPSU network within the PEEK domains, but this time coarser

compared to the *p*-PEI in Figure 6.3b (PPSU has more affinity for PEEK compared to PC, based on the interfacial tensions). Since the three components of this ternary PC/PEEK/PPSU are assumed to be immiscible (or borderline immiscible for PEEK/PPSU), PC probably forms the larger ~ 2 μm domains, whereas PPSU forms the smaller ones ~ 0.5 μm, separated by PEEK.

Since PEEK tends to form a layer at the interface of the other two polymer phases, in all cases, the amount of PEEK was next decreased to 10 vol% to assess the level of continuity for very fine PEEK interfacial thin films. In Figure 6.3d, the material was subjected to a 30 min quiescent annealing step at 200 °C prior to the PC and *m*-PEI extraction, in order to maximize the crystallinity level and resulting mechanical properties of the residual interfacial PEEK phase. PEEK recrystallization leads to *m*-PEI expulsion within the remaining PEEK-rich and *m*-PEI-rich amorphous phases, resulting in a complex microstructure comprising crystalline PEEK domains with interlamellar, interfibrillar and interspherulitic amorphous regions [69, 72, 73, 80], which can explain why the morphology in Figure 6.3d appears less tenuous than expected, even though 90% of the material has been extracted, as confirmed by gravimetry. In Figure 6.3e, the material underwent the same annealing step at 200 °C for 30 min. This time, the ultraporous PEEK microstructure is clearer, with the PEEK forming thin walls roughly 150 nm thick. PEEK spherulites/crystalline domains are also visible. Closer inspection shows that the spherulites appear to be present only on one side of the PEEK walls - most probably the side in contact with the PC phase. Indeed, the annealing step was conducted at 200 °C, higher than the T_g of PC (150 °C), but also lower than the T_g of *p*-PEI (225 °C). Hence, the PC and PEEK both possess relatively high molecular mobility at this temperature compared to *p*-PEI, allowing PEEK to form spherulites when in contact with PC, but not at the PEEK/*p*-PEI interface. To better understand the morphology in this complex ternary system, **Figure S6.4b** presents the same composition, without annealing, when only the PC phase is selectively extracted with benzene. The *p*-PEI domains appear as granular sub-inclusions within the PEEK phase. Finally, in Figure 6.3f, a clear tubular morphology composed of thin PEEK walls is observed. This morphology is expected when looking at the morphologies observed for the PC/PPSU binary blend (Figure 6.1c) (see also Figure S6.4c when only the PC phase is extracted). In this micrograph, the material was not subjected to an annealing step since the PEEK was already completely localized at the interface between the PC and PPSU phases, producing a sufficiently strong material even at such a low composition.

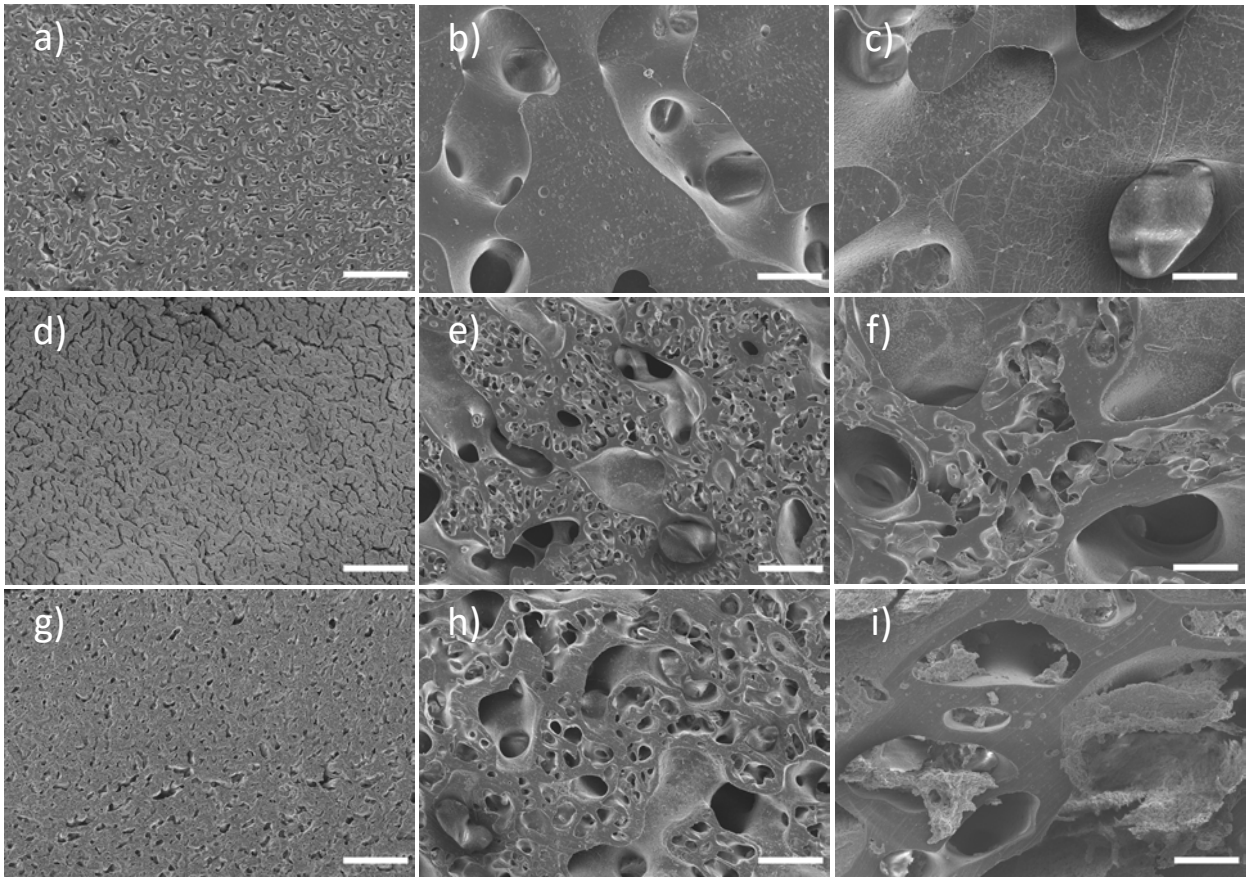

Figure 6.4 Morphology of the three ternary systems, all at a fixed composition of 40/30/30, first in the quenched state right after processing (left column), and after 1 and 3 min of quiescent annealing (center and right columns, and identified by C1 and C3, respectively). PC, *p*-PEI, and PPSU were completely extracted. a) PC/PEEK/*m*-PEI Q; b) PC/PEEK/*m*-PEI C1; c) PC/PEEK/*m*-PEI C3; d) PC/PEEK/*p*-PEI Q; e) PC/PEEK/*p*-PEI C1; f) PC/PEEK/*p*-PEI C3; g) PC/PEEK/PPSU Q; h) PC/PEEK/PPSU C1; i) PC/PEEK/PPSU C3. White scale bars represent 20 μm.

Figure 6.4 again directly compares the three different ternary systems, but this time after a quiescent annealing step over the PEEK melting temperature. The global level of immiscibility increases, from the miscible PEEK/*m*-PEI pair (top row), compared to the partially miscible pair of PEEK/*p*-PEI (middle row), and finally to the nearly immiscible pair of PEEK/PPSU (bottom row). From the left to the right, the micrographs compare quenched samples to C1 (1 min) and then to C3 (3 min) annealed samples.

Coarsening exacerbates the trends observed in Figure 6.3. For the PC/PEEK/*m*-PEI system, *m*-PEI is miscible with PEEK and forms a homogeneous phase, which explains why no coarsening within the PEEK/*m*-PEI blend phase is observed. However, the PC and (PEEK+*m*-PEI) blend phases show

significant coarsening, consistent with the existence of an interfacial tension between these two phases, driving coarsening in order to minimize the interfacial free energy. Extraction of both PC and *m*-PEI phases after coarsening should then lead to two increasingly distinct networks of pores: (1) a network of mesopores nearly constant in size stemming from the extraction of the *m*-PEI phase within the PEEK phase [81, 83, 125], and (2) a second network of macropores increasing in average size as annealing time is prolonged, by extracting the PC phase – *i.e.* the two distributions should gradually separate with increasing annealing time.

For the other two systems, each displaying three phases, coarsening is observed for all phases. For the PC/PEEK/*p*-PEI system, the *p*-PEI-rich phase, within the PEEK-rich phase, coarsens more slowly compared to the PC phase – the two networks can be clearly distinguished in Figure 6.4d-f. For the PC/PEEK/PPSU system, the PPSU phase, within the PEEK phase, also coarsens rapidly, and both PC and PPSU networks are nearly impossible to distinguish after 3 min of coarsening (Figure 6.4i). For both the PC/PEEK/*p*-PEI and PC/PEEK/PPSU systems, the rates of phase coarsening and characteristic phase size as a function of time is a complex interplay of various factors, including (1) the interfacial tensions (higher interfacial tension speeds up coarsening), (2) phase viscosity, which slows down the process as it increases, (3) the initial average phase size, etc. The relative coarsening rates and characteristic sizes of the *p*-PEI and PPSU phases (the former coarsens much less rapidly) can be explained following these guidelines: *p*-PEI is nearly twice as viscous as the PPSU phase, whereas the PEEK/*p*-PEI interfacial tension is nearly twice as low compared to the PEEK/PPSU tension (0.18 mN/m VS 0.32 mN/m). Considering that the PPSU phase is already coarser at the beginning (see Figure 6.3b and c), all of these factors explain why the coarsening rate of the PPSU phase and the resulting characteristic phase size as a function of annealing time are higher. Understanding these effects provides levers to finely control the morphological features in ternary systems.

6.3.3 Predicting the phase behavior in ternary systems comprising partially miscible and nearly miscible binary polymer pairs based on the spreading coefficients

The previous results illustrate that all three systems can display complex morphologies, with a certain level of organization – *i.e.* the PEEK phase always tends to situate and completely separate the other two polymers (PC is separated from *m*-PEI, *p*-PEI, and from PPSU). This level of

organization has been explained in previous publications using spreading coefficients theory for fully immiscible ternary systems of commodity thermoplastics [90, 140, 149]. To the best of our knowledge, no attempt has been made for ternary systems comprising partially miscible pairs (herein PEEK/*p*-PEI and PEEK/PPSU), or, at the limit, miscible pairs (PEEK/*m*-PEI herein) (as mentioned previously, it is not clear whether PEEK and PC are partially miscible, or immiscible).

Spreading coefficients (λ) basically compare the interfacial free energy between the four distinct morphologies a 3-phase system can adopt at thermodynamic equilibrium, *i.e.* the tendency of each phase to spread at the interface of the other two, ultimately completely separating them. As such, three spreading coefficients need to be calculated. If one out of the three coefficients is positive (*i.e.* if $\lambda_{ijk} = \gamma_{ik} - (\gamma_{ij} + \gamma_{jk}) > 0$), it indicates that phase *j* spreads at the interface and separates phases *i* and *k* – *i.e. j* completely wets the *ik* interface. In that case, the other two coefficients (λ_{ikj} and λ_{jik}) are negative. Overall, there are three possible equilibrium morphologies associated with complete wetting scenarios. The fourth possibility arises when all three coefficients are negative, indicating that none of the phases completely spreads at the interface of the other two. In that case, the three phases meet along a common line of contact – *i.e.* a 3-phase line of contact, with characteristic contact angles related to the ratios of the interfacial tensions [149].

For every ternary system in this work, the lowest interfacial tension among the constitutive binary pairs is always between PEEK and the third component (PEEK/PPSU, PEEK/*p*-PEI, or PEEK/*m*-PEI). Next is the interfacial tension between PC and PEEK. Finally, the largest interfacial tension is between PC and the third component (PC/PPSU, PC/*p*-PEI, or PC/*m*-PEI): $\gamma_{PC/PPSU} > \gamma_{PC/m\text{-}PEI} > \gamma_{PC/p\text{-}PEI} > \gamma_{PC/PEEK} > \gamma_{PEEK/PPSU} > \gamma_{PEEK/p\text{-}PEI} > \gamma_{PEEK/m\text{-}PEI} = 0$. **Table 6.3** presents the spreading coefficient values calculated with the interfacial tensions measured by the breaking thread method and reported in Table 6.2. For the PC/PEEK/*p*-PEI system (with the PEEK/*p*-PEI partially miscible pair), $\lambda_{PC,PEEK,pPEI} > 0$ and indicates that PEEK should spread at the PC/*p*-PEI interface and separate both polymers. Schematically, this corresponds to the scenarios shown in **Figure 6.5a** when PEEK is the minor phase or comparable in volume fraction to PC and *p*-PEI, or Figure 6.5b when PEEK forms the matrix, and PC and *p*-PEI form dispersed phases. In all cases, PEEK completely separates PC and *p*-PEI. This is confirmed experimentally when looking at the SEM micrographs in Figure 6.2 to Figure 6.4. For the PC/PEEK/PPSU (with PEEK/PPSU nearly immiscible or slightly partially miscible), spreading coefficients also predict the complete

separation of PC and PPSU by the PEEK phase ($\lambda_{PC,PEEK,PPSU} > 0$). This is illustrated schematically in Figure 6.5c, which is also confirmed experimentally (Figure 6.2 to Figure 6.4). For the limiting scenario, *i.e.* for the PC/PEEK/*m*-PEI system comprising the miscible PEEK/*m*-PEI binary system, $\gamma_{PEEK/m\text{-}PEI}$ is set to 0, resulting in $\lambda_{PC,PEEK,m\text{-}PEI} > 0$, corresponding schematically to PEEK forming a complete layer between PC and *m*-PEI (Figure 6.5d). Whether a very fine pure PEEK layer forms at the interface of the PC phase and (PEEK+*m*-PEI) blend phase – *i.e.* interfacial enrichment in PEEK – remains to be validated. However, the spreading coefficients still predict the correct trend.

Table 6.3 Interfacial tensions and spreading coefficients for the three ternary systems and their constitutive polymer pairs

	Interfacial tensions (γ_{ij}) at 375 °C (mN/m)	Spreading coefficients (λ_{ijk})
PC/PEEK/*p*-PEI		
PC/PEEK	0.7 ± 0.12	$\lambda_{PEEK,pPEI,PC} = 0.70 - 0.18 - 1.70 = -1.18 \pm 0.30$
PEEK/*p*-PEI	0.18 ± 0.05	$\lambda_{pPEI,PC,PEEK} = 0.18 - 1.70 - 0.70 = -2.22 \pm 0.30$
PC/*p*-PEI	1.70 ± 0.13	$\lambda_{PC,PEEK,pPEI} = 1.70 - 0.70 - 0.18 = \mathbf{0.82 \pm 0.30}$
PC/PEEK/PPSU		
PC/PEEK	0.7 ± 0.12	$\lambda_{PEEK,PPSU,PC} = 0.70 - 0.32 - 2.75 = -2.37 \pm 0.50$
PEEK/PPSU	0.32 ± 0.04	$\lambda_{PPSU,PC,PEEK} = 0.32 - 2.75 - 0.70 = -3.13 \pm 0.50$
PC/PPSU	2.75 ± 0.33	$\lambda_{PC,PEEK,PPSU} = 2.75 - 0.70 - 0.32 = \mathbf{1.73 \pm 0.50}$
PC/PEEK/*m*-PEI		
PC/PEEK	0.7 ± 0.12	$\lambda_{PEEK,mPEI,PC} = 0.70 - 0 - 1.76 = -1.06 \pm 0.26$
PEEK/*m*-PEI	0 [a]	$\lambda_{mPEI,PC,PEEK} = 0 - 1.76 - 0.70 = -2.46 \pm 0.26$
PC/*m*-PEI	1.76 ± 0.14 [b]	$\lambda_{PC,PEEK,mPEI} = 1.76 - 0.70 - 0 = \mathbf{1.06 \pm 0.26}$

[a] Set to 0 since the pair is fully miscible.

[b] Measured at 340 °C.

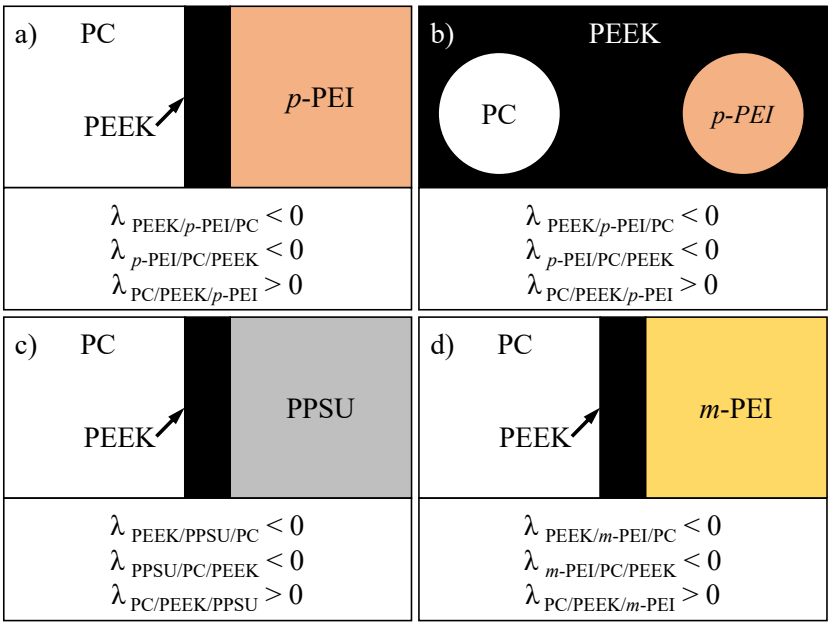

Figure 6.5 Schemes of the different morphologies predicted by the spreading coefficients and encountered in this work. In all cases, PEEK (in black) is predicted to separate PC (in white) from the third component: *p*-PEI in (a) and (b) (in orange), PPSU in (c) (in gray), and *m*-PEI in (d) (in yellow).

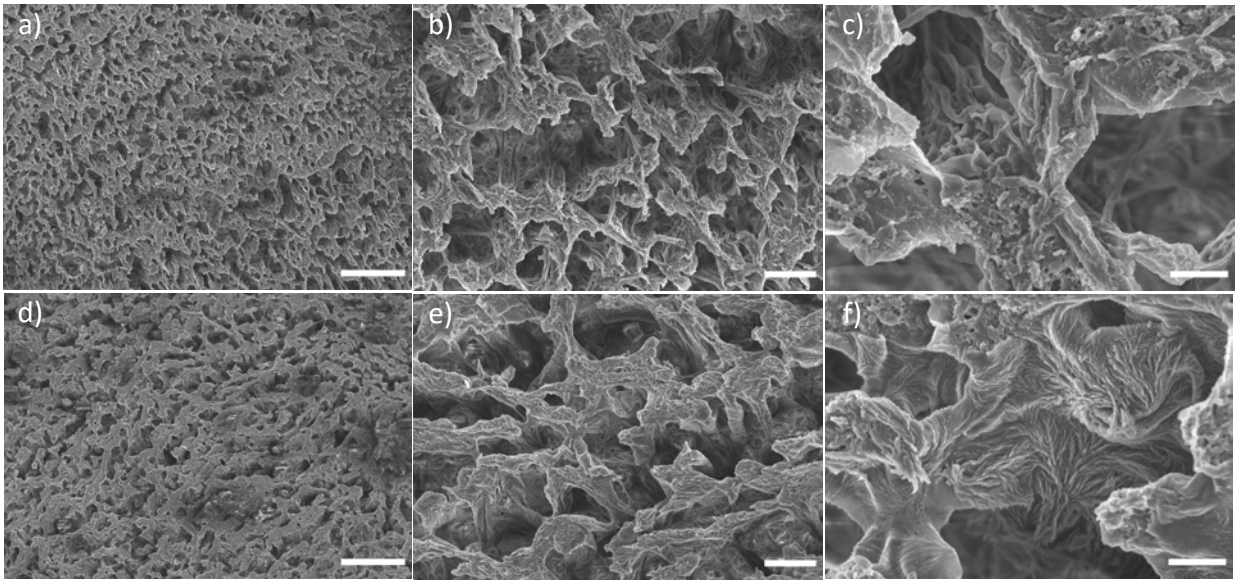

Figure 6.6 Microstructure of the PC/PEEK/*p*-PEI system for two annealed compositions: 47.5/5/47.5 (a, b, c) and 45/10/45 (d, e, f) at different levels of magnification. White scale bars represent 20 µm (a, d), 4 µm (b, e), and 1 µm (c, f).

The spreading coefficients indicate that it is then theoretically possible to form a very thin layer of PEEK at the interface of the other two phases (PC and *p*-PEI, PC and PPSU, or PC and *m*-PEI),

which, when extracted, could yield ultraporous PEEK monoliths (with tunable pore size by employing quiescent annealing).

Figure 6.6 demonstrates the approach with the PC/PEEK/*p*-PEI system, at 5 and 10 vol% of PEEK (and equal volume fractions of PC and *p*-PEI). Following annealing at 200 °C to recrystallize the PEEK phase, the extraction of both PC and *p*-PEI yielded ultraporous PEEK monoliths, with a fully open porosity and very thin PEEK domains. In particular, at 5 vol% of PEEK, what remains after the extraction step forms an ultraporous, platelet-like microstructure (Figure 6.6a-c). Figure S6.4a shows the morphology at the same composition, this time quenched, after the selective extraction of the PC phase only, helping visualize the interface between the PEEK and the PC phases. No spherulites are apparent at this composition, probably because of the very low volume fraction of PEEK, contrary to what is observed at 10 vol% (see Figure 6.6c-f). Additionally, in Figure 6.6c, we can clearly distinguish the walls of PEEK folding in on themselves like a sheet, revealing a certain flexibility at this very low percentage of PEEK. Finally, while we did not go below 5 vol% in PEEK, it would be of interest to see what would be the minimum composition yielding self-supporting structures.

6.3.4 Discussion

For all three ternary systems presented above, PC is always relatively coarse when it forms a continuous phase, and its extraction always yields a network of macropores, as it is nearly immiscible with the other polymers. Based on the interfacial tensions, PC also has overall the lowest level of affinity with the other polymers, explaining why a layer of PEEK always separates it from the third component. The hierarchical porous structure is then provided by the complementary pair formed by PEEK and the third component it encapsulates, once this third component is selectively extracted to form a second network of pores: (1) a micro/mesoporous network when *m*-PEI, miscible with PEEK, is the third component; (2) a sub-μm network with *p*-PEI, partially miscible with PEEK; (3) a larger but still sub-μm network with PPSU, also partially miscible with PEEK, but to a lesser degree compared to *p*-PEI since the T_g's are less shifted compared to the pure components, and the interfacial tension is slightly higher. As demonstrated, these trends and results can be fairly accurately predicted based on the binary pairs' miscibility and interfacial tension properties.

It is of interest to note that all binary systems in this work display (very) low interfacial tensions, with examples of partial miscibility (PEEK/*p*-PEI or PEEK/PPSU) or full miscibility (PEEK/*m*-PEI), whereas all binary combinations involving PC are borderline immiscible (we could not conclude for certain for PC/PEEK due to the close T_g's and low interfacial tension, but the relatively coarse PC/PEEK morphology in Figure 6.1d suggests nearly full immiscibility). As a result, the morphologies of all binary and ternary systems are quite fine and even show sub-μm features in some cases (PEEK/*p*-PEI), without the addition of interfacial compatibilizers.

The partial miscibility behavior of some polymer pairs (PEEK/*p*-PEI and PEEK/PPSU) also imposes limits on the precision of the interfacial tension values, as they are measured by the breaking thread method with the pure polymers, whereas more precise measurements would require the two phases to be at equilibrium. This, in addition, would provide more precise estimations for the spreading coefficients. The spreading coefficients, however, predict quite well the equilibrium morphologies. In all cases, PEEK completely separates the other two phases and, at the limit of low PEEK content, acts as a "pseudo-compatibilizer" by forming a thin layer at the interface, as predicted by the spreading coefficients. To the best of our knowledge, it is the first time that spreading coefficients are used to explain the morphological features of ternary systems comprising partially miscible and/or fully miscible polymer pairs, and for systems comprised of high-performance polymers.

From a practical perspective, these systems open the way, for example, towards the preparation of hierarchically porous PEEK monoliths with a high level of control over the porosity: fully interconnected pores, bimodal pore size distributions, ultraporosity, etc. Compared to other methods used to prepare ultraporous PEEK monoliths, such as foams or aerogels, the approach developed in this work offers faster preparation time, possible bimodal pore size distributions, and more control over the desired PEEK weight fraction (in our case, not limited by dissolution limits in certain solvents), which subsequently impacts mechanical properties [121, 122, 150]. For example, one could target a bimodal distribution with two maxima: one at the nm scale level (micro- or mesoporosity), and a second maximum at tens of μm (macroporosity). This could be achieved, for example, with the PC/PEEK/*m*-PEI system, first by annealing the blend to let the PC phase coarsen (the *m*-PEI phase will not coarsen since it is miscible with PEEK), then by extracting both the PC and *m*-PEI phases, respectively yielding the macro and micro/mesopores.

To provide even more control over the morphological features, playing on the ratio of both PEIs would represent an interesting approach, since it also tunes the miscibility between PEEK, *m*-PEI, and *p*-PEI [146]. For example, developing a quaternary system of PC/PEEK/*p*-PEI(+*m*-PEI) could also allow complete control over the size of the smaller network of pores inside the PEEK phase, by playing on the interfacial tension, miscibility, and relative coarsening rates between the PC, PEEK, and PEIs phases.

Considering the high level of morphological control achievable in these high-performance polymer-based systems, one of the next steps would be to evaluate if it is possible to further tailor and improve, for example, the toughness, tenacity, and impact properties of these already highly mechanically resistant materials.

6.4 Conclusion

This work demonstrates how melt-processed PEEK-based high-performance ternary polymer systems, with highly controlled hierarchical morphologies, can be comprehensively designed and prepared based on the miscibility level and interfacial tension of the individual binary pairs. It highlights the critical role of binary pair miscibility in dictating the final morphology, which can evolve from biphasic systems, as observed when PEEK is combined with PC and *m*-PEI, to fully triphasic systems when PEEK is instead combined with PC and *p*-PEI or PPSU.

All three PEEK-based ternary systems investigated in this work presented highly hierarchical and organized morphologies, with PEEK systematically and fully separating the other two components. Interfacial tension values were then determined for all binary pairs to calculate spreading coefficients, which proved successful in predicting the observed morphologies. To the best of our knowledge, this is the first time that spreading coefficients are employed for such complex ternary systems involving miscible or partially miscible polymer pairs.

These insights then enabled the preparation of hierarchically porous PEEK monoliths comprised simultaneously of both macro- and meso-porous network structures, with tunable pore sizes spanning a considerable range of nearly 4 orders of magnitude, from a few nanometers to several microns. Moreover, ultraporous PEEK materials containing as little as 5 vol% PEEK were successfully prepared using the PC/PEEK/*p*-PEI ternary system, underscoring the potential of such blends for very lightweight, high-performance applications. This work presents new opportunities to engineer advanced morphologies in high-performance PEEK-based polymer systems, opening

avenues for designing PEEK porous monoliths with application-specific thermal, mechanical, and morphological properties.

6.5 Supporting information: Additional morphological analysis

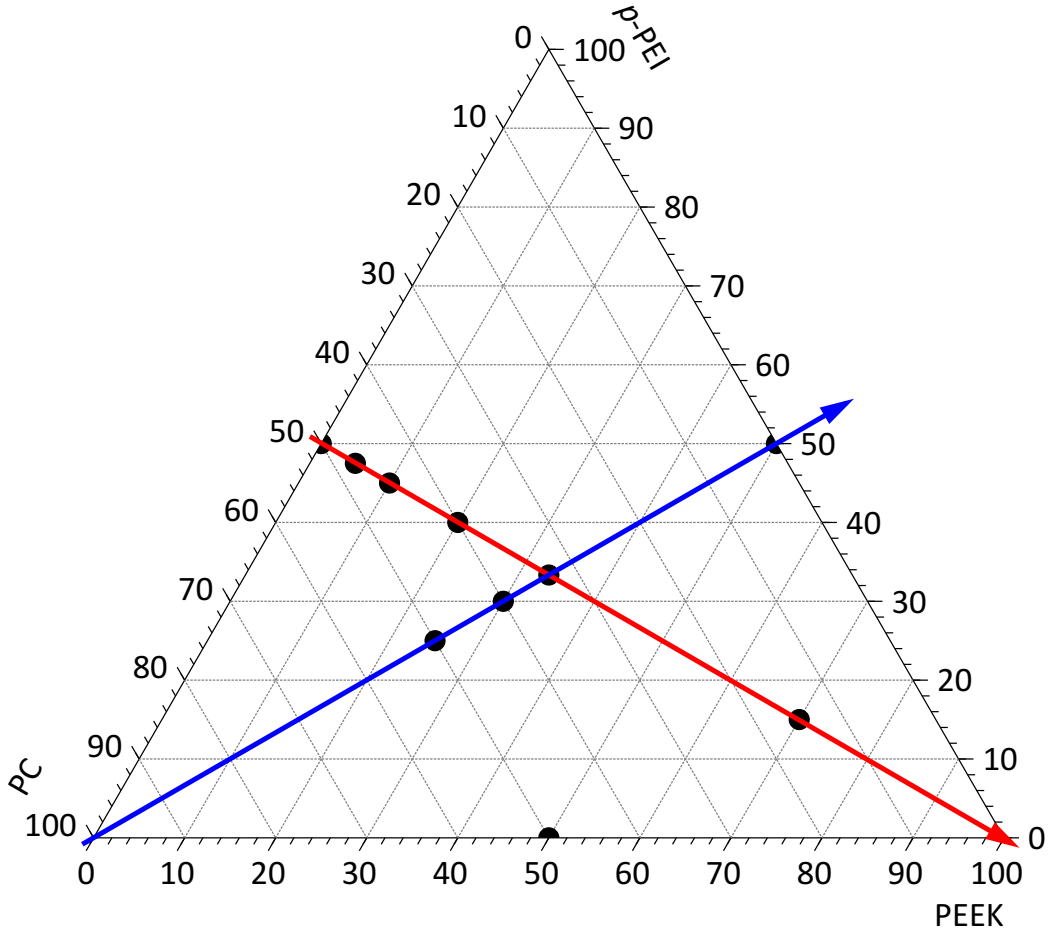

Figure S6.1. Ternary diagram representing all the binary and ternary compositions prepared for the PC/PEEK/*p*-PEI system. Isopleth with a constant ratio of PEEK/*p*-PEI equal to 1 (blue arrow). Isopleth with a constant ratio of PC/*p*-PEI equal to 1 (red arrow).

A)

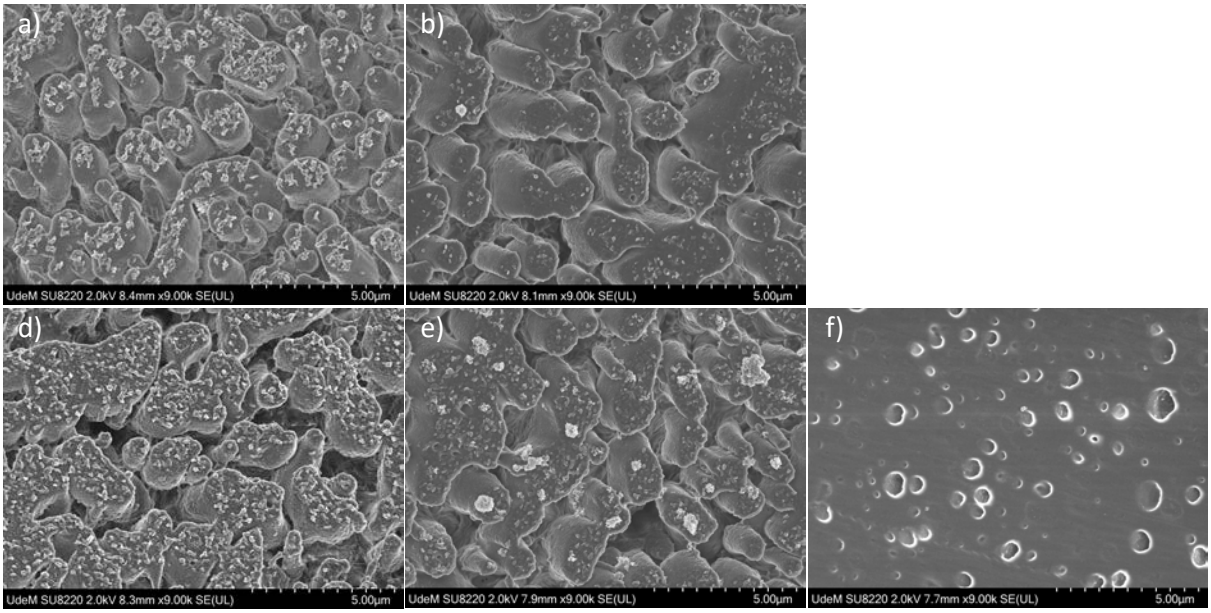

B)

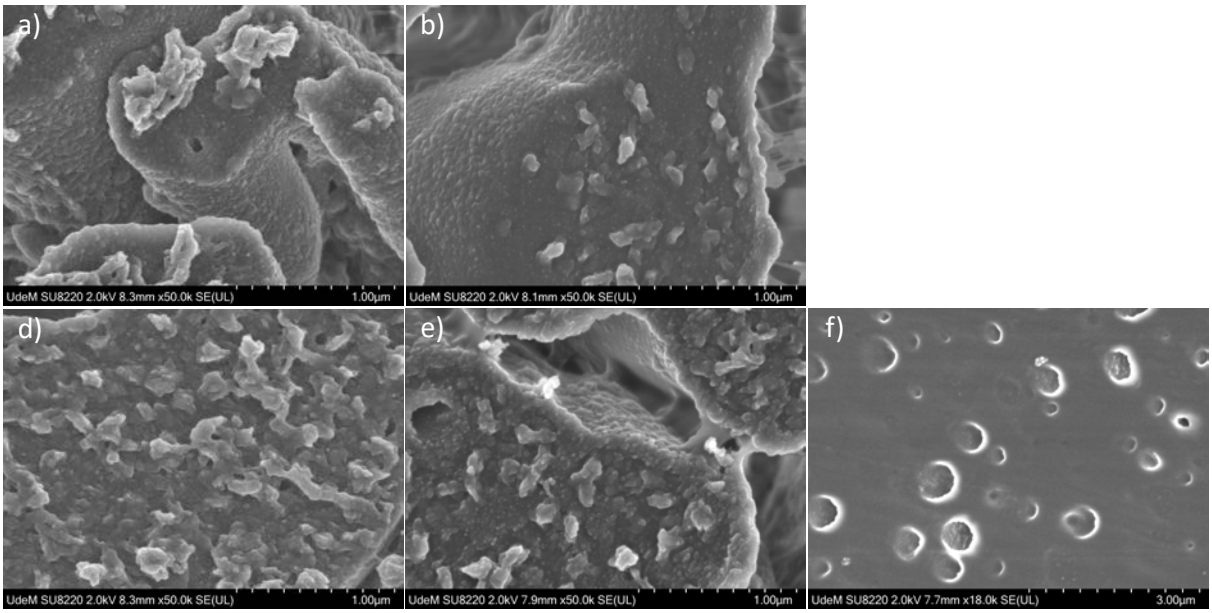

Figure S6.2. Morphology of quenched ternary PC/PEEK/*p*-PEI blends as revealed after the selective benzene-based extraction of PC. Compositions in vol%: a) 50/25/25; b) 40/30/30; ~~c) 33/33/33~~; d) 45/10/45; e) 40/20/40; f) 15/70/15. Panel **A)**: lower magnification with scale bars representing 5 µm. Panel **B)**: Higher magnification.

A)

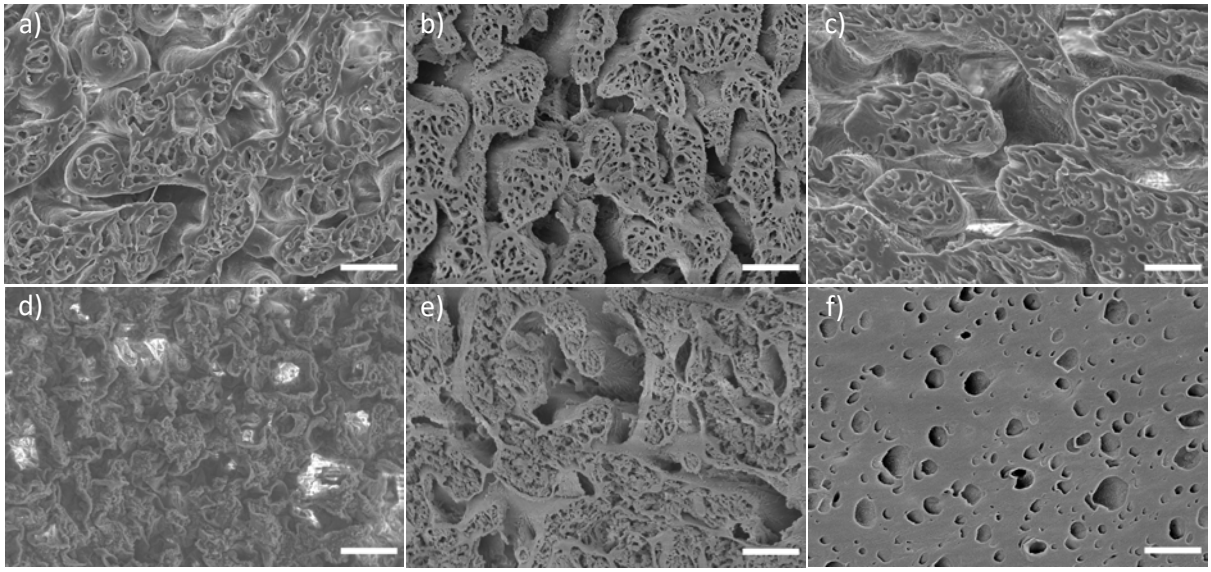

B)

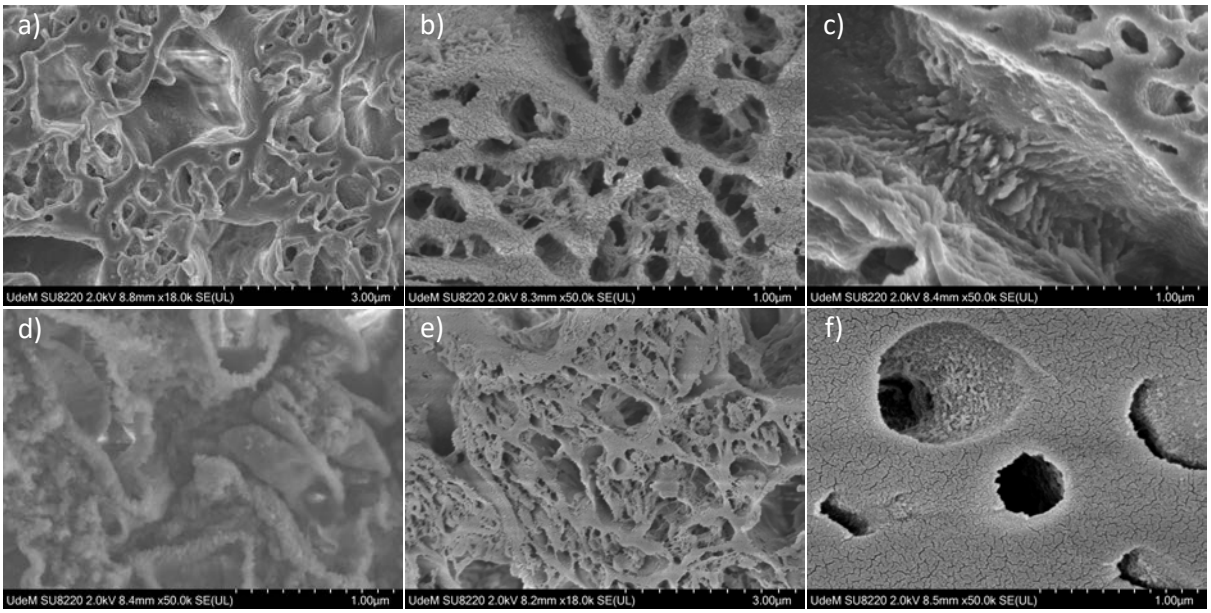

Figure S6.3. Morphology of quenched ternary PC/PEEK/*p*-PEI blends as revealed after the selective extraction of PC and *p*-PEI. Compositions in vol%: a) 50/25/25; b) 40/30/30; c) 33/33/33; d) 45/10/45; e) 40/20/40; f) 15/70/15. Panel **A)**: lower magnification with scale bars representing 2 µm. Panel **B)**: Higher magnification.

A)

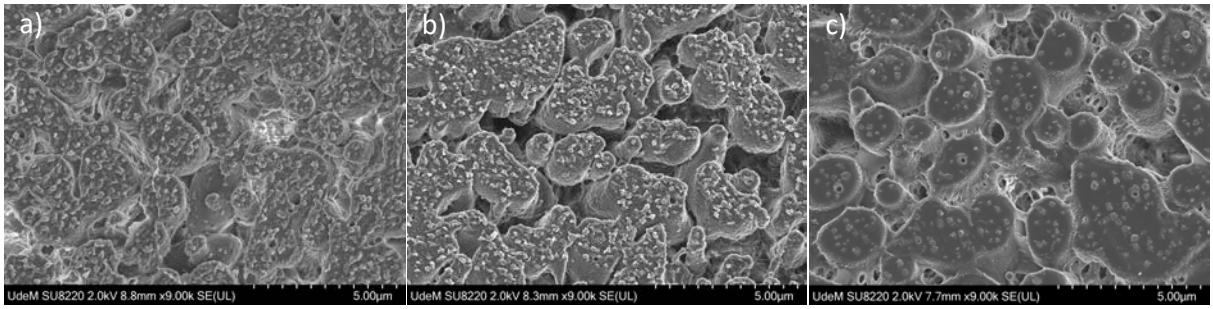

B)

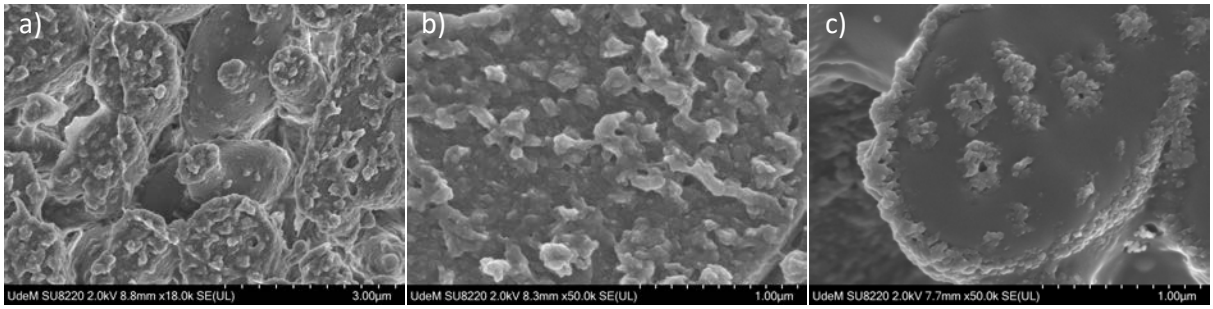

Figure S6.4. Morphology of low PEEK content quenched ternary systems as revealed after the selective benzene-based extraction of PC. Compositions in vol%: a) PC/PEEK/*p*-PEI 47.5/5/47.5; b) PC/PEEK/*p*-PEI 45/10/45; c) PC/PEEK/PPSU 45/10/45. Panel **A)**: lower magnification with scale bars representing 5 µm. Panel **B)**: Higher magnification.

CHAPTER 7 GENERAL DISCUSSION

This thesis work was part of a broader project encompassing multiple research fields, from numerical simulation to 3D printing and induction welding. The initial plan was conceived as a stepwise collaboration between the Ph.D. students, where the developed material formulations were supposed to be prepared under 3D filament spools and directly shared with students working on 3D printing applications. As is often the case in research, practical constraints with equipment, materials, and investigation scope meant the original plan could not be fully implemented – but it also led to unexpected opportunities and results. The onset of the COVID-19 pandemic at the beginning of this doctoral research also had an undeniable impact, bringing well-known disruptions to both professional and personal life.

7.1 Challenges associated with the processing of high-performance polymers

Working with high-performance thermoplastics requires specialized equipment capable of reaching the high processing temperatures they demand. Although we had access to a micro-compounder (5 c.c.) and an internal mixer (60 c.c.), the lab's available twin-screw extruder needed an upgrade to reach temperatures as high as 450 °C, which unfortunately only became available toward the end of the project. This delay made it impossible to produce enough quantity of polymer blends to allow for the preparation of 3D filament spools or standard mechanical test specimens during most of this research. Another factor worth noting is that this was the first project in the group involving high-performance polymers, meaning that many of the methods had to be developed for the first time – which turned out to be a considerable challenge. For these reasons, the thesis focused primarily on fundamental findings relating to polymer blends rather than directly on the development of structural materials for lunar applications. However, calorimetric analysis and preliminary mechanical results have nevertheless revealed the ability of these blends to increase the T_g by several tens of degrees Celsius while improving the Young's modulus, compared to neat PEEK. These observations should encourage the development of future composites incorporating these advantages for the choice of their thermoplastic matrix (*e.g.* PEEK/*m*-PEI 70/30 or 50/50 and PEEK/*p*-PEI 80/20 or 50/50).

As an example, it was initially considered to perform the morphological analyses by TEM. However, after more than a year of testing staining procedures, many ultramicrotomed samples, and limited interesting results, this method was abandoned. The staining procedure used vapor of OsO_4 to stain PEEK, but either ended staining all the sample or not sufficiently. In parallel, AFM and SEM techniques were also explored as alternatives for efficient morphological analysis tools. AFM proved costly and challenging due to the difficulty in observing partially miscible finely phase-separated systems, where the difference in chemical and physical interactions with the AFM tip was faint. At the same time, SEM observation was made possible thanks to the finding in the literature of a composite solvent allowing the depolymerization and efficient extraction of both *m*-PEI and *p*-PEI phases. Even with this approach, difficulties remained in the observation of fine morphological details by SEM, such as ~10 nm pores created after the selective extraction of *m*-PEI in annealed PEEK/*m*-PEI 50/50 blend. Observing such small details requires very high magnification, no electron-beam-related surface charging, high-vacuum SEM, low air humidity, and defect-free sample preparation, which are obviously difficult to assemble for every observation. The nm to sub-µm morphological scale in these systems, combined with the high chemical resistance of high-performance thermoplastics and their tendency to form miscible or partially miscible systems, turned out to be quite a challenge for morphological analyses.

One of the many challenges associated with the processing of PEEK is related to its very short half-crystallization time (~1 min). A quick analysis of the non-isothermal calorimetric data of PEEK and its binary blends with *m*-PEI and *p*-PEI revealed that the addition of PEI only starts to significantly slow crystallization at around 60-70 vol% of PEI. This crystallization kinetics is quite important when considering the different processing steps of a PEEK-based material. For example, in 3D printing, a fast crystallization rate can lead to defects such as warping due to crystallization-related stress concentration on one side. During this research, different annealing protocols were tested on the materials, especially on the PEEK/*m*-PEI 50/50 blend, with the annealing temperature varying from 190 °C to 300 °C (see CHAPTER 4). Those different temperatures led to distinctive PEEK crystalline morphologies, which in turn produced distinct *m*-PEI segregation length scales, from a few nm to a few µm. Such a different arrangement of crystalline and amorphous phases must impact the mechanical properties of the final material, which unfortunately could not be evaluated within the timeframe of this research.

By the end of the project, some 3D printing filament spools of PEEK/*m*-PEI (70/30, 50/50) and PEEK/*p*-PEI (80/20, 50/50) blends were successfully extruded. The fine control of their diameter remains a challenge because of the pulling belt-conveyor that made the filament slip unpredictably and whose speed was difficult to adjust. However, some sections of the filaments, with a constant 1.75 mm diameter, could be printed without difficulty through a 0.4 mm high-temperature 3D printer nozzle, supporting their future potential use in such applications.

7.2 Composites and nanocomposites investigation

During this research work, a lot of liberty was given to explore new material formulations. Among them, some composites and nanocomposites were investigated to broaden the range of properties and possible fields of applications, thanks to the addition of specialty fillers. Therefore, a few PEEK/*m*-PEI and PEEK/*p*-PEI binary blends were melt-blended with different loadings (10 wt%, 20 wt%, or 40 wt%) of short carbon fibers to qualitatively observe the impact on their processing. A quick conclusion is that the porosity level increases continually at loadings higher than 10 wt% of fillers (Figure 7.1). It is known that a competition exists between the creation of porosity and the increase in Young's modulus attributed to the addition of fillers, sometimes resulting in a plateau or even a decrease in the mechanical enhancement.

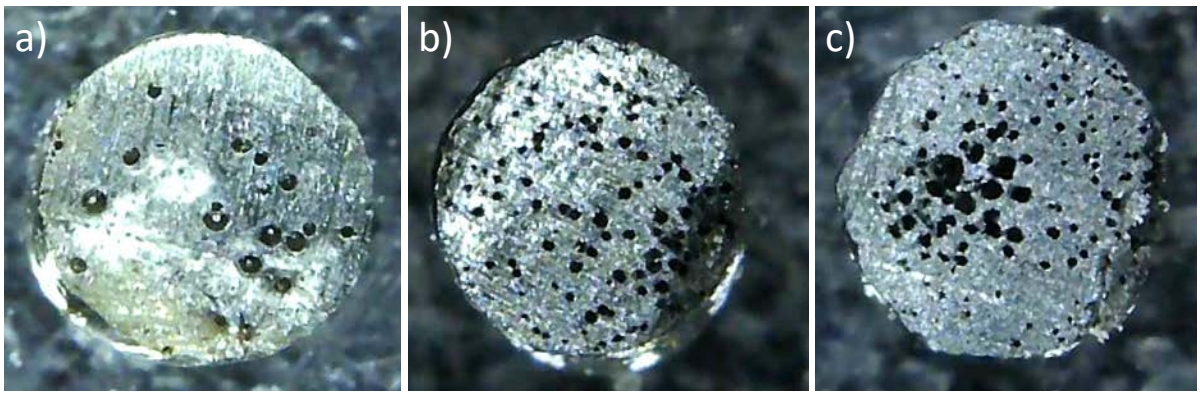

Figure 7.1 PEEK/*m*-PEI 70/30 + carbon fibers (wt%) composites: a) 10 wt%; b) 15 wt%; c) 20 wt%.

Regarding the investigation of nanocomposites, the PEEK/*p*-PEI 50/50 composition was chosen as the reference matrix due to its co-continuous morphology, and distinct fillers were tested: multi-walled carbon nanotubes (MWCNT), graphene, hexagonal boron nitride (h-BN), hydroxyapatite,

and nanosilica. The 2D platelet-like nanoparticles (graphene and h-BN) were especially difficult to exfoliate and correctly disperse in the polymer blend matrix, possibly due to the low melt viscosity of PEEK; thus, using a different grade could help in future work. Furthermore, since their aggregates' characteristic sizes (10 µm for graphene and 3 µm for h-BN) were typically larger than the characteristic morphological length scale of PEEK/*p*-PEI blends (0.3 µm), their localization in one of the two phases was difficult to assess. However, for the system containing h-BN, the nanoparticles clearly localized in the *p*-PEI-rich phase upon a 30 min quiescent annealing, highlighting its phase-separated morphology without solvent extraction (Figure 7.2a). For the other 1D (MWCNT) and spherical (hydroxyapatite and nanosilica) nanoparticles, their limited size allowed them to be directly localized inside the *p*-PEI-rich phase, as confirmed through SEM analysis (Figure 7.2b). No dispersion tests were attempted using a PEEK/*m*-PEI matrix; however, the impact of its fine phase separation behavior, due to PEEK crystallization, on the localization of the nanoparticles would be interesting for future investigation. Lastly, because it is possible to precisely control its phase-separated morphology as a matrix, some PEEK/*m*-PEI/*p*-PEI nanosilica nanocomposites were also prepared. The nanosilica were localized in the PEI-rich phase, and some were pulled out during microtomy (Figure 7.2c). In the future, this spatial confinement could be leveraged to further tailor the nanocomposite physical properties, *e.g.* electrical conductivity with the addition of MWCNT.

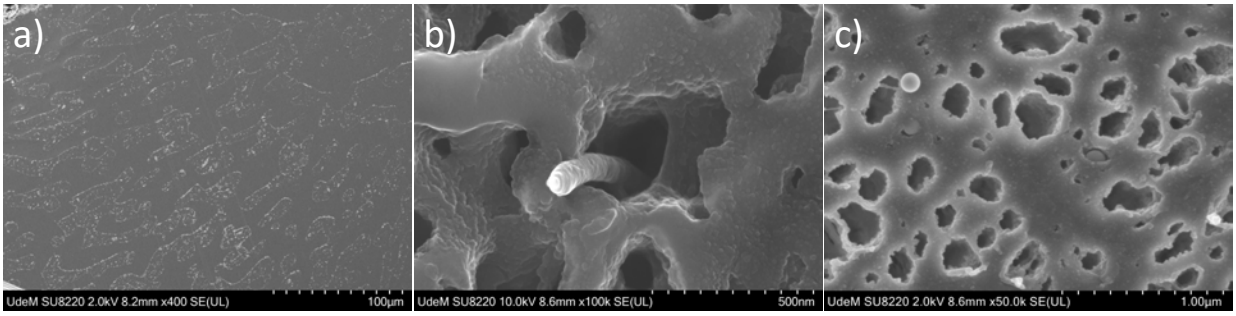

Figure 7.2 Different nanocomposites morphologies: a) non-extracted and 30 min annealed PEEK/*p*-PEI 50/50 + 5 wt% of h-BN; b) quenched PEEK/*p*-PEI 50/50 + 1 wt% of MWCNT; c) quenched PEEK/*m*-PEI/*p*-PEI 50/15/35 + 3 wt% of nanosilica.

7.3 Ternary systems considerations

The 2nd article, presented in CHAPTER 5, is a fundamental investigation on PEEK/*m*-PEI/*p*-PEI ternary systems, which led us to an attempt at calculating the composition of the phases at equilibrium in phase-separated ternary blends. A set of 8 equations and 8 unknown variables was developed to describe the system as a whole. Six out of the eight equations were mass balances for: the PEEK, the *m*-PEI, the *p*-PEI, the PEEK-rich phase, the PEI-rich phase, and the entire system. The two remaining equations associated the values of the two T_g's to the mass fractions of their components thanks to empirical equations describing miscible blends (Fox or Gordon-Taylor). For the Gordon-Taylor equation, the *K* fitting parameter was determined beforehand by "training" the equation on fully miscible ternary blends of known compositions (*i.e.* displaying only one T_g). The 8 unknown variables then corresponded to: the PEEK-rich and the PEI-rich phases' mass fractions relative to the entire blend; the PEEK, *m*-PEI, and *p*-PEI mass fractions relative to the PEEK-rich phase; and finally, the PEEK, *m*-PEI, and *p*-PEI mass fractions relative to the PEI-rich phase. By using a numerical solver, a unique solution for each variable that satisfied all the equations was expected to be found. However, the resulting variables' values were dependent on the initial guesses. This behavior needs to be analyzed while considering the following aspects: 1) the chosen ternary system was made from a binary polymer pair displaying really close T_g's (215 °C for *m*-PEI and 225 °C for *p*-PEI), which complexifies the precise measurement of their distinct contribution to the overall blend's T_g; 2) the semi-crystalline nature of PEEK adds a level of complexity to the analysis by changing the measured T_g between the DSC cycles. Through crystallization, PEEK creates a phase separation in the miscible amorphous parts of the blends, which concentrates PEEK-rich amorphous phases with additional PEEK, and segregates PEI to PEI-rich amorphous phases. This phenomenon changes the molecular compositions of the phases at equilibrium and modifies the calorimetric data from one heating cycle to another; 3) the precision of the DSC equipment, allowing measurement to the second decimal, is probably a limiting factor for the precise numerical resolution of the equations' set. In the future, those limitations would need to be alleviated in order to push forward the theoretical analysis of ternary systems and particularly for the calculation of the composition of their phases at equilibrium.

Additionally, about the difficulties caused by PEEK crystallization, its impact on obtaining the χ segmental binary interaction parameters was calculated for PEEK/*m*-PEI and PEEK/*p*-PEI blends.

Since PEEK crystals do not contribute to miscibility with the *m*-PEI in the amorphous part of the blend, their mass fraction can be subtracted from the total PEEK mass fraction in order to perform calculations only on the mass proportions of the amorphous part of the blend. Thus, for the PEEK/*m*-PEI system, the compositions affected by this consideration are those with a low proportion of crystallized PEEK, despite the quench (*i.e.* 90/10 to 60/40 vol%). Once the interaction parameter calculations have been readjusted for these compositions, the new average $\chi_{PEEK/m\text{-}PEI}$ obtained is -0.101 ± 0.057 instead of the original -0.109 ± 0.050. The variation is therefore relatively small but not negligible. In the case of the PEEK/*p*-PEI system, the recalculations give a $\chi_{PEEK/p\text{-}PEI}$ of 0.040 ± 0.004 instead of the original 0.041 ± 0.004. The crystallization of PEEK is therefore an aspect that should not be overlooked in these tedious theoretical calculations.

Another interesting observation appeared during some tensile mechanical tests on ternary systems of PEEK/*m*-PEI/*p*-PEI, during which an increase in the Young's modulus (~11 %) was observed for the miscible 50/37.5/12.5 composition compared to the reference PEEK/*m*-PEI 50/50. The full miscibility of this ternary composition was characterized in CHAPTER 5, it is thus suggested that it is possible to replace a fraction of *m*-PEI by some *p*-PEI, without producing phase-separation, to create a synergistic mechanical behavior between the polymeric components. This hypothesis would need further investigation, especially by studying PEEK-rich ternary compositions (*e.g.* 70/20/10 or 80/15/5) and the impact of their level of crystallinity, controlled by thermal annealing. Finally, exploring the mechanical properties (*e.g.* tensile, impact, or heat deflection temperature) of phase-separated PEEK/*m*-PEI/*p*-PEI systems would also be of great interest, because of the known potential such morphologies can demonstrate when they are properly compatibilized. This is the case here, with an expected strong interfacial adhesion between the phases at equilibrium, due to the pronounced partial miscibility behavior observed in such ternary systems.

7.4 Fundamental contributions

Overall, this thesis work led to several fundamental contributions, barely or not reported elsewhere in the literature. Firstly, the measurements of various interfacial tensions between different high-performance polymers by the breaking thread method were investigated in detail. This relatively fast and sensitive technique allowed us to obtain the unreported interfacial tensions between PEEK and different high-performance polymers – *e.g.* *m*-PEI, *p*-PEI, PPSU, and PC. Those values are fundamental tools to analyse the global affinity between the polymers, but also to predict different morphological behaviors. Furthermore, it was found that at such high processing temperatures (375 °C), the interfacial tensions between all the characterized polymers display low values compared to classical immiscible blends of commodity polymers.

The newly obtained interfacial tensions were then used to apply the spreading coefficients theory, where the relative affinity between the polymer pairs is compared to each other in order to predict the resulting morphologies of their ternary blends. The spreading coefficients were never applied to ternary systems displaying such complex miscible and partially miscible behaviors among their constitutive pairs. In this work, this tool proved accurate in the prediction of the resulting morphologies, even when a completely miscible constitutive pair (*i.e.* PEEK/*m*-PEI) was involved.

During the fundamental study performed on the PEEK/*m*-PEI/*p*-PEI ternary system, polymer-polymer binary interaction parameters were calorimetrically determined for all the pairs involved. Such data are scarce in the literature due to the complexity in their precise determination but are of fundamental interest to accurately understand and predict the molecular interactions between the polymers in complex blends. Thus, previously unreported PEEK/*p*-PEI and *m*-PEI/*p*-PEI binary interaction parameters were obtained and used to predict the phase separation behavior of their ternary blends. These values will greatly interest any study investigating such high-performance polymer pairs and their more complex multiphase blends.

Finally, some shear-induced miscibility behaviors were observed with the same ternary system, a rarely reported feature. Miscibility in the melt state was observed by SEM, after the application of some mechanical work (extrusion processing) on specific compositions (*e.g.* 50/25/25 and 50/20/30). However, such compositions underwent phase separation when exposed to a quiescent annealing step. These observations could be of interest to further investigate such complex phase

behaviors in ternary systems, helping improve the fundamental knowledge and prediction of phase separation mechanisms.

7.5 Additional remarks

The different articles of this thesis demonstrate that morphological control can be achieved through thermal annealing of the polymer blends. However, such behavior could also limit their scale-up production due to undesired morphology evolution during the multiple processing steps (*e.g.* extrusion, injection molding, hot-pressing, welding, etc.). Consequently, it is of prime importance to fully understand the morphological behavior of such systems and to tailor their processing according to their final application. For example, it would be recommended to extrude the blends directly in a film form for their future use as membranes, to avoid an additional melt pressing step.

Additionally, porous PEEK-based materials prepared via melt blending and selective extraction remain uncommon in the literature, even though their potential spans across critical fields such as aerospace, biomedicine, catalysis, and advanced filtration. Thus, an important contribution of this research work is the fact that such porous PEEK monoliths could be obtained after the selective extraction of the amorphous polymers. What was at first used to investigate the precise morphology of the polymer blends, could now become a tool to produce robust porous PEEK-based materials, resistant to harsh environments where high temperature, aggressive solvents and chemicals are used. The morphological work on porous PEEK-based materials presented in this thesis is already leveraged in more applied research projects, aiming at different application fields such as biocatalytic reactors, filtration membranes, conductive nanocomposites, or fuel cell membranes.

CHAPTER 8 CONCLUSION AND RECOMMENDATIONS

8.1 Conclusions

This work set out to develop multiphase polymer materials based on poly(ether ether ketone) (PEEK), with highly controlled morphologies, and capable of withstanding the lunar environment as part of the structure of a lunar rover. The motivation stemmed from the unique challenges of lunar applications (extreme thermal cycling, abrasive regolith, vacuum, and radiations), which require materials that combine high thermal resistance, mechanical performance, low density, on-site repair capability, and environmental durability. By blending PEEK with *m*-PEI and *p*-PEI, as well as with other high-performance thermoplastics, this project explored fundamental relationships between processing history, composition, miscibility, morphology, thermal behavior, and mechanical properties.

The first phase of this work established the distinct miscibility and morphological behaviors of PEEK/*m*-PEI and PEEK/*p*-PEI binary blends. The less explored PEEK/*p*-PEI system was directly compared to the more widely studied PEEK/*m*-PEI, enabling the assessment of the consequences arising from the change in chemical link position within the PEI structure. PEEK/*p*-PEI was found to be partially miscible, exhibiting two distinct T_g values under DSC analysis and sub-μm phase-separated morphologies (0.3 μm) under SEM. Interfacial tension, measured via the breaking thread method, by observing distortions of molten PEEK threads encapsulated in molten *p*-PEI films, yielded an exceptionally low value of 0.14 mN/m, among the lowest reported for polymer systems. Subsequent quiescent annealing in the melt state enabled precise control over the phase-separation length scale, coarsening from 0.3 μm to over 15 μm in just 30 min. In contrast, PEEK/*m*-PEI was confirmed to be fully miscible in the amorphous state by DSC, yet could be phase-separated through controlled PEEK crystallization during annealing. This process generated morphologies characterized extensively by SEM, at a level of detail not previously reported, revealing *m*-PEI segregation from a few nanometers to micrometers. Tensile testing of the binary blends revealed a synergistic effect in compositions containing 20 to 30 vol% of either PEI, with higher Young's modulus values than neat PEEK. Annealing at 200 °C for 30 min led to increased crystallinity in all blends, accompanied by greater rigidity compared to quenched samples. Finally, selective extraction of the PEI phases using a specific composite solvent produced porous PEEK materials with tunable pore sizes, from ~5 nm to over 15 μm, depending on the PEI type.

The second stage of this research consisted in the development of PEEK/*m*-PEI/*p*-PEI ternary systems. The influence of the processing speed, blend's composition, and quiescent annealing on the resulting miscibility and phase-separation behaviors, was investigated. It was shown, for instance, that compositions displaying finely phase-separated structures (< 0.1 µm) could be made miscible by the action of higher shear rate during the processing step. This rarely reported shear-induced miscibility was then lost when blends were subjected to quiescent annealing in the melt state, where phase-separation could occur. Depending on the composition and thermal treatment, the systems displayed distinct morphologies, from fully miscible to biphasic phase-separated, with domain size ranging from a few nanometers to over tens of micrometers. This phase separation could be finely controlled by the variation of the *m*-PEI over *p*-PEI ratio, without the need for interfacial compatibilizers. Calorimetric data were used to calculate the Flory-Huggins' polymer-polymer interaction parameter, thanks to thermodynamical equations that directly relate the blend's T_g's to the χ_{ij}. Never reported values were then obtained for the PEEK/*p*-PEI and the *m*-PEI/*p*-PEI systems. Furthermore, spinodal phase separation regions were plotted on ternary diagrams and compared to SEM experimental results, by using the three previously calculated binary interaction parameters. This visualization of miscibility behavior provides fundamental insights for the design of materials based on such complex blends. Lastly, porous PEEK monoliths with precisely tunable pore sizes were obtained after the selective extraction of both PEIs, opening opportunities in advanced filtration or biomedical applications.

Finally, the research extended to more complex ternary systems composed of PEEK and PC, associated with either *m*-PEI, *p*-PEI, or PPSU. The impact of the constitutive pairs' miscibility on the final morphology of the blends was characterized in detail by SEM analysis. When the miscible PEEK/*m*-PEI pair is included in the blend, the resulting morphologies were observed to be biphasic. In contrast, more complex triphasic morphologies were characterized with the partially miscible pairs of PEEK/*p*-PEI and PEEK/PPSU. Previously unreported interfacial tensions between all the component pairs were obtained by the breaking thread method, revealing low values (< 3 mN/m) compared to classical immiscible blends. In the blend's resulting morphology, PEEK was shown to always intercalate at the interface between the PC and the third component. This observation was correctly predicted by the simple spreading coefficients, calculated from the previously measured interfacial tensions. Lastly, taking advantage of PEEK localization in the blends, bimodal

porous (with both nm and μm pore sizes) and ultraporous (with as little as 5 vol% of solid) PEEK monoliths were prepared by the selective extraction of the amorphous polymers.

To conclude, this thesis focused on the preparation and study of binary and ternary PEEK-based systems, with a detailed investigation of their miscibility, morphology, and thermal behavior as influenced by processing history. This work establishes a fundamental understanding of how morphological control, from the nanoscale to the micron-scale, can be achieved in PEEK-based multiphase systems without the use of external compatibilizers. These findings open new opportunities for high-performance materials development for extreme environments, such as thermoplastics composites, lightweight structural components, thermal or acoustic insulation, filtration membranes, fuel cell membranes, etc.

8.2 Original contributions

The original contributions of this research work are the following:

1. Producing an extended and detailed morphological analysis of the PEEK/*m*-PEI system, different from what was previously reported in the literature.
2. Demonstrating the partial miscibility of the PEEK/*p*-PEI system and the resulting impact on the blend's properties, such as morphology, interfacial tension, χ_{ij} parameter, etc.
3. Developing a new ternary PEEK/*m*-PEI/*p*-PEI system, and characterizing it through calorimetric analysis, detailed morphological analysis, and theoretical background to support and predict its miscibility behavior. Obtention of the polymer-polymer binary interaction parameters for all the pairs involved, such as the previously unreported PEEK/*p*-PEI and *m*-PEI/*p*-PEI. This new ternary system demonstrates the utility of tailored composition to control the miscibility and morphology without the need for any added interfacial compatibilizers.
4. Developing three new ternary systems to understand the role of pair miscibility on the resulting morphology. The detailed morphological analysis and the newly obtained interfacial tensions proved that the spreading coefficients theory, never applied to such systems before, can accurately predict the resulting morphology in blends composed of

miscible or partially miscible pairs. This observation was leveraged to create novel complex ultraporous or hierarchical porous PEEK monoliths.

5. Producing a systematic morphological study on PEEK-based multiphase systems that allows the development of future applied research projects – *e.g.* conductive nanocomposites, filtration membranes, fuel cell membranes, or biocatalytic enzyme support.

8.3 Recommendations

It is recommended that future research focus on the following aspects:

1. Test the outgassing properties of the different multiphase PEEK-based blends to verify if they respect the standard requirements, like the pure thermoplastics.
2. Characterize with powerful methods, such as electron tomography, the fine co-continuous morphology produced after the selective extraction of *m*-PEI in annealed binary PEEK/*m*-PEI blends.
3. Investigate the impact of PEEK crystalline form, *e.g.* ~20 nm nodules or ~1 µm spherulites, on the resulting mechanical properties for annealed binary PEEK/*m*-PEI systems.
4. Explore the PEEK reticulation by electron beam irradiation in binary PEEK/PEI blends to improve its subsequent stability for membrane applications.
5. Study the impact of controlled PEEK crystallization behavior and the associated phase separation in PEEK/*m*-PEI/*p*-PEI ternary blends.
6. Prepare new high-performance binary or ternary blends involving one of the following newly commercialized thermoplastics: low-melting poly(aryl ether ketone) (LMPAEK™ from Victrex), thermoplastic polyimide (Extem™ from Sabic), or amorphous/slow-crystallization PEKK (Kepstan® from Arkema).
7. To extend the theoretical analysis of ternary systems, especially the obtention of reliable χ_{ij} parameters through calorimetric analysis, the studied blends should include non-crystallizable components that display largely different T_g (separated by at least 20 °C). This would improve the subsequent calculations of the spinodal phase separation region

and the composition of the phases at equilibrium. Completely amorphous PC/PEKK/PEI or PC/PEKK/PPSU could be systems of interest.

8. Compare the χ_{ij} parameters obtained through calorimetric analysis (T_g and melting point depression) to the ones obtained with more accurate techniques such as small-angle neutron scattering.

9. Optimize the ternary systems' compositions used in the preparation of ultraporous PEEK: 1) a higher amount of PC compared to *p*-PEI in the PC/PEEK/*p*-PEI 47.5/5/47.5 composition; 2) a lower amount of PC compared to PPSU in the PC/PEEK/PPSU 45/10/45 composition; 3) change the PPSU for poly(ether sulfone) (PES) if it can increase the localization of PEEK at the PC/PES interface due to a higher interfacial tension between PEEK and PES.

10. Prepare quaternary blends of PC/PEEK/*p*-PEI+*m*-PEI to control even more finely the pore sizes in the bimodal porous PEEK, prepared from compositions close to the PC/PEEK/*p*-PEI 40/30/30 vol%. It is expected that adding *m*-PEI to the *p*-PEI in such systems could present two effects: 1) decrease the size, in quenched samples, of the network of pores initially present inside the PEEK phase, as compared to the reference ternary PC/PEEK/*p*-PEI; 2) stabilize the *p*-PEI phase during quiescent annealing, in contrast to the fast coarsening PC phase.

11. Investigate the preparation of nanocomposites based on the developed complex multiphase systems, and especially the control of nanoparticles localization to tailor physical properties in such blends.

12. Explore hydrothermal polymerization of PEEK to obtain a greener pathway for its synthesis, as has already been done for PEIs.

REFERENCES

[1] D. Vaniman, R. Reedy, G. Heiken, G. Olhoeft, and W. Mendell, "The lunar environment," *The lunar Sourcebook, CUP,* pp. 27-60, 1991.

[2] S. A. Thibeault, J. H. Kang, G. Sauti, C. Park, C. C. Fay, and G. C. King, "Nanomaterials for radiation shielding," *MRS Bulletin,* vol. 40, no. 10, pp. 836-841, 2015, doi: 10.1557/mrs.2015.225.

[3] J. Simpson, "Composition and origin of cosmic rays," *Mathematical and Physical Sciences,* vol. 107, 1983.

[4] J.-P. Meyer, L. O. C. Drury, and D. C. Ellison, "Galactic cosmic rays from supernova remnants. I. A cosmic-ray composition controlled by volatility and mass-to-charge ratio," *The Astrophysical Journal,* vol. 487, no. 1, p. 182, 1997, doi: 10.1086/304599.

[5] A. Sharma, H. Bhojraj, V. Kaila, and H. Narayanamurthy, "Anodizing and inorganic black coloring of aluminum alloys for space applications," *Metal Finishing,* vol. 95, no. 12, pp. 14-20, 1997.

[6] V. Netti, J. Lopez Jr, P. Morgan-Dimmick, and S. Oliver, "Design of a modular utility vehicle for teleoperated and manned Lunar South Pole exploration," 2020.

[7] R. J. Rioja and J. Liu, "The Evolution of Al-Li Base Products for Aerospace and Space Applications," *Metallurgical and Materials Transactions A,* vol. 43, no. 9, pp. 3325-3337, 2012, doi: 10.1007/s11661-012-1155-z.

[8] O. Lutz. "Navigating LA with 65,000 Pounds of NASA Space Shuttle History." https://www.jpl.nasa.gov/edu/news/2016/5/18/navigating-la-with-65-000-pounds-of-nasa-space-shuttle-history/ (accessed January 27, 2021).

[9] G. Wang, Y. Zhao, and Y. Hao, "Friction stir welding of high-strength aerospace aluminum alloy and application in rocket tank manufacturing," *Journal of Materials Science & Technology,* vol. 34, no. 1, pp. 73-91, 2018, doi: 10.1016/j.jmst.2017.11.041.

[10] R. Brandt and G. Neuer, "Electrical Resistivity and Thermal Conductivity of Pure Aluminum and Aluminum Alloys up to and above the Melting Temperature," *International Journal of Thermophysics,* vol. 28, no. 5, pp. 1429-1446, 2007, doi: 10.1007/s10765-006-0144-0.

[11] Sabic. "GRADE COMPARISON: ULTEM™ RESIN 1000 ; ULTEM™ RESIN 1010 ; ULTEM™ RESIN CRS5001." https://www.sabic.com/en/products/compare?ids=c42faad7-e0d8-e611-819b-06b69393ae39,d52faad7-e0d8-e611-819b-06b69393ae39,9933aad7-e0d8-e611-819b-06b69393ae39&regions=ee05ec09-ed6d-4fed-80ac-229549245c91,ee05ec09-ed6d-4fed-80ac-229549245c91,ee05ec09-ed6d-4fed-80ac-229549245c91 (accessed February 16, 2021).

[12] Victrex. "VICTREX® PEEK 90G Datasheet." https://www.victrex.com/~/media/datasheets/victrex_tds_90g.pdf (accessed February 16, 2021).

[13] V. Mittal, "High Performance Polymers: An Overview," in *High Performance Polymers and Engineering Plastics*, 2011, pp. 1-20.

[14] S. M. Kurtz, W. Andrew, Ed. *PEEK Biomaterials Handbook*, 2 ed. Elsevier Science, 2019, p. 465.

[15] S. Dutton, D. Kelly, and A. Baker, *Composite materials for aircraft structures*. American Institute of Aeronautics and Astronautics, 2004.

[16] Victrex. "VICTREX® PEEK CHEMICAL RESISTANCE." https://www.victrex.com/~/media/literature/en/victrex_chemical_resistance_en_us.pdf (accessed April 05, 2021).

[17] Victrex. "VICTREX® PEEK 650G Datasheet." https://www.victrex.com/~/media/datasheets/victrex_tds_650g.pdf (accessed April 05, 2021).

[18] NASA. "Outgassing Data for Selecting Spacecraft Materials Online." https://outgassing.nasa.gov (accessed April 05, 2021).

[19] Solvay. "Radel® PPSU, Veradel® PESU & Acudel® modified PPSU, Design Guide." https://www.solvay.com/sites/g/files/srpend221/files/2018-07/Radel-PPSU-Veradel-PESU-Acudel-PPSU-Design-Guide_EN.pdf (accessed May 05, 2021).

[20] Sabic. "LEXAN™ Resin 101." https://www.sabic.com/en/products/compare?ids=d42faad7-e0d8-e611-819b-06b69393ae39&regions=ee05ec09-ed6d-4fed-80ac-229549245c91 (accessed July 22, 2025).

[21] J. Ahmad and M. G. Niasar, "Aging Behavior of PEEK, PTFE, and PI Insulation Materials Under Thermal Oxidative and Humid Conditions for Aerospace Applications," *Journal of Applied Polymer Science,* vol. 142, no. 19, 2025, doi: https://doi.org/10.1002/app.56858.

[22] E. Courvoisier, Y. Bicaba, and X. Colin, "Multi-scale and multi-technical analysis of the thermal degradation of poly(ether imide)," *Polymer Degradation and Stability,* vol. 147, pp. 177-186, 2018, doi: https://doi.org/10.1016/j.polymdegradstab.2017.12.002.

[23] E. Richaud, P. Ferreira, L. Audouin, X. Colin, J. Verdu, and C. Monchy-Leroy, "Radiochemical ageing of poly(ether ether ketone)," *European Polymer Journal,* vol. 46, no. 4, pp. 731-743, 2010, doi: https://doi.org/10.1016/j.eurpolymj.2009.12.026.

[24] K. K. de Groh and B. A. Banks, "MISSE-Flight Facility Polymers and Composites Experiment 1-4 (PCE 1-4)," NASA/TM-20205008863, 2021. [Online]. Available: https://ntrs.nasa.gov/api/citations/20205008863/downloads/TM-20205008863%2003.29.21.pdf

[25] K. K. de Groh and B. A. Banks, "Atomic Oxygen Erosion Data from the MISSE 2-8 Missions," NASA/TM—2019-219982, 2019. [Online]. Available: https://ntrs.nasa.gov/api/citations/20190025445/downloads/20190025445.pdf

[26] A. Guo, G. T. Yi, C. C. Ashmead, G. G. Mitchell, K. K. de Groh, and B. A. Banks, "Embrittlement of MISSE 5 Polymers After 13 Months of Space Exposure," NASA/TM—2012-217645, 2012. [Online]. Available: https://ntrs.nasa.gov/api/citations/20120014249/downloads/20120014249.pdf

[27] W. A. Campbell Jr., R. S. Mamott, and J. J. Park, "Outgassing Data for Selecting Spacecraft Materials," 1984. [Online]. Available: https://ntrs.nasa.gov/api/citations/20030053424/downloads/20030053424.pdf

[28] L. Lin, X.-Q. Pei, R. Bennewitz, and A. K. Schlarb, "Tribological Response of PEEK to Temperature Induced by Frictional and External Heating," *Tribology Letters,* vol. 67, no. 2, 2019, doi: https://doi.org/10.1007/s11249-019-1169-4.

[29] Q. Wang, F. Zheng, and T. Wang, "Tribological properties of polymers PI, PTFE and PEEK at cryogenic temperature in vacuum," *Cryogenics,* vol. 75, pp. 19-25, 2016, doi: https://doi.org/10.1016/j.cryogenics.2016.01.001.

[30] M. Nikonovich, A. Ramalho, and N. Emami, "Cryogenic cyclic aging effect on thermal, mechanical and tribological performance of PEEK-based materials," *Wear,* vol. 564-565, 2025, doi: https://doi.org/10.1016/j.wear.2024.205709.

[31] M. Nikonovich, A. Ramalho, and N. Emami, "Effect of cryogenic aging and test-environment on the tribological and mechanical properties of PEEK composites," *Tribology International,* vol. 194, 2024, doi: https://doi.org/10.1016/j.triboint.2024.109554.

[32] J. Sukumaran, J. D. Pauw, P. D. Neis, L. F. Tóth, and P. De Baets, "Revisiting polymer tribology for heavy duty application," *Wear,* vol. 376-377, pp. 1321-1332, 2017, doi: https://doi.org/10.1016/j.wear.2017.01.018.

[33] J. Hanchi and N. S. Eiss, "The Tribological Behavior of Blends of Polyetheretherketone (PEEK) and Polyetherimide (PEI) at Elevated Temperatures," *Tribology Transactions,* vol. 37, no. 3, pp. 494-504, 1994, doi: 10.1080/10402009408983322.

[34] Y. Jong Hyun and N. S. Eiss, "Tribological behavior of blends of polyether ether ketone and polyether imide," *Wear,* vol. 162-164, pp. 418-425, 1993, doi: 10.1016/0043-1648(93)90525-q.

[35] J. Bijwe, U. S. Tewari, and P. Vasudevan, "Friction and wear studies of bulk polyetherimide," *Journal of Materials Science,* vol. 25, no. 1, pp. 548-556, 1990, doi: https://doi.org/10.1007/BF00714072.

[36] J. W. Barlow and D. R. Paul, "Polymer blends and alloys—a review of selected considerations," *Polymer Engineering & Science,* vol. 21, no. 15, pp. 985-996, 1981, doi: https://doi.org/10.1002/pen.760211502.

[37] L. A. Utracki, G. Z. H. Shi, D. Rodrigue, and R. Gonzalez-Núñez, "Compounding Polymer Blends," in *Polymer Blends Handbook*, 2014, ch. Chapter 11, pp. 919-1028.

[38] A. Ajji and L. A. Utracki, "Interphase and compatibilization of polymer blends," *Polymer Engineering & Science,* vol. 36, no. 12, pp. 1574-1585, 1996, doi: https://doi.org/10.1002/pen.10554.

[39] M. Xanthos and S. S. Dagli, "Compatibilization of polymer blends by reactive processing," *Polymer Engineering & Science,* vol. 31, no. 13, pp. 929-935, 1991, doi: https://doi.org/10.1002/pen.760311302.

[40] M. Gonzalez-Garzon, S. Shahbikian, and M. A. Huneault, "Properties and phase structure of melt-processed PLA/PMMA blends," *Journal of Polymer Research,* vol. 25, no. 2, 2018, doi: https://doi.org/10.1007/s10965-018-1438-1.

[41] G. Zhang, J. Zhang, S. Wang, and D. Shen, "Miscibility and phase structure of binary blends of polylactide and poly(methyl methacrylate)," *Journal of Polymer Science Part B: Polymer Physics,* vol. 41, no. 1, pp. 23-30, 2002, doi: https://doi.org/10.1002/polb.10353.

[42] S. Wu, "Entanglement between dissimilar chains in compatible polymer blends: poly(methyl methacrylate) and poly(vinylidene fluoride)," *Journal of Polymer Science Part B: Polymer Physics,* vol. 25, no. 3, pp. 557-566, 1987, doi: https://doi.org/10.1002/polb.1987.090250308.

[43] J. H. Wendorff, "Concentration fluctuations in poly(vinylidene fluoride)-poly(methyl methacrylate) mixtures," *Journal of Polymer Science: Polymer Letters Edition,* vol. 18, no. 6, pp. 439-445, 1980, doi: https://doi.org/10.1002/pol.1980.130180607.

[44] S. Ravati and B. D. Favis, "Morphological states for a ternary polymer blend demonstrating complete wetting," *Polymer,* vol. 51, no. 20, pp. 4547-4561, 2010, doi: https://doi.org/10.1016/j.polymer.2010.07.014.

[45] A.-L. Esquirol, P. Sarazin, and N. Virgilio, "Tunable Porous Hydrogels from Cocontinuous Polymer Blends," *Macromolecules,* vol. 47, no. 9, pp. 3068-3075, 2014, doi: 10.1021/ma402603b.

[46] C. R. López-Barrón and C. W. Macosko, "Rheological and morphological study of cocontinuous polymer blends during coarsening," *Journal of Rheology,* vol. 56, no. 6, pp. 1315-1334, 2012, doi: https://doi.org/10.1122/1.4739067.

[47] C. R. Lopez-Barron and C. W. Macosko, "Coarsening of PS/SAN Blends with Cocontinuous Morphology Studied with 3D Image Analysis," *Macromolecular Symposia,* vol. 283–284, no. 1, pp. 348-353, 2009, doi: https://doi.org/10.1002/masy.200950941.

[48] P. Sarazin, X. Roy, and B. D. Favis, "Controlled preparation and properties of porous poly(L-lactide) obtained from a co-continuous blend of two biodegradable polymers," *Biomaterials,* vol. 25, no. 28, pp. 5965-78, Dec 2004, doi: https://doi.org/10.1016/j.biomaterials.2004.01.065.

[49] Z. Yuan and B. D. Favis, "Coarsening of immiscible co-continuous blends during quiescent annealing," *AIChE Journal,* vol. 51, no. 1, pp. 271-280, 2004, doi: https://doi.org/10.1002/aic.10281.

[50] P. Sarazin and B. D. Favis, "Morphology control in co-continuous poly(L-lactide)/polystyrene blends: a route towards highly structured and interconnected porosity in poly(L-lactide) materials," *Biomacromolecules,* vol. 4, no. 6, pp. 1669-79, Nov-Dec 2003, doi: https://doi.org/10.1021/bm030034+.

[51] F. S. Bates and G. H. Fredrickson, "Block copolymer thermodynamics: theory and experiment," *Annual review of physical chemistry,* vol. 41, no. 1, pp. 525-557, 1990.

[52] J. Noolandi, "Recent advances in the theory of polymeric alloys," *Polymer Engineering & Science,* vol. 24, no. 2, pp. 70-78, 1984, doi: https://doi.org/10.1002/pen.760240203.

[53] E. Helfand, "Block copolymers, polymer-polymer interfaces, and the theory of inhomogeneous polymers," *Accounts of Chemical Research,* vol. 8, no. 9, pp. 295-299, 1975.

[54] P. Cigana, B. D. Favis, and R. Jerome, "Diblock copolymers as emulsifying agents in polymer blends: Influence of molecular weight, architecture, and chemical composition," *Journal of Polymer Science Part B: Polymer Physics,* vol. 34, no. 9, pp. 1691-1700, 1996, doi: https://doi.org/10.1002/(SICI)1099-0488(19960715)34:9<1691::AID-POLB18>3.0.CO;2-2.

[55] L. Leibler, "Emulsifying effects of block copolymers in incompatible polymer blends," *Makromolekulare Chemie. Macromolecular Symposia,* vol. 16, no. 1, pp. 1-17, 1988, doi: https://doi.org/10.1002/masy.19880160103.

[56] A. Belguise *et al.*, "Confinement and distribution of the composition in semicrystalline/amorphous miscible blends of PEKK/PEI: a calorimetry study," *Macromolecules,* vol. 54, no. 16, pp. 7364-7376, 2021, doi: https://doi.org/10.1021/acs.macromol.1c00344.

[57] C. Ye, J. Zhao, L. Ye, Z. Jiang, J. You, and Y. Li, "Precise inter-lamellar/inter-fibrillar localization and consequent fabrication of porous membranes with crystallization-modulated pore-size," *Polymer,* vol. 142, pp. 48-51, 2018, doi: https://doi.org/10.1016/j.polymer.2018.02.004.

[58] P. J. Flory, *Principles of polymer chemistry*. Cornell university press, 1953.

[59] A. Zirkel, S. M. Gruner, V. Urban, and P. Thiyagarajan, "Small-Angle Neutron Scattering Investigation of the Q-Dependence of the Flory−Huggins Interaction Parameter in a Binary Polymer Blend," *Macromolecules,* vol. 35, no. 19, pp. 7375-7386, 2002, doi: https://doi.org/10.1021/ma010576o.

[60] D. Richter, "Neutron scattering in polymer physics," *Physica B: Condensed Matter,* vol. 276-278, pp. 22-29, 2000, doi: https://doi.org/10.1016/S0921-4526(99)01357-5.

[61] U. R. Bidkar and I. C. Sanchez, "Neutron scattering from compressible polymer blends: a framework for experimental analysis and interpretation of interaction parameters," *Macromolecules,* vol. 28, no. 11, pp. 3963-3972, 1995.

[62] R.-J. Roe and W.-C. Zin, "Determination of the polymer-polymer interaction parameter for the polystyrene-polybutadiene pair," *Macromolecules,* vol. 13, no. 5, pp. 1221-1228, 1980.

[63] T. Nishi and T. K. Kwei, "Cloud point curves for poly(vinyl methyl ether) and monodisperse polystyrene mixtures," *Polymer,* vol. 16, no. 4, pp. 285-290, 1975, doi: https://doi.org/10.1016/0032-3861(75)90172-X.

[64] L. Zhao and P. Choi, "Determination of solvent-independent polymer–polymer interaction parameter by an improved inverse gas chromatographic approach," *Polymer,* vol. 42, no. 3, pp. 1075-1081, 2001, doi: https://doi.org/10.1016/S0032-3861(00)00412-2.

[65] T. Nishi and T. T. Wang, "Melting point depression and kinetic effects of cooling on crystallization in poly (vinylidene fluoride)-poly (methyl methacrylate) mixtures," *Macromolecules,* vol. 8, no. 6, pp. 909-915, 1975, doi: https://pubs.acs.org/doi/pdf/10.1021/ma60048a040.

[66] X. Lu and R. A. Weiss, "Relationship between the glass transition temperature and the interaction parameter of miscible binary polymer blends," *Macromolecules,* vol. 25, no. 12, pp. 3242-3246, 1992, doi: https://doi.org/10.1021/ma00038a033.

[67] W. N. Kim and C. M. Burns, "Blends of polycarbonate and poly (methyl methacrylate) and the determination of the polymer-polymer interaction parameter of the two polymers," *Macromolecules,* vol. 20, no. 8, pp. 1876-1882, 1987, doi: https://doi.org/10.1021/ma00174a030.

[68] A. Arzak, J. I. Eguiazábal, and J. Nazábal, "Mechanical performance of directly injection-molded PEEK/PEI blends at room and high temperature," *Journal of Macromolecular Science, Part B,* vol. 36, no. 2, pp. 233-246, 1996, doi: https://doi.org/10.1080/00222349708220428.

[69] G. Crevecoeur and G. Groeninckx, "Binary blends of poly (ether ether ketone) and poly (ether imide): Miscibility, crystallization behavior and semicrystalline morphology," *Macromolecules,* vol. 24, no. 5, pp. 1190-1195, 1991, doi: https://doi.org/10.1021/ma00005a034.

[70] M. Frigione, C. Naddeo, and D. Acierno, "Crystallization behavior and mechanical properties of poly(aryl ether ether ketone)/poly(ether imide) blends," *Polymer Engineering & Science,* vol. 36, no. 16, pp. 2119-2128, 1996, doi: https://doi.org/10.1002/pen.10608.

[71] A. A. Goodwin and G. P. Simon, "Glass transition behaviour of poly(ether ether ketone)/poly(ether imide) blends," *Polymer,* vol. 37, no. 6, pp. 991-995, 1996, doi: https://doi.org/10.1016/0032-3861(96)87282-X.

[72] S. D. Hudson, D. D. Davis, and A. J. Lovinger, "Semicrystalline morphology of poly(aryl ether ether ketone)/poly(ether imide) blends," *Macromolecules,* vol. 25, no. 6, pp. 1759-1765, 1992, doi: https://doi.org/10.1021/ma00032a021.

[73] A. M. Jonas, D. A. Ivanov, and D. Y. Yoon, "The Semicrystalline Morphology of Poly(ether−ether−ketone) Blends with Poly(ether−imide)," *Macromolecules,* vol. 31, no. 16, pp. 5352-5362, 1998, doi: https://doi.org/10.1021/ma9711607.

[74] H. S. Lee and W. N. Kim, "Glass transition temperatures and rigid amorphous fraction of poly(ether ether ketone) and poly(ether imide) blends," *Polymer,* vol. 38, no. 11, pp. 2657-2663, 1997, doi: https://doi.org/10.1016/S0032-3861(97)85599-1.

[75] M. J. Jenkins, "Relaxation behaviour in blends of PEEK and PEI," *Polymer,* vol. 41, no. 18, pp. 6803-6812, 2000, doi: https://doi.org/10.1016/S0032-3861(00)00033-1.

[76] J. F. Bristow and D. S. Kalika, "Investigation of semicrystalline morphology in poly(ether ether ketone)/poly(ether imide) blends by dielectric relaxation spectroscopy," *Polymer,* vol. 38, no. 2, pp. 287-295, 1997, doi: https://doi.org/10.1016/S0032-3861(96)00517-4.

[77] H.-L. Chen, J.-W. You, and R. S. Porter, "Intermolecular interaction and conformation in poly(ether ether ketone)/poly(ether imide) blends - An infrared spectroscopic investigation," *Journal of Polymer Research,* vol. 3, no. 3, pp. 151-158, 1996, doi: https://doi.org/10.1007/BF01494524.

[78] Y. S. Chun, H. S. Lee, H. C. Jung, and W. N. Kim, "Thermal properties of melt-blended poly(ether ether ketone) and poly(ether imide)," *Journal of Applied Polymer Science,* vol.

72, no. 6, pp. 733-739, 1999, doi: https://doi.org/10.1002/(SICI)1097-4628(19990509)72:6<733::AID-APP1>3.0.CO;2-Y.

[79] T. Nemoto, J. Takagi, and M. Ohshima, "Nanocellular foams-cell structure difference between immiscible and miscible PEEK/PEI polymer blends," *Polymer Engineering & Science,* vol. 50, no. 12, pp. 2408-2416, 2010, doi: https://doi.org/10.1002/pen.21766.

[80] C. H. Lee, T. Okada, H. Saito, and T. Inoue, "Exclusion of non-crystalline polymer from the interlamellar region in polymer blends: poly(ether ether ketone)/poly(ether imide) blend by small-angle X-ray scattering," *Polymer,* vol. 38, no. 1, pp. 31-34, 1997, doi: https://doi.org/10.1016/S0032-3861(96)00454-5.

[81] G. Chen, Y. Chen, T. Huang, Z. He, J. Xu, and P. Liu, "Pore Structure and Properties of PEEK Hollow Fiber Membranes: Influence of the Phase Structure Evolution of PEEK/PEI Composite," *Polymers (Basel),* vol. 11, no. 9, Aug 26 2019, doi: https://doi.org/10.3390/polym11091398.

[82] X. Cheng *et al.*, "Crystallization-template-induced PEEK membranes for particulate matter capture at high temperature and separation of emulsion containing corrosive component," *Journal of Environmental Chemical Engineering,* vol. 10, no. 3, 2022, doi: https://doi.org/10.1016/j.jece.2022.107469.

[83] Y. Ding and B. Bikson, "Preparation and characterization of semi-crystalline poly(ether ether ketone) hollow fiber membranes," *Journal of Membrane Science,* vol. 357, no. 1-2, pp. 192-198, 2010, doi: https://doi.org/10.1016/j.memsci.2010.04.021.

[84] T. Huang, G. Chen, Z. He, J. Xu, and P. Liu, "Pore structure and properties of poly(ether ether ketone) hollow fiber membranes: influence of solvent-induced crystallization during extraction," *Polymer International,* vol. 68, no. 11, pp. 1874-1880, 2019, doi: https://doi.org/10.1002/pi.5897.

[85] Y. Huang *et al.*, "Template-assisted fabrication of polyether ether ketone hollow fiber membrane for highly efficient separation of binary dye mixtures," *Journal of Membrane Science,* vol. 698, 2024, doi: https://doi.org/10.1016/j.memsci.2024.122634.

[86] R. H. Mehta and D. S. Kalika, "Characteristics of poly(ether ether ketone) microporous membranes prepared via thermally induced phase separation (TIPS)," *Journal of Applied Polymer Science,* vol. 66, no. 12, pp. 2347-2355, 1997, doi: https://doi.org/10.1002/(SICI)1097-4628(19971219)66:12<2347::AID-APP16>3.0.CO;2-X.

[87] R. H. Mehta, D. A. Madsen, and D. S. Kalika, "Microporous membranes based on poly(ether ether ketone) via thermally-induced phase separation," *Journal of Membrane Science,* vol. 107, no. 1-2, pp. 93-106, 1995, doi: https://doi.org/10.1016/0376-7388(95)00106-M.

[88] J. E. Harris and L. M. Robeson, "Miscible blends of poly(aryl ether ketone)s and polyetherimides," *Journal of Applied Polymer Science,* vol. 35, no. 7, pp. 1877-1891, 1988, doi: https://doi.org/10.1002/app.1988.070350713.

[89] L. Zeman and D. Patterson, "Effect of the Solvent on Polymer Incompatibility in Solution," *Macromolecules,* vol. 5, no. 4, pp. 513-516, 1972, doi: https://doi.org/10.1021/ma60028a030.

[90] S. Torza and S. G. Mason, "Three-phase interactions in shear and electrical fields," *Journal of Colloid and Interface Science,* vol. 33, no. 1, pp. 67-83, 1970, doi: https://doi.org/10.1016/0021-9797(70)90073-1.

[91] W. D. Harkins and A. Feldman, "Films. The spreading of liquids and the spreading coefficient," *Journal of the American Chemical Society,* vol. 44, no. 12, pp. 2665-2685, 1922, doi: https://pubs.acs.org/doi/pdf/10.1021/ja01433a001.

[92] W. D. Harkins, "A general thermodynamic theory of the spreading of liquids to form duplex films and of liquids or solids to form monolayers," *The Journal of Chemical Physics,* vol. 9, no. 7, pp. 552-568, 1941, doi: https://doi.org/10.1063/1.1750953.

[93] R. L. Scott, "The Thermodynamics of High Polymer Solutions. V. Phase Equilibria in the Ternary System: Polymer 1—Polymer 2—Solvent," *The Journal of Chemical Physics,* vol. 17, no. 3, pp. 279-284, 1949, doi: https://doi.org/10.1063/1.1747239.

[94] H. Tompa, "Phase relationships in polymer solutions," *Transactions of the Faraday Society,* vol. 45, 1949, doi: https://doi.org/10.1039/TF9494501142.

[95] A. Su and J. Fried, "Phase behavior of ternary polymer blends," *Polymer Engineering & Science,* vol. 27, no. 22, pp. 1657-1661, 1987, doi: https://doi.org/10.1002/pen.760272203.

[96] Y. S. Chun, H. S. Kwon, W. N. Kim, and H. G. Yoon, "Compatibility studies of sulfonated poly(ether ether ketone)-poly(ether imide)-polycarbonate ternary blends," *Journal of Applied Polymer Science,* vol. 78, no. 14, pp. 2488-2494, 2000, doi: https://doi.org/10.1002/1097-4628(20001227)78:14<2488::AID-APP80>3.0.CO;2-T.

[97] E. M. Woo and Y.-C. Tseng, "Analysis and characterization of unusual ternary polymer miscibility in poly(ether diphenyl ether ketone), poly(ether ether ketone), and poly(ether imide)," *Macromolecular Chemistry and Physics,* vol. 201, no. 14, pp. 1877-1886, 2000, doi: https://doi.org/10.1002/1521-3935(20000901)201:14<1877::AID-MACP1877>3.0.CO;2-C.

[98] R. E. S. Bretas and D. G. Baird, "Miscibility and mechanical properties of poly(ether imide)/poly(ether ether ketone)/liquid crystalline polymer ternary blends," *Polymer,* vol. 33, no. 24, pp. 5233-5244, 1992, doi: https://doi.org/10.1016/0032-3861(92)90806-8.

[99] A. R. Morales and R. E. S. Bretas, "Polyetherimide/poly(ether ether ketone)/liquid crystalline polymer ternary blends—I. Calorimetric studies and morphology," *European Polymer Journal,* vol. 32, no. 3, pp. 349-363, 1996, doi: https://doi.org/10.1016/0014-3057(95)00126-3.

[100] A. R. Morales and R. E. S. Bretas, "Polyetherimide/poly(ether ether ketone)/liquid crystalline polymer ternary blends—II. Approximated interaction parameters and phase diagrams," *European Polymer Journal,* vol. 32, no. 3, pp. 365-373, 1996, doi: https://doi.org/10.1016/0014-3057(95)00127-1.

[101] S. Bicakci and M. Cakmak, "Phase behaviour of ternary blends of poly(ethylene naphthalate), poly(ether imide) and poly(ether ether ketone)," *Polymer,* vol. 39, no. 17, pp. 4001-4010, 1998, doi: https://doi.org/10.1016/S0032-3861(97)10227-0.

[102] S. Bicakci and M. Cakmak, "Development of structural hierarchy during uniaxial drawing of PEEK/PEI blends from amorphous precursors," *Polymer,* vol. 43, no. 1, pp. 149-157, 2002, doi: https://doi.org/10.1016/S0032-3861(01)00607-3.

[103] X. Zhou and M. Cakmak, "Influence of composition and annealing on the structure development in biaxially stretched PEN/PEI/PEEK ternary blends," *Polymer,* vol. 47, no. 18, pp. 6362-6378, 2006, doi: https://doi.org/10.1016/j.polymer.2006.07.007.

[104] X. Cheng, J. Wang, M. Ding, Y. B. Yang, and J. Bae, "Fabrication and manipulation of hierarchically porous PEEK membranes based on crystallization-induced phase segregation and sea-island structures," *Journal of Polymer Science,* vol. 62, no. 20, pp. 4687-4697, 2024, doi: https://doi.org/10.1002/pol.20240490.

[105] C. Jian-bing, G. Wen-he, L. Zhun-zhun, and T. Li-ming, "Crystalline and thermal properties in miscible blends of PEEK, PPS and PEI obtained by melt compounding," *Functional materials,* vol. 23, no. 1, pp. 55-62, 2016, doi: http://dx.doi.org/10.15407/fm23.01.055.

[106] M. Iannone, F. Esposito, and A. Cammarano, "Thermoplastic matrix composites for aeronautical applications – The amorphous/semi-crystalline blends option," *AIP Conference Proceedings,* vol. 1599, no. 1, pp. 66-69, 2014, doi: https://doi.org/10.1063/1.4876779.

[107] R. l'Abee, F. DaRosa, M. J. Armstrong, M. M. Hantel, and D. Mourzagh, "High temperature stable Li-ion battery separators based on polyetherimides with improved electrolyte compatibility," *Journal of Power Sources,* vol. 345, pp. 202-211, 2017, doi: http://dx.doi.org/10.1016/j.jpowsour.2017.02.005.

[108] D. J. Blundell and B. N. Osborn, "The morphology of poly(aryl-ether-ether-ketone)," *Polymer,* vol. 24, no. 8, pp. 953-958, 1983, doi: https://doi.org/10.1016/0032-3861(83)90144-1.

[109] N. Marin and B. D. Favis, "Co-continuous morphology development in partially miscible PMMA/PC blends," *Polymer,* vol. 43, no. 17, pp. 4723-4731, 2002, doi: https://doi.org/10.1016/S0032-3861(02)00280-X.

[110] J. A. Galloway, M. D. Montminy, and C. W. Macosko, "Image analysis for interfacial area and cocontinuity detection in polymer blends," *Polymer,* vol. 43, no. 17, pp. 4715-4722, 2002, doi: https://doi.org/10.1016/S0032-3861(02)00282-3.

[111] M. Yuan, J. A. Galloway, R. J. Hoffman, and S. Bhatt, "Influence of molecular weight on rheological, thermal, and mechanical properties of PEEK," *Polymer Engineering & Science,* vol. 51, no. 1, pp. 94-102, 2011, doi: https://doi.org/10.1002/pen.21785.

[112] E. L. Gilmer, C. Mansfield, J. M. Gardner, E. J. Siochi, D. G. Baird, and M. J. Bortner, "Characterization and Analysis of Polyetherimide: Realizing Practical Challenges of Modeling the Extrusion-Based Additive Manufacturing Process," in *Polymer-Based Additive Manufacturing: Recent Developments* vol. 1315, (ACS Symposium Series, 2019, ch. 5, pp. 69-84.

[113] M. R. Nobile, D. Acierno, L. Incarnato, and L. Nicolais, "The rheological behavior of a polyetherimide and of its blends with a thermotropic copolyester," *Journal of Rheology,* vol. 34, no. 7, pp. 1181-1197, 1990, doi: https://doi.org/10.1122/1.550080.

[114] D. C. Chappelear, "Interfacial tension between molten polymers," *Polym. Prepr,* vol. 5, pp. 363-371, 1964.

[115] R. H. Olley, D. C. Bassett, and D. J. Blundell, "Permanganic etching of PEEK," *Polymer,* vol. 27, no. 3, pp. 344-348, 1986, doi: https://doi.org/10.1016/0032-3861(86)90147-3.

[116] J. Li, P. L. Ma, and B. D. Favis, "The Role of the Blend Interface Type on Morphology in Cocontinuous Polymer Blends," *Macromolecules,* vol. 35, no. 6, pp. 2005-2016, 2002, doi: https://doi.org/10.1021/ma010104+.

[117] H. S. Lee and E. S. Kim, "Linear Viscoelasticity and the Measurement of Interfacial Tension in a Partially Miscible Polymer Mixture," *Macromolecules,* vol. 38, no. 4, pp. 1196-1200, 2005, doi: https://doi.org/10.1021/ma0485179.

[118] Z. Wu, Y. B. Zheng, H. X. Yu, M. Seki, and R. Yosomiya, "Effect of thermal history on crystallization behavior of polyetheretherketone studied by differential scanning calorimetry," *Die Angewandte Makromolekulare Chemie,* vol. 164, no. 1, pp. 21-34, 1988, doi: https://doi.org/10.1002/apmc.1988.051640102.

[119] J. Wang *et al.*, "Hierarchically porous membranes with isolated-round-pores connected by narrow-nanopores: A novel solution for trade-off effect in separation," *Journal of Membrane Science,* vol. 604, 2020, doi: https://doi.org/10.1016/j.memsci.2020.118040.

[120] M. Thommes *et al.*, "Physisorption of gases, with special reference to the evaluation of surface area and pore size distribution (IUPAC Technical Report)," *Pure and Applied Chemistry,* vol. 87, no. 9-10, pp. 1051-1069, 2015, doi: https://doi.org/10.1515/pac-2014-1117.

[121] S. J. Talley, S. L. Vivod, B. A. Nguyen, M. A. B. Meador, A. Radulescu, and R. B. Moore, "Hierarchical Morphology of Poly(ether ether ketone) Aerogels," *ACS Appl Mater Interfaces,* vol. 11, no. 34, pp. 31508-31519, Aug 28 2019, doi: https://doi.org/10.1021/acsami.9b09699.

[122] L. Meng *et al.*, "A Novel PEEK Foam with Ultra-High Temperature-Resistant by Temperature Induced Phase Separation," *Macromolecular Materials and Engineering,* vol. 308, no. 5, 2022, doi: https://doi.org/10.1002/mame.202200559.

[123] V. Heshmati and B. D. Favis, "High performance poly (lactic acid)/bio-polyamide11 through controlled chain mobility," *Polymer,* vol. 123, pp. 184-193, 2017, doi: http://dx.doi.org/10.1016/j.polymer.2017.07.009.

[124] P. A. Bhadane, A. H. Tsou, J. Cheng, M. D. Ellul, and B. D. Favis, "Enhancement in interfacial reactive compatibilization by chain mobility," *Polymer,* vol. 55, no. 16, pp. 3905-3914, 2014, doi: https://doi.org/10.1016/j.polymer.2014.05.023.

[125] A. Lassus, D. Therriault, B. D. Favis, and N. Virgilio, "Tailoring the morphology in partially and fully miscible mixtures of PEEK and PEI," *Polymer,* vol. 326, 2025, doi: https://doi.org/10.1016/j.polymer.2025.128315.

[126] J. Reignier and B. D. Favis, "Control of the Subinclusion Microstructure in HDPE/PS/PMMA Ternary Blends," *Macromolecules,* vol. 33, no. 19, pp. 6998-7008, 2000, doi: https://doi.org/10.1021/ma991954g.

[127] T. S. Valera, A. T. Morita, and N. R. Demarquette, "Study of Morphologies of PMMA/PP/PS Ternary Blends," *Macromolecules,* vol. 39, no. 7, pp. 2663-2675, 2006, doi: https://doi.org/10.1021/ma052571n.

[128] D. J. Duffy, H. D. Stidham, S. L. Hsu, S. Sasaki, A. Takahara, and T. Kajiyama, "Effect of polyester structure on the interaction parameters and morphology development of ternary blends: Model for high performance adhesives and coatings," *Journal of Materials Science,* vol. 37, no. 22, pp. 4801-4809, 2002, doi: https://doi.org/10.1023/A:1020826616745.

[129] B. K. Hong, J. Y. Kim, W. H. Jo, and S. C. Lee, "A closed-loop phase behaviour of ternary homopolymer blend composed of three miscible binaries," *Polymer,* vol. 38, no. 17, pp. 4373-4375, 1997, doi: https://doi.org/10.1016/S0032-3861(96)01017-8.

[130] P. Zoller, T. A. Kehl, H. W. Starkweather Jr, and G. A. Jones, "The equation of state and heat of fusion of poly (ether ether ketone)," *Journal of Polymer Science Part B: Polymer Physics,* vol. 27, no. 5, pp. 993-1007, 1989, doi: https://doi.org/10.1002/polb.1989.090270503.

[131] J. S. Yu, M. Lim, and D. M. Kalyon, "Development of density distributions in injection molded amorphous engineering plastics. Part I," *Polymer Engineering & Science,* vol. 31, no. 3, pp. 145-152, 1991, doi: https://doi.org/10.1002/pen.760310302.

[132] H. L. Chen and R. S. Porter, "Melting behavior of poly(ether ether ketone) in its blends with poly(ether imide)," *Journal of Polymer Science Part B: Polymer Physics,* vol. 31, no. 12, pp. 1845-1850, 1993, doi: https://doi.org/10.1002/polb.1993.090311217.

[133] S. A. Madbouly and T. Ougizawa, "Rheological Investigation of Shear Induced-Mixing and Shear Induced-Demixing for Polystyrene/Poly(vinyl methyl ether) Blend," *Macromolecular Chemistry and Physics,* vol. 205, no. 9, pp. 1222-1230, 2004, doi: https://doi.org/10.1002/macp.200400030.

[134] S. Madbouly, M. Ohmomo, T. Ougizawa, and T. Inoue, "Effect of the shear flow on the phase behaviour of polystyrene/poly(vinyl methyl ether) blend," *Polymer,* vol. 40, no. 6, pp. 1465-1472, 1999, doi: https://doi.org/10.1016/S0032-3861(98)00369-3.

[135] S. A. Madbouly, T. Ougizawa, and T. Inoue, "Phase Behavior under Shear Flow in PMMA/SAN Blends: Effects of Molecular Weight and Viscosity," *Macromolecules,* vol. 32, no. 17, pp. 5631-5636, 1999, doi: https://doi.org/10.1021/ma9813946.

[136] W. N. Kim and C. M. Burns, "Thermal behavior, morphology, and the determination of the Flory–Huggins interaction parameter of polycarbonate–polystyrene blends," *Journal of Applied Polymer Science,* vol. 34, no. 3, pp. 945-967, 1987, doi: https://doi.org/10.1002/app.1987.070340307.

[137] W. N. Kim and C. M. Burns, "Thermal behavior, morphology, and some melt properties of blends of polycarbonate with poly(styrene-co-acrylonitrile) and poly(acrylonitrile-butadiene-styrene)," *Polymer Engineering & Science,* vol. 28, no. 17, pp. 1115-1125, 1988, doi: https://doi.org/10.1002/pen.760281706.

[138] W. N. Kim and C. M. Burns, "Phase behavior of blends of polycarbonate with partially miscible polymers," *Journal of Applied Polymer Science,* vol. 41, no. 7-8, pp. 1575-1593, 1990, doi: https://doi.org/10.1002/app.1990.070410718.

[139] H. S. Lee, W. N. Kim, and C. M. Burns, "Determination of the Flory-Huggins interaction parameter of polystyrene-polybutadiene blends by thermal analysis," *Journal of Applied Polymer Science,* vol. 64, no. 7, pp. 1301-1308, 1997, doi: https://doi.org/10.1002/(SICI)1097-4628(19970516)64:7<1301::AID-APP9>3.0.CO;2-N.

[140] J. Reignier, B. D. Favis, and M.-C. Heuzey, "Factors influencing encapsulation behavior in composite droplet-type polymer blends," *Polymer,* vol. 44, no. 1, pp. 49-59, 2003, doi: https://doi.org/10.1016/S0032-3861(02)00684-5.

[141] N. Virgilio, C. Marc-Aurèle, and B. D. Favis, "Novel Self-Assembling Close-Packed Droplet Array at the Interface in Ternary Polymer Blends," *Macromolecules,* vol. 42, no. 9, pp. 3405-3416, 2009, doi: https://doi.org/10.1021/ma802544q.

[142] Y. Zhu, W. Wu, M. Gao, J. Yan, and B. Wang, "Molecular Compatibility and Hydrogen Bonding Mechanism of PES/PEI Blends," *Polymers (Basel),* vol. 14, no. 15, Jul 27 2022, doi: https://doi.org/10.3390/polym14153046.

[143] S. Nara and H. T. Oyama, "Effects of partial miscibility on the structure and properties of novel high performance blends composed of poly(p-phenylene sulfide) and poly(phenylsulfone)," *Polymer Journal,* vol. 46, no. 9, pp. 568-575, 2014, doi: https://doi.org/10.1038/pj.2014.21.

[144] B. Nandan, L. D. Kandpal, and G. N. Mathur, "Poly(ether ether ketone)/poly(aryl ether sulfone) blends: Relationships between morphology and mechanical properties," *Journal of Applied Polymer Science,* vol. 90, no. 11, pp. 2887-2905, 2003, doi: https://doi.org/10.1002/app.13009.

[145] T. M. Malik, "Thermal and mechanical characterization of partially miscible blends of poly(ether ether ketone) and polyethersulfone," *Journal of Applied Polymer Science,* vol. 46, no. 2, pp. 303-310, 1992, doi: https://doi.org/10.1002/app.1992.070460211.

[146] A. Lassus, B. D. Favis, and N. Virgilio, "Controlling and modeling phase separation behavior in ternary systems of PEEK with *meta*- and *para*-PEI," (2025).

[147] J. Roovers, R. Ethier, and P. Toporowski, "The Properties of 'RADEL R' Polysulfone," *High Performance Polymers,* vol. 2, no. 3, pp. 151-163, 1990, doi: https://doi.org/10.1177/152483999000200301.

[148] L. E. Govaert and T. A. Tervoort, "Strain hardening of polycarbonate in the glassy state: Influence of temperature and molecular weight," *Journal of Polymer Science Part B: Polymer Physics,* vol. 42, no. 11, pp. 2041-2049, 2004, doi: https://doi.org/10.1002/polb.20095.

[149] N. Virgilio, P. Desjardins, G. L'Espérance, and B. D. Favis, "In Situ Measure of Interfacial Tensions in Ternary and Quaternary Immiscible Polymer Blends Demonstrating Partial Wetting," *Macromolecules,* vol. 42, no. 19, pp. 7518-7529, 2009, doi: https://doi.org/10.1021/ma9005507.

[150] L. Cafiero, S. Iannace, and L. Sorrentino, "Microcellular foams from high performance miscible blends based on PEEK and PEI," *European Polymer Journal,* vol. 78, pp. 116-128, 2016, doi: https://doi.org/10.1016/j.eurpolymj.2016.03.014.